

Trajectory Optimization Methods for Low-Thrust Kuiper Belt Flyby Missions

MSc Thesis

Kevin De hulsters



Trajectory Optimization Methods for Low-Thrust Kuiper Belt Flyby Missions

by

Kevin De hulsters

to obtain the degree of Master of Science
at Delft University of Technology
to be defended publicly on Wednesday February 15, 2023 at 14:00.

Student number: 4649486
Project duration: February 14, 2022 - January 31, 2023
Institution: Delft University of Technology
Place: Faculty of Aerospace Engineering, Delft
Supervisor: Ir. R. Noomen
Thesis committee: Dr. D.M. Stam, committee chair
Dr. S. Speretta, external committee member
Ir. R. Noomen, daily supervisor

Cover Image: Enhanced color view of Charon, a moon of Pluto, captured by New Horizons in 2015. Copyright of NASA/JHUAPL/SwRI [84].

Preface

I can still vividly remember when I first visited TU Delft during one of the open days in my final year of high school. Now, more than five years later I'm nearing the end of my time as a student at the university. I guess people are indeed correct when they tell you how fast time goes by.

For the last year I've spent most of my time either at my internship or working on this thesis project, in the form of a literature study and the actual thesis. Space has always been one of my biggest interests since I was young so I truly feel fortunate that I have been able to perform my study in a topic I adore. This specific thesis looks at trajectories towards Kuiper belt objects, a research topic inspired by incredible achievements by scientists and engineers who captured beautiful images of Pluto and Charon with their New Horizons mission. One of those images is shown on the front page. And it is also possible due to previous work by students such as L. van der Heyden and T. Roegiers. I want to thank them for their amazing work. As they say we always build on the knowledge of those before us. I also want to thank students and professors who helped me during my thesis by answering questions and helping me learn the ins and outs of Tudat: M. Avillez and D. Dirkx.

Besides my thesis I have also spent quite some time the last few years on side projects such as a video game called Invertigo which I have been developing together with other students. I want to thank all my fellow-developers at Invertigo for being flexible with work hours due to my thesis. Since February 2022 I've spent four out of five workdays per week on my thesis and the remaining day on Invertigo. I also want to thank my supervisor Ir. R. Noomen for his wisdom and tips throughout all these months as well as for allowing me to take a combined two months off from work for vacation as well as to be with family which flew over from Mexico. While on that topic, I would also like to thank my family for all their support. Not only during this thesis project, but during my entire university career.

By removing the vacation and Invertigo time I'm left with slightly less than eight months spent on the thesis from the first meeting with my supervisor to my thesis defense. And I must say that I thoroughly enjoyed it, even though it did get a bit busy near the end of it. And last, but certainly not least I want to thank my friends for supporting me throughout the whole thesis process, friends I could always go to for advice or just to vent some thoughts. I'm not going to try to name everyone out of fear of leaving people out, but you all know who you are.

*Kevin De hulsters
Delft, January 2023*

Summary

The Kuiper belt, a circumstellar disk beyond Neptune, is one of the last mostly unexplored regions in the Solar System. Due to the antiquity of some of the bodies in this region, exploration of the Kuiper belt can greatly increase humanity's understanding of the Solar System's formation and evolution. However, to date the New Horizons mission is the only one to have actively explored objects in the Kuiper belt. Furthermore, previous studies of Kuiper belt object (KBO) missions as well as current proposals mainly use conventional high-thrust propulsion. The use of low-thrust propulsion for KBO missions is a mostly unexplored topic and has the potential to improve the payload mass of the mission due to the high efficiency of its propellant. Therefore, this thesis can be considered as a feasibility study and aims to answer the following research question: "What methodology is required to optimize realistic low-thrust trajectories with the goal of Kuiper belt object flybys?".

The goal of the found methodology is to be able to construct low-thrust flyby missions with at least two KBOs in a single mission. This is to be done with current technologies in terms of the available power, encapsulated in the research question with the word 'realistic'. To simplify the problem, the hyperbolic excess velocity from the departure at Earth as well as the use of powered gravity assists are neglected. To obtain the required velocity to reach and enter the Kuiper belt and to shape the trajectory the methodology assumes a gravity assist with both Jupiter and Neptune. For this mission a launch window between 2040 and 2050 is considered. The trajectory is modelled using Tudat with a patched-conics assumption and spherical shaping as the trajectory parameterization method. Python-based code is used to perform the trajectory calculations.

For the optimization problem a two-objective problem is constructed with ΔV and the time-of-flight as objectives. MOEA/D is the chosen optimizer for this purpose and has been tuned with low-thrust problems for optimal performance. The optimization problem is split into two phases: one phase up to and including the first KBO flyby and a second phase to find subsequent flybys. A methodology is constructed which switches between high-thrust and low-thrust legs to constrain the input space for the low-thrust optimization problem as a workaround for the sensitivity of the low-thrust solution. Furthermore, certain trajectory legs are tackled separately to allow the low-thrust optimizer to converge. To expand the trajectory to a second KBO flyby this method is insufficient and new methods need to be constructed. By using close-approach graphs, using a larger pool of KBOs, and optimizing multiple KBO flybys at the same time a second KBO flyby is found.

The result of the thesis is a robust method to find KBO flyby trajectories with low-thrust propulsion. To illustrate this a number of low-thrust trajectories to KBOs are discussed including a flyby mission of Albion with a total ΔV of 9.68 km/s and a time-of-flight of 27.0 years, after local refinement cycles and a sensitivity study. A two-KBO flyby mission with K13WB4G and K15RS1R requires roughly 10.52 km/s of ΔV and a time-of-flight of 33.2 years. These two trajectories have mass propellant fractions of 1.39 and 1.43 after departure from Earth, respectively. With the high-thrust optimization method many more two-KBO flyby missions can be found, but it is not possible to convert these to low-thrust missions due to limitations of the spherical shaping method. No direct comparison is performed with high-thrust trajectories in this thesis, which would require an analysis of missions with higher launch energy values. However, based on results from other research it is concluded that at the very least the results found in this thesis are comparable or in some cases even more optimal than the mass fraction found in proposed high-thrust KBO missions.

Further analysis regarding the frequency of more distant KBO flybys during the main mission indicates that to perform such distant flybys with known KBOs it is not sufficient to rely on random encounters. Instead, such distant flybys should also actively be searched for in the objective description. A check with the real-life implications of the found missions indicates that launch windows are in the order of a few weeks and that for the majority of the mission time the thrust magnitude is below the maximum

thrust available with modern low-thrust propulsion. The use of a higher launch energy can resolve the increased thrust and thus power requirement in the initial mission phase where the thrust limit is exceeded.

In conclusion, a methodology which relies on switching between high-thrust and low-thrust trajectories and separately analyzing trajectory legs is developed to constrain the inputs for the low-thrust two-objective optimization problem and to come up with realistic solutions for the KBO mission. With the use of an evolutionary algorithm this allows for the design of many single-flyby KBO missions. Expanding this methodology to multiple KBO flybys is possible but challenging, in large part due to the limitations of the spherical shaping parameterization in terms of its requirements regarding trajectory curvature, the manner in which it solves for its free coefficient, and in general the high sensitivity to changes in the input space. Therefore, further study of the method is recommended with changes to spherical shaping or with other low-thrust shape-based trajectory parameterization methods. Nevertheless, the results show that the design and optimization of low-thrust KBO missions is possible and that the resulting trajectories are realistic in terms of the propellant mass fraction and thrust levels, thus firmly putting another propulsion possibility on the table when deep-space Kuiper belt missions are designed.

Contents

Preface	ii
Summary	iv
Nomenclature	x
1 Introduction	1
I Preparation	3
2 Background	5
2.1 Kuiper belt	5
2.1.1 History and evolution	5
2.1.2 Current state	6
2.1.3 Scientific relevance	8
2.1.4 Objects of interest	8
2.2 Low-thrust theory	10
2.3 Mission heritage	12
2.3.1 Previous deep-space missions	12
2.3.2 New Horizons	12
2.3.3 Proposed missions	14
2.3.4 Low-thrust and flyby missions	16
2.4 Research heritage	17
2.5 Summary	18
3 Mission description	19
3.1 Trajectory scenario	19
3.2 Science return	19
3.3 Spacecraft subsystems	20
3.3.1 Propulsion	20
3.3.2 Power	20
3.3.3 Spacecraft mass	21
3.3.4 Launch system	21
3.4 Decision variables	22
3.4.1 Departure date	22
3.4.2 Time-of-flight	23
3.4.3 Departure velocity	23
3.4.4 Flyby variables	23
3.5 Constraints	24
3.5.1 Flyby constraints	24
3.5.2 Other constraints	26
3.6 Objectives	27
3.6.1 ΔV objective	27
3.6.2 Time-of-flight	27
3.6.3 Other considerations: KBOs and penalties	27
3.7 Requirements	28
3.8 Problem structure	29
3.9 Summary	30

4	Astrodynamics	31
4.1	Tudat	31
4.2	Data sources	32
4.3	Model decisions	33
4.4	Trajectory parameterization	35
4.4.1	Parameterization options	35
4.4.2	Spherical shaping	37
4.5	Trajectory theory	39
4.5.1	Orbital mechanics	40
4.5.2	Kepler orbits	41
4.5.3	Gravity assists and flybys	42
4.6	Summary	43
II	Implementation	45
5	Software development	47
5.1	Coding design	47
5.1.1	Main model architecture	47
5.1.2	Auxiliary files	49
5.1.3	Calculation loop example	49
5.1.4	C++ adjustments	51
5.1.5	Launch implementation	52
5.1.6	Trajectory leg implementation	52
5.1.7	Gravity assist and flyby implementation	52
5.1.8	Kuiper belt flyby implementation	52
5.2	Verification	52
5.2.1	Thrust profile checks	53
5.2.2	GTOP verification	57
5.2.3	Low-thrust verification	58
5.3	Summary	59
6	Optimizer theory and tuning	61
6.1	Optimizer selection	61
6.2	MOEA/D theory	62
6.3	Optimizer parameters	63
6.4	Optimizer tuning for high-thrust trajectories	64
6.4.1	Initial analysis	65
6.4.2	Subsequent high-thrust tuning	65
6.5	Optimizer tuning for low-thrust trajectories	68
6.6	Summary	72
III	Application	73
7	Planetary and single KBO flyby analysis	75
7.1	Straightforward optimization problem	75
7.2	Separate analyses per leg	76
7.3	Convergence and root finder	78
7.4	Free, locked, and constrained trajectory solutions	80
7.5	High-thrust intermediate step	82
7.6	High-thrust to low-thrust translation	85
7.7	Final procedure	86
7.8	Summary	87

8 Multiple KBO flyby analysis	89
8.1 High-thrust to low-thrust leg	89
8.2 Alternative attempts	91
8.3 Close-approach graphs	91
8.4 Summary	94
9 Final results	95
9.1 Earth to Neptune	95
9.2 Single flyby results	96
9.2.1 Sensitivity study	97
9.3 Multiple flyby results	99
9.4 Distant flyby analysis	103
9.5 Thrust magnitude analysis	105
9.6 Requirements recap	107
9.7 Comparison with high thrust and industry	107
9.7.1 Comparison with high-thrust trajectory performance	107
9.7.2 Industry optimization methods	108
9.8 Summary	109
10 Conclusions	111
11 Recommendations	113
References	117
A Overview of unit tests	125

Nomenclature

Abbreviations

Abbreviation	Definition
AU	Astronomical unit
ASRG	Advanced Stirling radioisotope generator
BI	Boundary intersection
BOL	Beginning of life
BS	Bulirsch–Stoer
CFB	Close flyby
DE	Differential evolution
DFB	Distant flyby
DOPRI	Dormand–Prince
DSM	Deep space maneuver
E	Earth flyby node in trajectory sequence
ECLIP	Ecliptic coordinate system
EMTG	Evolutionary Mission Trajectory Generator
ESA	European Space Agency
GA	Gravity assist
GEN	General
GPHS	General-purpose heat source
GTOP	Global Trajectory Optimization Problems (database)
ICRF	International Celestial Reference Frame
IHP	Interstellar Heliocentric Probe
IHS	Improved harmony search
INL	Idaho National Laboratory
INSTR	Instrumentation
J	Jupiter flyby node in trajectory sequence
J2000	January 1, 2000 at 12:00 terrestrial time
JAXA	Japan Aerospace Exploration Agency
JD	Julian date/day
JHUAPL	Johns Hopkins University Applied Physics Laboratory
JPL	Jet Propulsion Laboratory
KBM	Kuiper belt mission
KBO	Kuiper belt object
LS	Local search
MJD	Modified Julian date
MJD ₂₀₀₀	Modified Julian date since J2000
MOEA/D	Multi-objective evolutionary algorithm based on decomposition
MPC	Minor Planet Center
MGA	Multiple gravity assist
MHACO	Multi-objective hypervolume-based ant colony optimizer
N	Neptune flyby node in trajectory sequence
NASA	National Aeronautics and Space Administration
Nobj	Number of objectives
NSGA2	Non-dominated sorting genetic algorithm
NSPSO	Non-dominated sorting particle swarm optimizer
LV	Launch vehicle
OOP	Object-oriented programming

Abbreviation	Definition
PaGMO	Parallel global multiobjective optimizer
POW	Power
PROP	Propulsion
PyGMO/Pygmo	Python parallel global multiobjective optimizer
Pu	Plutonium
RTG	Radioisotope thermoelectric generator
SDO	Scattered disk object
SOI	Sphere of influence
SPICE	Spacecraft Planet Instrument C-matrix Events
SSB	Solar System barycenter
SwRI	Southwest Research Institute
TNO	Trans-Neptunian object
TNW	Thrust, normal, out-of-plane
TOF	Time-of-flight
TRAJ	Trajectory
Tudat	TU Delft Astrodynamics Toolbox
Tudatpy	TU Delft Astrodynamics Toolbox in Python
USM	Unified State Model
V	Venus flyby node in trajectory sequence
VDFB	Very distant flyby

Symbols

Symbol	Definition	Unit
\vec{a}	Acceleration vector along the trajectory	[m/s ²]
a	Semi-major axis	[m]
a_x	Free coefficient x for the spherical shaping azimuthal function	[-]
B	Impact parameter	[m]
b_{rot}	3D rotation angle	[rad]
b_x	Free coefficient x for the spherical shaping elevation function	[-]
C_3	Launch energy	[m ² /s ²]
CR	Cross-over rate MOEA/D	[-]
C_{crit}	Convergence criterium	[m/s]
D or $D(\theta)$	Parabolic anomaly function	[rad]
d_r	Degradation rate	[-]
E	Eccentric anomaly	[rad]
\mathbf{e}	Unit vector	[-]
e	Eccentricity	[-]
\mathbf{F}	Force vector	[N]
F	Scale factor MOEA/D	[-]
G	Gravitational constant	[m ³ kg ⁻¹ s ⁻²]
g	Gravitational acceleration	[m/s ²]
g_0	Standard gravitational constant	[m/s ²]
gen_{lim}	Generation limit	[-]
I_{sp}	Specific impulse	[s]
i	Inclination	[rad]
L_{stable}	Stable length	[-]
M	Mean anomaly	[rad]
m	Mass	[kg]
m_0	Initial mass	[kg]

Symbol	Definition	Unit
m_f	Final mass	[kg]
N_{KBO}	KBO index number	[-]
n_r	Number of full revolutions	[-]
p	Semi-latus rectum	[m]
$R(\theta)$	Radial distance spherical shaping function	[m]
R/r	Radius/radial distance	[m]
\mathbf{r}	Radial position vector	[m]
r_{min}	Minimum flyby distance	[m]
r_p or r_3	Pericenter distance	[m]
Realb	Diversity preservation chance	[-]
$T(\theta)$	Time-related spherical shaping function	[s]
T	Neighbourhood size MOEA/D	[-]
T	Thrust	[N]
t	Time	[s]
t_f or TOF	Time-of-flight	[s]
t_y	Time in years	[years]
U	Uncertainty parameter	[-]
\mathbf{u}	Low-thrust control vector	[m/s ²]
u	Thrust acceleration	[m/s ²]
V	Velocity	[m/s]
\mathbf{V}_∞	Heliocentric excess velocity vector	[m/s]
V_∞	Heliocentric excess velocity magnitude	[m/s]
V_p or V_3	Velocity at pericenter distance	[m/s]
$\tilde{\mathbf{v}}$	Velocity vector along the trajectory	[m/s]
v_C	Circular velocity	[m/s]
v_E	Escape velocity	[m/s]
W	Power	[W]
\mathbf{x}	State vector	[various]
x	Cartesian x-coordinate	[m]
y	Cartesian y-coordinate	[m]
z	Cartesian z-coordinate	[m]
α	Asymptotic bending angle	[rad]
β	Angular conversion auxiliary variable	[-]
γ	Flight path angle	[rad]
ΔV or Delta V	Velocity maneuver magnitude	[m/s]
ΔV_{lim}	ΔV limit	[m/s]
ϵ	Fractional error	[-]
η	Thrust efficiency	[-]
η_m	Distribution index MOEA/D	[-]
θ	Azimuthal angle	[rad]
θ	True anomaly	[rad]
μ	Gravitational parameter	[m ³ /s ²]
ν	True anomaly	[rad]
Φ or $\Phi(\theta)$	Elevation angle spherical shaping function	[rad]
ϕ	Elevation angle	[rad]
Ω	Right ascension/Longitude of the ascending node	[rad]
ω	Argument of pericenter	[rad]

Subscripts and superscripts

Note that this list is not exhaustive. Unique and/or deviating subscripts and superscripts or ones that are always combined with the same symbol are mentioned in the previous table.

Symbol	Definition
\square'	First derivative with respect to θ
\square''	Second derivative with respect to θ
$\dot{\square}$	First derivative with respect to time
$\ddot{\square}$	Second derivative with respect to time
$\frac{dx}{dy}$	Derivative of x with respect to y
0, 1, 2...	Sequential numbering
arr	Arrival
dep	Departure
E	Earth
f	Final
ga	Gravity assist
h	Out-of-plane component
i	Initial/Current iteration
i+1	Next iteration number
KBO	Related to a Kuiper belt object
J	Jupiter
N	Neptune
n	Normal component
r	Radial component
t	Tangential component
x	Cartesian x-component
y	Cartesian y-component
z	Cartesian z-component
θ	Azimuthal component
ϕ	Elevation component

Introduction

Developments in the spaceflight sector have led to successful missions to most major bodies in the Solar System. All of the planets and many of their moons have been explored by at least one space mission. Despite this, there are vast regions of the Solar System which are almost completely unexplored. The Kuiper belt is a circumstellar disc which extends roughly from 30 to 50 AU from the Sun. It is scattered with rocky and icy bodies, ranging in size from small asteroids to dwarf planets [33]. Many of these bodies have been in the Kuiper belt for billions of years. As such, they are the closest available in-situ representation of the primordial state of the Solar System. The study of the Kuiper belt can therefore greatly increase humankind's understanding of the origin and evolution of the Solar System as well as the general mechanics of stellar systems [113]. Multiple space missions such as Voyager 1 and 2 as well as Pioneer 10 and 11 have already passed through the Kuiper belt. However, it was not until the New Horizons mission that a spacecraft performed a close approach with a Kuiper belt object (KBO). New Horizons performed a flyby of Pluto in 2015 and later also of KBO 486958 Arrokoth in 2019 [83]. This final KBO flyby was only decided upon until shortly before the Pluto flyby. As of 2021 New Horizons has also left the Kuiper Belt [86].

The main limiting factor of the previously mentioned missions is their high radial velocity, which causes them to only spend a brief time in the Kuiper belt. For example, New Horizons left the region after only six years [86]. While New Horizons has been of monumental value for the scientific community, a new mission which could stay inside the Kuiper Belt for a longer amount of time could visit more KBOs and expand on its findings. By visiting more KBOs, information on a diverse selection of bodies in the Kuiper belt can be gathered [113], which will increase the knowledge of these ancient areas of the Solar System greatly. This thesis builds on a previous study by L. van der Heyden [43], whose work indicates that long-term trajectories which stay in the Kuiper belt for more than 100 years are feasible by means of multiple gravity assists (GAs) and deep space maneuvers (DSMs).

The next step, which will be performed in this thesis, is to look at the methodology required to optimize Kuiper belt missions. Unlike the long-term trajectories analyzed by L. van der Heyden, this thesis specifically looks at optimizing close flyby trajectories with KBOs. This will be done with the TU Delft astrodynamics toolbox (Tudat), a framework developed by TU Delft [21]. The flybys analyzed concern close approaches like the ones performed by New Horizons with Pluto and Arrokoth. Later in the thesis the possibility of more distant flybys, which only allow partial scientific measurements, is analyzed as well.

Previous work on KBO missions has mainly regarded the use of high-thrust propulsion. The use of low-thrust propulsion for a KBO mission is a mostly unexplored topic and could be beneficial for a flyby mission due to the large associated ΔV requirements. The methodology to tackle deep-space high-thrust missions already exists, but such a plan of attack is less readily available for low-thrust optimization. This thesis can be considered as a feasibility study and combines the KBO trajectory and low-thrust topics by means of the following research question:

“What methodology is required to optimize realistic low-thrust trajectories with the goal of Kuiper belt object flybys?”

To fully answer this research question, the following set of subquestions can be identified:

- How is the science return of a KBO flyby mission defined?
- Which thrust parameterization and physics description is best used for the low-thrust trajectory design and how does this need to be implemented in Tudat?
- What is the best performing optimizer including tuning for a low-thrust flyby mission?
- What is the optimal planetary gravity assist sequence for Kuiper belt trajectories?
- What is the required optimization strategy to expand the trajectory to the Kuiper belt with optimal objective values?
- What kind of Kuiper belt flyby trajectories are possible with the found optimization strategy?
- How many distant flybys can one expect to encounter during a long-term Kuiper belt mission?
- What impact does a sensitivity study of the inputs of the trajectory have on the found optimal Kuiper belt trajectories?
- How feasible are the found Kuiper belt flyby trajectories with current power and low-thrust propulsion technologies?
- How does the wet-to-dry mass fraction of the designed low-thrust missions compare to potential high-thrust missions?

These subquestions are tackled one by one throughout this thesis. In larger terms the thesis is split into three parts. The first part, preparation, looks at all the heritage analyses and theory required to prepare the study of KBO missions. Background information on the topic is provided in Chapter 2. This concerns the Kuiper belt, past missions, and low-thrust propulsion in general. Afterwards, the specific mission scenario for this project is described in Chapter 3. This is followed by a chapter on astrodynamics used in this thesis in Chapter 4. Together, the aforementioned chapters answer the first two subquestions regarding the science return and the physics description of the mission.

The second part of the thesis looks at the implementation of the new low-thrust KBO optimization method and strategy. Chapter 5 discusses the trajectory implementation in Python code as well as the verification of the code. The selection and tuning of the optimizer is discussed in Chapter 6. The final part of the thesis, application, discusses the methods to construct KBO flybys and provides examples of KBO flybys and the conclusions based on the findings. This part starts with the construction of low-thrust optimization methods for single-KBO flyby trajectories and multiple-KBO flyby trajectories in Chapters 7 and 8, respectively. Chapter 9 shows the final found trajectories as well as results regarding distant flybys, the thrust profile, and the sensitivity study. These results will also indicate the feasibility of the trajectories and this thus regards the ‘realistic’ term within the research question. The thesis is concluded with conclusions and recommendations for future work in Chapters 10 and 11, respectively.

Part I

Preparation

2

Background

This chapter provides relevant background information for the thesis. Firstly, more information is given about the Kuiper belt in terms of its history, structure, and scientific relevance. Secondly, relevant heritage missions and research papers are discussed. Finally, a brief summary of the chapter is provided.

2.1. Kuiper belt

The end goal of this thesis project is to have a methodology to design a Kuiper belt exploration mission with example trajectories. This section explains what the Kuiper belt is and how it came to be. Furthermore, the current structure of the Kuiper belt is discussed as well as its scientific relevance and objects of interest.

2.1.1. History and evolution

The Kuiper belt is a circumstellar disk or torus-shaped band of icy objects, which can be found beyond the outer planet Neptune [54]. To understand the state of the Kuiper belt it is important to know the history of the Solar System. In the early stages of the Solar System the stellar disk around the Sun coalesced into larger bodies, eventually forming the planets of today. However, not all of the matter in the disk ended up in planetary systems. Under influence of the outer planets, many smaller objects in the Solar System were organized into different regions such as the asteroid belt between Mars and Jupiter. This also resulted in multiple groups of bodies beyond Neptune, the so-called trans-Neptunian objects (TNOs). These objects inhabit the Kuiper belt, the scattered disc, and the hypothesized Oort cloud [33]. While the precise origin of the Kuiper belt is still heavily debated, one of the most commonly accepted models for the Solar System's and thus also the Kuiper belt's formation is the so-called Nice model.

The Nice model describes the migration of the four giant planets of the Solar System. Specifically, it addresses the migration of Uranus and Neptune to the outer regions of the Solar System with more eccentric orbits [52]. Migration of the planets is caused by two different processes: the torque from the protoplanetary disk (type I and type II migration) and planetesimal-induced migration [54]. The latter process is considered to have been dominant in the creation of the current TNO structure.

Gravitational stirring by Uranus and Neptune caused minor objects to move closer to the Sun and thus closer to Saturn and Jupiter. Once they reached Jupiter they would often be catapulted to the Oort cloud [54]. The changes in angular momentum conversely moved these planets outwards, while Jupiter moved slightly inward due to expelling bodies to the Oort cloud [54]. This migration resulted in the formation of resonance objects and high-eccentricity orbits, especially with Neptune [54]. Later stabilization of the planetary orbits and crossing of planetary mean-motion resonances caused another migration of planets and planetesimals and eventually resulted in the different categories of TNOs that can currently be found [52]. Note that the Nice model does not account for all features of the Solar System, which is why it has been modified over the years and other hypotheses regarding planetary migration exist as well. The current distribution of objects is shown in Figure 2.1 [20].

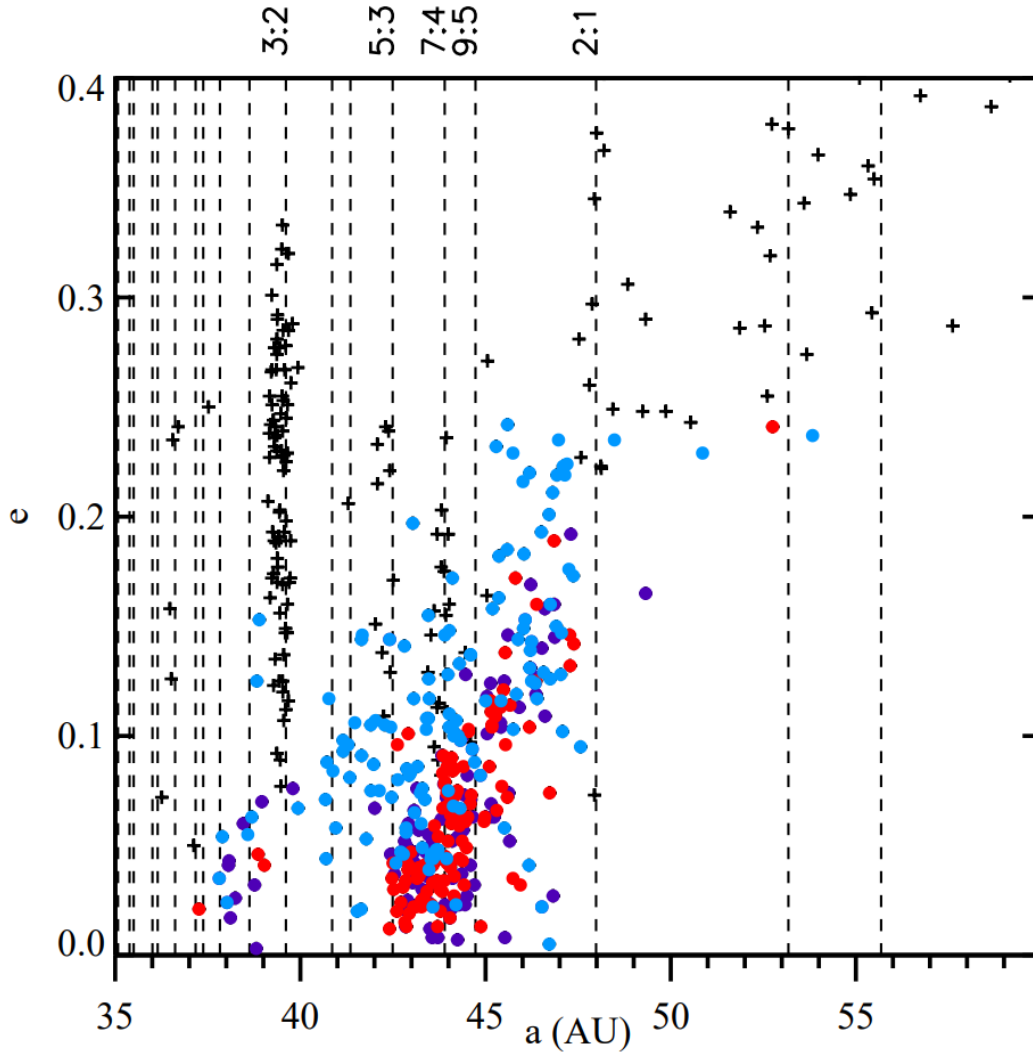


Figure 2.1: An overview of the distribution of objects in and near the Kuiper belt in terms of their semi-major axis (a) and their eccentricity (e) [20]. Resonant objects and scattered objects are indicated by plus-symbols. The cold classical population is indicated in blue, the hot population in red, and intermediate objects in purple. The dashed lines indicate resonance bands with Neptune. The meaning of these different categories of TNOs is explained in the next subsection.

2.1.2. Current state

The Kuiper belt currently consists of multiple distinct groups of objects with varying properties, origins, and reasons for study. Therefore, this subsection discusses the structure, composition, and distribution of the Kuiper belt.

As already mentioned, the Kuiper belt is located beyond the orbit of Neptune. Neptune's orbit has a semi-major axis of roughly 30.1 astronomical units (AU) [54]. Any object with a semi-major axis beyond this orbit is considered to be a TNO. Kuiper belt objects (KBOs) are a subset of TNOs. While the precise definition of the Kuiper belt is not absolute, generally it is considered to refer to a region 30 to 50 AU from the Sun [68]. Note that different definitions of the Kuiper belt do exist, but that the 30 - 50 AU boundary will be used for this thesis. Because of this limitation not all TNOs are included in the research. Two collections of objects that are excluded from the analysis are the scattered disk objects (SDOs) and detached objects. The orbits of objects in the scattered disk are fundamentally different from those in the Kuiper belt. As the name implies these bodies have been scattered by the giant planets and are still being perturbed by Neptune [62]. Because of this they have higher eccentricities and inclinations than most KBOs and often have aphelions many times larger than the outer extent of the Kuiper belt [118].

Beyond these, there are also the so-called detached or scattered-extended objects [25]. The perihelia of these objects are far beyond Neptune's orbit and therefore these objects are minimally affected by the bodies in the Solar System besides the Sun. The most distant objects of this sub-class fall under the category of Sednoids such as Sedna itself, which has an aphelion of over 900 AU [86]. Due to their high inclination and often distant location to the Sun, SDOs and detached objects are not included in the trajectory design for this research. Analysis of missions to any of the excluded groups of objects is recommended for future research.

The remaining TNOs are the KBOs which will be studied during this thesis. Information on these objects is taken from the Minor Planet Center (MPC), a database which keeps track of all objects in the Solar System [15]. The list of objects which is considered to be part of the Kuiper belt in this research concerns all objects with a semi-major axis between 30.0 and 50.0 AU. A full plot of the position of all KBOs with a semi-major axis between 30 and 50 AU as of 2021 is shown in Figure 2.2. This filtered list consists of more than 3000 catalogued objects.

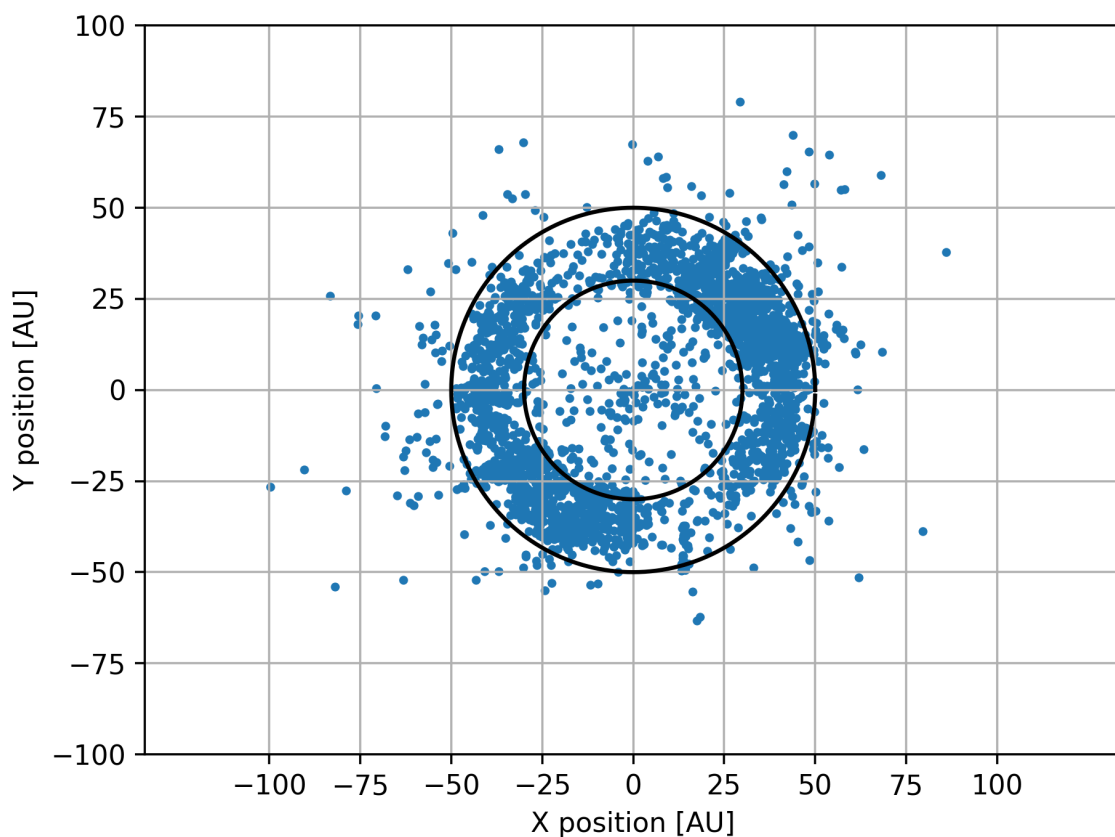


Figure 2.2: The position of the catalogued celestial objects with a semi-major axis between 30 and 50 AU and a distance from the Sun below 100 AU as of 2021. The black lines mark the defined 30 - 50 AU edges of the Kuiper belt region. Own work using raw data from [15].

These KBOs consist of distinct families. The first one is the classical belt, also known as cubewanos. The classical belt consists of stable objects with a semi-major axis smaller than 48 AU [52]. These bodies usually have small eccentricities below 0.1 and make up the majority of known KBOs [118]. This group of bodies best represents the original expectations of the Kuiper belt: stable bodies beyond Neptune which are not directly impacted by the outer planets [33]. The classical belt consists of a dynamically cold and hot population. The cold population has low inclinations below 4 or 5 degrees [34] and is theorized to have formed within the Kuiper belt [68]. The hot population has larger inclinations up to tens of degrees and likely formed near Neptune a long time ago before being scattered during planet migration [68].

The other main category consists of resonant TNOs such as Neptune trojans, plutinos, and twotinos. They are also in stable orbits, but are locked in some way with Neptune [68]. The trojans are in a 1:1 resonance with Neptune [64] with a semi-major axis of roughly 30 AU. The plutinos are in a 3:2 resonance with a semi-major axis around 39 AU [33]. As the name suggests this resonance band also contains Pluto. Twotinos are in a 2:1 resonance with Neptune with a semi-major axis around 47.8 AU [33]. This region denotes a clear boundary beyond which not many KBOs have been discovered [33]. Still different resonance bands exist or have been theorized as far out as 5:1 at 88 AU [25]. These bands are also visualized in Figure 2.1. The existence of more resonance bands and the lack of bodies in certain regions is not yet fully understood and could benefit greatly from in-situ measurements. This and more scientific reasons to visit the Kuiper belt again are discussed in the next subsection.

2.1.3. Scientific relevance

The New Horizons mission has given the scientific community much information about the characteristics of the Pluto-Charon system and by extension the Kuiper belt. However, this does not mean that all research questions about the Kuiper belt have been answered. While this thesis only focuses on trajectory design methodology and optimization to the Kuiper belt, it is still important to have a good understanding of the scientific relevance of such a mission, if only to define a proper objective function for the current research.

As has already been mentioned earlier in this chapter, the Kuiper belt is the closest representation of the primordial phase of the Solar System. The cold classical belt is an especially good analog since it consists of bodies which formed and have remained in the Kuiper belt since the early life of the Solar System. As such, further close-up study of the Kuiper belt can answer questions about the conditions during the early Solar System and about theories regarding Solar System formation and evolution. Theories regarding comet formation and evolution could strongly benefit from in-situ measurements of KBOs that can be compared with already existing comet measurements [93]. The study of multiple KBOs in a single mission is highly recommended since it allows more information to be gathered concerning the diverse properties of the bodies [93]. KBO missions with close flybys would also allow measurements of any volatiles or organic compounds that might be present on these distant bodies [93].

The discovery of many different classes of KBOs, as explained in the previous subsection, also means that the study and comparison of different types of KBOs is a valuable research objective [129]. By having a better understanding of the different characteristics of the varying types of KBOs, current understanding of the Kuiper belt and its evolution can be validated or updated. The study of different classes of KBOs has also been mentioned in a proposal for a New Horizons follow-up mission, specifically to determine the structure of the now long gone proto-planetary disk and how planetary accretion took place in the early Solar System [93]. The discovery of many binary objects as well as ring systems around KBOs has resulted in a large number of science questions which can only be answered by means of close observation [129]. Specific analyses of different classes of KBOs in one mission or visits to binary objects and ring systems are not specifically analyzed in this thesis, but are recommended beyond the preliminary design stage. More details regarding instrumentation options to answer these science questions follow in Chapter 3.

2.1.4. Objects of interest

Thousands of bodies have already been identified in the Kuiper belt [15] with many more expected to exist. During the trajectory design stage of this thesis, optimization will be performed with all bodies as well as with a subset of the database. For this subset a list with objects of interest is determined. One immediate body of interest would be Pluto as well as its moons. The Pluto-Charon system has already been visited by New Horizons in 2015. However, the findings by New Horizon have resulted in more science questions which would benefit from another flyby of the dwarf planet. Another highly recommended body to visit is Triton. Imagery of Pluto and Triton can be seen in Figure 2.3 [95] [87]. While not currently in the Kuiper belt, Triton is a moon of Neptune and most likely originated in the Kuiper belt [30]. During the migration of the outer planets Triton was captured by Neptune [54]. Since a gravity assist with Neptune is a realistic option in order to get the appropriate bending angle for a long Kuiper belt trajectory, a close approach of Triton would be a welcome by-product.

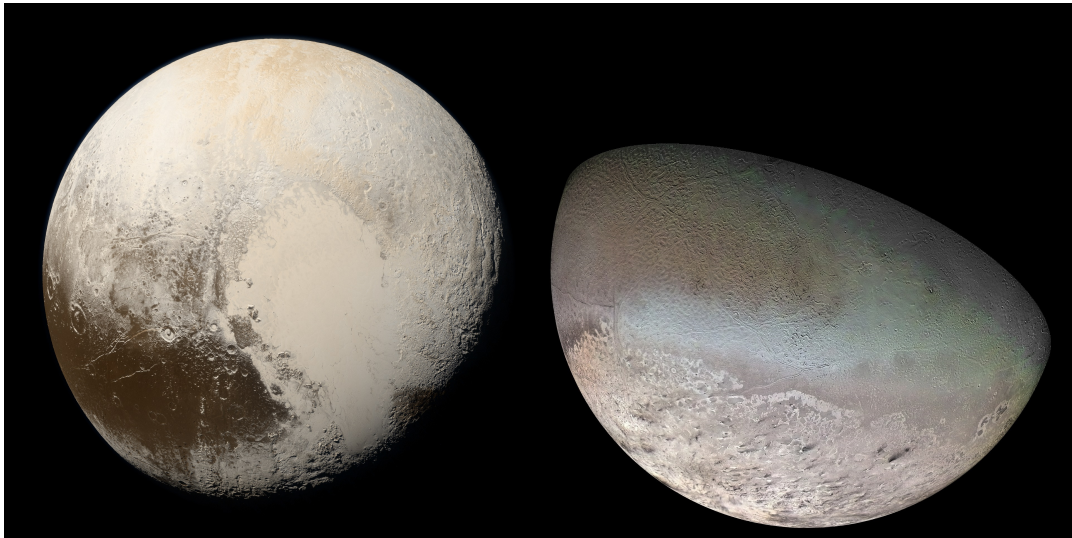


Figure 2.3: A multispectral composite image of Pluto made by New Horizons (left) [95]. A global color mosaic of Triton made by Voyager 2 during its flyby of Neptune (right) [87].

Another important parameter to determine bodies of interest is whether they can realistically be reached by a space mission. Due to the uncertainty in the future positions of KBOs, margins have to be taken into account in the propellant budget. Bodies for which this uncertainty is too high are preferably not included in the nominal description for trajectory design in this thesis project. A definitive selection of the bodies which will be considered based on this limiting factor is given in Chapter 3.

Furthermore, preference is given to the brightest objects since they can be easily detected and would result in a larger scientific data return. One of these large objects in the Kuiper belt is Haumea, which is also special due to its ring system, shown by means of an artist illustration in Figure 2.4 [4]. Specific preference could be given to bodies in the cold classical belt for previously mentioned science reasons. Giving a higher priority to other named objects is also recommended, since giving non-standard names to bodies is usually only done when they are of specific interest to the scientific community.

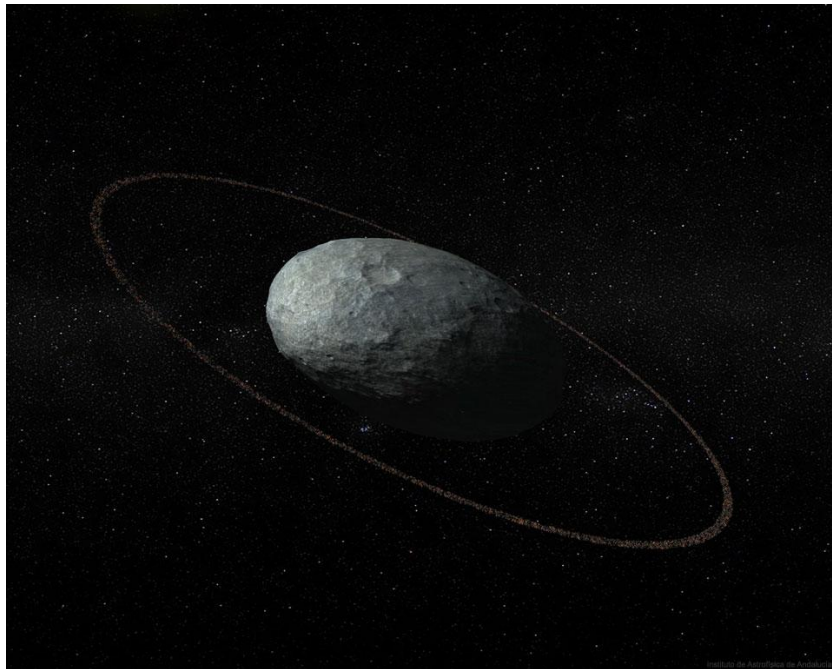


Figure 2.4: An artistic illustration of Haumea, an egg-shaped Kuiper belt object with a faint ring system [4].

It is also important to state what it means to 'visit' a KBO. The first type of visit regards close flybys (CFBs) which allow full scientific analyses. Based on the New Horizons flight path this is considered to be at a distance of 3,500 - 10,000 km [114]. Another type of flyby would be a distant flyby (DFB). This is a flyby during which some extended scientific measurements could take place while still staying at a large distance to the body. Based on the mission proposal for the Trident flyby of Triton the limiting distance for such a DFB is placed at 9 million km [30]. A final option would be very distant flybys (VDFBs), which are only close enough to allow basic detection of a KBO. Depending on the brightness of the KBO this distance ranges from 0.07 to 1.34 AU [42]. During this thesis only CFBs will be directly analyzed to simplify the optimization problem. However, near the end of the report it is checked how many DFBs and VDFBs are found as a by-product in the optimal trajectories.

2.2. Low-thrust theory

As was already mentioned in the introduction, the trajectories in this thesis are designed by using low-thrust propulsion. The precise parameterization and mathematical description of low-thrust theory is given in Chapter 4. This section will provide a brief overview regarding the definition of low-thrust propulsion and why it is chosen as the final propulsion method in this thesis instead of high-thrust propulsion.

All Kuiper belt missions to date have made use of high-thrust propulsion. This method burns propellant on its own once ignited and its large mass flow means that all of the mission's ΔV can be delivered in only a fraction of the mission lifetime. The total ΔV capabilities of different high-thrust deep-space mission are given in Table 2.1. This ΔV excludes any contributions by the launch vehicle. The ΔV is calculated using Equation 2.1 where g_0 is the standard gravity constant, $\frac{m_0}{m_f}$ is the ratio between the initial and final mass of the spacecraft, and I_{sp} is the specific impulse which is an indication of the efficiency of the propulsion method. These ΔV levels are reasonable for KBO missions as indicated by L. van der Heyden's conclusions [43]. However, much research has already been performed towards this option and just because it is a possibility does not mean it is the only option worth studying.

$$\Delta V = I_{sp} g_0 \ln\left(\frac{m_0}{m_f}\right) \quad (2.1)$$

Table 2.1: An overview of the relevant capabilities of different high-thrust missions [73] [74] [70] [71] [69] [29] [72].

Mission	$\frac{m_0}{m_f}$ [-]	ΔV [m/s]	Thrust [N]
Voyager (1 and 2)	1.14	280	3.6
Pioneer (10 and 11)	1.16	320	9
New Horizons	1.19	370	17.6
Rosetta	2.36	2700	40
Stardust	1.28	530	8

Low-thrust electrostatic electric propulsion ionizes the propellant and then expels it using electrodes [56]. The thrust levels of these systems are orders of magnitude smaller than of high-thrust propulsion, as shown in Table 2.2. However, since these systems can remain active during a large portion of the mission or even the entire mission, combined with the very high I_{sp} , the total ΔV generated by these systems is larger than with conventional propulsion methods. This results in more freedom of movement and could thus benefit a long mission such as one to the Kuiper belt. All mentioned low-thrust missions make use of ion engines as opposed to other low-thrust methods due to the simplicity of ion propulsion and its widespread usage as the low-thrust propulsion method to date. Therefore, ion propulsion is the only low-thrust method considered for this thesis project.

Table 2.2: An overview of the relevant capabilities of different low-thrust missions [78] [110] [82] [102].

Mission	I_{sp} [s]	$\frac{m_0}{m_f}$	ΔV [km/s]	Thrust [mN]
Dawn	3100	1.63	14.9	91
Deep Space 1	3300	1.30	8.5	91
Hayabusa	3000	1.34	8.6	24
Hayabusa 2	3000	1.24	6.3	28

The main issue with low-thrust propulsion is that the thrust levels mentioned here might be too low to shape trajectories fast enough for the Kuiper belt mission. The limitation of this shaping ability will be one of the main takeaways from this research. In the outer regions of the Solar System, nuclear-based radioisotope thermoelectric generators (RTGs) are the only reliable modern-day power source due to the low power levels that can be delivered by photovoltaic cells farther away from the Sun. Other methods such as batteries and fuel cells are not capable in view of the required mission times as of now, as is shown in Figure 2.5 [2].

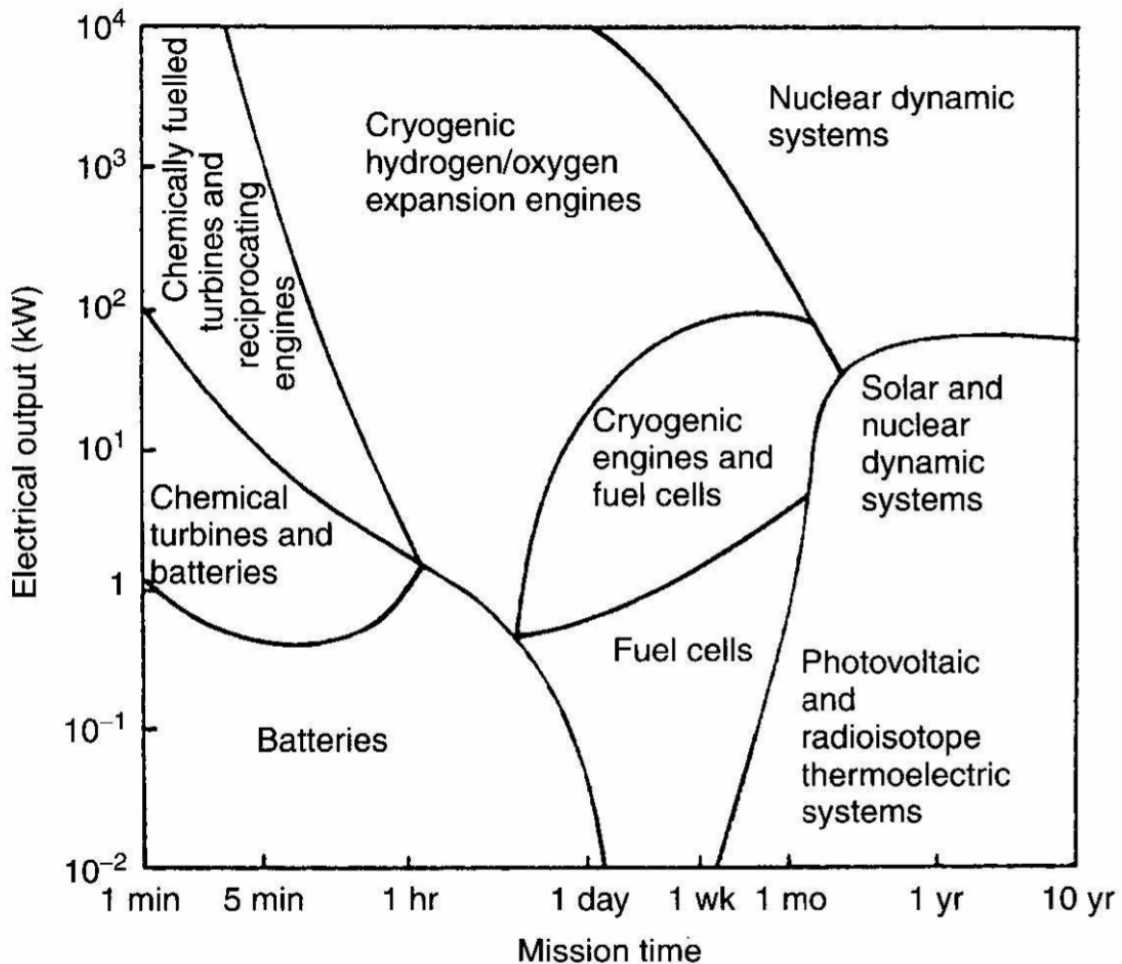


Figure 2.5: Power systems for space missions as a function of the electrical output and the mission time [2].

Using Equation 2.2 [35], where W is the power in W and η is the thrust efficiency (80% for Xenon ion engines) and with a specific impulse of 3000 s [17], it is found that three RTGs (900 W) can deliver roughly 49 mN of thrust. This is based on 300 W BOL (beginning of life) power per RTG [7]. The thrust value becomes lower over time due to degradation of RTGs. Research by J. Melman indicated that low-thrust propulsion was insufficient for a transfer mission to Neptune due to the power requirements [58]. However, this research did not analyze the possibilities of gravity assists in combination with low-thrust trajectories. Note that a hybrid system which uses solar power in the inner Solar system and nuclear power beyond is also a potential solution, but is deemed out of scope for this thesis.

Furthermore, one of the conclusions of this research could be that current RTGs are incapable of sufficiently powering a low-thrust Kuiper belt mission, but that an upcoming nuclear system such as an advanced Stirling radioisotope generator (ASRG) might be sufficient [66]. All in all, there is a distinct research gap towards the analysis of low-thrust propulsion for multi-KBO flyby missions and whether the power levels can be attained with modern technologies. L. van der Heyden also mentioned low-thrust

propulsion as an interesting topic for further study due to this very reason [43]. Therefore, a study towards low-thrust KBO missions is deemed to add a greater body of work to the scientific understanding of deep-space missions than analyzing the same problem with high-thrust propulsion.

$$T = \eta \frac{2W}{I_{sp}g_0} \quad (2.2)$$

2.3. Mission heritage

Multiple missions have already been sent to the Kuiper belt. The only one of these missions to be sent to this region for specific study within the Kuiper belt is New Horizons. Nevertheless, the conclusions from previous missions can be crucial for the trajectory design in this thesis research. Therefore, previous deep-space missions are briefly discussed. This is followed by a slightly more detailed description of the New Horizons mission. Previous low-thrust and flyby missions are also discussed, even if they did not occur in the Kuiper belt, as they are also relevant to this study. Finally, a few mission proposals are mentioned.

2.3.1. Previous deep-space missions

The spacecraft most distant from Earth currently is Voyager 1, which entered the 30 AU mark of the Kuiper belt in 1989 [86]. Both the Voyager 1 and Voyager 2 probes used a gravity assist with Jupiter in order to increase their heliocentric velocity. Voyager 1 performed a gravity assist with Jupiter and Saturn while Voyager 2 had additional gravity assists with Uranus and Neptune [81]. The latter mission remains the only mission to have visited Uranus and Neptune to date. Gravity assists have also been used for the Pioneer 10 and 11 missions, two other spacecraft which passed through the Kuiper belt. Pioneer 10 is the first spacecraft to enter the Kuiper belt, doing so in 1983 [86]. Note that a gravity assist with Jupiter is already sufficient to send a spacecraft on an escape trajectory from the Solar System [67], the other gravity assists were added due to the added scientific value of the flybys. However, for the work in this thesis the combination of multiple gravity assists would be of use as well since it allows more detailed and flexible shaping of the trajectory.

Both the Voyager and Pioneer missions made use of high-thrust propulsion and were powered by RTGs. While all of these missions passed through the Kuiper belt, none of them visited a KBO. Furthermore, all of these spacecraft have already left the 50 AU outer border of the Kuiper belt many years ago and thus did not spend a long time in the Kuiper belt. This was due to the high heliocentric radial velocities of the spacecraft. The trajectories of the Voyager and Pioneer missions are visualized in Figure 2.6. A larger bending angle during the gravity assists could extend the period that a spacecraft can remain in the Kuiper belt and is thus a desired property for the trajectories in this thesis. The only mission that did manage to study a KBO is New Horizons, which is discussed in the next subsection.

2.3.2. New Horizons

The New Horizons mission was launched in 2006 with the goal to explore the Pluto-Charon system and to gather information about the current state of the Kuiper belt as well as its history and evolution. This last goal also relates to the evolution of the Solar System in general. In 2015 New Horizons made its closest approach of Pluto at a distance of roughly 12,500 km from the surface [83]. This resulted in the first close study of Pluto and its moons. In order to reach Pluto, New Horizons only performed a gravity assist with Jupiter. Like the previously mentioned missions, New Horizons exclusively made use of high-thrust propulsion. Figure 2.7 gives an overview of the trajectory of New Horizons [76].

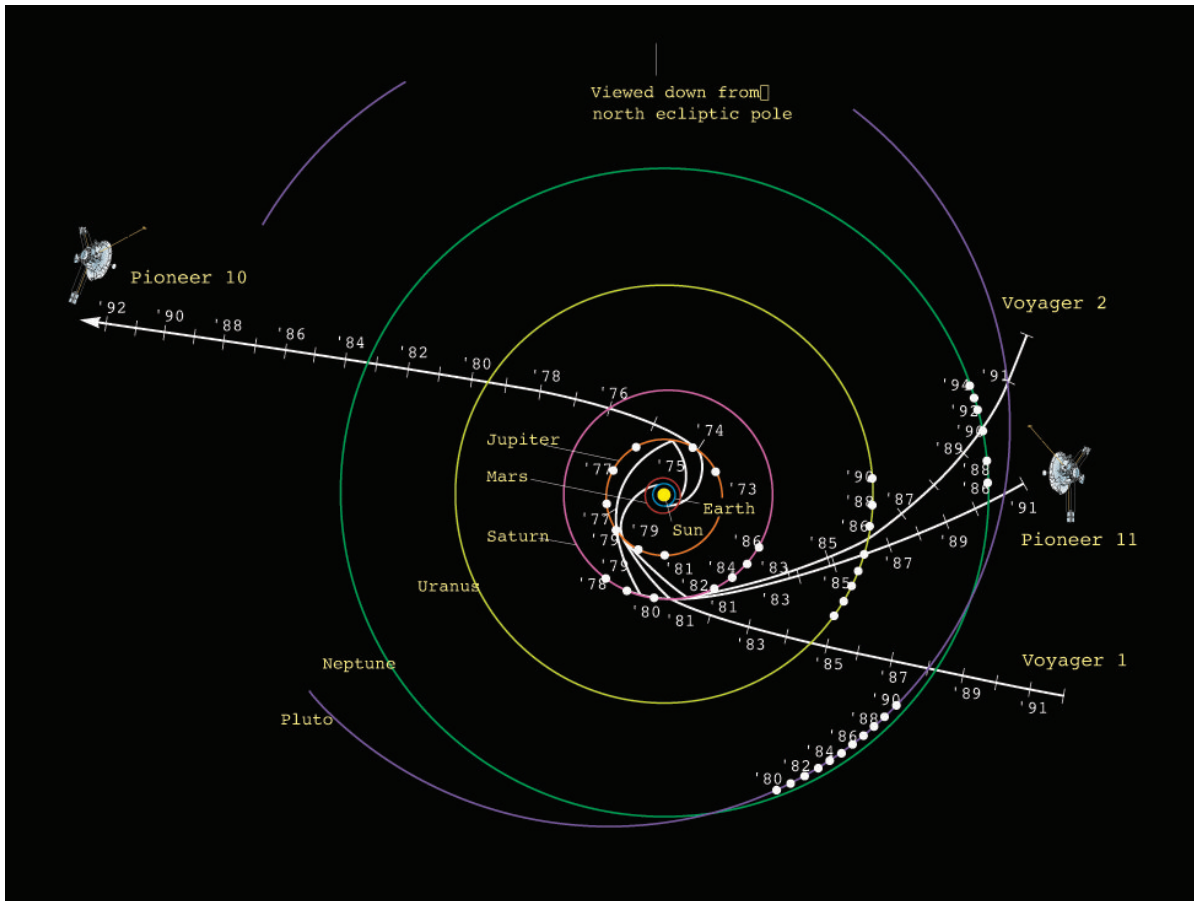


Figure 2.6: The trajectory of the Pioneer and Voyager missions [81].

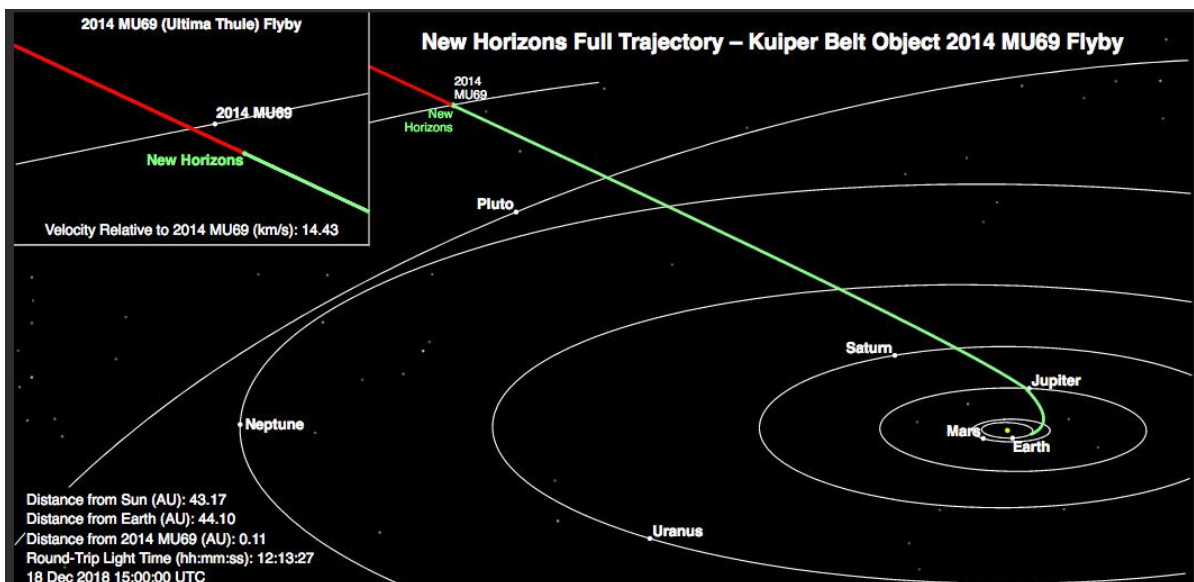


Figure 2.7: The trajectory of New Horizons up until the arrival at Arrokoth / 2014 MU69. The bodies are all shown in their position as of the 18th of December, 2018 [76].

After the flyby with Pluto the original mission of New Horizons was complete. However, with still some propellant left it was analyzed whether it was possible to visit another KBO while New Horizons was flying through the Kuiper Belt. This eventually led to a course correction in order to pass by 486958

Arrokoth at a distance of only 3,500 km [83]. A visual composite of Arrokoth made during the flyby is shown in Figure 2.8. New Horizons shows that it is indeed capable to successfully perform flybys of KBOs and that small correction burns are sufficient to resolve the uncertainties of the flyby objects. Since the decision to perform a flyby with Arrokoth was only made shortly before the Pluto flyby, the spacecraft had very limited maneuverability [89]. By planning a KBO flyby sequence in advance that is not linked to Pluto, as is done in this thesis, the possible number of flyby objects could potentially increase.

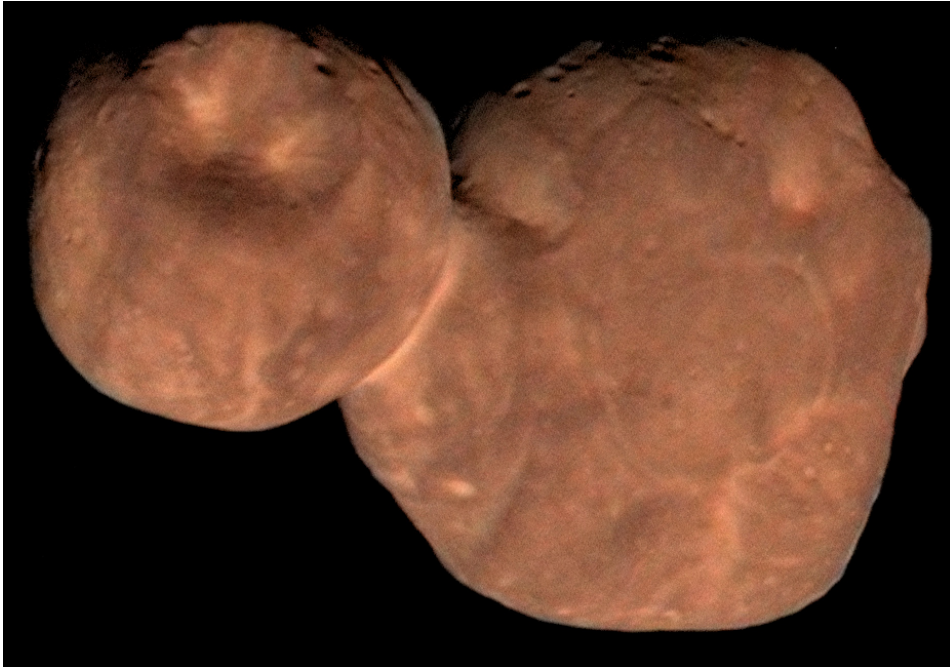


Figure 2.8: An enhanced color-composite image of Arrokoth made by New Horizons during its flyby of the KBO in 2019 [117].

2.3.3. Proposed missions

Considering that there are many research questions yet to be answered regarding the Kuiper belt and the Solar System's origin, it makes sense that space agencies and institutions also have concepts about potential future missions. Such proposed missions are discussed in this subsection.

One of the proposed missions was a potential follow-up to New Horizons called New Horizons II. The proposal for the mission was to reach the Kuiper belt by means of a gravity assist with Jupiter, followed by another one with Uranus or Neptune [77]. The final proposal contained a Uranus flyby instead of a Neptune flyby since this was the only body that could be reached during the planned mission time frame. An overview of a proposed trajectory is shown in Figure 2.9 [77]. The planetary flybys would be followed by one or several KBO flybys, possibly including another flyby of Pluto. The review panel for the New Horizons II mission proposal determined that there is still sufficient scientific reasoning for a new Kuiper belt mission, even though the results are not expected to be as paradigm altering as the original New Horizons mission [93]. The mission is described as technically feasible, but could not be performed mainly due to a lack of Pu-238 which would be required for the RTGs of the spacecraft [93].

However, since the mission review in 2005 the situation has changed sufficiently to reconsider the possibility of a Kuiper belt mission. A major issue for the follow-up KBO mission in 2005 evaluation was the lack of Pu-238 for the RTGs. However, the production of Pu-238 for space purposes has increased again with Idaho National Laboratory (INL) on track to produce 1.5 kg per year by 2026 [90]. Since the time scale of the mission is now much larger with a less strict launch window, a flyby with Neptune or any other planet is most likely possible in the research context and thus changes the possibilities for the KBO mission.

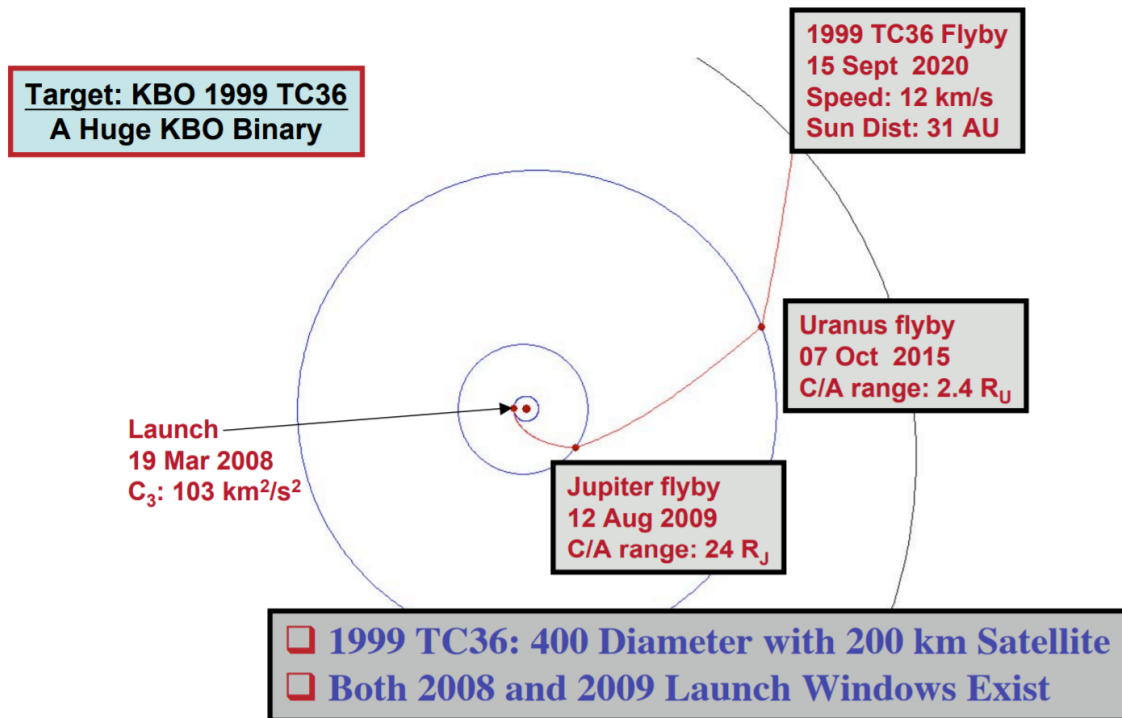


Figure 2.9: The proposed trajectory for New Horizons II. This mission would perform gravity assists with Jupiter and Uranus and end with a flyby of 1999 TC36 [77].

Furthermore, the New Horizons II review panel only analyzed high-thrust missions since low-thrust propulsion was not developed enough yet for use in such a large mission. Nowadays low-thrust propulsion efficiency and power has increased considerably as shown by multiple missions discussed in the next subsection. Besides, one of the questions in this research is to analyze how feasible low-thrust propulsion is for a Kuiper belt flyby mission. If the answer to this question would be that current low-thrust propulsion or RTG power generation is not yet powerful enough, that would be a viable answer in this research context. For the New Horizons II review panel this would not have been an interesting analysis to perform since they were concerned with the practical organization of a mission in the near future. For these reasons, the conclusions of the New Horizons II review panel not to pursue another KBO flyby mission can co-exist with the research question in this thesis project.

The New Horizons II mission is not the only proposed mission to the Kuiper belt. The Trident mission proposal is to travel to Neptune to study both Neptune and its moon Triton, a captured Kuiper belt object [101]. The mission uses an EVEEJN gravity-assist sequence; the Earth and Venus flybys in the beginning are able to reduce the total ΔV for the launch [60]. The abbreviation stands for the first letters of the flyby bodies in chronological order. After its flyby of Neptune and Triton, the Trident spacecraft would also end up in the Kuiper belt and could then possibly perform a KBO flyby similar to the one New Horizons performed.

A final proposed set of missions is the IHP-1 and IHP-2, both short for Interstellar Heliocentric Probe. These missions would also perform a gravity assist with Jupiter, followed by a flyby of Triton and a KBO [131]. However, the main purpose of this mission is the study of the heliospheric boundary and its structure. Specifically, it is theorized that the tail of the heliosphere is larger than its head, the latter being the only side that has been explored with deep-space missions to date [131]. All in all, these missions indicate the design of missions to KBOs is theoretically feasible and requires gravity assists, most of the time with Jupiter and Neptune and possibly with additional ones with Earth or Venus.

2.3.4. Low-thrust and flyby missions

Missions to the Kuiper belt are not the only heritage missions that are relevant to this study. Since the research question focuses on low-thrust flyby missions, other past missions involving low-thrust propulsion and/or flyby are also valuable as background information.

The first NASA (National Aeronautics and Space Administration) exploratory mission to use low-thrust (ion) propulsion is Dawn, launched in 2007 [78]. It was preceded by a technology demonstration of low-thrust propulsion with the Deep Space 1 mission in 1998. Dawn performed a gravity assist with Mars and subsequently entered an orbit around Vesta and later on around Ceres. With a total ΔV of roughly 11 km/s after the high-thrust launch [14], Dawn clearly showed the increased capabilities of low-thrust propulsion with regards to maneuverability in space. The 11 km/s value is slightly lower than the 14.9 km/s value mentioned in Table 2.2 since the table assumes perfect conditions. The full trajectory of Dawn is shown in Figure 2.10. A few years prior in 2003 JAXA (Japan Aerospace Exploration Agency) also launched an ion engine mission called Hayabusa. This mission rendezvoused with the asteroid Itokawa and brought surface samples back to Earth [102]. The follow-up mission Hayabusa2, launched in 2014, performed a similar mission by returning samples from the asteroid Ryugu [102]. The Hayabusa2 mission is still active and will perform two more asteroid flybys in 2026 and 2031 [44]. These missions show that performing flybys using low-thrust propulsion is feasible. Even the use of landers is a realistic capability. Due to the complexity of the trajectory design to the Kuiper belt, the additional use of landers is excluded from analysis in this thesis. However, it is recommended to study in further work.

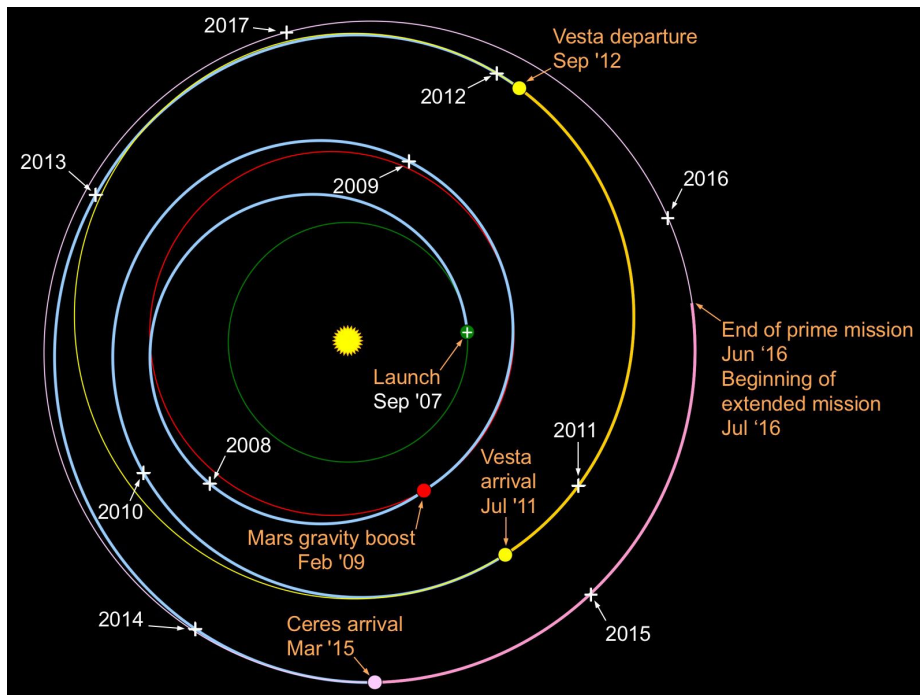


Figure 2.10: The trajectory of the Dawn mission [103].

Two final missions to note are Rosetta and Stardust. Both of these missions used high-thrust propulsion, but they are still relevant to this project. Rosetta was an ESA (European Space Agency) mission launched in 2004, which performed flybys of three different asteroids [5]. Gravity assists with the Earth and Mars were required to gain the required velocity and to shape the trajectory. NASA also performed a multi-asteroid flyby mission, Stardust, which used additional flybys with Earth in order to reach its three targets [72]. The important lesson from these missions for this thesis is that the planning of trajectories towards asteroids, even asteroids with relatively uncertain ephemerides, is possible by using a buffer in the propellant budget. As the spacecraft nears the target, updated ephemerides based on Earth-observations or visual detections by the spacecraft itself can be used to adjust the trajectory. The calculation of this buffer is not considered during this thesis, but recommended for future research.

2.4. Research heritage

Besides mission heritage there is also a large body of research heritage consisting of previous thesis projects as well as other academic research. First the thesis by L. van der Heyden is discussed since this thesis partly functions as a follow-up to his research. Afterwards, other relevant theses at TU Delft are mentioned as well as various academic papers on the topic of the Kuiper belt and flyby missions.

The research by L. van der Heyden was aimed at finding trajectories with a long time period in the Kuiper belt. The research used a high-thrust launch vehicle (LV), followed by high-thrust DSMs and gravity assists with various planets [43]. The trajectory was propagated by means of a patched-conics method. Besides the time in the Kuiper belt, the total mission time and ΔV used were also taken into account for the optimization. The conclusion of this thesis was that trajectories with a Kuiper belt period in excess of 100 years are feasible [43]. These trajectories are capable with modern launch vehicles. The most optimal trajectories have a VVEJS, EVEEJN or JN gravity-assist sequence [43]. An example of one of the found JN sequences is shown in Figure 2.11 [43].

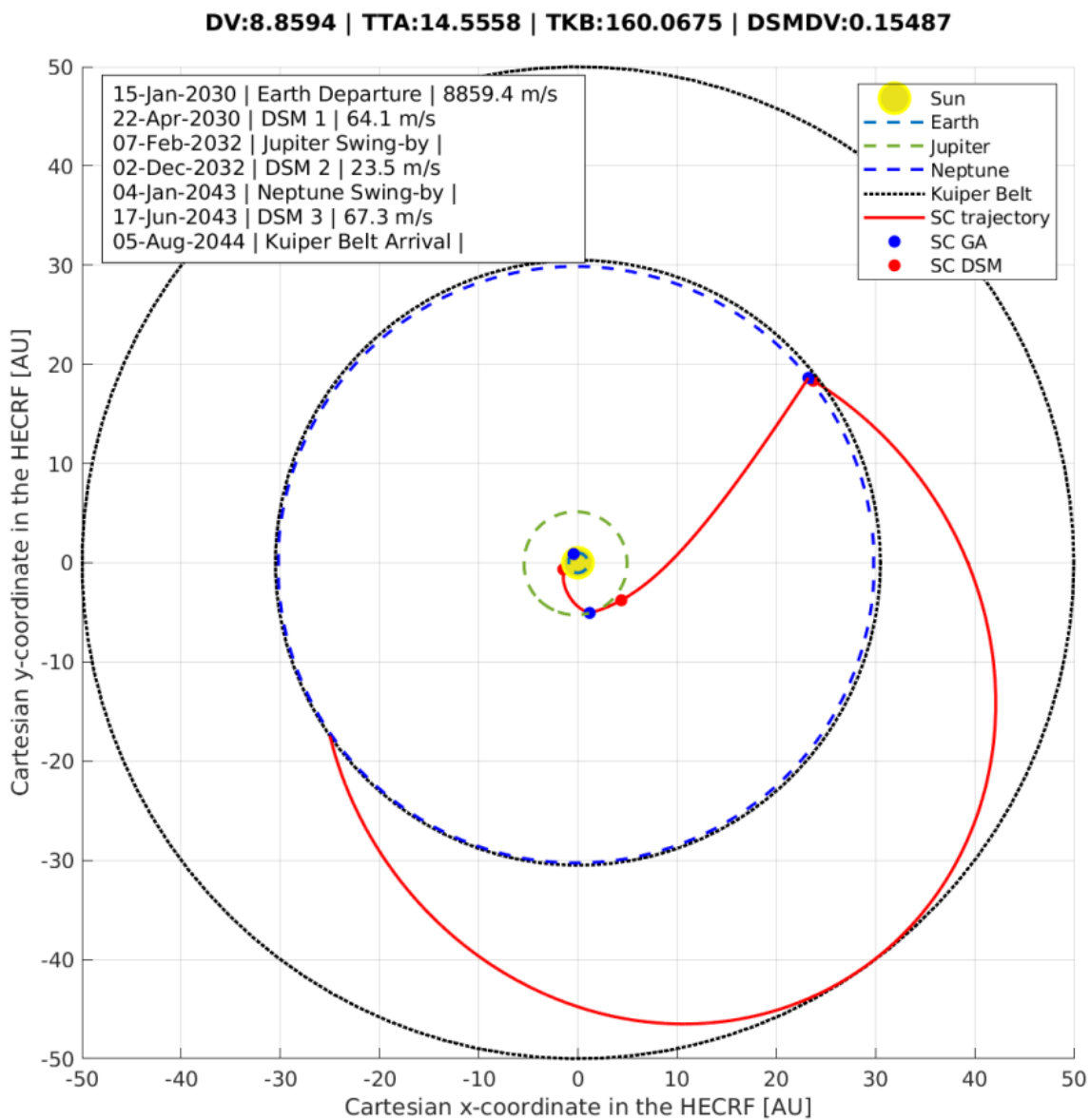


Figure 2.11: The optimal found trajectory in the thesis by L. van der Heyden for a long Kuiper belt mission with minimal ΔV using a JN gravity-assist sequence [43].

Other master theses at TU Delft have also delved into topics relevant for this project. A thesis by M.B. Penas analyzed the use of a grid-search method for a multi-KBO flyby mission with a low fidelity. The research indicates that the design of flyby missions in this manner is possible [98], even though the launch energy and ΔV results were not as optimal as in the research by L. van der Heyden. This thesis is distinctly different from the current topic since it only looked at high-thrust propulsion. Other less related but still somewhat relevant thesis projects regard a high-thrust optimization for a Neptune flyby [58] and a study to include coasting periods in low-thrust propulsion arcs [36]. However, the study of the Kuiper belt in combination with low-thrust propulsion is still an unexplored topic in these works.

Academic research outside of the TU Delft has also been looking at the possibility for missions to the outer regions of the Solar System. One example is a study for a flyby of Sedna, a TNO which lies beyond the traditional Kuiper belt. It was found that an Earth and Jupiter gravity-assist sequence would allow an optimal flyby of Sedna [132]. More research towards TNOs such as Pluto, Quaoar, Make-make, Eris, and Lempo gave a similar result that a Jupiter gravity assist would feasibly allow a KBO flyby [57] [108] [19], while the addition of a longer gravity-assist sequence could lower the required ΔV [107]. Note that all these papers only analyzed a single KBO flyby and used high-thrust propulsion. One of the few exceptions is a study for a short-term single high-thrust mission to Huya and Quaoar with promising results [47].

Research towards low-thrust deep-space trajectories also exists. However, this is mostly aimed at missions towards the outer planets instead of the Kuiper belt. Examples are missions to Jupiter [49] [61], the Jovian moons [26] [51] [120] and Neptune [92]. Specific low-thrust mission design towards Uranus and Neptune indicates that low-thrust propulsion could be more efficient than high-thrust propulsion for this purpose [50]. Research towards low-thrust Kuiper belt missions for example consists of a comparison between low- and high-thrust payloads and once again indicates that a mission to a KBO such a Quaoar can be done more efficiently with low-thrust propulsion [6]. Other low-thrust research has been aimed at analytically calculating low-thrust transfers [35] [106], but without the analysis of Kuiper belt missions. All research so far seems to indicate that low-thrust KBO missions are feasible, but a complete optimization methodology and result for long-term KBO missions has not been found, thus validating the potential of the research question of this thesis project.

2.5. Summary

This chapter has given an overview of the relevant background required to understand the setup for this thesis project. The Kuiper belt, a region 30 to 50 AU from the Sun, is the target area for missions in this report. The region contains many primordial bodies and as such can give more information about the formation and history of the Solar System. SDOs and detached objects will not be considered during this thesis, leaving a list of roughly 3000 catalogued objects. Specific objects of interest are bodies in the cold classical belt, named objects or the brightest bodies in general.

Furthermore, a background study of low-thrust propulsion theory shows that, while thrust levels are orders of magnitude lower than those of high thrust, the total ΔV delivered during low-thrust missions can be many times higher in the order of 10+ km/s. This makes low-thrust propulsion an interesting option for long-term missions with objects that are far removed from each other as the additional ΔV provides extra maneuverability.

Multiple missions have already visited the Kuiper belt, though New Horizons is the only one to have visited a KBO as well. The heritage missions indicate that a gravity assist with Jupiter is most likely required. Earlier gravity assists with the inner planets can be used to decrease the total launch ΔV , while gravity assists with other outer planets can also be used to shape the trajectory. The success of New Horizons as well as the planning of other deep-space missions indicates that KBO flybys are realistic to perform. However, no low-thrust missions have ever been done in this region, thus leaving a research gap. Academic research towards KBO missions is also abundant and shows promising results. But once again the combination of low-thrust propulsion and KBO flybys is almost untouched and justifies the research question and subquestions of this thesis.

3

Mission description

This chapter provides an overview of the mission profile to be studied in this thesis project. First the trajectory scenario for the mission is described as well as its science return. This is followed by a brief description of decisions regarding relevant spacecraft subsystems. Afterwards the decision variables or inputs for the mission are described, as well as constraints and specific objectives. A list of top-level requirements for the mission is also provided. The decisions in this chapter mostly follow from the literature study that preceded this thesis and is recommended material in case one wants to get a more extensive overview of the background information behind these decisions [45].

3.1. Trajectory scenario

The mission to be designed in this project will perform flybys of one or multiple KBOs. The mission starts with a launch from Earth followed by a number of gravity assists with planets in the Solar System. After entering the Kuiper belt, the spacecraft will perform close flybys with KBOs. This analysis will start aiming for a flyby with a single KBO and it will then be extended to more flybys. A literature study of heritage research in Chapter 2 indicates that missions with at least two KBO visits have already been designed using high-thrust propulsion. Therefore, the goal is for the methodology to result in trajectories with at least a similar number of close KBO visits.

In the final phase of the trajectory analysis it will also be analyzed how many DFBs and VDFBs are possible. These type of flybys would allow partial scientific analysis. Since no previous research has looked into these distant flybys and their occurrence, it is difficult to put a number on them. As such no minimum requirement is put on them, but the study later in this thesis will provide an indication how many DFBs/VDFBs should be expected if one does not optimize for them specifically.

3.2. Science return

The science return is one of the crucial elements of any mission. An extensive science requirement description is out of the scope of this research. It is only analyzed whether a science case for a KBO mission exists, as described in Chapter 2, and then the rest of the thesis focuses on trajectory design. Detailed science return descriptions are recommended for further research. Based on a literature search regarding instrumentation used in previous deep-space and KBO missions, the following list of instruments is assumed to be present for the science payload:

- VIR/IR imaging system [79] [102]
- IR/VIS/UV spectrometer [105]
- Photopolarimeter [80]
- Radio science system [73]
- Magnetometer [24]
- Solar wind/plasma spectrometer [80]
- Dust particle detector [18]

- Accelerometer [18]
- Ultra-stable oscillator [18]

The above list is cited from the literature study [45] and a more extensive discussion regarding the inclusion of these instruments can be found there. The overview of instruments is relevant for this thesis since it is required for estimates regarding spacecraft mass and power as well as decisions regarding the distance to KBOs during flybys.

3.3. Spacecraft subsystems

A detailed design of the spacecraft subsystems is out of the scope of this thesis and is recommended for future research. Communication subsystems, power distribution systems, data storage systems, and many other subsystem-related topics are not discussed in this thesis. However, it is impossible to perform trajectory design without some decisions regarding the subsystems, for example the decision to use low-thrust propulsion. Therefore, the relevant spacecraft subsystem decisions for this project are discussed in the following subsections.

3.3.1. Propulsion

The decision for the propulsion subsystem was already discussed in Chapter 2 including the reasoning why low-thrust propulsion will be tackled in this thesis. The trajectory legs in this thesis will make use of continuous low-thrust propulsion. The inclusion of coasting phases, periods in the arc without thrust, is recommended for future research, but is not tackled in this thesis as it would add more free variables and as such complexity. Previous thesis work by A.M. Gonzalez concludes that the inclusion of coasting phases in low-thrust arcs can reduce the peak acceleration, but only recommends it to be done after the first-order design stage [36].

The propulsion subsystem will make use of ion engines with Xenon as propellant which is the most common propellant for low-thrust spaceflight [125]. This means that the engines will have an I_{sp} of 3000 s. Degradation of the propulsion subsystem will be neglected and all degradation of thrust is assumed to be caused by a reduction in power, discussed in the next subsection. A study regarding the impact of long travel times on the thrust delivered by ion engines is recommended for future research.

3.3.2. Power

In order for low-thrust propulsion to work a continuous power supply to the propulsion subsystem is required. Furthermore, power is required for the instruments on the spacecraft as well as power which is needed for the spacecraft to perform its other station-keeping tasks. The main power source for most space missions comes from solar radiation, using solar panels. However, as discussed in the previous chapter, the use of solar power for deep-space missions is infeasible since solar power reduces quadratically with the distance from the Sun. This means that at the 30 AU border of the Kuiper belt the power density due to the Sun is $(1/30)^2 = 900$ times smaller than at Earth. Therefore, all deep-space missions to date have used nuclear power, specifically RTGs. RTGs make use of Pu-238 as their power source, which has a theoretical degradation rate of 0.79% per year [8]. Due to other issues such as thermoelectric degradation [41], the degradation rate in reality is slightly higher. The average degradation rate of the Voyager probes based on their power decrease from BOL to 2011 is roughly 1.6% per year [37]. This value will be used for the thesis.

A single GPHS-RTG requires 7.8 kg of Pu-238 and delivers 300 W of power at BOL [7], which would thus be reduced to roughly 60 W after 100 years as follows from the calculation in Equation 3.1. Here W represents the power generated at two points in time separated by t_y , the time in years and with a yearly degradation rate of the power system of d_r . The stockpile of Pu-238 was the major limiting factor in many recent deep-space mission proposals such as New Horizons II. However, the production of Pu-238 is increasing again and is set to become 1.5 kg per year by 2026 [90]. In combination with the departure date constraint, discussed in Section 3.4, this would allow for the production of three RTGs and thus 900 W of power before launch. This is the most optimistic scenario, but to prevent a reduction of design space during this preliminary study this case of three RTGs is used. If this power source is deemed insufficient then novel power source such as the ASRG or NASA's Kilopower reactor can be considered [31] [16].

$$W_1 = W_0 * d_r^{t_y} = 300 * 0.984^{100} \approx 60W \quad (3.1)$$

The final relevant aspect of the power subsystem is how the power is distributed. The mass and total power level required for the instruments mentioned in Section 3.2 are shown in Table 3.1. This means that on average 42.2 W of power will be needed when the instrumentation system is active and 82.2 W is needed upon closest approach during CFBs when the radio-science system is also active.

Table 3.1: An overview of the proposed set of instruments for the KBO mission taken from [18] [80]. The radio-science system is only needed at closest approach and thus does not count towards the total average power. The sum of the power column excluding the radio-science system is 42.2 W and 82.2 W if the radio-science system is included. The table is directly cited from the literature study [45].

Instrument	Mass [kg]	Power [W]
VIS/IR imaging system	8.6	5.0
IR/VIS/UV spectrometers	5.0	12.0
Photopolarimeter	4.4	2.4
Radio-science system	3.0	40.0
Magnetometer	3.3	3.0
Solar wind/plasma spectrometer	3.7	2.3
Dust particle detector	3.5	9.0
Accelerometer	3.5	3.0
Ultra-stable oscillator	1.5	5.5
Probe/lander	N/A	N/A
Total	36.5	42.2 - 82.2

Based on similar missions such as New Horizons it can safely be assumed that the instrumentation subsystem will work for an almost negligible fraction of the total flight time. Therefore, it is assumed that either the full instrumentation suite is active and the thrust system is inactive (42.2 - 82.2 W) or that the thrust system is active and the rest of the spacecraft is in hibernation mode. Other power usages that fall outside of the spacecraft's hibernation mode such as short bursts for communication with Earth are neglected.

3.3.3. Spacecraft mass

The spacecraft dry mass is based on the instrumentation-to-dry mass ratio for the New Horizons spacecraft. The instruments on the New Horizons together weigh 30.4 kg and the dry mass of the spacecraft is 401 kg [124]. By comparing this to the estimated instrument mass of 36.5 kg for this mission in Table 3.1 this results in a dry mass for this thesis of 481 kg, rounded to 500 kg for simplicity and since the instrument list is not definitive. In Table 2.2 it can be seen that Dawn performed its mission with a value of 1.63 for $\frac{m_0}{m_f}$. To keep the design space as big as possible a maximum value of 2 for $\frac{m_0}{m_f}$ will be assumed. This results in a maximum dry mass m_0 of 1000 kg. Excluding gravity losses, this would result in a total available low-thrust ΔV of roughly 20.4 km/s after decoupling from the launch vehicle. This will be considered as the maximum allowable ΔV for this mission.

3.3.4. Launch system

All the spacecraft subsystems so far have only discussed the eventual spacecraft itself. However, in order to put the spacecraft on its initial escape trajectory from Earth, a high-thrust launch vehicle is required. The launch itself will be modelled as an instantaneous ΔV boost which puts the spacecraft on its first trajectory leg. Any extended analysis of the launch is out of scope. However, a brief analysis of launch systems is done to understand which ones are realistic for use in this mission and what the relation is between the mass and launch energy.

An overview of modern launch vehicles (LVs) is given in Figure 3.1. This plot shows the launch energy, C_3 , in km^2/s^2 as a function of the spacecraft wet mass in kg. The C_3 of space missions varies depending on the mission type. The deep-space missions that eventually entered the Kuiper belt have C_3 values ranging from 87 km^2/s^2 (Pioneer 11) to 158 km^2/s^2 (New Horizons) [129]. New Horizons gained its additional C_3 by using a third stage on top of the launch vehicle [88]. The heritage values

indicate that only the most powerful launch vehicles such as the Vulcan 6 and Falcon Heavy Expendable are suitable options. Trident's mission proposal only uses a C_3 value of $26 \text{ km}^2/\text{s}^2$ and gains its additional velocity from extra gravity assists [60]. Results by L. van der Heyden also indicate that C_3 values of roughly $20 \text{ km}^2/\text{s}^2$ are possible if multiple gravity assists are performed in the inner Solar System and roughly $80 \text{ km}^2/\text{s}^2$ if only gravity assists with the outer planets are done [43]. Because of this result and the table of launch vehicles a limit at $100 \text{ km}^2/\text{s}^2$ is placed for the launch energy in this thesis.

Figure 3.1 indicates that this is only possible with the aforementioned maximum mass of 1000 kg if LVs such as the Vulcan or Falcon Heavy are used. Even then additional stages, similar to New Horizons, have to be used near the upper bound for C_3 of $100 \text{ km}^2/\text{s}^2$ as then both LVs can only carry roughly 750 kg [75]. The launch adds complexity to the optimization process by adding an excess velocity as well as orientation angles of that velocity. If complexity becomes an issue during the optimization process, setting the C_3 to $0 \text{ km}^2/\text{s}^2$ could be a method to reduce the complexity. This would represent a launch into a parabolic trajectory which would then become hyperbolic due to the additional ΔV of the low-thrust propulsion system. An analysis with high-velocity launches would then be recommended for future study.

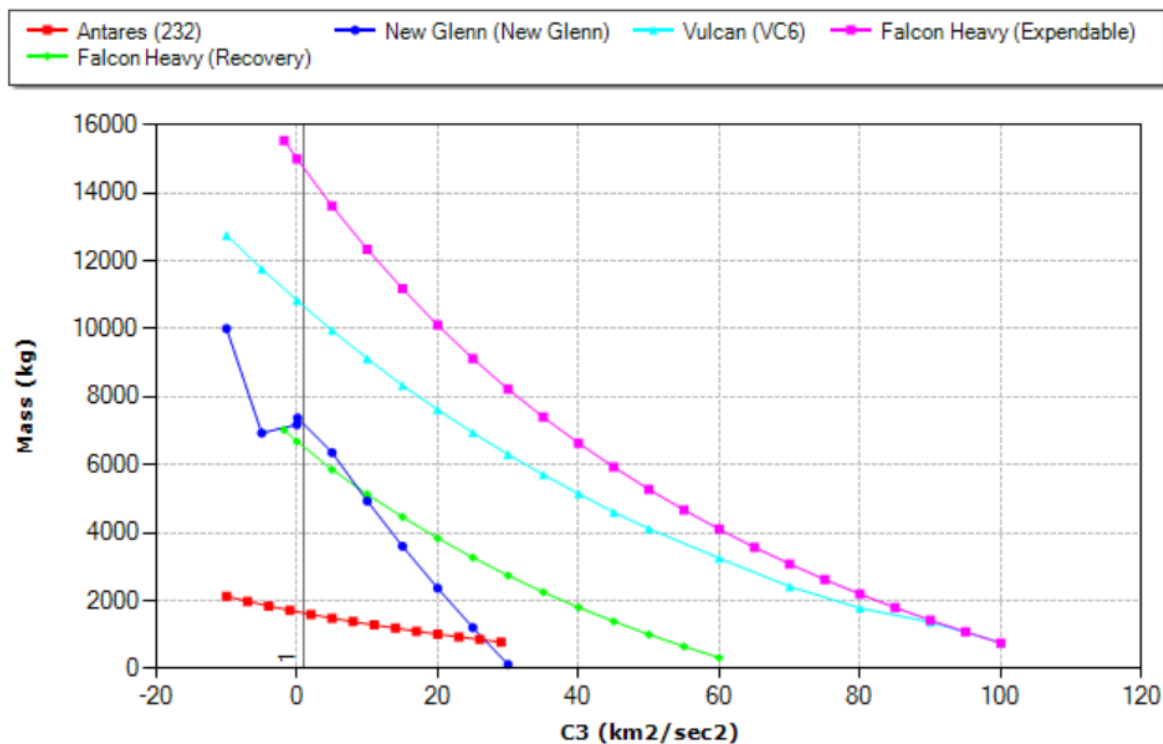


Figure 3.1: The launch energy of a range of different common launch vehicles as a function of the wet mass [75]. Negative C_3 values indicate that the spacecraft has insufficient energy to escape from Earth.

3.4. Decision variables

The variables for the trajectory settings in this thesis are split into three categories: decision variables, constraints, and objectives. First the decision variables are discussed. The decision variables are the inputs and other free parameters in the problem.

3.4.1. Departure date

Having too wide of a range for the departure date can result in an abundance of options and therefore inefficient optimization. On the one hand, it is important that the departure date is not too far in the future in order to limit uncertainty errors and to prevent the report from being outdated by the time of the desired launch date. On the other hand, enough time is required to allow for the Pu-238 production which is required for three RTGs. Based on the Pu-238 production rate an earliest launch date of

January 1, 2040 is chosen. A time window of 10 years is chosen to allow enough time for different optimal planet positions for gravity-assist combinations, thus until January 1, 2050. Specifically, the optimal Jupiter - Neptune alignment has a return period of 13 years and will thus occur once within this time period in 2043, as L. van der Heyden found another instance of this alignment is with a launch in 2030 [43]. Since the low-thrust trajectories in this thesis are slower than their high-thrust counterparts, the precise date of this optimal alignment might shift for low-thrust trajectories. Due to the departure date another decision variable, the departure position state, is also defined. This state is equal to the position of Earth at launch.

3.4.2. Time-of-flight

The complete time-of-flight of the mission is not a single decision variable. However, the time between the start and end of each trajectory leg is a direct input to the system. In accordance with other Kuiper belt studies [57] [129], the travel time of New Horizons, as well as the research by L. van der Heyden [43], a maximum desired time of 25 years is set to reach the Kuiper belt. How these 25 years are spread over the different trajectory legs depends on the specific flyby sequence and is determined by means of trial-and-error during the optimization process. In the optimization process a maximum time of 25 years per leg is used to keep the input space large enough for all possible trajectories, but the end goal is to have only 25 years for all legs until the Kuiper belt is reached.

The same goes for the time period between different CFBs in the Kuiper belt and between the last planet and the first KBO visit. Previous research found that a flyby between Quaoar and Haumea was possible with a travel time of roughly six years between the two KBOs [47]. Based on this a slightly looser constraint of 10 years is used as the maximum average time period between KBO CFBs in one trajectory as well as the maximum time between entry in the Kuiper belt and the first CFB. Similar to the planetary legs an input space of 25 years is used to prevent a lack of solutions during the optimization phase. This also allows for trajectories where one leg is longer than 10 years, but the average time between CFBs is below 10 years.

3.4.3. Departure velocity

Earlier in this section the departure date and thus the related departure position were discussed. However, the departure velocity is also required to describe the first leg of the trajectory. To do this the magnitude and direction of the hyperbolic excess velocity after launch needs to be known. The direction of this velocity is determined based on an in-plane and out-of-plane angle and the launch energy is set as a value between 0 and 100 km²/s² as discussed in Section 3.3.4. The hyperbolic excess velocity is the square root of the launch energy. The use of an in-plane and out-of-plane angle, right ascension and declination, in combination with the hyperbolic excess velocity magnitude is the most common description of the velocity vector in other research [27] [128] as well as the TU Delft Astronomical Toolbox (Tudat). The vector of the excess velocity is to be added to the heliocentric velocity of Earth at departure. If it is later decided to set the launch velocity to zero the two departure angles are also no longer relevant as they relate to the direction of this excess velocity.

3.4.4. Flyby variables

The variables so far mostly refer to the launch and the separate trajectory legs. However, in order to perform the full trajectory design the flybys with the planets and connections between different trajectory legs also need to be defined. As already mentioned, the initial launch leg is defined by means of an initial position state, an excess velocity vector with two directional angles, and the time-of-flight. Multiple revolutions in a single trajectory leg are neglected as these can result in unworkable flight times, especially for deep-space legs. The selection for the target planet/body is also one of the input variables. The gravity assist with the planet is then partially defined with similar variables: the incoming excess velocity magnitude of the spacecraft together with two angles which position this vector. The epoch of the gravity assist is already defined by the departure date and time-of-flight values.

For the gravity assist itself two different options exist. One option would be to use the gravity assist variables as the inputs: the periapsis distance, (optional) ΔV during a powered assist, and the asymptotic bending angle of the gravity assist. The second option would be to define the outgoing excess velocity and two angles, in other words the velocity vector at the start of the subsequent leg. Together

with the incoming velocity vector for the gravity assist at the end of the previous leg, these two velocity vectors completely define the flyby and lock the values for the three previously mentioned gravity assist variables.

For this thesis the gravity assists will be modelled with the incoming velocity vector and the three gravity assist variables (periapsis, ΔV , asymptotic bending angle). Due to the 3D simulation all these variables are required to fully define the flyby. The main reason for this is that the decision-variable space would become much larger if the alternative description with two velocity vectors is chosen. The vast majority of combinations of two random velocity vectors leads to theoretically infeasible trajectories and the design space would then thus become much bigger than the useful design space. A mathematical background regarding gravity assists is given in Chapter 4.

The flybys of KBOs are modelled in a similar manner with a few minor exceptions. Based on an analysis during the literature study it is determined to neglect the mass of KBOs during the gravity assists since this mass is often not well-known and is so small that its impact can be disregarded for a first-order design. Thus to model KBO flybys the trajectory will "overlap" with the ephemeris of the KBO at a certain point in time [45]. This means that the KBOs are considered to be nodes in the trajectory and do not impact the trajectory of the spacecraft. In other words, the incoming and outgoing velocity vectors of a KBO flyby are the same and no gravity assist variables are required.

3.5. Constraints

Besides the inputs to the system there are also other variables which limit the solution space of the problem. These variables are called constraints and are discussed in this section. The main constraints that have not been mentioned yet regard the flybys. Any remaining constraints are discussed in a subsection afterwards.

3.5.1. Flyby constraints

In the previous section the flyby variables were already discussed. The following paragraphs discuss the way the flybys are constrained by means of the flyby distance and sequences.

A minimum flyby distance for each of the planets should be put in place to constrain the gravity assist parameters. Since this study does not tackle the concept of planetary gravity assists in a different way compared to L. van der Heyden's thesis, the same minimum distances will be used [43]. The values are based on the flyby distances of similar missions and proposals. The full list of minimum flyby distances is given in Table 3.2. Due to the extra free variables with low-thrust trajectories, a maximum flyby distance must also be chosen. Of the spacecraft that have used gravity assists to reach the Kuiper belt (Pioneer 10 and 11, Voyager 1 and 2, New Horizons), the most distant gravity assist with respect to the planet's radius was performed by New Horizons which approached Jupiter up to 2.3 million km for its gravity assist [126], roughly 32 times the planet's radius. As a rough margin a factor 2 is applied to this ratio, which means that for every planet the maximum flyby distance is 64 times the minimum flyby distance.

Table 3.2: An overview of the minimum flyby distances for the planets in the Solar System, cited from the literature study [45] and originally taken from [43]. The conversion to flyby distances is made using the mean radius [54]. The distance is taken from the center of the planet, not the planet's surface.

Planet	Mercury	Venus	Earth	Mars	Jupiter	Saturn	Uranus	Neptune
r_{min} [km]	2806	6960	7327	3899	118,849	98,994	43,115	41,861

Another constraint for flybys is the flyby sequence. This concerns both flybys with planets in the Solar System as well as the KBO flybys. First the planetary flybys are discussed. To reduce the optimization complexity a single planetary flyby sequence is chosen beforehand. L. van der Heyden concluded that the following five flyby sequences would be optimal for a long-term Kuiper belt trajectory based on the ΔV and time-of-flight analysis: EJN, EEJN, EVEEJN, VEEJS, JN [43]. Note that the E for Earth in these abbreviations stand for a flyby with the Earth on top of the original launch from Earth.

Many heritage missions only make use of a Jupiter gravity assist or many inner Solar System flybys followed by a final Jupiter gravity assist. These trajectories, however, are not optimal for the problem tackled in this thesis as a gravity assist with at least two of the large planets (Jupiter, Saturn, Uranus, Neptune) can strongly increase the bending angle and is thus crucial for a long-term Kuiper belt trajectory. Other examples such as the JSUN sequence for the Voyager mission are not used due to the lack of proper planetary alignment. Trajectories without a Jupiter gravity assist are also not used as it was found by L. van der Heyden that the Jupiter gravity assist is most efficient for increasing time spent in the Kuiper belt [43]. To reduce complexity the flybys of inner Solar System planets are not tackled in this thesis, though they are recommended for future research. Due to the proximity of Neptune to the Kuiper belt as well as the added benefit of visiting Triton, the JN flyby sequence is used for study in this thesis.

The final constraint regarding flybys regards the KBO section of the trajectory. For each node in the Kuiper belt the next KBO to visit is either pre-selected or randomly selected from a group of objects depending on the optimization stage. In Chapter 2 it was already mentioned that a total of more than 3000 KBOs have been registered. However, due to the uncertainty in the future positions, also known as ephemerides, a subset of KBOs with small uncertainties is used as the nominal data set during this thesis. Research during the literature study determined that KBOs with an 'uncertainty parameter' U of 2 or smaller should have an ephemeris accurate enough that a minor ΔV correction can account for the position errors [45]. The uncertainty parameter is grouped in numbered categories where a higher number indicates a higher runoff of the uncertainty of a celestial body in arcseconds per decade. This filter of an uncertainty factor of 2 or smaller leaves 902 bodies for study. A scatter plot of these bodies is shown in Figure 3.2.

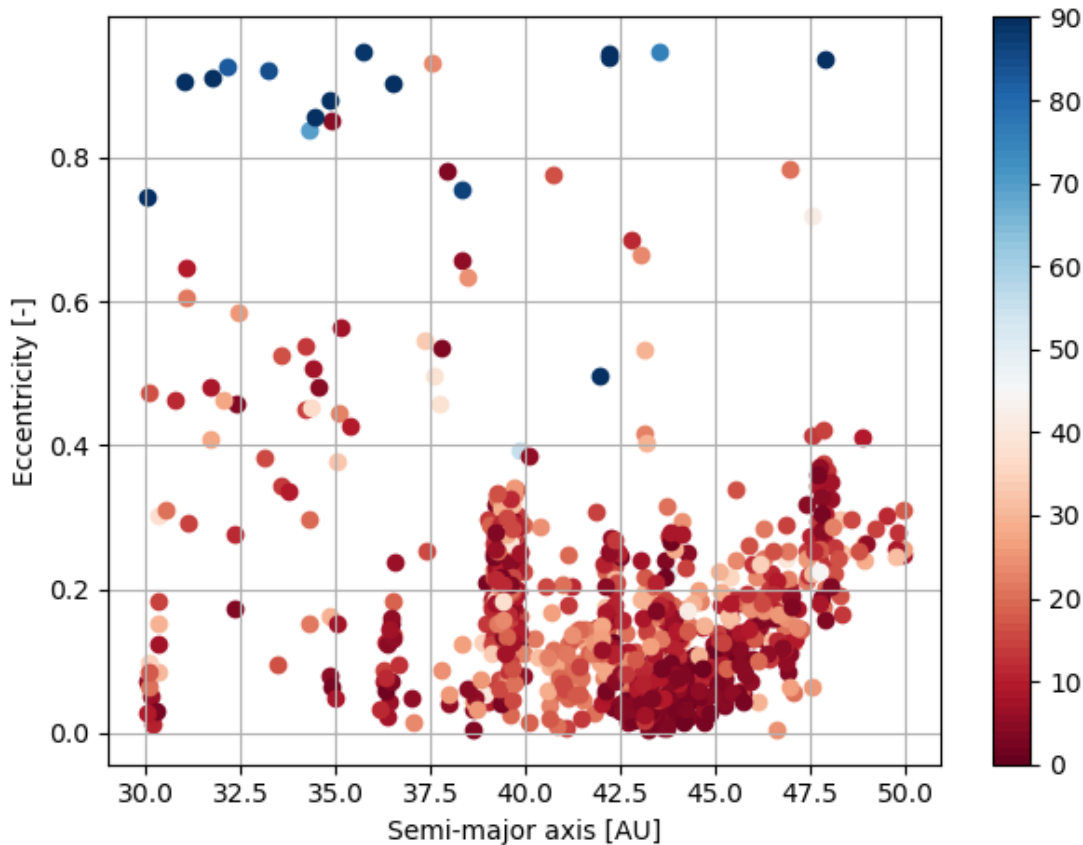


Figure 3.2: A scatter plot of the semi-major axis and eccentricity of all catalogued KBOs with an uncertainty parameter of 2 or less. The color represents the inclination of the orbit of the KBO in degrees. Taken from the literature study [45].

To reduce complexity further a smaller subset can be made of the most high-priority objects. As mentioned in Chapter 2 the most interesting objects are the brightest KBOs, brightest classical-belt KBOs, and named KBOs. All bodies with an absolute magnitude H below 4.0 are chosen [129], resulting in 15 of the brightest objects. Furthermore, 10 of the brightest cold-classical belt objects are chosen and the remaining 11 named objects are selected. Thus, the subset of bodies consists of 36 KBOs. The size of this subset is determined by weighing the advantage of having more options with the disadvantage of increasing the already quite large input space. A scatter plot of these bodies is shown in Figure 3.3. Depending on the stage of the optimization either these 36 or 902 bodies are used. If this is not deemed enough to find satisfactory trajectories the remaining bodies with a higher uncertainty factor can also be used. These data sets can also be further reduced based on the inclination of the KBOs if desired.

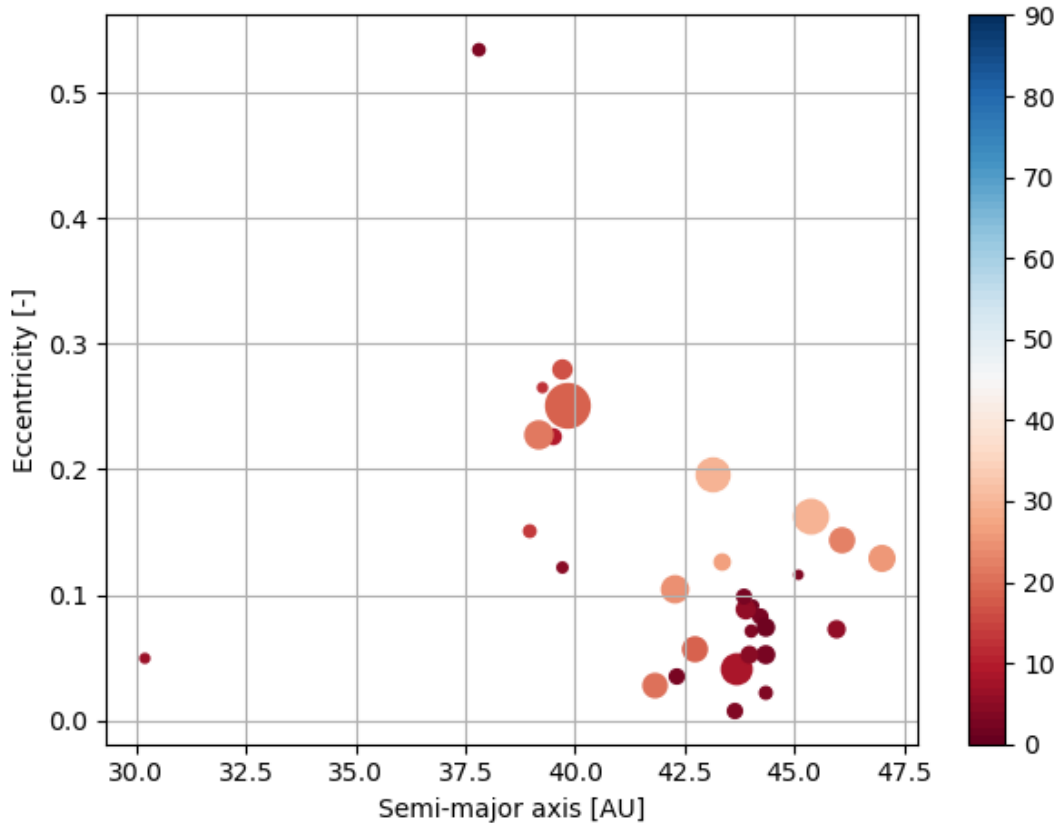


Figure 3.3: A scatter plot of the semi-major axis and eccentricity of the 36 KBOs which are given highest priority. The color represents the inclination of the orbit of the KBO in degrees. The size of the dots correlates with the size of the bodies. Taken from the literature study [45].

3.5.2. Other constraints

The remaining constraints are grouped together in this last subsection. The first of these constraints relates to the thrust of the spacecraft. It was already mentioned that the nominal BOL power of the spacecraft in this thesis is set at 900 W based on the use of three RTGs. Using Equation 2.2 with an efficiency factor of 0.8 and an I_{sp} of 3000 s it can be determined that a BOL thrust of 49 mN is possible. With the 1.6% degradation level this results in 22 mN after 50 years and 10 mN after 100 years. After the optimization process it is checked whether these variable thrust constraints are complied with.

The last constraints concern the thermal subsystem. Based on a maximum 40 degrees Celsius limit for the protection of computers and the propulsion system of the spacecraft [96] a constraint of 0.8 AU was set as the minimum distance to the Sun during the literature study based on the black-body radiation temperature [45]. Heritage research shows that this number could be slightly lower since trajectories to Venus would bring the spacecraft even closer to the Sun. However, since Venus is not considered as a flyby body in this thesis the constraint is not adjusted.

3.6. Objectives

The goal of an optimization process is to increase the fitness of objective functions as much as possible. This section describes the different objectives for the trajectory design in this thesis and how they are implemented into the optimization process. The two main objectives regard ΔV and time-of-flight. Finally, other considerations such as KBO visits and penalties are mentioned.

3.6.1. ΔV objective

The leading objective for most space missions is the amount of ΔV used. ΔV directly relates to the amount of propellant required and thus the mass of the spacecraft. Since all missions want to increase the payload mass as much as possible, a lower ΔV is preferred. Note that this thesis combines a high-thrust launch with low-thrust arcs. As such the two will need to be combined. Since the I_{sp} of hydrazine (high-thrust propellant) is 220 s [3] while the I_{sp} of low-thrust Xenon propellant is 3000 s [17], the two ΔV 's can not simply be added up. Instead their efficiencies will have to be taken into account to come up with the total mass fraction of the mission. If the launch energy is set to 0 km²/s² then this combining step is no longer relevant and the ΔV from low-thrust can directly be used as the objective. The same goes for any high-thrust impulsive ΔV used during gravity assists.

3.6.2. Time-of-flight

Another objective concerns the total time-of-flight (TOF). As with all space missions or projects in general it is beneficial to perform the task as quickly as possible while still meeting all the desired mission criteria. In order to make this a fair comparison only missions with a similar scientific return can be compared. In other words, only missions with the same number of trajectory legs can be directly compared in terms of their time-of-flight. While it is indeed true that this thesis studies long-term KBO missions, the time-of-flight is still a critical objective. Getting results sooner increases their relevance for the scientific community and reduces the chance of crucial spacecraft parts failing too soon or technology becoming obsolete.

3.6.3. Other considerations: KBOs and penalties

The use of two objectives, ΔV and time-of-flight, allows for the creation of 2D Pareto fronts which indicate a range of optimal members in a population. Since the ΔV is considered the leading objective in this thesis the member with the lowest ΔV will be chosen as the best one during later stages of the research.

However, besides these two objectives there are also other variables that were considered. One of these is to include a KBO-related objective. This objective could count the number of CFBs and DFBs, and could take into account the type of KBO which would be visited during the flyby. A CFB counter as objective is not necessary. This is since at first the trajectory will consist of multiple planetary flybys followed by one KBO flyby. Later in the thesis the number of KBO flybys is extended one by one as far as possible. The optimization is thus always only performed with a population which has the same number of CFBs. DFBs will not be taken into account during the optimization process and are only analyzed afterwards. Analyzing DFBs as well as the type of KBO encountered as an objective is recommended for future research, but is out of scope for this thesis.

One other consideration is to add penalty functions to the objectives. This could be either through a separate penalty objective or by adding a penalty to the other objectives [22]. An advantage of these penalty systems is that they can guide the optimizer away from unrealistic solutions. However, they also increase complexity by adding objectives or can make the meaning of the existing objective values less clear if the penalties are directly added to those objectives. The original intent for this thesis was to implement a few penalty objectives, specifically the following ones.

- Thrust setting above the maximum based on the power output (49 mN limit at BOL).
- ΔV in powered gravity assists above the set limit (50 m/s).
- Total low-thrust ΔV used should be below the limit based on a wet-to-dry mass ratio of 2.0 and an I_{sp} of 3000 s (20.4 km/s).
- The final mass of the spacecraft must be larger than the dry mass of 500 kg.

- The minimum distance to the Sun is not exceeded.
- The maximum launch ΔV is not exceeded.
- Time to the Kuiper belt is below 25 years.

However, it is determined that no penalties are required. Penalties such as the one regarding the launch ΔV and time-of-flight are eventually constrained by means of the input range and are thus not needed. Furthermore, as will be explained in later chapters, powered gravity assists are not considered thus eliminating that potential penalty. The results also indicate that there are no trajectories in the JN sequence which approach the Sun closer than the previously mentioned 0.8 AU constraint, thus negating the use of that penalty. In every optimization the total ΔV eventually dipped below the 20.4 km/s, which was partially taken care of by a convergence system explained in Chapter 7. The thrust setting is also not as much of a constraining factor as anticipated and as such no penalty systems will be used in the optimization process.

3.7. Requirements

The mission description in this chapter automatically also leads to a list of associated requirements. These requirements are grouped together in this section. Note that this list of requirements is only top-level since for example a detailed spacecraft subsystem design is out of the scope of this thesis. Furthermore, only elements of the mission relevant for the trajectory optimization process are discussed and the requirement generation is thus not necessarily complete. The KBM abbreviation in the requirement classification stands for 'Kuiper belt mission', GEN stands for 'general', 'PROP' stands for 'propulsion', 'POW' stands for 'power', 'INSTR' stands for 'instrumentation', 'LV' stands for 'launch vehicle', 'TRAJ' stands for 'trajectory'. 'TIME' is not abbreviated.

- KBM-GEN-01 The spacecraft shall perform a close flyby with a periapsis less than 10,000 km from the surface of the body with at least two KBOs.
- KBM-GEN-02 The mission objective of KBM-GEN-01 shall be reached before the end of the mission. The end of the mission is defined as the moment the spacecraft leaves the 50 AU border of the Kuiper belt or otherwise 100 years after launch.
- KBM-GEN-03 The total wet mass of the spacecraft shall be no more than 1000 kg.
- KBM-GEN-03.1 The dry mass of the spacecraft shall be no less than 500 kg.
- KBM-INSTR-01 The power budget of the instrumentation subsection of the spacecraft shall be below 50 W for general usage.
- KBM-INSTR-01.1 The power budget of the instrumentation subsection of the spacecraft shall be below 100 W for peak usage.
- KBM-PROP-01 The spacecraft shall make use of low-thrust Xenon ion propulsion as its main thrust method.
- KBM-PROP-01.1 The maximum theoretical thrust of the spacecraft, based on the ion propulsion system requirements and available power, shall not be exceeded.
- KBM-POW-01 The spacecraft shall be powered by means of three GPHS-RTGs, capable of delivering 900 W of power at BOL.
- KBM-LV-01 The spacecraft shall be placed on its initial interplanetary trajectory leg with a maximum launch energy of $100 \text{ km}^2/\text{s}^2$.
- KBM-TIME-01 The spacecraft shall be launched between January 1, 2040 and January 1, 2050.
- KBM-TIME-02 The spacecraft shall reach the 30 AU Kuiper belt border within 25 years after launch.
- KBM-TIME-03 During the active phase of the mission the average time between CFBs shall be no more than 10 years.
- KBM-TRAJ-01 The mission trajectory shall consist of a low-thrust arc to Jupiter, followed by a low-thrust arc to Neptune, followed by CFBs of KBOs.
- KBM-TRAJ-01.1 None of the individual trajectory legs shall complete one full revolution around the Sun or more.
- KBM-TRAJ-01.2 The gravity assists with the planets shall be limited by minimum and maximum periapsis distances based on heritage missions.

- KBM-TRAJ-01.3 None of the sections of a trajectory leg shall approach the Sun by less than 0.8 AU.
- KBO-TRAJ-02 The Kuiper belt mission shall be performed with close flybys of KBOs with an uncertainty factor of 2 or lower.

3.8. Problem structure

The final goal of this research is to find a working methodology for low-thrust KBO optimization and to then find optimal trajectories for such a mission. It is decided to split this main goal into multiple sub-goals or phases, which will be tackled one by one during the thesis. The first phase regards the tuning of the chosen optimizer on low-thrust trajectories. Afterwards, the second phase studies the planetary flybys and can be used to test the capabilities of the low-thrust optimizer. The third phase then includes a single KBO flyby. If needed, the optimization method can be adjusted here. Afterwards, the KBO sequence is extended and the found trajectories are analyzed until they are deemed acceptable. The final phase of the research is a retrospective analysis regarding the sensitivity of the found solutions as well as the number of DFBs found in the trajectories. A schematic overview of the different thesis phases can be found in Figure 3.4. Before the phases it is first decided whether a fully propagated approach or a patched-conics approach is used for the trajectory propagation.

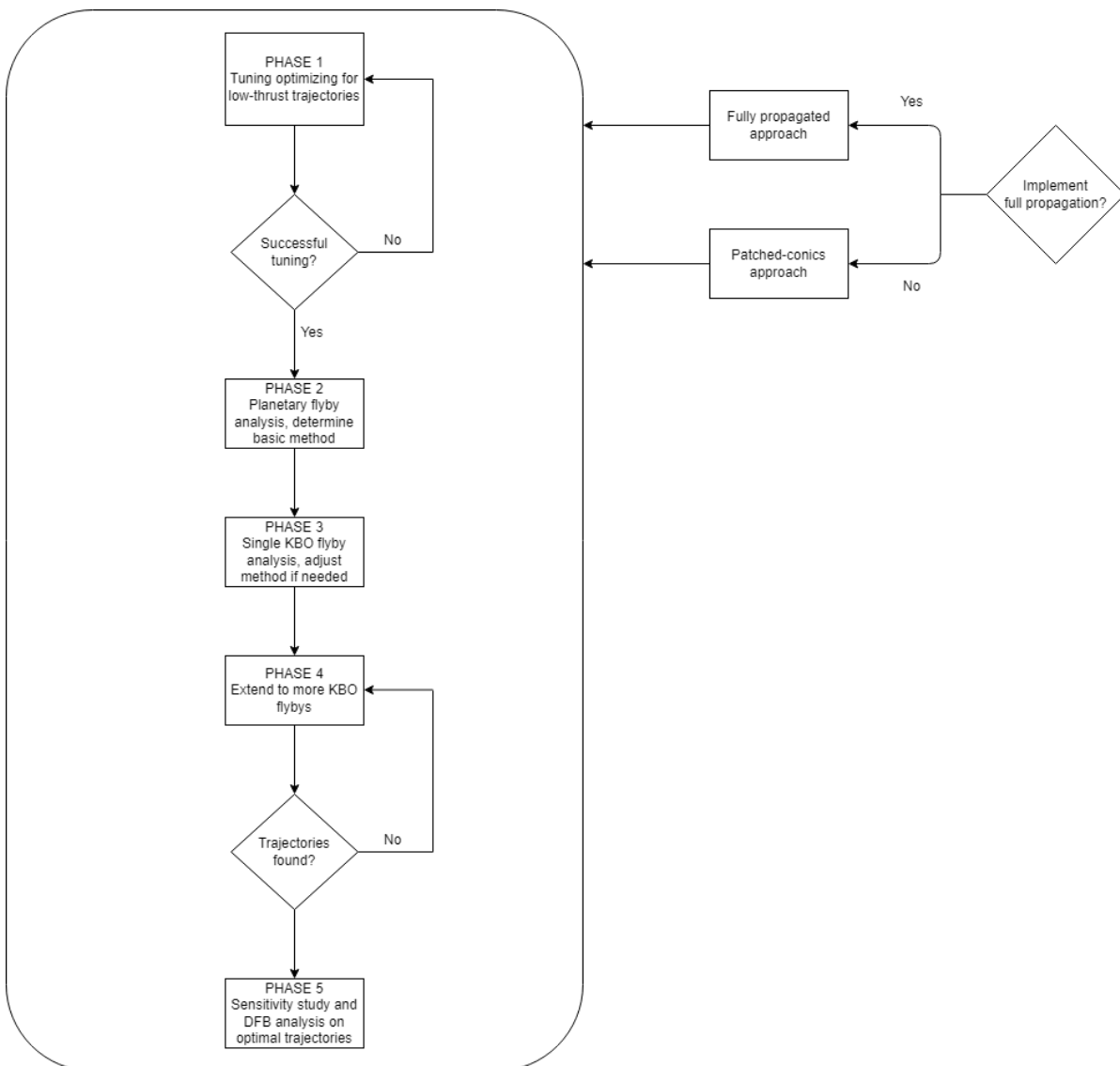
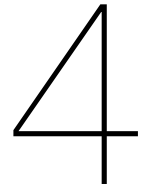


Figure 3.4: A flow chart of the different phases of the thesis project.

3.9. Summary

This chapter provides an overview of the mission description. The goal of the trajectory design is to find trajectories to KBOs with at least two CFBs in a single mission. DFBs are not analyzed during the optimization, but are only looked at afterwards. Based on the science instruments a spacecraft dry mass estimate of 500 kg is made with a maximum wet-to-dry mass ratio of 2. Using the larger launch systems allows a launch energy up to $100 \text{ km}^2/\text{s}^2$. Ion engines with an I_{sp} of 3000 s are assumed and are powered by three RTGs with a BOL power of 900 W and a degradation level of 1.6% per year.

The trajectories are defined by a departure date, time-of-flight values, a launch velocity, and flyby values which regard the incoming velocity for the flyby and three variables of the gravity assist itself. A list of constraints has been made for the flybys including the planetary flyby sequence, which will be Jupiter - Neptune (JN). A decision regarding KBOs has been made and multiple selections of bodies are used during the thesis project: the full set of known KBOs, 902 bodies with a sufficiently small uncertainty parameter and 36 high-priority bodies. The trajectory fitness is defined by the ΔV and time-of-flight, which allows the usage of Pareto fronts. The ΔV is the leading objective out of the two. Finally, an overview is provided of the requirements based on the mission description as well as the problem structure as it will be tackled during the rest of the project.



Astrodynamics

There are multiple ways to mathematically tackle the design of interplanetary trajectories. This chapter tackles the astrodynamics theory related to the thesis topic. The chapter starts with a discussion on Tudat, the coding framework used for this thesis, as well as the used data sources since they are relevant for some of the astrodynamics decisions. Afterwards, model decisions such as the coordinate system, time system, and reference frame are discussed. This is followed by a discussion of the trajectory parameterization. Finally, the remaining mathematical theory is discussed which contains orbital mechanics, Kepler orbits, and gravity assists.

4.1. Tudat

Tudat (TU Delft Astrodynamics Toolbox) is a toolbox written in C++ and developed by TU Delft [21]. The coding implementation of all trajectory design in this thesis is done using Tudat. Since the advantages and limitations of Tudat are also relevant for the astrodynamics description, the toolbox is discussed in this chapter. This section discusses what Tudat is, why it is chosen for this thesis and what its general capabilities are.

Tudat is a toolbox developed and used by TU Delft. To make the toolbox easier to use and to combine it with many other frameworks and modules in Python, Tudatpy has been made as well. Tudatpy (TU Delft Astrodynamics Toolbox in Python) is a library which exposes the functions of Tudat such that they can be directly used in Python [21]. Any fundamental changes to the workings of the toolbox can only be made in C++. However, if the tools are available the use of the Python version allows for easier customization and combination with other programs and coding modules. Unless explicitly mentioned, the coding in this thesis is done in Python with Tudatpy.

The main purpose of Tudat is to allow users to perform astrodynamics simulations in an intuitive manner and to provide many of the common functions required for such research. This includes numerical simulation-related capabilities such as the availability of many different integrators and propagators. Mathematical settings and tools such as coordinate frames, interpolators, and state descriptions (such as Kepler elements) are implemented. Tudat allows the user to set up a numerical simulation with a set of bodies, vehicles, and different types of trajectories. Trajectories such as the ones for multiple gravity assist (MGA) missions are already implemented in Tudat and can thus easily be accessed. The body models of planets can be adjusted with specific environment properties and acceleration models. Custom bodies can also be added. Tudatpy can also be used together with optimization modules which allows trajectory optimization to be performed in Python. Python's matplotlib package will be used for the visualization of the results in this thesis.

Tudat was not the only tool considered for trajectory design and optimization for this thesis. Figure 4.1 shows an overview other trajectory design software such as NASA's Evolutionary Mission Trajectory Generator (EMTG) package, which has also been used in many previous MSc theses [26]. The decision for Tudat is based on multiple reasons. Firstly, Tudat is specifically made while keeping the needs of

(thesis) students in mind and thus has a very high level of customization. Secondly, contributions by previous MSc students such as L. van der Heyden are available in Tudat and this allows the thesis to be a natural continuation of their work. Thirdly, because Tudat is developed and maintained by students and staff from TU Delft, it is easy to make contact with developers in order to ask for the status of specific modules, request prioritization for certain parts of the code, and to ask for support when problems are encountered. Specifically, contact with D. Dirx has been made extensively to discuss the current state of Tudat. Contact with fellow master student M. Avillez was also frequent as he implemented the low-thrust MGA legs into Tudat. Separate spherical shaping legs were already implemented in Tudat by T. Roegiers and later re-implemented into its current version by M. Chambe [36].

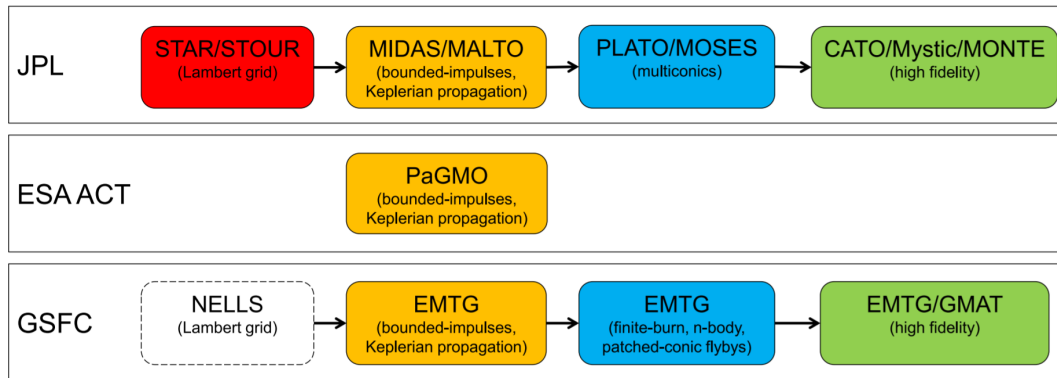


Figure 4.1: Trajectory design software used by various other institutions. The software displayed on the right is the most advanced and used for later design stages [26].

4.2. Data sources

To understand how the astrodynamics components of the thesis work it is also relevant to know which type of input data is used.

The position of the planets of the Solar System, stored in ephemerides, are taken from SPICE, which stands for Spacecraft Planet Instrument C-matrix Events. During this thesis the DE440 version of SPICE is used, which was released in 2020. There is also a DE441 version of SPICE, but it is less accurate than DE440 [94]. DE441 covers a time period of roughly 30,000 years while DE440 only covers a period of roughly 4,000 years [94]. However, for this thesis the DE440 time range is more than enough and is more accurate for the relevant time period.

The SPICE ephemeris provides the properties and positions of the planets for the relevant time period of the thesis simulation. However, the KBOs themselves are not included in this database and must thus be added in a different manner. For this data from the Minor Planet Center (MPC) is used. MPC keeps a database of all known and catalogued objects in the Solar System [15]. The Kepler elements at a specified point in time can be retrieved from its database and are used to construct unperturbed Kepler orbits of the KBOs in Tudatpy.

There is a possibility to generate perturbed ephemerides from the MPC website, but the main issue here is that the tool only runs 60 years into the future and could thus limit KBO mission analysis due to the long expected time-of-flight values [39]. Another option would be to use the JPL Horizon interface, which runs up to 2500 AD and can generate a look-up table for a perturbed KBO trajectory [86]. The position at a certain time can then be found through interpolation of the table. Since this study regards a preliminary analysis the Kepler orbits are deemed sufficient as the use of the JPL Horizon ephemerides would slow down the optimization process. For future detailed analysis, the use of the JPL Horizon ephemerides is recommended. An extensive analysis of the impact of neglecting the perturbations for the KBOs is also recommended. The uncertainty due to the omission of perturbations is at least equal to the angular runoff of the uncertainty parameter, which is based on the perturbed trajectory from MPC [15]. For an uncertainty value of 2 the position accuracy for a body at a distance of 40 AU over a period of 50 years is roughly 0.02 AU [45].

4.3. Model decisions

In order to design the trajectories in this thesis a number of model decisions have to be made. These regard the trajectory description, reference frame, time system, integrator, propagator, and models for the spacecraft, environment, and acceleration. These decisions are discussed in this section.

The most fundamental decision regarding the model is whether a fully propagated approach is chosen or whether patched conics are assumed, the latter being shown in Figure 3.4. The main advantage of a fully propagated approach is its increased accuracy by being able to implement detailed acceleration models. However, its main drawback is its increased runtime which would be orders of magnitude lower than the alternative, patched conics [23]. Instead of propagating the trajectory with many acceleration models, patched conics simplifies the trajectory to a two-body problem [21]. During the large interplanetary sections the only force acting on the spacecraft, besides the thrust, is the point-mass gravity of the Sun. Once the spacecraft enters the planet's sphere of influence (SOI) the main body switches from the Sun to the respective planet [21]. During preliminary design this patched-conics approach is often used as it can greatly increase the sample size of the analysis with only a limited loss in accuracy. This is especially the case for this analysis as the time spent near the planets is very short relative to the time span of the interplanetary legs. Therefore, the patched-conics approach is chosen for this thesis.

Other simplifications of Tudat's patched-conics approach in combination with MGAs is that each trajectory leg performs a maximum of one full revolution or less and that the trajectory is counter-clockwise, in the same direction as the orbital motion of the planets [21]. An example of a patched-conics approach to Mars with a switch from an Earth-centric, to a Sun-centric, to a Mars-centric trajectory is shown in Figure 4.2 [97]. By using the patched-conics method the gravity assists are seen as instantaneous maneuvers, which are used to patch the two trajectory legs together.

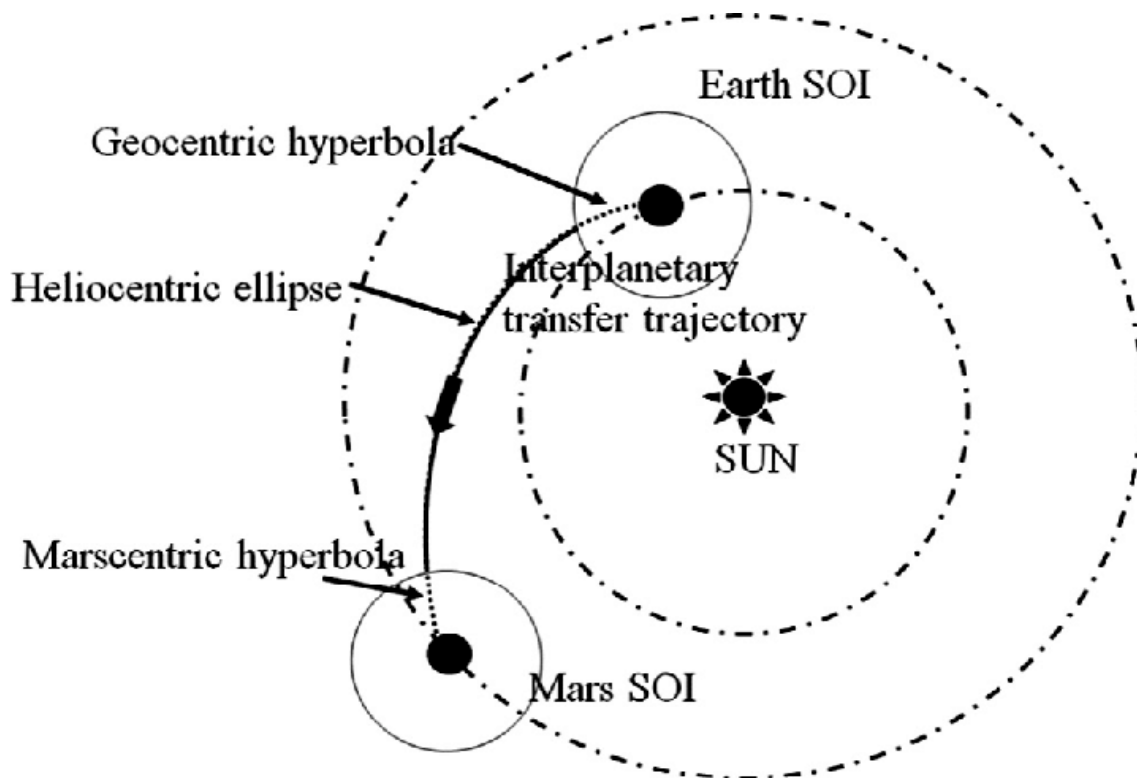


Figure 4.2: An illustration of a patched-conics trajectory from Earth to Mars with the different SOIs [97].

The Solar System barycenter (SSB) will be used as the global frame origin during this thesis with an inertial ecliptic coordinate frame orientation based on the Solar System as of January 1, 2000 at noon (ECLIPJ2000). This frame has an xy -plane in the ecliptic plane, which goes through the ascending

node of the Sun's equator at J2000 [85]. The z-axis is known as the Ecliptic North Pole [85]. This reference frame is one of the default frames for interplanetary missions in Tudat and is also used in the ephemeris data from MPC and the JPL Horizon interface through the international celestial reference frame at J2000 (ICRFJ2000), which is considered equivalent for preliminary analyses [65]. A visual overview of the ECLIPJ2000 reference frame is given in Figure 4.3.

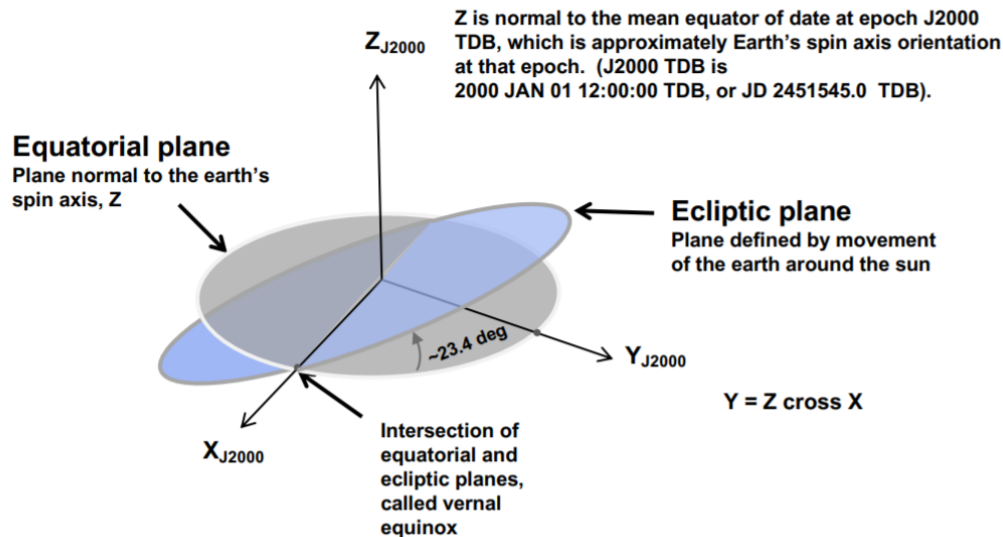


Figure 4.3: An overview of the ECLIPJ2000 reference frame [65].

The time system used during this thesis is based on the Julian day system, which has a zero point at noon on January 1, 4713 BC [115]. There is also a shifted version of this system with the zero point at noon on January 1, 2000 AD. This system is called J2000. Another time system called MJD_{2000} starts at 00:00 on January 1, 2000 AD. Finally, the Modified Julian Date (MJD) has a zero point at 00:00 on November 17, 1858 AD [32]. Unless specified otherwise, the Tudat software makes use of MJD_{2000} .

Another decision regarding the trajectory is the use of an integrator and propagator. The initial idea during the literature study was to make use of a high-order Bulirsch–Stoer (BS) or Dormand-Prince (DOPRI8(7)) integrator together with the Unified State Model (USM) as the propagator [45]. However, this decision still assumes a fully propagated trajectory. This selection changed due to the decision to use a patched-conics approach. Since the gravity assist is considered to be an instantaneous maneuver, the spacecraft is in practice always in the Sun-centered frame. The shape of low-thrust shape-based trajectories with a thrust profile and a constant central body can be completely described by mathematical functions. Therefore, no numerical integration is required and a semi-analytical low-thrust trajectory can be used. If detailed design with a fully propagated trajectory is done in future research, the previously mentioned integrator and propagator are recommended.

The decision to use semi-analytical legs vastly increases the speed of the analysis and makes it realistic to study a larger number of trajectory options. During the experiment phase of the thesis it is also found that this increase in computation speed is required in order to study the desired number of trajectory options. The description of these semi-analytical legs is dependent on the trajectory parameterization and is discussed in Section 4.4.

The decision to use semi-analytical patched conics also simplifies the environment, acceleration, and spacecraft models. The environment models regard the properties of bodies or objects in the Solar System. The bodies used during the simulation are the Sun, the planets in the Solar System relevant for the trajectory, and the KBOs with which the flybys are performed. The ephemerides of these bodies have already been discussed earlier in this chapter.

The acceleration models concern the consequences of certain decisions on the acceleration of the spacecraft. The only main decisions made here regard the fact that for the planets a point-mass gravitational acceleration will be used and that for the flybys in the Kuiper belt the mass of the KBOs themselves is neglected completely since their acceleration is multiple orders of magnitude lower than those of the planets. A more detailed quantitative comparison regarding KBO gravitational attraction was performed in the literature study [45]. This decision simplifies the KBO section of the trajectory as the outgoing position and velocity from the KBO flyby is the same as the incoming position and velocity. The only other modelled acceleration is the thrust of the spacecraft.

Besides environment and acceleration models there is also the spacecraft itself which will need to be modelled in some capacity. Some of these settings have already been mentioned in previous chapters such as the maximum wet mass of 1000 kg and the minimum dry mass of 500 kg. The propellant efficiency is modelled with an I_{sp} of 3000 s for the ion engine and 220 s for any high-thrust maneuvers. Further specifications for the spacecraft including rough dimensions and the radiation pressure coefficient are recommended for further research when a fully propagated trajectory is used, but are out of scope of this thesis. The most important model decision that has not been discussed yet is the trajectory parameterization. The next section discusses this topic in detail.

4.4. Trajectory parameterization

Besides the gravitational acceleration due to the Sun and the planets during the gravity assists, the thrust is the major force experienced by the spacecraft during its trajectory. There are many different methods to parameterize the thrust arc. The different options were extensively studied during the literature study [45]. First these different options are summarized and a parameterization is chosen. Afterwards, this option is explained in more detail.

4.4.1. Parameterization options

Low-thrust trajectory parameterizations can generally be split into direct, indirect, hybrid, and shape-based methods. Direct and indirect methods discretize the problem thereby changing the continuous low-thrust problem in a defined set of nodes. One of the most common direct methods, the Sims-Flanagan method, splits the trajectory into a number of nodes and applies an instantaneous ΔV at the center of each segment. An illustration of this method is given in Figure 4.4 [112]. As the number of nodes increases this method approaches the result of a continuous low-thrust arc. Due to the large number of nodes for the long-term mission studied here, which would result in many free variables, in combination with the fact that Sims-Flanagan is more suited for already defined trajectories instead of preliminary design [1] this method is not used nor is any other direct method. Once the trajectory is more well-defined, Sims-Flanagan would be an interesting option for further research.

Indirect methods do not solve the nodes directly, but instead solve for the costates of the problem. Like direct methods, this method already requires a good initial guess in order to converge and its formulation is susceptible to any change in the simulation. Therefore, these methods are also not chosen for this thesis. Hybrid options which combine direct and indirect methods are an interesting alternative, but are also not chosen due to limitations in adding detailed environment models. Furthermore, the low-thrust hybrid methods that were found are all optimized for Earth-centered orbits. The design of a hybrid method for deep-space missions is an intriguing topic, but is out of scope for this thesis.

The remaining class of options thus consist of shape-based methods. Shape-based methods formulate trajectories based on a set of mathematical functions and, as the name implies, use specific mathematical shapes in order to design the trajectory. These methods are highly recommended for preliminary trajectory design due to their fast computational speed while retaining accuracy [55]. Within the shape-based method class there are also multiple options which all use different mathematical base functions. The exponential sinusoids and inverse polynomial methods have been used in previous MSc theses at TU Delft, but both struggle with boundary conditions and free variables [35] [99] [123].

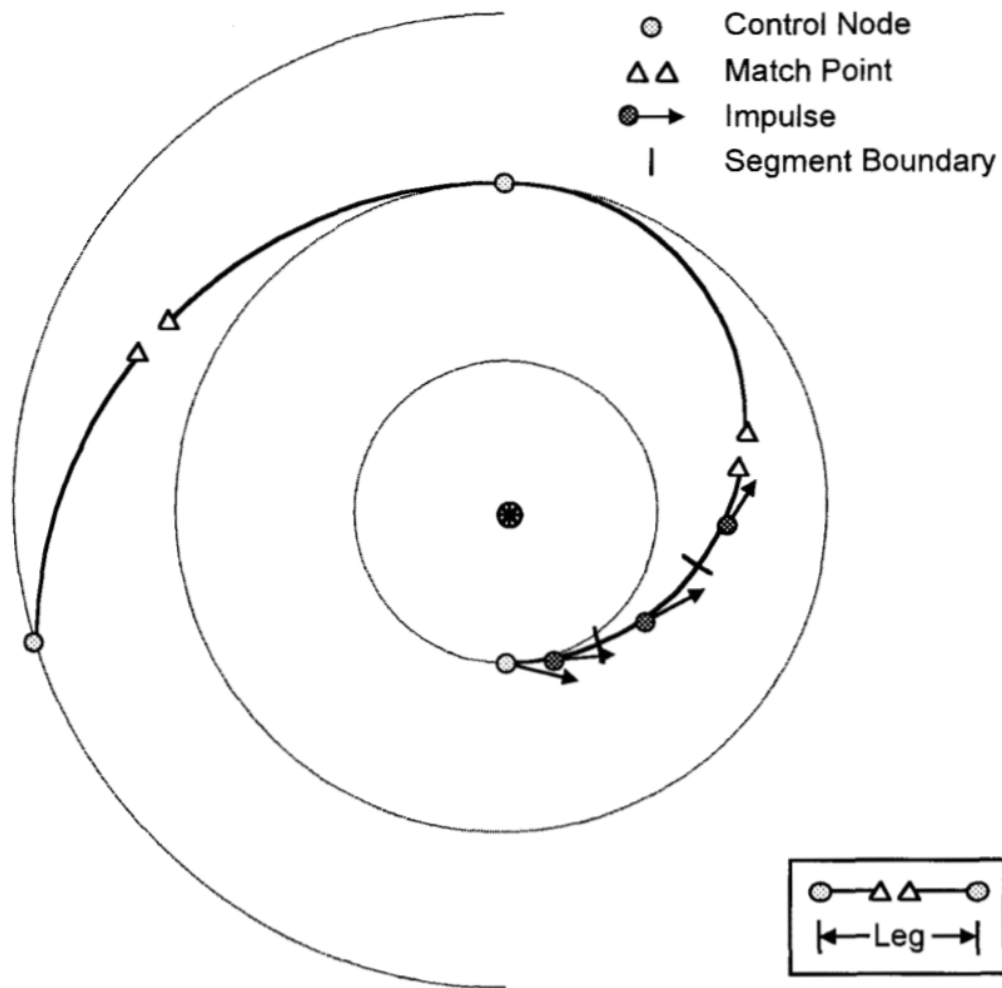


Figure 1. Trajectory Structure

Figure 4.4: A trajectory illustrating the principle of the Sims-Flanagan method [112].

The two most intriguing shape-based methods for this thesis are spherical shaping and hodographic shaping. The basic radial description of spherical-shaping legs is given by Equation 4.1 [123]. The method is thus a combination of an inverse second-order polynomial together with a sine/cosine wave function to calculate the radial distance R . The 'a' components represent the free coefficients of the function. Hodographic shaping uses the velocity hodograph to shape the trajectory as illustrated in Figure 4.5 [35]. Unlike the previously mentioned shaping methods, hodographic shaping has free coefficients to tune the trajectory and also has a vast array of different base functions. The main advantage of this is that hodographic shaping works for nearly all trajectory inclinations, while the nominal description of spherical shaping is only accurate up to an inclination of roughly 15 degrees [121].

$$R = \frac{1}{a_0 + a_1\theta + a_2\theta^2 + (a_3 + a_4\theta)\cos(\theta) + (a_5 + a_6\theta)\sin(\theta)} \quad (4.1)$$

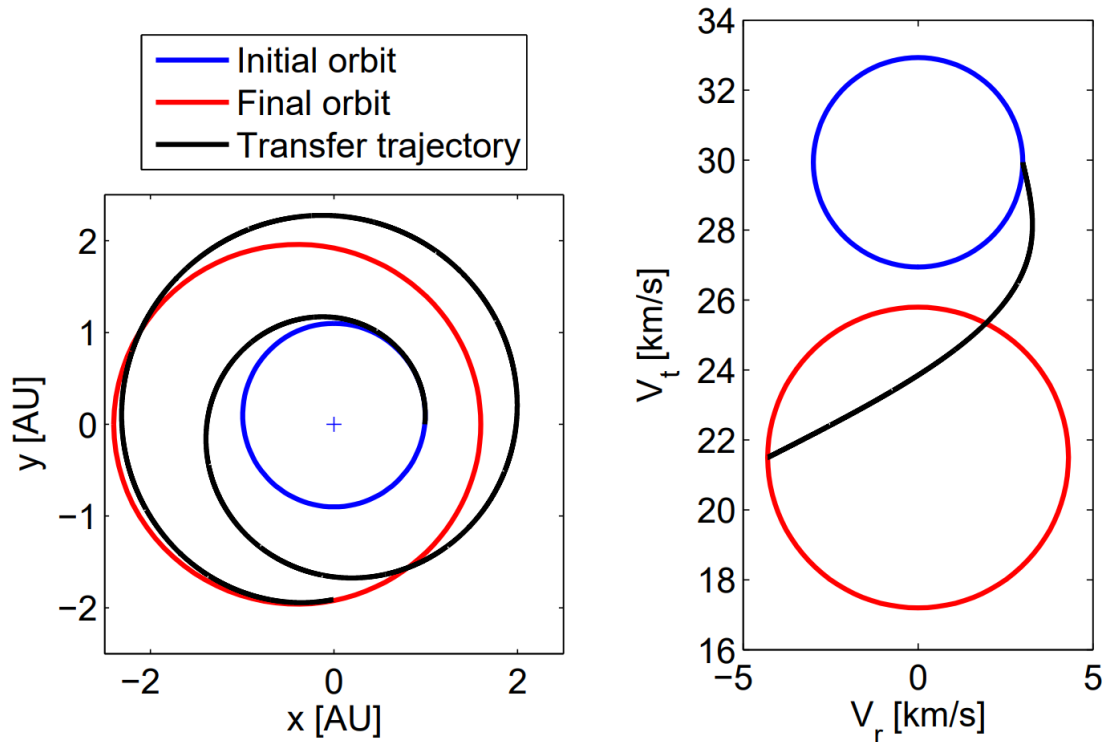


Figure 4.5: A trajectory shaped using hodographic shaping (left) and the corresponding velocity hodograph (right) [35].

The final decision on the shaping method is between spherical and hodographic shaping. A major disadvantage of hodographic shaping for the time plan of this specific thesis is that much time will have to be spent on exploring the optimal base functions and the tuning of the free coefficients. This would shift the main focus of the thesis away from low-thrust KBO trajectory methods and towards the study of hodographic shaping. While still an interesting topic, this is not within the scope of the thesis. Therefore, spherical shaping is chosen as the thrust parameterization for the thesis.

Due to the use of spherical shaping only KBOs with an inclination magnitude smaller than or equal to 15 degrees are considered during the nominal phase of the thesis as the method can have trouble calculating trajectories with high inclinations [121]. This implies that of the 902 bodies which passed the uncertainty parameter filter in the previous chapter, 590 also pass the 15 degree inclination filter. The selection can be expanded if the desired results can not be reached with these 590 bodies. Spherical shaping is tackled in more detail in the next subsection.

4.4.2. Spherical shaping

This subsection provides the theoretical basics for spherical shaping. This explanation is sufficient to understand the inner workings of spherical shaping, but is not detailed enough to replicate the method from scratch. For this full mathematical derivation the previous work by D. Novak and T. Roegiers is recommended [91] [106].

D. Novak was the first to describe the version of spherical shaping which is used in Tudat. A slightly adjusted version of this method was eventually implemented in Tudat by T. Roegiers and M. Chambe. As the name implies spherical shaping is based on spherical coordinates. Spherical coordinates make use of one radial and two angular coordinates and can be described using Equations 4.2, 4.3, and 4.4 as is also shown in Figure 4.6 [92]. Here r is the radius, θ is the azimuthal angle, and ϕ is the elevation angle while x , y , z are the standard Cartesian coordinates.

$$r = \sqrt{x^2 + y^2 + z^2} \quad (4.2)$$

$$\theta = \text{atan2}(y, x) \quad (4.3)$$

$$\phi = \arcsin\left(\frac{z}{r}\right) \quad (4.4)$$

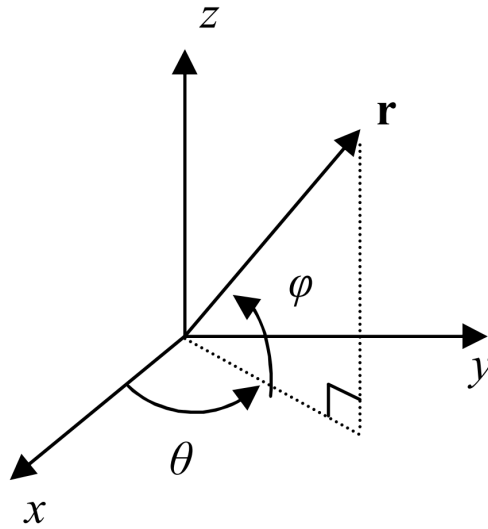


Figure 4.6: A schematic overview of a spherical coordinate system [92].

These spherical coordinates are used during the rest of the description of spherical shaping. However, throughout the rest of the thesis the nominal Cartesian coordinates (x, y, z) are used as well as Kepler elements to describe properties of the trajectories. Kepler elements and orbits are discussed in more detail in Section 4.5.

Spherical shaping assumes a negligible spacecraft mass compared to that of the planetary bodies. Parameterization of the trajectory is done by means of the azimuthal angle θ . The state vector is thus a function of θ instead of time t . This state vector is shown in Equation 4.5 [106]. Here $r = R(\theta)$, $t = T(\theta)$, $\phi = \Phi(\theta)$ are functions of θ . Similarly the velocity and acceleration can also be rewritten as a function of θ . Based on the solution of these functions the required thrust can be calculated.

$$\mathbf{x} = \left[r, t, \phi, \frac{dr}{d\theta}, \frac{dT}{d\theta}, \frac{d\Phi}{d\theta} \right] \quad (4.5)$$

The first step of the spherical-shaping process is to input the decision variables as discussed in Chapter 3. This is used to determine the initial and final state vector as a function of the azimuthal angle as is shown in Equation 4.5. Furthermore, a list of boundary conditions can be set up. A full derivation and description of these boundary conditions can be found in T. Roegier's work [106]. The two shaping functions are the previously shown Equation 4.1 and Equation 4.6 for the elevation [106].

$$\Phi = (b_0 + b_1\theta)\cos(\theta) + (b_2 + b_3\theta)\sin(\theta) \quad (4.6)$$

The boundary conditions together with the shaping functions as well as their derivatives can be used to solve for the coefficients a_x and b_x by setting up matrices. The only coefficient without a closed analytical solution is a_2 . A different value for a_2 affects the time-of-flight of the trajectory. Thus, an iterative process by means of a bisection root finder is used to get the value for a_2 that corresponds with the desired time-of-flight. The time-of-flight can be calculated with Equations 4.7 and 4.8 where D is given by Equations 4.9 and 4.10 [106]. Here μ is the gravitational parameter of the central body, θ_i and θ_f are the initial and final azimuth values of the trajectory, n_r is the number of revolutions of the trajectory, u_n is the normal

thrust acceleration, and γ is the flight-path angle. The D function is the parabolic anomaly function that regards the geometry of the trajectory. As can be seen from Equation 4.7 the time and thus the trajectory is only feasible if D has a positive value. The real-life context of this is that a positive value of D relates to a trajectory which curves towards the central body as shown in Figure 4.7 [106].

$$T'(\theta) = \frac{dT}{d\theta} = \sqrt{\frac{D(\theta)R(\theta)^2}{\mu}} \quad (4.7)$$

$$TOF = \int_{\theta_i}^{\theta_f + 2\pi n_r} T' d\theta \quad (4.8)$$

$$D\dot{\theta}^2 = \frac{\mu}{r^2} + \frac{u_n}{\cos(\gamma)} \quad (4.9)$$

$$D = -R'' + 2\frac{R'^2}{R} + R'\Phi' \frac{\Phi'' - \sin(\Phi)\cos(\Phi)}{\Phi'^2 + \cos^2(\Phi)} + R(\Phi'^2 + \cos^2(\Phi)) \quad (4.10)$$

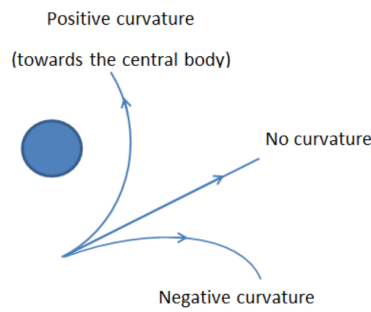


Figure 4.7: The implication of the curvature of the trajectory depending on the value of D. A positive D value means that the trajectory curves towards the body while it curves away with a negative value of D [106].

The final steps are now to calculate the acceleration vector of the spacecraft over time $\tilde{\mathbf{a}}$ and, related to that, the control vector or in other words the low-thrust vector \mathbf{u} . This is done with Equations 4.11 and 4.12, respectively. The acceleration is given in the spherical coordinate system. The tilde indicates that the acceleration is expressed in the spherical coordinates along the trajectory. Here \mathbf{e} is a unit vector in radial (r), tangential (t), normal (n) or out-of-plane (h) direction. $\tilde{\mathbf{v}}$ is the velocity vector along the trajectory. The full derivation of these descriptions can be found in T. Roegiers' thesis [106]. The total ΔV is then the $|\mathbf{u}| \frac{dT}{d\theta}$ integrated over the azimuthal angle of the trajectory, which is done by means of an RK4 integrator with a time step of $\frac{2\pi}{100}$ [106].

$$\tilde{\mathbf{a}} = \begin{bmatrix} \tilde{a}_r \\ \tilde{a}_\theta \\ \tilde{a}_\phi \end{bmatrix} = \begin{bmatrix} r'' - r(\phi'^2 + \cos^2(\phi)) \\ 2r'\cos(\phi) - 2r\phi'\sin(\phi) \\ 2r'\phi' + r(\phi'' + \sin(\phi)\cos(\phi)) \end{bmatrix} \quad (4.11)$$

$$\mathbf{u} = \begin{bmatrix} u_t \\ u_n \\ u_h \end{bmatrix} = \begin{bmatrix} \frac{\mu}{r^2} \mathbf{e}_r * \mathbf{e}_t + \dot{\theta} \tilde{\mathbf{v}} * \mathbf{e}_t \\ \frac{\mu}{r^2} \mathbf{e}_r * \mathbf{e}_n + \dot{\theta}^2 \tilde{\mathbf{a}} * \mathbf{e}_n \\ \dot{\theta}^2 \tilde{\mathbf{a}} * \mathbf{e}_h \end{bmatrix} \quad (4.12)$$

4.5. Trajectory theory

With the spherical-shaping methodology described, the only astrodynamics topic which still has to be discussed regards basic theory about trajectory design and physics. First a short overview of the laws of physics is given that determine orbital mechanics. Afterwards, Kepler orbits as well as gravity assists are discussed in more detail. Unless otherwise specified, the information in this section is derived from K.F. Wakker's 'Fundamentals of Astrodynamics' [122]. As such the entire section references this source and it is not mentioned in every sentence, unless citations are used.

4.5.1. Orbital mechanics

The basics of orbital mechanics follow from Isaac Newton's laws of motion, which are as follows:

- First law: "Every particle continues in its state of rest or uniform motion in a straight line relative to an inertial reference frame, unless it is compelled to change that state by forces acting upon it." [122] (Wakker, 2015, p1)
- Second law: "The time rate of change of linear momentum of a particle relative to an inertial reference frame is proportional to the resultant of all forces acting upon that particle and is collinear with and in the direction of the resultant force." [122] (Wakker, 2015, p1)
- Third law: "If two particles exert forces on each other, these forces are equal in magnitude and opposite in direction." [122] (Wakker, 2015, p1)

The third law in particular describes how an action results in an equal and opposite reaction. This concept is used in spaceflight to propel the spacecraft: by expelling propellant at a high speed a thrust force is generated in the opposite direction. This relates to a much more recent equation, namely Tsiolkovsky's rocket equation, repeated in Equation 4.13. The high specific impulse of low-thrust propulsion allows for a much larger ΔV budget than is capable with high-thrust propulsion.

$$\Delta V = I_{sp} g_0 \ln\left(\frac{m_0}{m_f}\right) \quad (4.13)$$

Another of Newton's laws regards gravitation and is shown in Equation 4.14. It shows the force exerted on body 2 by body 1 where G is the gravitational parameter and \mathbf{r}_2 is the vector from body 2 to body 1. Note that, as follows from Newton's third law, an opposite force is also exerted on body 1. However, if body 1 is assumed to be the planet and body 2 the spacecraft, the force on body 1 is often negligible in terms of affecting the planet's inertia. The problem tackled in this thesis is at all times a two-body problem due to the use of the patched-conics assumption. In this simplified state the acceleration of the spacecraft can be formulated with Equation 4.15. This function can also have an additional thrust term (normalized with the spacecraft mass) if there is thrust active.

$$\mathbf{F}_2 = G \frac{m_1 m_2}{r_2^2} \mathbf{r}_2 \quad (4.14)$$

$$\ddot{\mathbf{r}} = -\mu \frac{\mathbf{r}}{r^3} \quad (4.15)$$

The movement of the spacecraft around celestial bodies, if simplified to a two-body problem, is a conic section. In other words: an ellipse, a parabola or a hyperbola. A visual explanation of these orbits is shown in Figure 4.8 [100]. Since many heritage missions gained enough velocity during its Jupiter gravity assist to escape the Solar System, it is expected that the trajectories in this thesis will have hyperbolic orbits with respect to the Sun once they reach the Kuiper belt. This means that the velocity of the spacecraft is larger than the Solar System's escape velocity V_E . A more rigorous way to talk about the properties of orbits is by using Kepler elements, which is discussed in the next subsection.

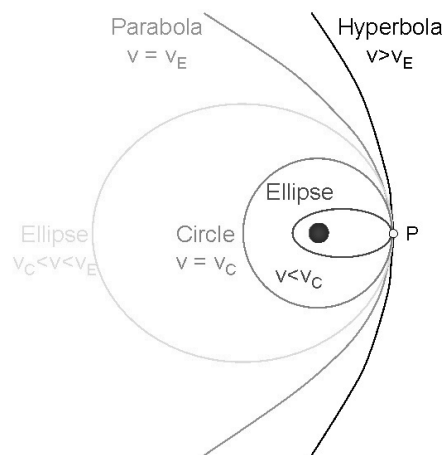


Figure 4.8: An illustration of an elliptical, parabolic, and hyperbolic orbit around a body with a common point P [100]. The parameter v represents the velocity in point P.

4.5.2. Kepler orbits

The radial distance of a particle in an orbit around a central body is given by Equation 4.16. Here p is the semi-latus rectum of the orbit, while e and θ are the eccentricity and the true anomaly, respectively. The last two terms are two of the Kepler orbital elements. A full list of these elements is: the semi-major axis a , eccentricity e , inclination i , the argument of pericenter ω , the right ascension or longitude of the ascending node Ω , and the true anomaly θ . An overview of all of these elements is given in Figure 4.9 [111]. In this figure the true anomaly is denoted by ν .

$$r = \frac{p}{1 + e \cos(\theta)} = \frac{a(1 - e^2)}{1 + e \cos(\theta)} \quad (4.16)$$

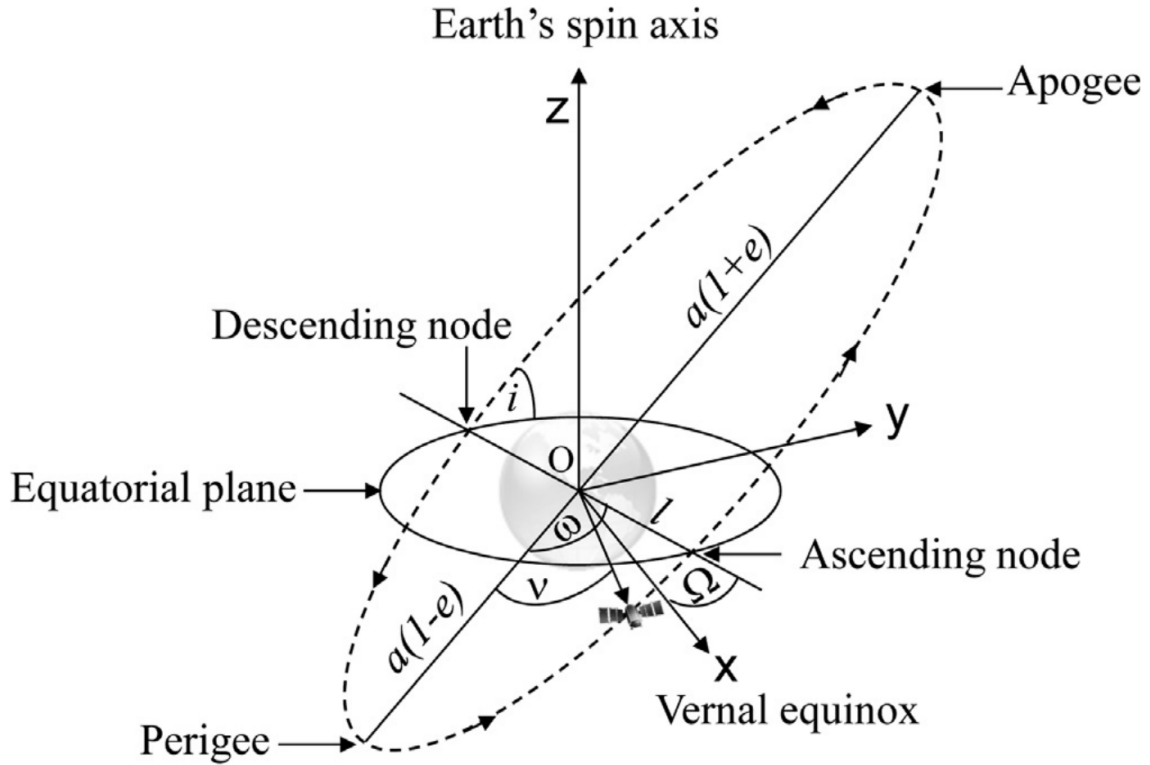


Figure 4.9: A schematic overview of an orbit with all the Kepler orbital elements, in this example for an Earth-centered elliptical orbit [111].

The time-of-flight in a Kepler orbit is given by Equation 4.17. In the case that the time-of-flight for just a section of an orbit is required Equation 4.18 can be used. Here E is the eccentric anomaly at point 1 and 2. This version is also known as Lambert's problem, which is solved in Tudat by using an algorithm developed by D. Izzo [46].

$$t_f = 2\pi \sqrt{\frac{a^3}{\mu}} \quad (4.17)$$

$$t_f = (E_2 - E_1 + e(\sin(E_1) - \sin(E_2))) \sqrt{\frac{a^3}{\mu}} \quad (4.18)$$

Many sources such as MPC do not provide the true anomaly, but instead use the mean anomaly. In these cases Equation 4.19 is used to go from the mean anomaly M to the eccentric anomaly E in an iterative process. For the first iteration E is assumed to be $\frac{M}{1-e}$. Afterwards, Equation 4.20 can be used to go from the eccentric anomaly to the true anomaly where β is given by Equation 4.21. Tudat also has another set of equations to solve this problem in case of hyperbolic orbits [21]. Finally, it is often

required to switch between the Keplerian elements and the Cartesian ones during analysis, which can be done with built-in functions from Tudat.

$$E_{i+1} = E_i + \frac{M - E_i + e \sin(E_i)}{1 - e \cos(E_i)} \quad (4.19)$$

$$\theta = E + 2 * \text{atan2}(\beta \sin(E), 1 - \beta \cos(E)) \quad (4.20)$$

$$\beta = \frac{e}{1 + \sqrt{1 - e^2}} \quad (4.21)$$

4.5.3. Gravity assists and flybys

The final theory discussed in this chapter regards gravity assists (GAs). In the trajectories analyzed gravity assists are used to patch the different interplanetary legs together. But not only that, the gravity assists themselves are used to change the heliocentric heading and velocity of the spacecraft. This means that less ΔV is required to complete the mission. For this reason gravity assists are commonplace in interplanetary trajectories. This subsection is largely based on the findings from the literature study [45].

Gravity assists make use the gravitational attraction of a flyby body in order to change the spacecraft's velocity in the planetocentric frame. This change results in both a change in the magnitude of the velocity as well as its direction in the heliocentric frame. A schematic overview of a gravity assist is provided in Figure 4.10 [122].

In this figure the spacecraft approaches the planet up to a distance r_3 , which will be referred to as r_p (pericenter distance) from now on. The value of this pericenter distance is given by Equation 4.22 [122]. At this distance the velocity of the spacecraft in the planetocentric frame is V_3 or V_p , described by Equation 4.23 [122]. In this equation B is called the impact parameter and represents the distance between the flyby planet and the asymptote of the flyby trajectory. After the flyby the heliocentric excess velocity in the tangential direction V_{∞_t} has changed to $V_{\infty_t}^*$ and the direction of the trajectory has changed by an angle α , the asymptotic deflection angle. Due to the conservation of angular momentum Equation 4.24 can be used [122]. The ΔV change during such a gravity-assist maneuver is described by Equation 4.25 [122].

In the 3D case a 3D rotation angle, b_{rot} , is required [43]. Due to using the incoming velocity as well as the gravity assist variables the 3D rotation angle is then fixed. The rotation angle is used within the Tudat calculations, but is not required as an explicit input. A more extensive explanation of the 3D gravity assist case can be found in the thesis by L. van der Heyden [43].

$$r_p = \frac{\mu}{V_{\infty_t}^2} \left(\sqrt{1 + \frac{B^2 V_{\infty_t}^4}{\mu^2}} - 1 \right) \quad (4.22)$$

$$V_p = \sqrt{\frac{2\mu}{r_3} + V_{\infty_t}^2} = \frac{\mu}{B V_{\infty_t}} \left[\sqrt{1 + \frac{B^2 V_{\infty_t}^4}{\mu^2}} + 1 \right] \quad (4.23)$$

$$B V_{\infty_t} = r_p V_p \quad (4.24)$$

$$\Delta V = 2 V_{\infty_t} \sin\left(\frac{1}{2}\alpha\right) = \frac{2 V_{\infty_t}}{\sqrt{1 + \frac{B^2 V_{\infty_t}^4}{\mu^2}}} \quad (4.25)$$

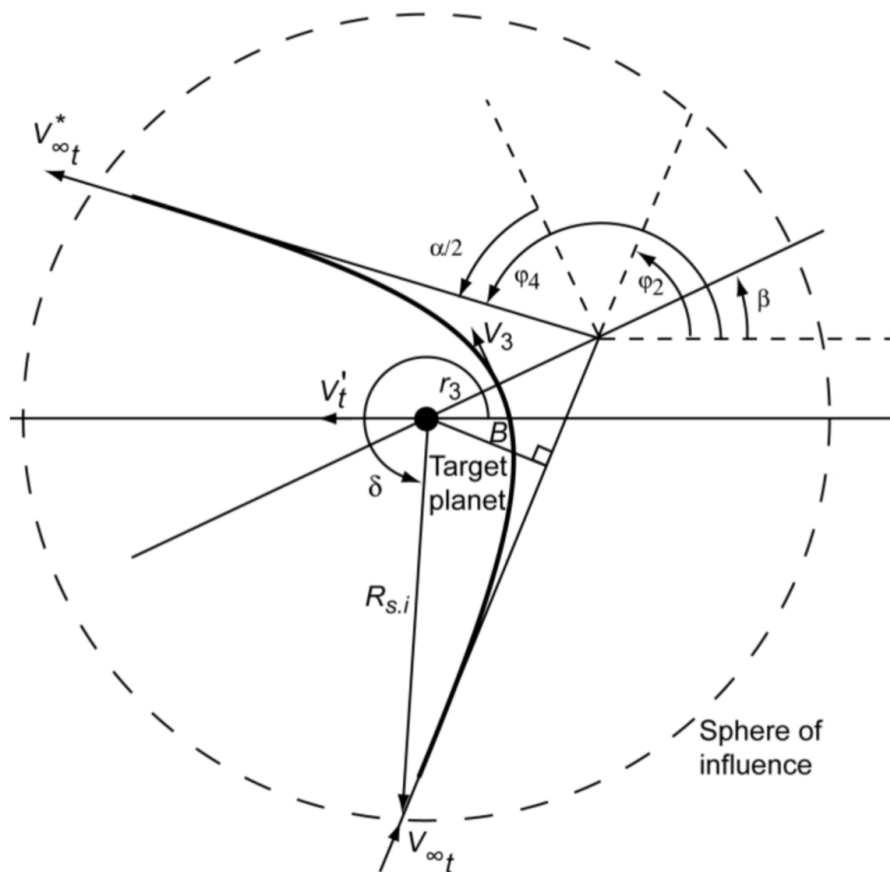


Figure 4.10: A schematic overview of a gravity assist [122].

One additional method to increase the effect of a gravity assist is to perform a ΔV boost during the flyby, which is called a powered gravity assist. Powered gravity assists make it easier to connect different legs of the trajectory and previous thesis work by P. Musegaas found an improvement of 7.8% in terms of the spacecraft wet mass in case powered gravity assists were used for high-thrust trajectories [63]. The nominal description of this thesis does not include powered gravity assists in order to keep the analysis completely focused on the capabilities of low-thrust propulsion. A powered gravity boost would need to be performed with high-thrust propulsion. Also, the use of aerogravity assists, where drag due to the atmosphere of the planet is used to influence the gravity assist, is considered out of scope of this thesis. An extensive analysis of the effect of powered gravity assists and aerogravity assists on low-thrust KBO trajectories is recommended for future research. During KBO flybys the mass of the flyby body is neglected and no gravity assist takes place. The KBO can be seen as a node in the trajectory and does not impact the velocity of the spacecraft.

4.6. Summary

This chapter describes the astrodynamics relevant for this thesis. The decision for Tudat as the software toolbox has been explained. Tudat is used in Python through Tudatpy with data for the planets retrieved from MPC and SPICE. To limit runtime and since this is a preliminary analysis, it is decided to use the patched-conics assumption. This patched-conics method is semi-analytical and only takes into account the main body's gravitational attraction and the thrust force by the spacecraft.

For the thrust a spherical shaping parameterization is used due to its relative simplicity and speed and thus more realistic chance at finding optimal low-thrust solutions since two of the bottlenecks of the low-thrust analysis will be its complexity and runtime. The chapter also provides an overview of relevant orbital mechanics and theory regarding Kepler orbits and gravity assists. In the nominal description only unpowered gravity assists are considered.

Part II

Implementation

5

Software development

This chapter describes the way in which the astrodynamics and mission description of the previous chapters have been implemented by means of Python code. The first section of the chapter provides an overview of the coding design while the second section regards verification of this code.

5.1. Coding design

The analysis of the thesis was fully done by means of Tudatpy in Python and a few tweaks to the C++ code in Tudat. First the full model architecture in Python is described. This is followed by a step-by-step example of a calculation loop for one trajectory. Afterwards, the C++ adjustments made to Tudat are discussed. Finally, the launch, trajectory leg, and gravity assist implementation are all briefly covered.

5.1.1. Main model architecture

This section discusses the architecture of the model used for the trajectory design of low-thrust KBO flyby trajectories. The optimization code is not discussed, but is tackled in Chapter 6. The model designed for this thesis makes use of the MGA tool available in Tudat. This tool allows the user to design a trajectory with several gravity assists and can be combined with low-thrust spherical shaping legs in between the gravity assists. The main part of the code in Python is spread across three files: a trajectory file, a problem file, and a utilities file.

The trajectory file is the main file which is run in order to perform the trajectory design and later also the trajectory optimization. Like with every Python file in this framework the file starts with imports of packages from Tudatpy as well as other Python packages and files within the framework. In this file the Solar System bodies are generated including the KBOs. The environment is made and the relevant settings such as the vehicle mass and specific impulse are set. Afterwards the settings for the specific trajectory are defined such as the departure time, time-of-flight, and flyby bodies. Based on these settings a so-called MGATrajectory object is made. This object-oriented programming (OOP) approach makes it easy to keep all results from a trajectory together to easily request and store them. Afterwards functions can be called to evaluate the trajectory. The functioning of the MGATrajectory object itself is done in the problem file.

The problem file defines and describes the MGATrajectory object class. The Python code for this thesis works with OOP where each instance of a trajectory is encapsulated by an MGATrajectory object. This object contains all the relevant variables for the trajectory and can be used to perform specific functions on the trajectory. A line from the trajectory file calls the problem file in order to make a new MGATrajectory object. The problem file defines functions for the MGATrajectory object such as the ability to get the trajectory parameters or the state history, to return the shaped trajectory or to calculate the values of the objectives for the trajectory. For the most part the problem file is simply a container for these functions. The actual implementation of the functions can be found in a third file, the utilities file.

The utilities file contains the implementation of the functions from the MGATrajectory class and also contains any other relevant functions for pre- or post-processing of the data. Functions to for example evaluate the trajectory, visualize the results, calculate the thrust profile, set up the body system in Tudat and many more can be found here. This thus results in a system with three files where the main trajectory file calls the problem file to produce MGATrajectory objects and the problem file then calls the utilities file for the implementation of functions for the MGATrajectory objects. To provide an overview of the capabilities and the relations of the main files all the functions present can be seen in Figure 5.1. For simplicity the inputs for the functions of the utilities file are omitted since many require a large portion or all of the variables of the MGATrajectory object. The numbers and letters behind each function indicate which other functions they call. After the greater-than-sign the returned variables are listed. If these variables are returned optionally based on settings of the function they are listed in italics. The working of each function and a more practical overview of how they link with each other when performing a calculation are discussed in Section 5.1.3.

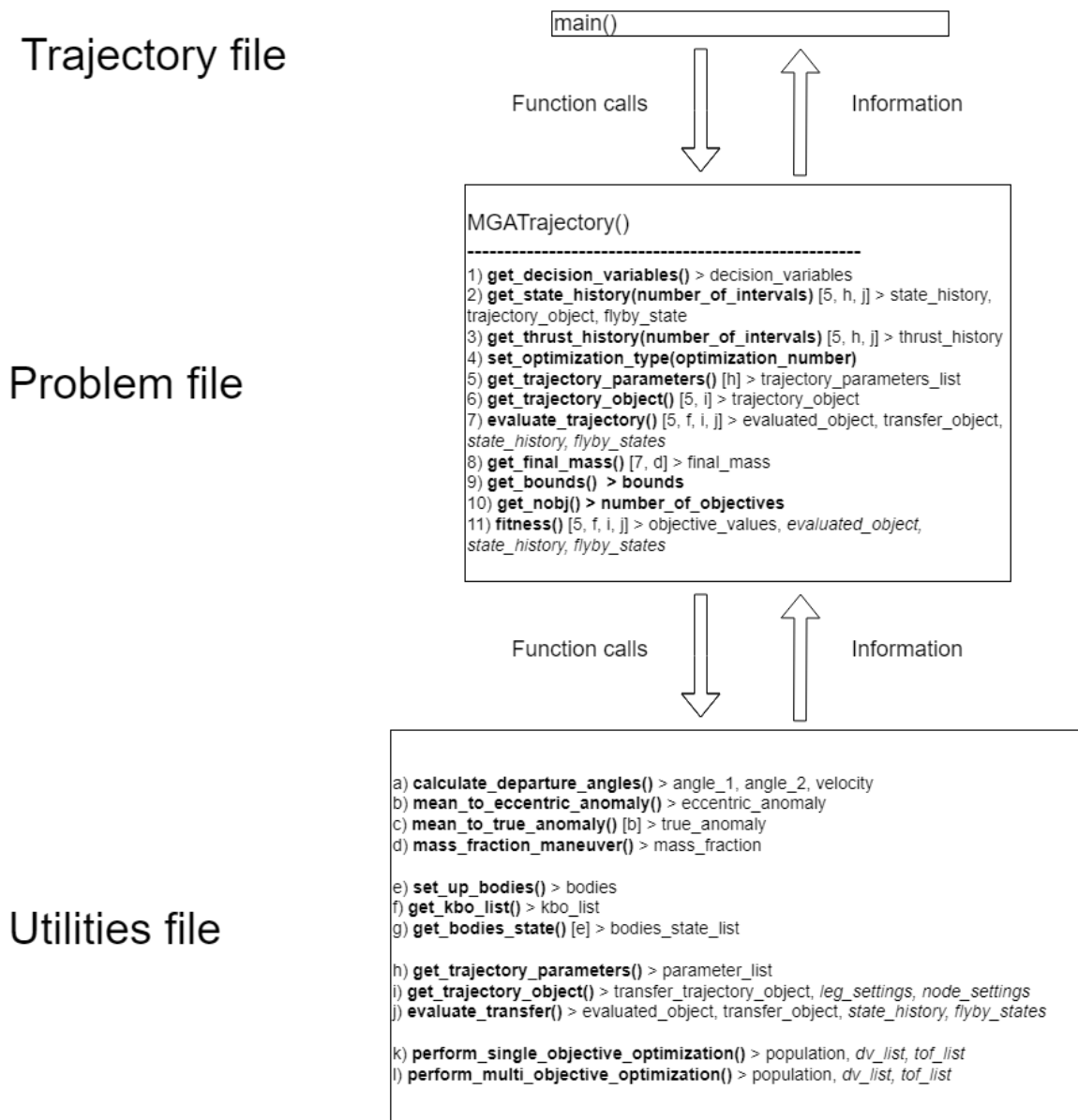


Figure 5.1: A schematic overview of the functions present in the different python files.

These three main files, however, are not the only ones that have been used for this thesis. Other relevant Python files are discussed in the next subsection.

5.1.2. Auxiliary files

Two other auxiliary files have been made for pre-processing purposes. The first of these is the KBO database file. It is used to gather the orbital elements of all the KBOs from MPC and to filter them based on the input settings. These input settings are the required uncertainty parameter, the maximum inclination or a manual list of KBOs to search for. A second file is made to interact with the JPL Horizon interface through Python to be able to request the tabulated ephemerides for all KBOs. Tabulated ephemerides were eventually not used during the thesis, but if this topic is picked up in further research this file could be used to get more detailed ephemerides.

In Figure 5.1 the main file is called the trajectory file. In reality there is not a single main file but instead there are many. This is done in order to group experiments by specific phases of the thesis. There is for example a tuning file used for trajectories during the optimizer tuning phase of the thesis. Similarly there are also separate files for the single KBO flyby analysis and the search for multiple KBO flybys.

Finally, two more files have been made with unit tests and system tests, respectively. Running these files causes all of the tests to be performed. Automatic assertions have been added such that it can quickly be seen whether any of the tests were to fail. A discussion of these tests follows in Section 5.2.

5.1.3. Calculation loop example

To illustrate the function of the different files and to provide an easy-to-follow overview of the trajectory design, this subsection will show how a trajectory can be calculated step-by-step. The model that has been made can work with both high-thrust (MGA or MGA-DSM) as well as low-thrust (MGA) trajectories. The trajectory in this example is a low-thrust spherical-shaping trajectory from Earth to Neptune with a gravity assist at Jupiter. The trajectory is designed in the main trajectory file. The list of steps follows below.

1. Import the relevant Python and Tudaipy modules as well as the functionalities from the problem and utility files and the SPICE kernels.
2. Set the vehicle and propellant settings: mass and specific impulse.
3. Set up the bodies by calling the `set_up_bodies` function from the utilities file.
4. Define the input values for the trajectory. These are the departure and arrival conditions (semi-major axis and eccentricity), which are both set to departure and arrival at the edge of the sphere of influence. This is hard-coded in the program by giving an infinite semi-major axis and an eccentricity of zero. Other input variables are the trajectory order (Earth, Jupiter, Neptune), a departure time, and two time-of-flight values, one for each leg.
5. Define the free parameters for the legs and nodes. These are the number of full revolutions per leg (set to zero for both legs), the departure velocity magnitude from Earth with two associated angles, the arrival velocity with two angles at Jupiter and Neptune, and the gravity-assist variables at Jupiter. If one wants to generate a random pool of input variables instead, a decision variable range array can be made which contains the lower and upper range of each of the decision variables. This is done during the initial population of the optimization phase of the project.
6. Generate the `MGATrajectory` object with all the information from the previous steps. The leg type should also be specified, which is a low-thrust spherical leg for this example.
7. Run the `evaluate_trajectory` function from the problem file. This function also gives the possibility to return, print, and plot the results. With this function the ΔV of the trajectory is calculated, split by each node and leg.
8. If desired other aspects of the trajectory can now be called through the problem file. This can be the state history, thrust history, trajectory parameters, trajectory object or final mass. For the optimization stage the fitness function is used to evaluate the trajectory. The optimization type, bounds, and number of objects (`nobj`) functions also relate to this optimization stage. If one wants the objective values of a single trajectory the fitness function in the problem file can be called.
9. The utilities file can also be called directly for a few functions. This can be done to calculate departure angles from certain planets (needed during optimization), convert between mean, true, and eccentric anomalies, to get the numbered list of KBOs and their states for post-processing and visualization, or to initiate an optimization algorithm.

Figure 5.2 shows a trajectory to Neptune with input values according to Table 5.1. Here the 'dep' and 'arr' subscripts stand for the departure and arrival conditions at the different planets. The specific input values are simply one of the intermediate results in the later optimization process. The total ΔV to reach the SOI of Neptune in this example is 11,418 m/s with a time-of-flight of 6530.6 days. The trajectories studied in this thesis start with a launch from Earth, followed by gravity assists with planets in the Solar System. Afterwards, one or more CFBs are performed in the Kuiper belt, where the gravitational impact of the KBOs on the spacecraft is neglected. A number of CFBs is performed as well as DFBs in between, the latter only being evaluated in post-processing. This results in a generic trajectory shape as indicated in Figure 5.3.

Table 5.1: An overview of the input variables for the example trajectory from Earth to Neptune by means of a gravity assist with Jupiter.

$t_{dep} = 14,948.44$ days	$V_{dep,E} = 2.06$ m/s	$V_{arr,J} = 6114.8$ m/s
$TOF_1 = 1208.72$ days	$\theta_{dep,E} = 0.988$ rad	$\theta_{arr,J} = 2.826$ rad
$TOF_2 = 5321.85$ days	$\phi_{dep,E} = 0.906$ rad	$\phi_{arr,J} = 0.0385$ rad

$r_p = 151,431$ km	$V_{arr,N} = 7825.9$ m/s
$\alpha = -1.357$ rad	$\theta_{arr,N} = 4.425$ rad
$\Delta V_{ga} = 0$ m/s	$\phi_{arr,N} = 0.107$ rad

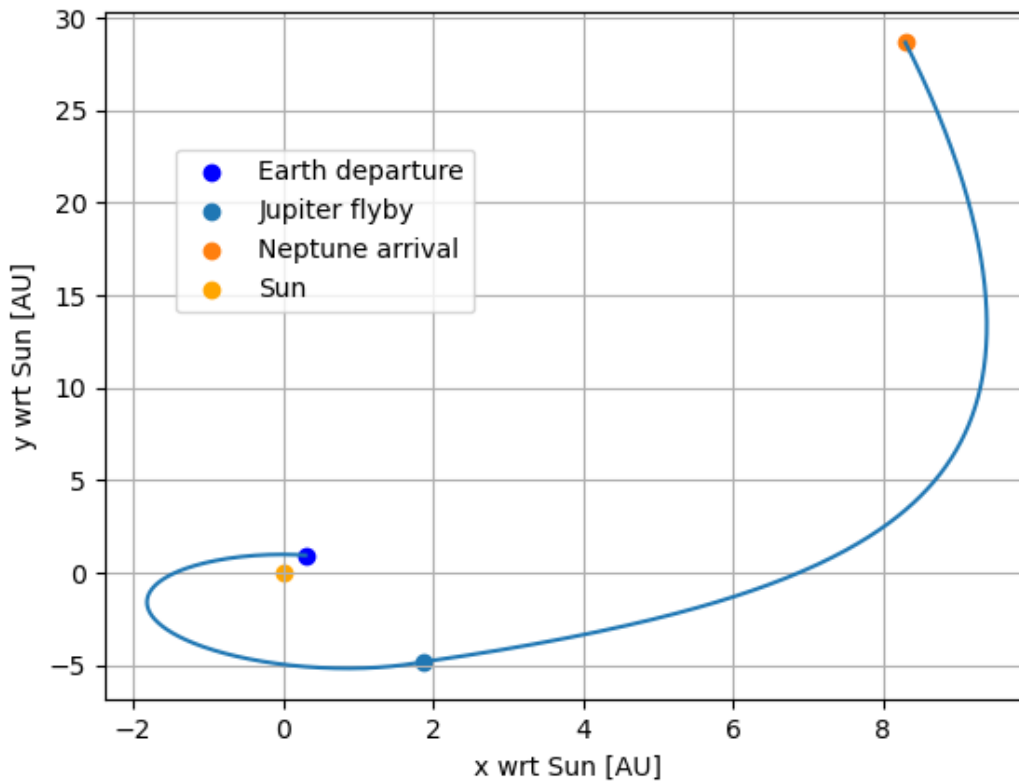


Figure 5.2: A 2D representation of the test trajectory from Earth to Neptune via Jupiter. Note that the axes in this figure are not equally scaled.

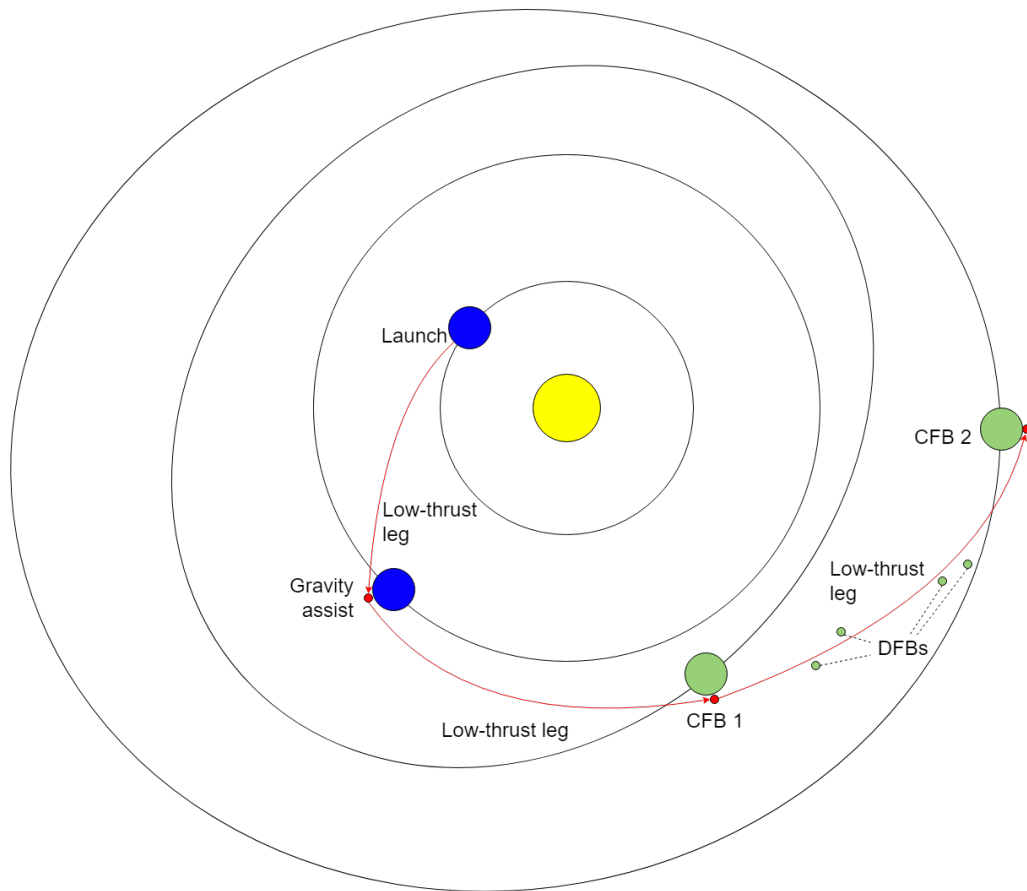


Figure 5.3: A schematic overview of a Kuiper belt trajectory which will be studied during this thesis. The yellow circle indicates the Sun, the blue circles planets in the Solar System, and the green circles KBOs.

5.1.4. C++ adjustments

While the majority of the analyses in this thesis project is done using the Python interface, some small changes also had to be made to the C++ code in order to get the functions to work as intended. These adjustments are discussed in this subsection.

The main adjustment made to C++ is the possibility to retrieve and test the value of the a_2 variable in the spherical-shaping algorithm. As explained in Chapter 4, this variable is used to make sure the time-of-flight of the trajectory matches the input. During the analysis it was found that sometimes the a_2 root finder does not find a solution at all or that it might converge to different roots depending on its starting value and search range. These different roots result in vastly different objective values. Therefore, the C++ code in Tudat is adjusted to allow the user to calculate the time-of-flight based on the a_2 value. In this way plots of the time-of-flight as a function of a_2 can be made. The implementation during this thesis only allows one to calculate the a_2 function if at least one value can be found by the user for which the trajectory is feasible so with a positive value for the D function. If this is not the case the a_2 function can not be returned. To increase understanding of this function it is recommended to add the functionality to always be able to view the a_2 value in future research.

The other addition, related to the previous paragraph, is the possibility to look at data from separate legs in an MGA low-thrust trajectory. This is a prerequisite to get to the a_2 value since it is a unique value for each trajectory leg.

5.1.5. Launch implementation

The previous subsections explained the general working of the code system. Now each phase of the trajectory is shortly discussed in terms of its implementation in Tudat.

The first phase of the trajectory is the launch. This launch will not be modelled in detail. Instead the trajectory design is initiated at the edge of the sphere of influence of the initial departure body (Earth) with a specified outgoing excess velocity vector at departure $\mathbf{V}_{\infty,dep}$. The magnitude of this launch velocity is directly related to the maximum mass that can be brought on-board of the mission as was already shown in Chapter 3. Together with this magnitude the in- and out-of-plane outgoing angles at departure θ_{dep} and ϕ_{dep} , respectively, are required. The range for θ runs from 0 to 2π while the range of ϕ runs from -0.5π to 0.5π . The angles are defined by the spacecraft velocity relative to the departure planet in the ECLIPJ2000 system.

5.1.6. Trajectory leg implementation

Each trajectory leg of the mission consists of a low-thrust spherical-shaping arc. Only the launch arc requires the velocity vector to be given at the start of the leg. For all the other legs the required inputs are listed below and are given as of arrival at a celestial body.

- $V_{\infty,arr}$ = the incoming excess velocity magnitude upon entering the upcoming flyby, at the end of the leg.
- θ_{arr} = the in-plane angle of the velocity vector upon entering the upcoming flyby, at the end of the leg.
- ϕ_{arr} = the out-of-plane angle of the velocity vector upon entering the upcoming flyby, at the end of the leg.
- t_f/TOF = the time-of-flight of the leg to the body.

The two angles are relative to the planet the spacecraft is approaching. The end of the leg corresponds to the gravity assist with the upcoming (planetary) body.

5.1.7. Gravity assist and flyby implementation

Every leg which ends at a planet will then be directly followed by a gravity assist. While in reality the gravity assist is a dynamic process, the maneuver will be considered instantaneous for the purposes of this thesis. During a gravity assist the spacecraft approaches the planet up to a pericenter distance r_p , which results in an asymptotic bending angle α of the spacecraft trajectory. During the gravity assist there is a possibility to perform a high-thrust corrective maneuver ΔV_{ga} , which makes the gravity assist a 'powered assist'. This last variable is not considered during this thesis and is set to zero. These parameters then fully define the velocity vector of the outgoing leg of the gravity assist.

5.1.8. Kuiper belt flyby implementation

The main difference between Kuiper belt flybys and planetary flybys in this thesis is that the mass of KBOs is neglected. Furthermore, the velocity vector at the start of the subsequent leg is set as identical to the vector at the end of the previous leg. This ensures that the Kuiper belt flyby functions merely as a node for the trajectory instead of being affected by the KBO itself. The thrust profile does change after the KBO flyby as a new trajectory leg begins. For the purposes of this thesis the KBO is given a negligible mass with a μ value of $1 \text{ m}^3/\text{s}^2$ and the spacecraft approaches the KBO up to one million km with an α value of 0 rad. This ensures that the KBO does not affect the trajectory and the one million km offset is a negligible error margin at this preliminary design stage and is assumed to equal an overlap of the CFB trajectory. For future research it is recommended to add a new type of leg in the C++ framework of Tudat: a leg to a certain location at a certain time (based on the ephemerides of the KBO), but with no specific action such as a gravity assist at the end of this leg.

5.2. Verification

One final step which needs to be performed before the actual research problem can be tackled is verification and validation. Verification makes sure that the code and mathematical framework behaves as expected and is implemented without errors. Validation ensures that the same code and framework is

not only behaving as expected, but also accurately replicates the reality that it attempts to model. The section starts with a discussion of thrust profile checks. Afterwards, system tests using ESA's Global Trajectory Optimization Problems (GTOP) database and low-thrust trajectories are discussed. At the end of the chapter possibilities for validation are also mentioned.

In order to verify the code, unit tests have been implemented for every written function. Many of these verification checks are trivial and not useful going over in the main body of the thesis. In the end all unit verification tests are passed. An overview of the unit tests performed is given in Appendix A.

5.2.1. Thrust profile checks

This subsection looks at logic checks of the thrust-profile generation for low-thrust trajectories. This way it can be confirmed whether the thrust behavior of spherical shaping is as expected. Similar tests have already been performed in detail by T. Roegiers in a previous thesis [106]. However, due to the updates made to Tudat since then and for completeness in this thesis, a somewhat similar but reduced set of checks is shown in this report. The checks are split into 2D trajectories (without an inclination change) and 3D trajectories.

2D trajectories

Two different types of 2D trajectories were tested. The first one is a shaping trajectory with the same start and end orbit, including phasing. In practice this means a 'transfer' from a 1 AU orbit to the same 1 AU orbit some time in the future. Since the trajectory does not change it is thus expected that no ΔV is required to fly this trajectory as the transfer corresponds to natural phasing of the orbit. This test is performed for orbits with an inclination of 0 degrees and orbits which both have an inclination of 10 degrees. Both of these trajectories are performed with a fixed time-of-flight of 100 days and 0 full revolutions. The trajectory starts and ends at the edge of a sphere of influence of a fictional body with a perfect circular Kepler orbit with a semi-major axis of 1 AU. Since patched conics are used the gravitational parameter of this body is not important for the simulation and has been set to $1 \text{ m}^3/\text{s}^2$. The thrust profiles for these two trajectories can be seen in Figures 5.4 and 5.5. This thrust is split up into tangential (u_t), normal (u_n), and out-of-plane (u_h) components.

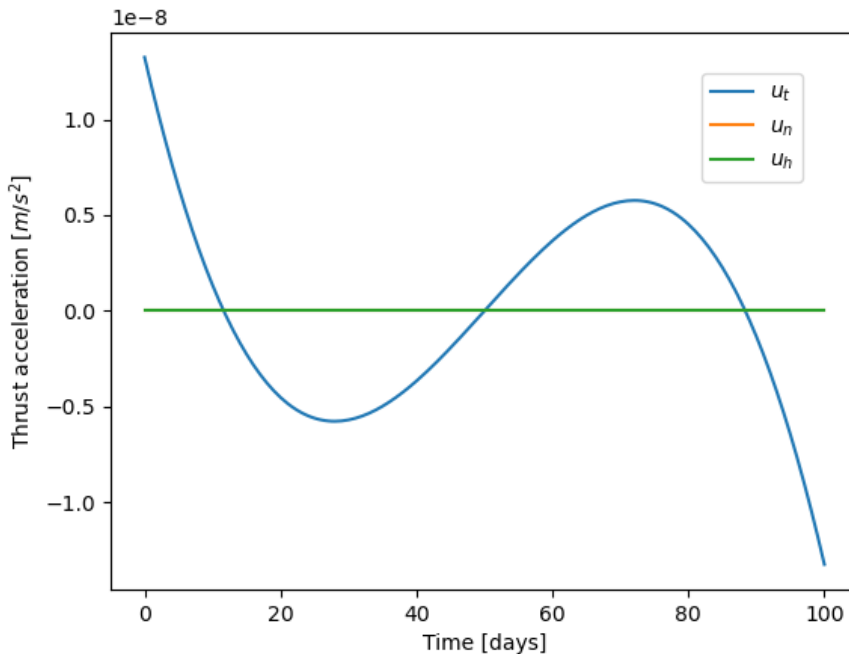


Figure 5.4: The tangential, normal, and out-of-plane thrust acceleration for a circular trajectory with a start and end position 1 AU from the Sun and a constant inclination of 0 degrees.

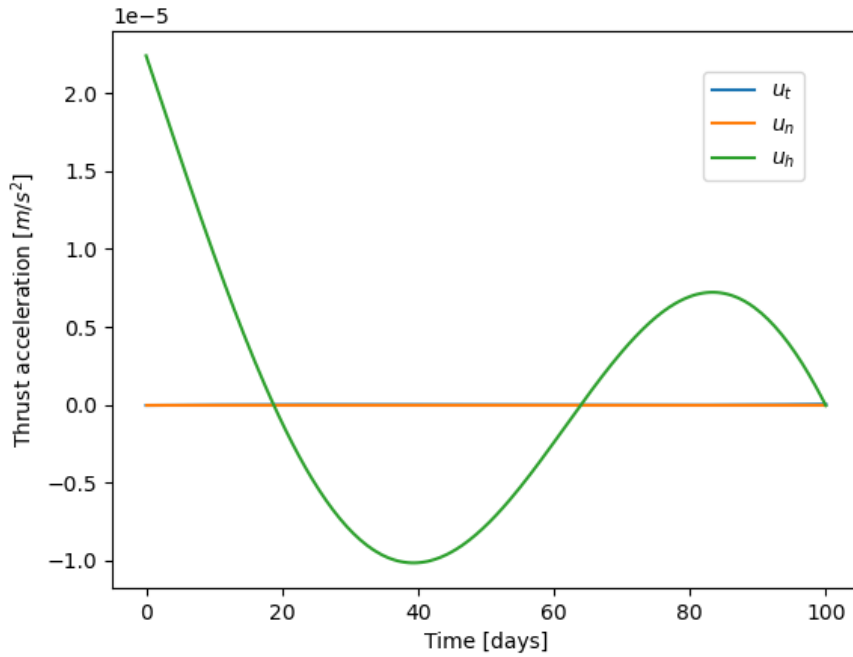


Figure 5.5: The tangential, normal, and out-of-plane thrust acceleration for a circular trajectory with a start and end position 1 AU from the Sun and a constant inclination of 10 degrees.

In order to shape the time evolution u_n is always set to zero for spherical shaping calculations in Tudat. For the theoretical background of this decision see the work of T. Roegiers [106]. The only value for u_n which can remain is a machine error in the order of 10^{-18} m/s 2 and this is indeed what is found for u_n in both plots. It is expected that the out-of-plane thrust acceleration u_h is zero for both cases since there is no change in inclination. u_h is indeed zero for the case with a constant 0 degrees inclination, but it is non-zero in the case with a constant inclination of 10 degrees. Such behavior has already been documented in previous verification of the Tudat spherical-shaping software and is related to the inherent inability of the implemented version of spherical shaping to provide a perfect representation of inclined trajectories [106]. For the purposes of this thesis the errors due to the inclination are ignored and target bodies with an inclination deemed too large are not included in the nominal description.

Furthermore, one would expect the trajectories to have a ΔV of 0 m/s since they stay on their original trajectory. The inclined orbit has a ΔV of 56.4 m/s, caused by the aforementioned inclination inaccuracy of spherical shaping. However, the 0 degrees inclination trajectory also has a non-zero, albeit smaller, ΔV of 0.04 m/s. It is caused by a non-zero tangential thrust value u_t . This can be caused by a variety of reasons such as small rounding deviations in the calculation process or minor differences between body settings such as the gravitational parameter. The precise cause for this error has not been found, but due to its small size it is deemed sufficiently verified for the purposes of this thesis.

A final 2D test is a trajectory with a constant 0 degrees inclination, but this time with a transfer from a circular 1 AU orbit to a circular 3 AU orbit. The thrust profile for this trajectory as well as the trajectory shape can be found in Figures 5.6 and 5.7, respectively. A time-of-flight of 575 days is used for this trajectory, even though the precise value is not relevant, as long as it results in a feasible trajectory, since it is an unoptimized problem. Once again u_n and u_h are zero, excluding machine errors. Since it is a planar problem the thrust is fully defined by the tangential parameter u_t , which peaks at roughly 100 days and then switches sign. When looking at the trajectory shape as shown in Figure 5.7 this makes sense. At this point of roughly 100 days the trajectory reaches its closest point to the Sun.

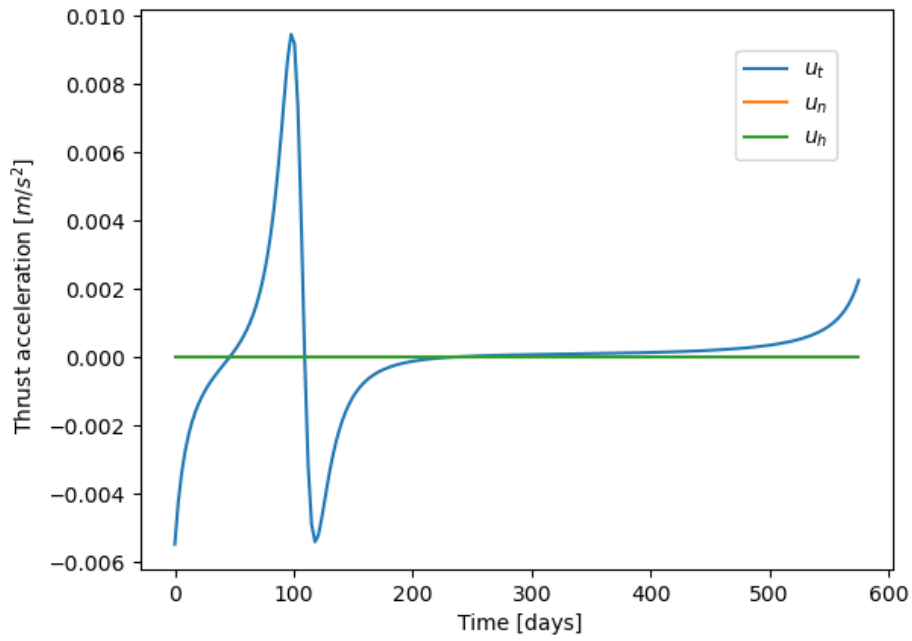


Figure 5.6: The tangential, normal, and out-of-plane thrust acceleration for a transfer trajectory which starts at a circular trajectory at 1 AU and ends at a circular trajectory of 3 AU. The time-of-flight for this trajectory is 575 days.

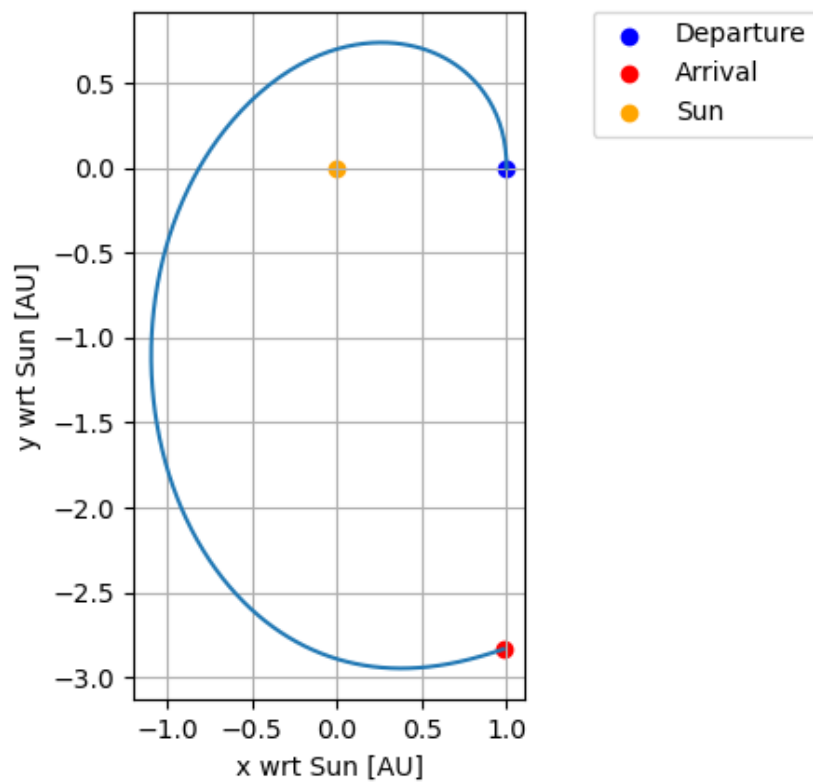


Figure 5.7: The trajectory shape for an orbit transfer from 1 AU to 3 AU.

3D trajectories

All test trajectories so far only concern planar trajectories. The transfers in this paragraph require an inclination change. This is done for the 1 AU to 1 AU trajectory as well as for the trajectory from 1 to 3 AU. In both cases the trajectory starts at an inclination of 0 degrees and ends with an inclination of 10 degrees. The 1 AU to 1 AU has a time-of-flight of 100 days, while the 1 AU to 3 AU trajectory has a time-of-flight of 575 days. The thrust profiles for both trajectories are shown in Figures 5.8 and 5.9, respectively.

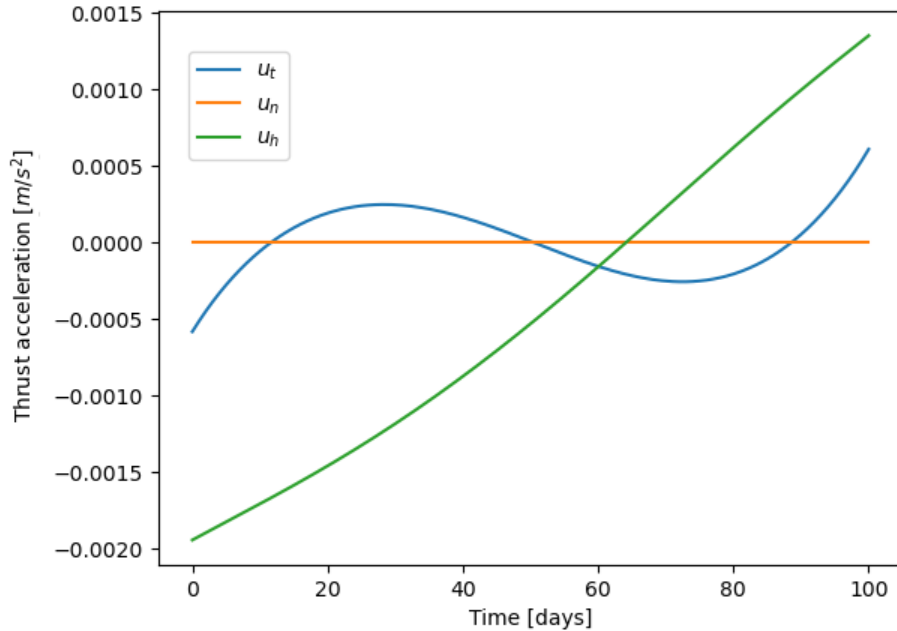


Figure 5.8: The tangential, normal, and out-of-plane thrust acceleration for a circular low-thrust trajectory with a start and end position 1 AU from the Sun and an inclination change from 0 to 10 degrees.

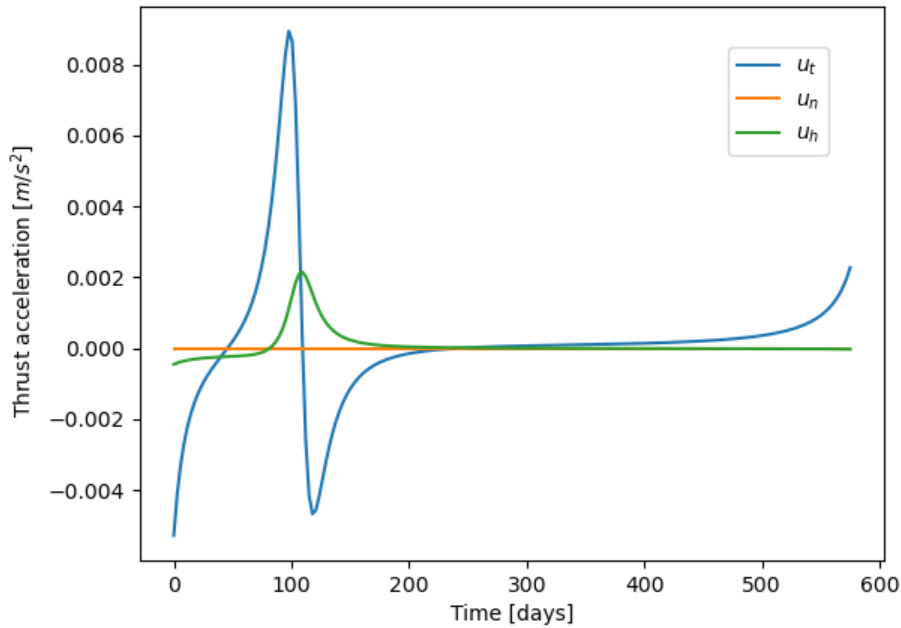


Figure 5.9: The tangential, normal, and out-of-plane thrust acceleration for a circular low-thrust trajectory with a start position at 1 AU, an end position at 3 AU, and an inclination change from 0 to 10 degrees.

In both cases u_n is once again zero, as expected. This time there is also a significant u_h component due to the inclination change. The peak value of u_h is in the same order of magnitude for both trajectories, which is expected since both have an inclination change of 10 degrees. Since the 1 to 3 AU trajectory also requires a large semi-major axis change it is expected that here the u_t component is dominant. Note that the u_h peak in Figure 5.9 is reached around the same time as the periapsis of the trajectory. This makes it an inefficient inclination change, since these type of out-of-plane maneuvers are most effective as far from the central body as possible. However, as already mentioned this is not an optimized trajectory. With all the inputs provided there is only one solution for the spherical-shaping algorithm, which in this case results in a feasible albeit inefficient thrust profile. With these tests, the thrust of the spherical shaping algorithm has been checked.

5.2.2. GTOP verification

Another method to verify the working of the code when designing trajectories is to make use of ESA's GTOP database [28]. All of these problems only regard high-thrust MGA or MGA-DSM problems. GTOP does not contain any low-thrust problems. While this test will thus not be sufficient to test the low-thrust trajectory design function, all the other functions that do not regard the thrust calculation during the trajectory legs should still work the same with high- and low-thrust missions. So by checking the working of these GTOP problems the code can still partially be verified. In these paragraphs it is checked whether filling in the correct decision variables gives the same output for the objectives.

In total three high-thrust GTOP problems are tested: Cassini 1, Messenger (reduced) and Cassini 2. Cassini 1 represents a high-thrust MGA problem to Saturn with multiple gravity assists and no DSMs. Messenger and Cassini 2 on the other hand do use DSMs. This means that for Cassini 1 the only variables are the departure time and the time-of-flight values between the different planets. For the other two trajectories the DSM fraction is required as well as the periapsis distance and bending angle for each gravity assist. All these trajectories only consider unpowered gravity assists. In all tests the only objective is to lower the ΔV as much as possible. The optimal values for the optimization problem, as far as they are known, are posted on the GTOP website and have been taken as the input values for this verification test [28]. Table 5.2 shows the resulting ΔV if this trajectory is implemented in Tudat as well as the relative fractional error ϵ with the official value posted by GTOP. An example of one of the trajectories, specifically Cassini 2, is shown in Figure 5.10.

Table 5.2: An overview of the ΔV results for the tested GTOP trajectories when calculated with a Tudat patched-conics method. The resulting ΔV is compared to the value posted by GTOP and the relative fractional difference between the two values is shown. The test is performed with the standard Tudat ephemerides and the updated DE440 ephemerides. The data for the GTOP results are taken from [28]. * = No higher significance value is available.

Test	GTOP ΔV [m/s]	Tudat ΔV [m/s]	Rel. ϵ [-]	Tudat ΔV (DE440) [m/s]	Rel. ϵ [-]
Cassini 1	4930.7*	4930.633	$\approx 1 * 10^{-5}$	103,639.6	20
Messenger	8630.832	8630.854	$2.5 * 10^{-6}$	24,323.85	1.8
Cassini 2	8383.184	8700.970	$3.8 * 10^{-2}$	17,695.16	1.1

The relative error of the ΔV in Tudat compared to GTOP ranges from the order 10^{-6} to 10^{-2} . These errors are in the same order of magnitude as the verification tests by L. van der Heyden whose relative errors were $1.6 * 10^{-3}$ for Messenger and $3.2 * 10^{-2}$ for Cassini 2 [43]. Still it should be noted that the relative error of roughly 3.8% for Cassini 2 could be considered quite high for a verification test. Here it is important to note the difference between the Tudat tests and the GTOP tests. There is a slight deviation between the ephemerides used by Tudat and by GTOP. This was spotted by L. van der Heyden and P. Musegaas during their verification tests [43] [63]. Specifically, the z-coordinate of the planets has a large impact on the Lambert targeter and thus the optimal solution. Verification tests by P. Musegaas have shown that using the GTOP ephemerides gets rid of the majority of these errors [63]. Since the Tudat ephemerides are more accurate than the GTOP ephemerides this is not considered an issue.

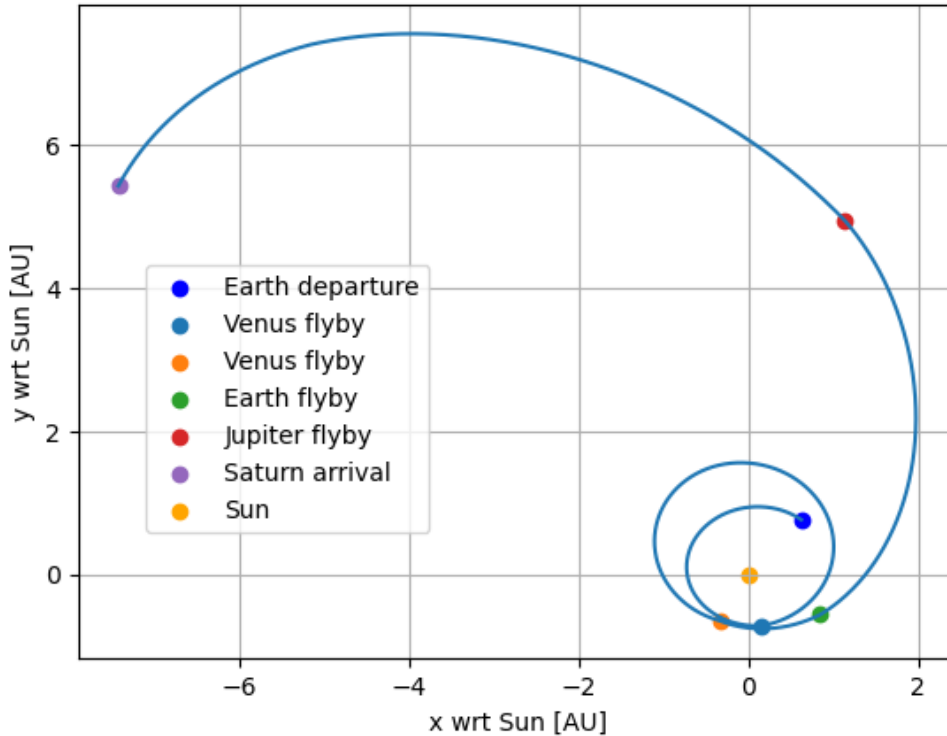


Figure 5.10: An overview of the optimal trajectory for the Cassini 2 GTOP problem as modelled by Tudat code.

The final two columns of Table 5.2 use a more accurate ephemeris based on the DE440 data. This results in relative fractional errors larger than 1 and increases the ΔV to unrealistic levels, in the most extreme case for Cassini 1 a value above 100 km/s. Like before, this is caused by the high sensitivity of the Lambert targeter to relatively small changes in the coordinates of the planets. It is not the case that the actual optima for these trajectories are found at wildly different input values. If a 5% margin is put on an untuned single-objective differential evolution (DE) optimizer around the decision variables for these problems then the optima are found at nearly exactly the same decision variables as with GTOP. In the case of Cassini 1 an even lower optimal ΔV of 4734 m/s is found. This improved ΔV is only possible due to the slightly different arrangement of the planets in the DE440 ephemerides. A similar result is obtained for the Messenger and Cassini 2 examples where the optimal found ΔV are 9140 m/s and 8730 m/s, respectively. Thus, while the precise input values from GTOP give very different results, this sanity check is sufficient to verify the updated ephemerides as well.

5.2.3. Low-thrust verification

Besides the high-thrust system tests, multiple low-thrust trajectories are tested as well. GTOP does not contain any low-thrust examples and thus these tests have to be taken from another source. T. Roegiers mentions four rendezvous low-thrust test cases which will also be used in this thesis to verify the code: Earth-Mars, Earth-Neptune, Earth-1989ML, and Earth-Tempel-1 [106]. These tests were initially formulated in work by D. Novak [91].

Like with the high-thrust examples the optimal values found by the grid search by T. Roegiers are directly used as inputs [106] and these verification tests thus serve to verify the trajectory design module. The only objective in these cases is ΔV . The results for the missions to Mars and Neptune are given in Table 5.3. The relative errors range from 10^{-2} to 10^{-4} and are thus similar in terms of their order of magnitude as the high-thrust examples. The slightly larger errors for the DE440 ephemerides are most likely caused by the difference in ephemerides while the error in the regular Tudat ephemerides is dominated by errors due to the different integration settings for the semi-analytical leg calculation

as well as updates to Tudat since T. Roegier's tests. Since the order of magnitude is similar to the high-thrust cases these verification tests are also passed.

Table 5.3: An overview of the ΔV results for the tested low-thrust trajectories when calculated with a Tudat patched-conics method. The resulting ΔV is compared to the optimal value found by T. Roegiers [106] and the relative fractional difference between the two values is shown. The different notation styles for the ΔV are due to the fact that not more significant digits are available for T. Roegiers' data.

Target	T. Roegiers ΔV [m/s]	Tudat ΔV [m/s]	Rel. ϵ [-]	Tudat ΔV (DE440) [m/s]	Rel. ϵ [-]
Mars	$5.70 * 10^3$	5698.368	$\approx 3 * 10^{-4}$	5702.189	$\approx 4 * 10^{-4}$
Neptune	$1.548 * 10^4$	15,281.83	$\approx 1 * 10^{-2}$	15,141.26	$\approx 2 * 10^{-2}$

For the examples to the asteroid 1989ML and the comet Tempel-1 slightly more explanation is required. The ephemerides of 1989ML and Tempel-1 are not available in Tudat or in DE440. This means that the two bodies should be added in a similar manner as the KBOs. This can be done by using the Kepler elements of the bodies or by using tabulated ephemerides from the JPL Horizon interface. Since both bodies are located within the inner Solar System they are highly perturbed by other planets and thus the tabulated ephemerides are used for this verification test. The results for the test are shown in Table 5.4. The Tempel-1 trajectory results in a very similar ΔV as was found by T. Roegiers. For 1989ML no trajectory is found with the input parameters from T. Roegiers. This could be related to the high sensitivity of low-thrust trajectory design to differences in the input. Therefore, a local search (LS) is performed with the decision variables within 10 % of the optima by T. Roegiers. This results in a stable optimum with a ΔV very similar to the one found by T. Roegiers. Based on these tests the trajectory design capabilities, both using high- and low-thrust trajectories, are considered verified.

No low-thrust trajectories to the Kuiper belt have ever flown, making it difficult to perform a validation test. Furthermore, trajectories by low-thrust missions such as Dawn are so atypical that they will not fit in the spherical-shaping format anyways. However, since the tests above are based on proposed and realistic flybys and have previously been checked with already validated tools, the passing of these tests is also considered to be validation for the code of this thesis. Other flybys which could be used for tests in subsequent research include trajectories from other papers such as the high-thrust mission to Huya and Quaoar [47].

Table 5.4: An overview of the ΔV results for the tested low-thrust trajectories with 1989ML and Tempel-1 when calculated with a Tudat patched-conics method. The resulting ΔV is compared to the optimal value found by T. Roegiers [106] and the relative fractional difference between the two values is shown. The different notation styles for the ΔV are due to the fact that not more significant digits are available for T. Roegiers' data.

Target	T. Roegiers ΔV [m/s]	Tudat ΔV [m/s]	Rel. ϵ [-]	LS ΔV [m/s]	Rel. ϵ [-]
1989ML	$4.53 * 10^3$	-	-	4705.587	$\approx 4 * 10^{-2}$
Tempel-1	$1.151 * 10^4$	11,487.10	$\approx 2 * 10^{-3}$	-	-

5.3. Summary

This chapter provides an overview of the software implementation of the trajectory design for this thesis. The main model for this thesis consists of three files: a trajectory, problem and utilities file which interact with each other to create MGATrajectory objects. Another file takes care of the data from the KBO database from MPC. An example of a trajectory calculation loop shows the inner workings and the links between these different files. An overview of the implementation of the different trajectory elements (launch, trajectory leg, gravity assist, KBO flyby) is also provided.

Afterwards, the code is verified by means of unit tests and system tests. The system tests regard checks of the thrust profile in both 2D and 3D trajectories. Furthermore, tests with GTOP problems are done to verify the core of the system while example flybys to Mars, Neptune, 1989ML, and Tempel-1 verify the low-thrust and custom body addition sections of the code.

Optimizer theory and tuning

As was shown at the end of Chapter 3 the first step of the research process is to tune the optimizer for the low-thrust trajectories. To do this an optimizer first needs to be selected. This is done in the first section of this chapter. Afterwards, a brief overview of the theory of the optimizer is given and the parameters of the optimizer are discussed. This is followed by the tuning process, which is split in tuning for high-thrust and low-thrust. The reason why high-thrust tuning is still required, despite this thesis investigating low-thrust trajectories, is discussed in the respective section.

6.1. Optimizer selection

As mentioned in Chapter 3 two objectives, ΔV and time-of-flight, are optimized. Ignoring the option to combine them in a single objective, this necessitates a multi-objective optimizer. The result of such a two-objective optimization process is a Pareto front of which a generic example is given in Figure 6.1. The members which are closest to the lower-left side of the curve together form the final Pareto front of optimal members. For this thesis the entire Pareto front is shown, but the trajectory with the lowest ΔV on the front is chosen as the option to continue with in further analysis as ΔV is considered to be the leading objective, essential creating a single-objective optimization. In further research other Pareto optimal elements can be chosen as well based on a more detailed trade-off between ΔV and time-of-flight.

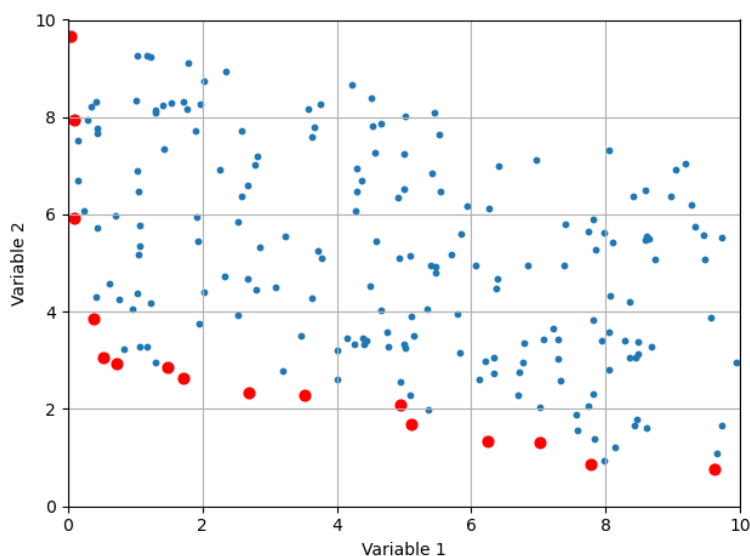


Figure 6.1: A generic example of a Pareto front with two objectives. The individuals along the optimal front within the figure are shown in red with larger markers.

A global optimizer is required since the optimum of the thesis or even its rough placement within the input space is unknown as of yet. The first decision to be made regards the type of global optimizer: enumerative, calculus-based, or heuristic [109]. Due to the complexity of the low-thrust optimization problem an enumerative method such as a grid search or Monte Carlo search is not used. Due to the lack of a strong initial estimate and of a closed mathematical description of the problem a calculus-based method is also not selected. This leaves a heuristic optimizer. A heuristic optimizer explores the design space with the intent to converge to an optimum in that space over time [22]. Heuristic algorithms are particularly favored for problems with an unknown input and solution space [55]. For these reasons a heuristic optimizer is chosen for this thesis.

There are many multi-objective heuristic optimizers to choose from. The package from Python which is used for this thesis is PyGMO (derived from PaGMO2) [12]. The five multi-objective heuristic optimizers in PyGMO are: non-dominated sorting genetic algorithm (NSGA2), multi-objective evolutionary algorithm with decomposition (MOEA/D), multi-objective hypervolume-based ant colony optimizer (MHACO), non-dominated sorting particle swarm optimizer (NSPSO), and improved harmony search (IHS) [12]. Analyses of multi-objective Pareto fronts show that the MOEA/D algorithm performs the best for complex Pareto fronts [53] [130], beating the previous best performing model NSGA2. Due to the many KBO targets and large number of variables it is expected that the Pareto fronts will be non-trivially shaped. For this reason MOEA/D is chosen as the optimizer in this thesis. Only the so-called island version of the optimizer is used. The alternative would be an archipelago version where multiple islands of optimized results are present and members of a population can migrate between them [9]. While this could result in improved results, it was not possible to implement this within the time span of the thesis and is instead recommended for future research.

6.2. MOEA/D theory

The optimizer used during this thesis is thus MOEA/D. MOEA/D is an evolutionary optimizer [130]. This means that a population evolves through a number of generations with the goal that each subsequent generation gets closer to the optimum objective value. The evolution of each generation is influenced by typical evolutionary algorithm concepts such as selection, crossover, and mutation [10]. As the name implies, MOEA/D makes use of decomposition to optimize a problem. This means that the problem is split up into multiple scalar single-objective sub-problems which are solved at the same time and whose results influence each other [130]. This influence of the different problems on each other depends on the neighborhood variable of the algorithm. Weight vectors are used to decompose the problem and optimization along each weight vector is tackled as a separate problem. The weight vectors for MOEA/D are visualized in Figure 6.2 [48]. The dots in the figure indicate solutions of the weight vector which form in clouds around the weight vectors, called membranes [48]. The black dots are solutions which are found with multiple weight vectors.

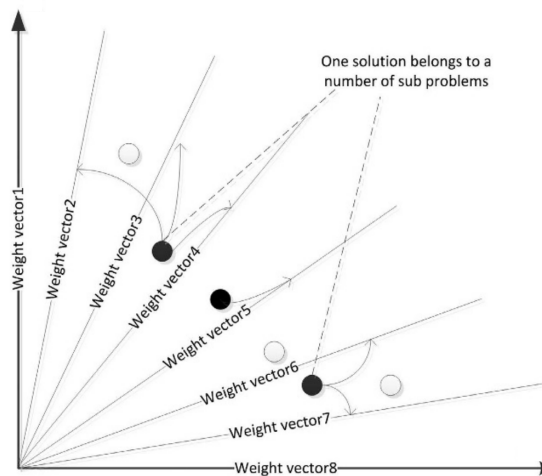


Figure 6.2: The solution method by means of weight vectors for the MOEA/D algorithm [48].

MOEA/D itself only describes the decomposition of the problem. To evolve the population towards the optimum through multiple generations another optimizer is used. MOEA/D uses differential evolution (DE) for this [13]. Differential evolution works by adding weighted differences between two population vectors to create mutated vectors. Each vector contains the parameters that are to be optimized. The mutated vector is then added to another third vector, the target vector, to create the trial vector. It is then checked whether the trial vector improves the objective function or not. If so, this trial vector replaces the old vector [116].

The optimization function is included as one of the functions in the Utilities file, previously mentioned in Chapter 5. The code works by initializing a population with the given population size and evolving this population for the number of generations given. The data is stored with a population list and a fitness list. After the final population the fitness values are returned to the user. The implementation of the optimizer is taken care of by the PyGMO module in Python. The MOEA/D optimizer is initialized with certain values for the optimizer parameters, which are discussed in the next section.

6.3. Optimizer parameters

The MOEA/D algorithm has multiple parameters which can be tweaked to optimize its performance for different types of problems. These settings are listed in Table 6.1 and are explained afterwards in more detail. The information in the table is derived from [11].

Table 6.1: An overview of the different settings for the MOEA/D optimizer as listed by Pygmo. A short definition of the setting is given as well as the nominal value used by Pygmo [11].

Setting	Definition	Default
Generations	Number of optimization cycles	1
Population size	Number of members in one generation	-
Weight generation	Method by which the weights are generated	Grid
Decomposition method	Method by which a multi-objective problem is decomposed to a scalar objective	Tchebycheff
Neighbourhood size (T)	Size of the weight's neighborhood	20
Cross-over rate (CR)	The rate at which cross-overs between population members occur, used for the DE operator	1
Scale factor (F)	Scaling factor for the DE operator	0.5
Distribution index (η_m)	Distribution index used by the polynomial mutation	20
Diversity preservation (Realb)	Chance that the neighbourhood is used instead of the entire population	0.9
Seed	Value to initialize quasi-random numbers	-
Preserve diversity	When "true" it activates diversity preservation	True
Limit	Maximum copies reinserted in the population	2
Verbosity	Frequency with which logs are printed	0

Some of the settings are fairly self-explanatory. As was already discussed before, MOEA/D is an evolutionary algorithm and thus requires a number of generations which have a certain population size and a specific seed to initialize it. There are different methods which can be used to generate the weights used during the decomposition. These are a regular-grid method, a random method or a low-discrepancy method [11]. For the decomposition method itself the following options are available: Tchebycheff, weighted, and boundary intersection (BI). The theory of these different options is quite extensive and not covered in this thesis, but can be read about in the original MOEA/D paper [130].

The neighborhood size relates to the number of close-by population members which can influence each other. A neighborhood with size four is shown in Figure 6.3 [59]. The cross-over rate is the chance with which mutant vectors are generated in the DE algorithm. The weight of the difference between the two original vectors used for the generation of these mutant vectors is given by the scale factor F. The distribution index affects the recombination during the mutation process where larger values correspond to mutated members which are further removed from the original members [40].

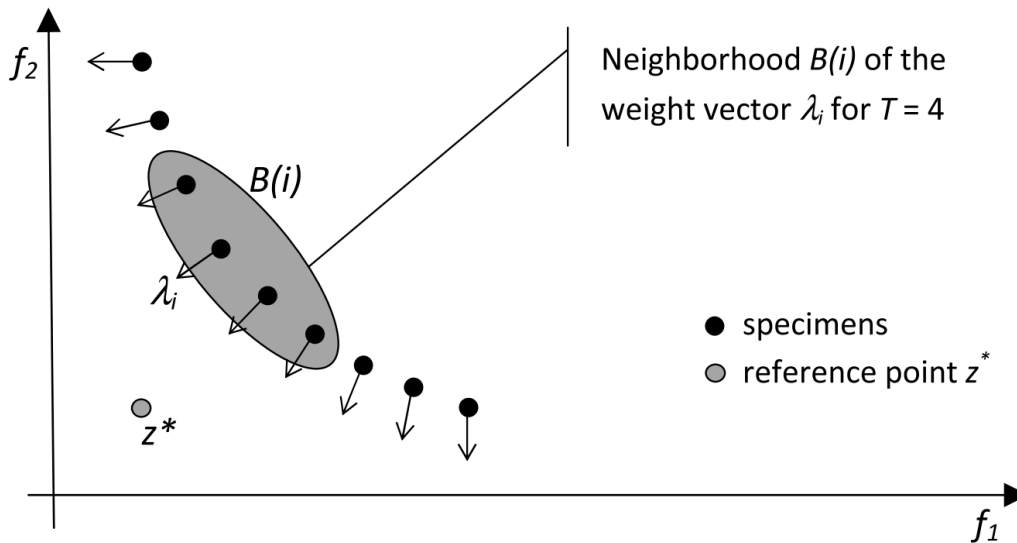


Figure 6.3: A schematic overview of the neighborhood concept for MOEA/D in case of $T = 4$ [59].

The diversity preservation setting determines the chance that the members can mutate with members which are only inside their own neighborhood or with members from the whole population. Whether this parameter is used at all is determined by the Boolean setting called preserve diversity. The limit setting determines how many copies can be directly reinserted in the population without mutation. Finally, verbosity regards whether logs about the state of the population are printed for the user. Since it is purely a setting for the user it is not mentioned again during the tuning process.

6.4. Optimizer tuning for high-thrust trajectories

Before the optimization process can be performed the previously mentioned settings first need to be tuned. The tuning process, just like the rest of the research, is performed with two objectives: ΔV and TOF. Here ΔV is considered the leading objective, but TOF and the shape of the resulting Pareto fronts are also taken into account during the decision-making process.

The first step is to tune the settings of the optimizer for high-thrust benchmark trajectories. Even though high-thrust trajectories are not used in the problem description of this thesis, it is still a good point to start. This is because it can provide a good initial guess for the optimizer settings for the later tuning of the low-thrust trajectories. Furthermore, previous theses such as the one by L. van der Heyden [43] have already tuned optimizers for high-thrust trajectories and that makes it thus easier to compare and to make sure that comparable results are obtained. This will thus also function as verification of the tuning process. With the tuning results for the high-thrust trajectories the search space for later low-thrust trajectories and tuning can be reduced, but this is only done if certain values of the settings perform badly to such a degree that there is sufficient certainty that the value will also be inferior for the low-thrust case.

For the high-thrust tuning phase the Cassini 2 problem is tackled, since it is sufficiently complex by having multiple gravity assists and can also directly be compared to earlier work by L. van der Heyden who also performed tuning with this GTOP problem. Since it is a GTOP problem there is also sufficient information about the optimal solution. Finally, the use of a DSM during each of the legs closer approximates a low-thrust trajectory than the Cassini 1 GTOP problem, which does not use DSMs. The variations analyzed for each of the settings can be seen in Table 6.2. All problems are performed with 1000 generations and a population size of 100. While these values are most likely not optimal, they are put to this relatively low value to ensure that the checking of the other parameters can be done more efficiently. Once the optimal settings have been found for the low-thrust problem, the generation and population values are tackled.

Table 6.2: An overview of the range of settings used for the MOEA/D optimizer tuning for the Cassini 2 problem.

Setting	Variation	Step size
Generations	Not varied	N/A
Population size	Not varied	N/A
Weight generation	Grid/Random/Low discrepancy	N/A
Decomposition method	Weighted/Tchebycheff/BI	N/A
Neighbourhood size (T)	20 - 80	20
Cross-over rate (CR)	0.5 - 1.0	0.1
Scale factor (F)	0.2 - 0.8	0.1
Distribution index	10 - 50	10
Chance for diversity preservation (Realb)	0.5 - 1.0	0.1
Seed	N/A	N/A
Preserve diversity	False/True	N/A
Limit	1 - 5	1
Verbosity	Not varied	N/A

6.4.1. Initial analysis

The high-thrust tuning tests are performed with the Cassini 2 problem, which uses one DSM per leg to reach Saturn by performing a gravity assist with Venus, Venus, Earth and Jupiter, in that order. The precise decision variables and ranges for the Cassini 2 problem can be found on the GTOP pages of the ESA website [28]. The current optimum in terms of ΔV is 8701 m/s using the Tudat ephemerides as was already mentioned in Chapter 5.

Performing tests with all permutations listed in Table 6.2 would result in an unworkable number of analyses. Thus, the first decision is to vary one variable at a time, while keeping the rest at the default values listed in Table 6.1. Only the generation (1000) and population (100) variables are both always kept constant as they are tuned separately later on. Due to co-dependencies of the different variables this method is insufficient to get the optimal value for all the optimizer settings. However, it will allow to remove clearly infeasible results. For tuning in future research alternative methods that combine uncertainties from multiple parameters such as the Taguchi method are recommended to be explored [119]. Each of the test cases is performed for five seeds (1, 2, 3, 4, 5). The five seeds allow an analysis of the best performing individual in each seed as well as the variance across seeds. The decision on five seeds stems from a trade-off between robustness and runtime.

Based on the initial results of the Cassini 2 optimization problem a few of the settings could already be discarded. In terms of ΔV and TOF all the weight-generation methods produce roughly equal results. However, the Pareto front is more complete and better spread out for the grid method. Therefore, only this option is kept. Similarly, Tchebycheff is the only decomposition method which results in a filled Pareto front and is thus chosen. Turning off diversity preservation similarly results in a non-uniform Pareto front. Thus, only options with diversity preservation are used from now on.

Regarding the neighbourhood size, cross-over rate, Realb, and limit no clear conclusions can be made based on these initial tests. While the scale factor and distribution index need to be tuned further, partial conclusions can already be made. Scale factors of 0.3 or lower result in sub-optimal ΔV results and incomplete Pareto fronts and are thus discarded. Furthermore, distribution indices of 40 or 50 resulted in a clumped Pareto front near higher values of the TOF and ΔV . These options are also discarded for later tests.

6.4.2. Subsequent high-thrust tuning

For the remaining settings the previous initial analysis is insufficient to determine one optimal value for each of the settings. The next step is to test all permutations of the remaining variables. Doing this with all the remaining options would still result in a too large data set. Therefore, the six remaining variables were split into two groups which were tuned separately. The first group consists of the cross-over rate, the scale factor, and the distribution index while the second group consists of Realb, the neighbourhood size, and the limit. The first group mainly regards the mutation generation with the DE operator while

the second group regards the neighbourhood functionality.

First the results of group 1 are discussed. Each permutation is performed with five seeds. Afterwards, the results are grouped for each value of every setting, for example a CR of 0.6. Then the lowest ΔV value for each seed with a CR value of 0.6 is taken and the average of these ΔV values is calculated. This is done for all values of each of these three variables and the results can be seen in Table 6.3.

Table 6.3: An overview of the average best ΔV in km/s across all seeds for each of the values of the CR, F, and η_m settings.

CR	F	η_m
0.5: 15.26	0.4: 17.17	10: 14.02
0.6: 15.07	0.5: 15.31	20: 14.07
0.7: 13.48	0.6: 13.61	30: 14.56
0.8: 14.06	0.7: 13.15	
0.9: 12.83	0.8: 11.84	
1.0: 14.61		

Based on the statistical results two options are kept for each of the parameters. The kept values for CR, F, and η_m are as follows:

- Cross-over rate = 0.7 and 0.9
- Scale factor = 0.7 and 0.8
- Distribution index = 10 and 20

This results in eight remaining permutations for these three settings. These options are tested with 1000 population members and 3000 generations with five different seeds. These extended runs ensure better convergence and can give a more definitive answer regarding the optimal settings. Based on these tests it is found that the combination of a cross-over rate of 0.7, a scale factor of 0.7, and a distribution index of 10 result in the lowest average ΔV value as well as the lowest standard distribution, thus indicating robustness. The found average optimal ΔV for these settings is 10.67 km/s with a standard deviation of 1.89 km/s. L. van der Heyden's tuning did not include the distribution index [43]. In his work five combinations of variables were chosen for further study, all of which were in the 0.9 - 1.0 range for the cross-over rate and the 0.5 - 0.7 range for the scale factor [43]. The cross-over rate of 0.7 falls outside of the 0.9 - 1.0 range by L. van der Heyden, but here it should be noted that a cross-over rate of 0.9 is only barely worse than 0.7 in the tuning analysis of this thesis.

Three of the variables have not been varied yet. These are the neighbourhood size, Realb, and the limit. Once again all permutations are tested with 100 population members and 1000 generations. The results are shown in Table 6.4. These tests use the default values for the other parameters, which is why the ΔV values in Table 6.4 are higher than some of the values in Table 6.3.

Table 6.4: An overview of the average best ΔV in km/s across all seeds for each of the values of the T, Realb, and limit settings.

T	Realb	Limit
20: 16.70	0.5: 15.92	1: 13.19
40: 15.16	0.6: 15.30	2: 14.29
60: 15.09	0.7: 15.13	3: 15.88
80: 16.56	0.8: 16.90	4: 17.93
	0.9: 15.03	5: 18.11
	1.0: 16.99	

This analysis does not lead to clear winners, but does result in the following statistical best options:

- Neighbourhood size = 40 and 60
- Realb = 0.6, 0.7, and 0.9
- Limit = 1 and 2

Performing extended tests with 3000 generations on the permutations of these remaining options results in the lowest ΔV values for a neighbourhood size of 60, Realb of 0.6, and a limit of 1. The found average optimal ΔV for these settings is 11.21 km/s with a variance of 2.33 km/s across all seeds. Technically the Realb value of 0.9 results in a lower ΔV , but on the other hand this value also results in much less consistent Pareto fronts and thus unpredictable results depending on the seed used. This problem is not present with Realb values of 0.6.

The found values for these three settings are similar to the ones found by L. van der Heyden [43]. The limit value was not tested during L. van der Heyden's tuning. The neighbourhood size of 60 - 100 was found as ideal during L. van der Heyden's tuning so the value of 60 is within that range. The found Realb value is within L. van der Heyden's result range of 0.6 - 0.7. All combined this means that the following optimal settings are found for the high-thrust tuning process of the Cassini 2 problem:

- Cross-over rate = 0.7
- Scale factor = 0.7
- Distribution index = 10
- Neighbourhood size = 60
- Realb = 0.6
- Limit = 1

The results for the Cassini 2 problem with 1000 population and 3000 generations with these settings is shown in Figure 6.4. To illustrate the robustness of the method this specific figure is split per seed. Especially for lower ΔV values the scatter plot almost overlaps for all five of the seeds. The best ΔV found in this analysis is 8701.08 m/s, very close to the true optimum of 8700.97 m/s as mentioned in Table 5.2.

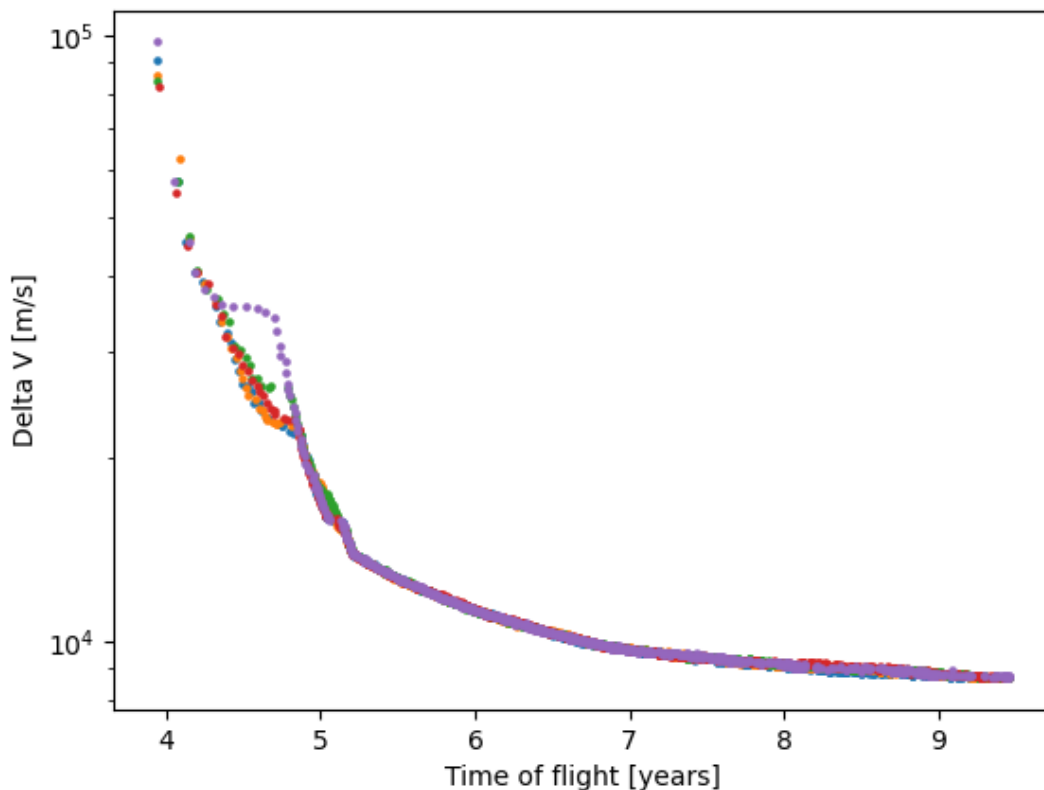


Figure 6.4: An overview of the optimal trajectory for the Cassini 2 GTOP problem as modelled by Tudat code with the tuned high-thrust MOEA/D optimizer settings. Each color represents population members of a different seed.

The final tuning step is to see whether changes in the population size or generation number are required. For the population size the number of 1000 is kept as, from a visual standpoint, it is deemed sufficient to result in a fully filled Pareto front. The optimal value of the Cassini 2 problem in the Tudat system is 8701.08 m/s. The code is considered sufficiently converged if the lowest ΔV value is within 5% of the true optimal value in all five of the test seeds. This test is performed with a generation number of 500, 1000, 1500, 2000, 2500, and 3000. For a generation number of 2000 the ΔV is within 0.55% and 1.93% of the optimum depending on the used seed. This is considered sufficient for the initial convergence step. As such the final settings for high-thrust analyses are a population of 1000 and a generation number of 2000. During the optimization process itself these values can be changed depending on the behavior of the results. The other optimizer settings, however, will be kept the same.

6.5. Optimizer tuning for low-thrust trajectories

The same optimization process is repeated for the low-thrust trajectory example from Earth to Mars. However, instead of the full choice of optimizer settings only the reduced settings from the second high-thrust tuning round are used. In the high-thrust tuning case this is done with a population of 1000 members and 3000 generations with five different seeds. However, performing the tuning with low-thrust members with these settings for all 20 permutations would result in a runtime of multiple days. Furthermore, the tuning process converges much sooner and with fewer population members in the low-thrust case. One case is performed with 100 members and 250 generations, but with these settings the problem already converges to a point that no difference can be identified independent of the chosen values for the settings. Multiple reruns are performed, but even at only 100 members with 20 generations the found differences between settings are minor. This is because the trajectory setup assumes arrival and departure at the sphere of influence of Earth and Mars, both with no excess velocity. Therefore, the only free variables are the departure time, time-of-flight, and number of revolutions, which results in a relatively simple problem.

In order to have more conclusive low-thrust trajectory tuning the complexity of the problem must be increased to something more similar to the actual problem tackled in this thesis. This will thus require a trajectory with a gravity assist. No launch velocity or use of powered gravity assists is assumed for this tuning problem. The trajectory chosen for this case is a low-thrust mission from Earth to Mars and back to Earth. The final arrival at Earth is a rendezvous at the SOI of Earth and thus does not require excess velocity or velocity angles. Like in the eventual mission only trajectories with no full revolutions around the Sun per leg are considered. The other needed input variables are the departure time, the arrival velocity with its two angles for Mars, the time-of-flight from Earth to Mars and from Mars to Earth, and the gravity assist periapsis and bending angle. A full overview of the ranges for the decision variables is given in Table 6.5.

Table 6.5: An overview of the decision variable ranges for the Earth-Mars-Earth low-thrust tuning problem. Departure velocity from Earth, number of revolutions, and arrival velocity at Earth are all excluded from this table as they equal zero.

Trajectory stage	Variable	Lower bound	Upper bound	Units
Earth departure	t_0	7000	9000	MJD ₂₀₀₀
Earth to Mars	$t_{f,1}$	200	2000	days
Mars to Earth	$t_{f,2}$	200	2000	days
Arrival Mars	V_∞	10	10,000	m/s
Arrival Mars	θ	0	2π	rad
Arrival Mars	ϕ	-0.5π	0.5π	rad
GA Mars - pericenter radius	r_p	6354	63,540	km
GA Mars - bending angle	α	$-\pi$	π	rad

This analysis is performed with the same 20 permutations as the previous low-thrust problem, but with 100 members and 100 generations. While these results are not sufficient to conclusively pick only one option, clear patterns can be found to further reduce the possible options to analyze. The full data is shown in Table 6.6.

Table 6.6: An overview of the average best ΔV in km/s for the Earth-Mars-Earth problem across all seeds for each of the values of the CR, F, η_m , T, Realb, and limit settings for the low-thrust tuning process.

CR	F	η_m	T	Realb	Limit
0.7: 10.46	0.7: 10.53	10: 10.49	40: 10.78	0.6: 10.72	1: 11.07
0.9: 10.57	0.8: 10.50	20: 10.54	60: 10.90	0.7: 10.94	2: 10.61
				0.9: 10.86	

The conclusions based on these results are shown below. The standard deviation values between brackets regard the variance based on the lowest ΔV for each seed of a certain setting.

- Cross-over rate = The average ΔV found with a cross-over rate of 0.7 is more than one standard deviation (67 m/s) better than with a cross-over rate of 0.9. Thus, only the cross-over rate of 0.7 is kept.
- Scale factor = Due to the large standard deviation of 117 m/s and 28 m/s for an F of 0.7 and 0.8, respectively, no decisions are made for this variable.
- Distribution index = The distribution index of 10 is roughly one standard deviation (86 m/s) better than the average optimum found with a distribution index of 20. Thus, only the distribution index of 10 is kept.
- Neighbourhood size = Due to the large standard deviation of 341 m/s and 276 m/s for a T of 40 and 60, respectively, no decisions are made for this variable.
- Realb = Both Realb values of 0.6 and 0.9 perform better than 0.7. A value of 0.6 performs best by almost one standard deviation (200 m/s), but for now both 0.6 and 0.9 are kept.
- Limit = The limit of 2 is more than one standard deviation (290 m/s) better than the limit of 1. Thus, the limit value 2 is kept. Higher limit tests are also tested to see whether this trend of improvement for higher limit values continues, but this is not the case.

The remaining options are thus:

- Cross-over rate = 0.7
- Scale factor = 0.7, 0.8
- Distribution index = 10
- Neighbourhood size = 40, 60
- Realb = 0.6, 0.9
- Limit = 2

Using all permutations this leads to a remaining set of eight possibilities. These possibilities are all tested with 100 members and 600 generations to discover more nuanced differences between them. Each of the options is executed with five seeds. The average optimal ΔV is within 100 m/s for all of the permutations. However, when sorting per setting it can be seen that the Realb of 0.6 and the scale factor of 0.7 both perform roughly one standard deviation better than the alternatives. Thus, the only remaining decision regards the neighbourhood size. These two options are tested with 2500 generations and have ΔV results within 1 m/s of each other. It thus seems that both options are roughly equal. However, as can be seen in Figures 6.5 and 6.6, the option with a T of 40 converges to a single front whereas the alternative converges to a less optimized front. Here Figure 6.6 is split per seed to illustrate that all seeds find the right-most front, but not all seeds find the fronts to the left, which results in a unexpected shape of the Pareto front in Figure 6.6. For a T of 40 every seed finds both major fronts.

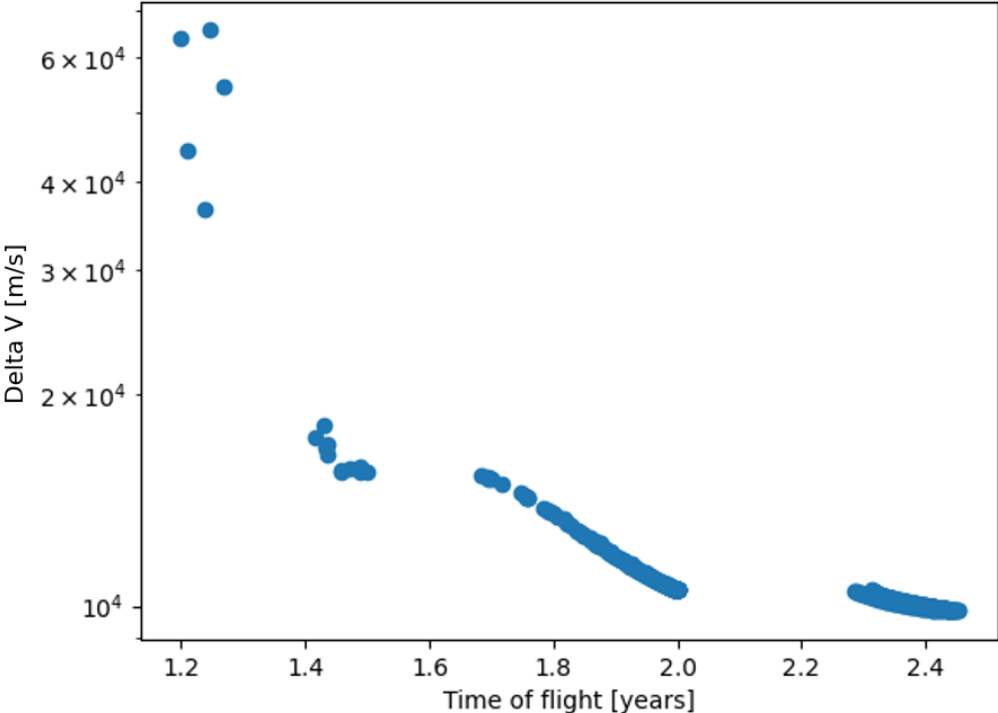


Figure 6.5: The ΔV and TOF of all members in the low-thrust tuning test across five seeds for a T value of 40.

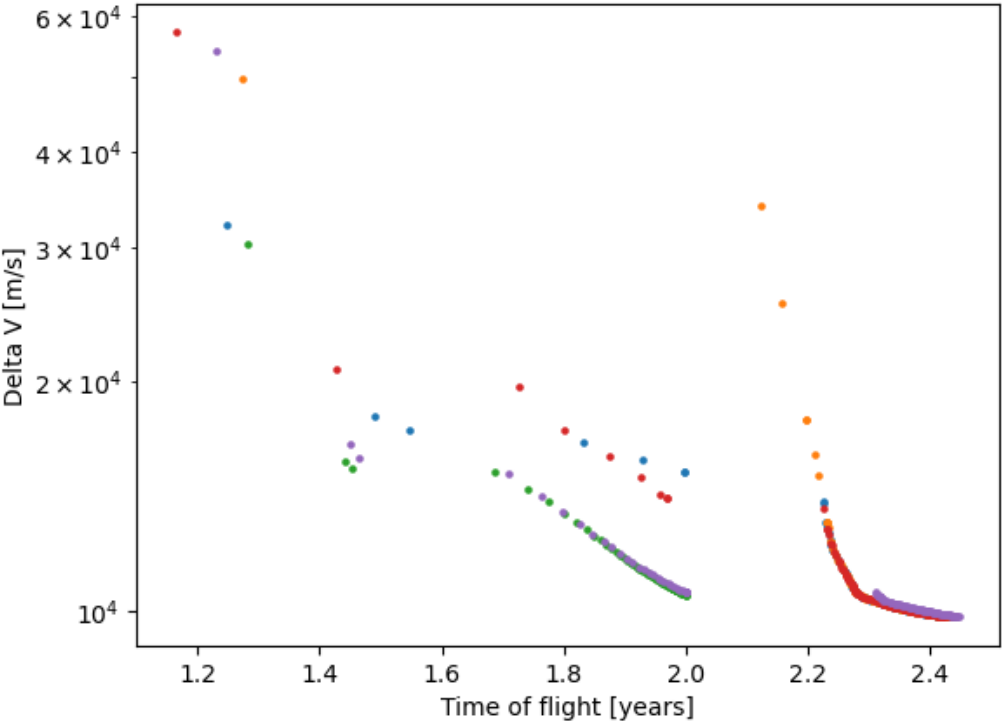


Figure 6.6: The ΔV and TOF of all members in the low-thrust tuning test across five seeds for a T value of 60. Each color represents population members of a different seed.

One final adjustment which is made is to lower the cross-over rate even further to 0.6 as subsequent tuning indicates that this stabilizes the Pareto fronts further in a similar manner as the lower neighbourhood size does. The final chosen settings for the low-thrust problem are thus:

- Cross-over rate = 0.6
- Scale factor = 0.7
- Distribution index = 10
- Neighbourhood size = 40
- Realb = 0.6
- Limit = 2

Finally, the population size and generation numbers are discussed. The population number is kept at 100 since, based on the plots, it appears sufficient to create a full Pareto front. Furthermore, an increase in population size has a large impact on the runtime and it is decided that this time resource can be better spent on more generations or more time to determine the optimization method itself. The long runtime of the low-thrust trajectories is expected to be the bottleneck for the number of analyses which can be performed during this thesis. In terms of generations it is found that the results show virtually no change beyond 1500 generations (tests included 500, 1000, 1500, 2000, 2500 generations). Thus, 1500 generations are used as the nominal number of generations. The scatter plot for the chosen low-thrust settings and the low-thrust benchmarking problem is shown in Figure 6.7. The trajectory for the lowest ΔV member in this plot is shown in Figure 6.8.

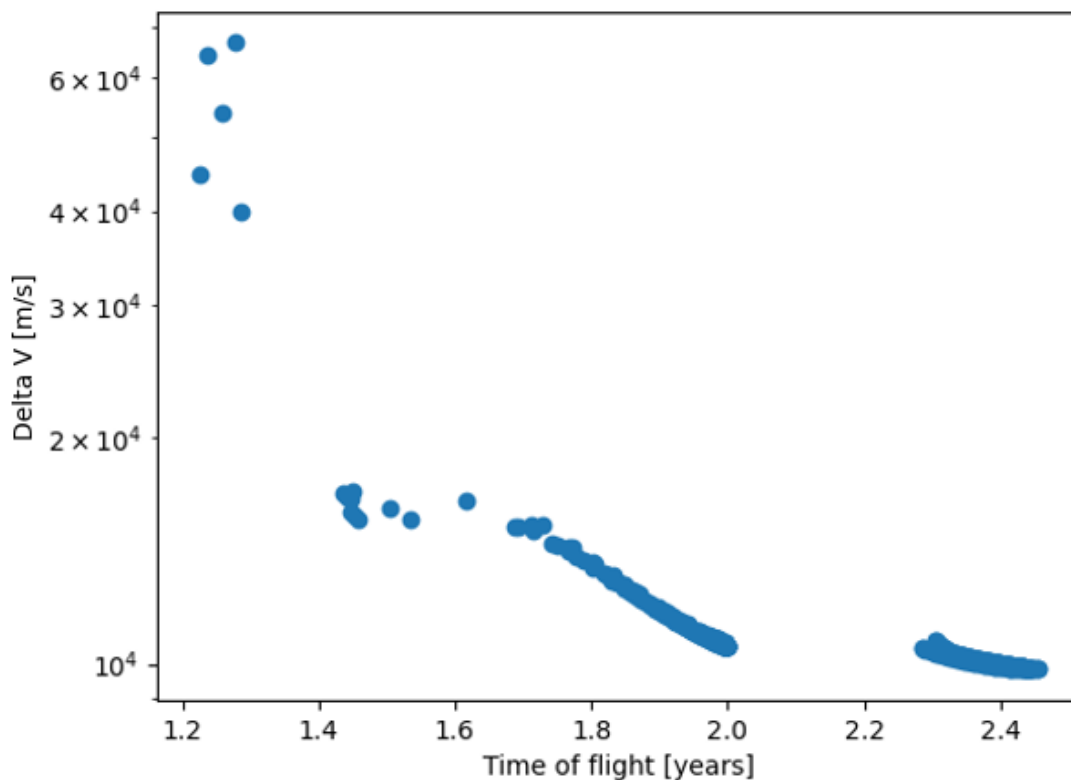


Figure 6.7: A scatter plot of the Earth-Mars-Earth low-thrust ΔV and TOF performance with the final tuned low-thrust settings.

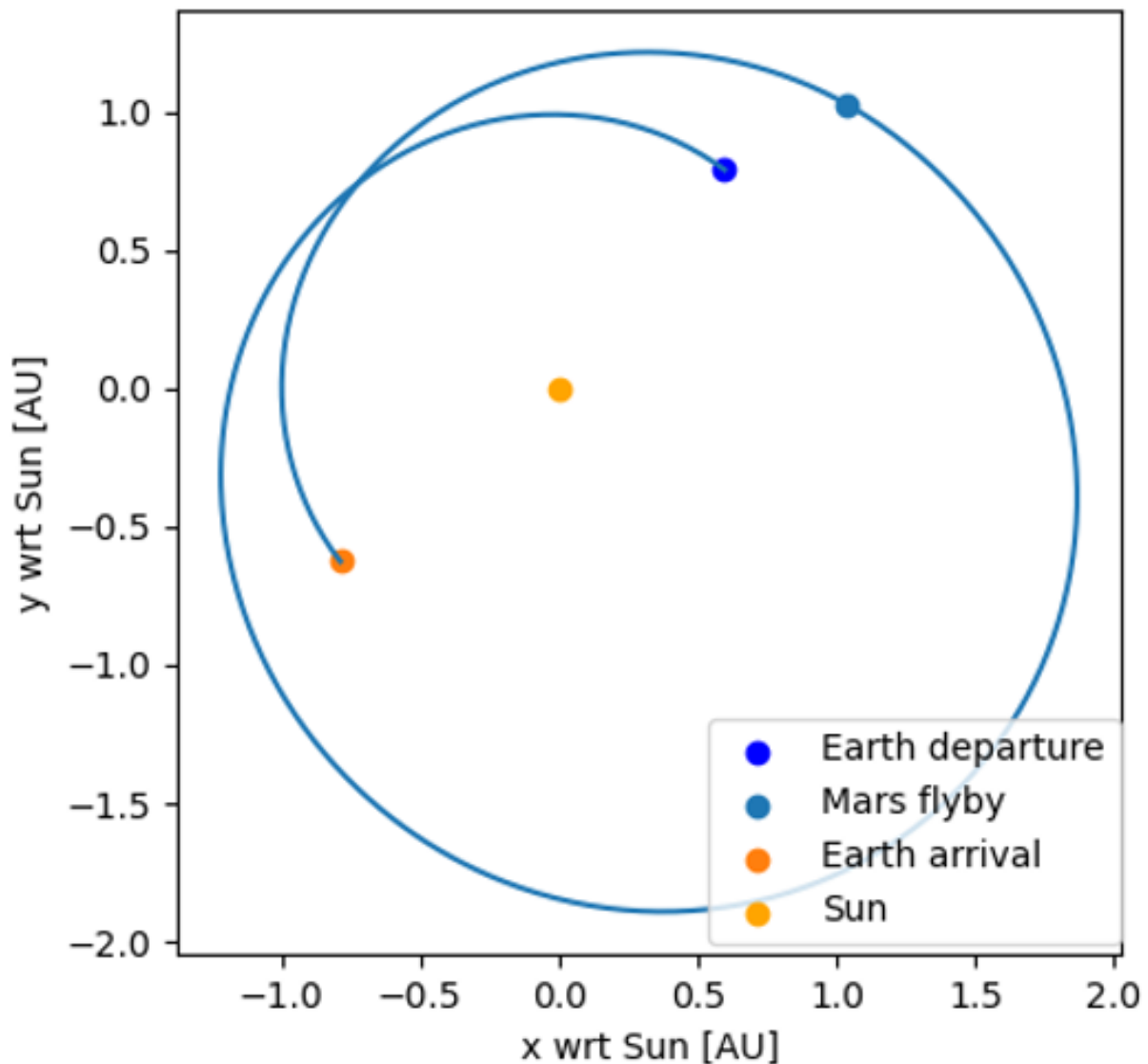


Figure 6.8: A 2D representation of the optimal (= lowest ΔV) Earth-Mars-Earth low-thrust trajectory found with the settings from the low-thrust tuning process.

6.6. Summary

This chapter describes the selection of the optimizer as well as the tuning process for both high-thrust and low-thrust trajectories. Based on its performance in similar problems the MOEA/D multi-objective optimizer is chosen.

A tuning process for the high-thrust trajectory is performed to verify the tuning process with L. van der Heyden's results, to provide a decreased search space for the low-thrust tuning, and in case high-thrust trajectories are still needed later in this thesis. Based on multiple stages of testing the following high-thrust settings are found: cross-over rate 0.7, scale factor 0.7, distribution index 10, neighborhood size 60, Realb 0.6, limit 1, population size 1000, generation number 2000.

This process is also repeated for a low-thrust trajectory from Earth back to Earth via a gravity assist with Mars. This results in the following tuned low-thrust settings: cross-over rate 0.6, scale factor 0.7, distribution index 10, neighborhood size 40, Realb 0.6, limit 2, population size 100, generation number 1500.

Part III

Application

Planetary and single KBO flyby analysis

With the optimizer tuned, the optimizer can be applied by analyzing flyby trajectories. The next two phases according to Figure 3.4 are the planetary flyby analysis and the single KBO flyby analysis. During these analyses it is found that it is easiest to combine them and thus they are also discussed together in this report. It is already decided that the planetary flyby sequence consists of a departure from Earth, a gravity assist with Jupiter, and a gravity assist with Neptune. This is then followed by a flyby of a KBO for the single KBO flyby case. The optimization method for this problem starts in a straightforward manner, but this does not yield the desired results. As such a number of different methods are tested which are discussed chronologically in this chapter. At the end the final working procedure with the single KBO flyby method is described.

7.1. Straightforward optimization problem

The first attempted method is the simplest one: optimizing the trajectory from Earth to a KBO in one go. For this first an overview of the decision variables in the optimization process is provided in Table 7.1 including their used ranges.

Table 7.1: An overview of the decision variable ranges for the Earth-Jupiter-Neptune-KBO low-thrust optimization problem. Departure velocity from Earth, number of revolutions, and powered gravity assists are all excluded from this table as they equal zero.

Trajectory stage	Variable	Lower bound	Upper bound	Units
Earth departure	t_0	14609.5	18262.5	MJD ₂₀₀₀
Earth to Jupiter	$t_{f,1}$	365	9125	days
Jupiter to Neptune	$t_{f,2}$	365	9125	days
Neptune to KBO	$t_{f,3}$	365	9125	days
Arrival Jupiter	$V_{\infty,J}$	10	10,000	m/s
Arrival Jupiter	θ_J	0	2π	rad
Arrival Jupiter	ϕ_J	-0.5π	0.5π	rad
GA Jupiter	$r_{p,J}$	118,849	7,606,336	km
GA Jupiter	α_J	$-\pi$	π	rad
Arrival Neptune	$V_{\infty,N}$	10	10,000	m/s
Arrival Neptune	θ_N	0	2π	rad
Arrival Neptune	ϕ_N	-0.5π	0.5π	rad
GA Neptune	$r_{p,N}$	41,861	2,679,104	km
GA Neptune	α_N	$-\pi$	π	rad
Arrival KBO	$V_{\infty,KBO}$	10	10,000	m/s
Arrival KBO	θ_{KBO}	0	2π	rad
Arrival KBO	ϕ_{KBO}	-0.5π	0.5π	rad
Arrival KBO	N_{KBO}	-0.49	21.49	-

The bounds for the variables stem from the mission description in Chapter 3 and the physical limitations

of certain angles such as the arrival angles and the gravity assist asymptotic bending angle. For the time-of-flight a wide range of 1 to 25 years is chosen for each leg. The last variable, N_{KBO} , is rounded to the nearest integer and each integer corresponds to one of 22 KBOs from the reduced list of high-priority targets. It is only with these KBOs with which flybys are attempted with this initial method. Note that the reduced list in Chapter 3 consists of 36 KBOs. The reduction to 22 is due to an inclination constraint of 15 degrees placed upon the KBOs. The minimum arrival velocity with each body is set to 10 m/s since lower arrival velocities periodically result returns matrix errors while calculating the trajectory.

Furthermore, the departure velocity (magnitude and angles) as well as the ΔV for potential powered assists are not included in Table 7.1. As will be a theme in this chapter, the main drawback of the low-thrust description is its sensitivity and complexity. Therefore, simplifications to the problem description are required. The use of powered gravity assists is the first option to be discarded. The other one is to assume no excess velocity for the spacecraft at the edge of the SOI of Earth. This will increase the total ΔV required during the trajectory legs and will result in longer flight times, but disregarding this excess velocity should not have a substantial impact on the shape or behavior of the trajectories. Therefore, this simplification is also applied. In follow-up research the addition of an excess launch velocity and the use of powered gravity assists is recommended.

With these simplifications the entire optimization process is performed in one go from Earth to a KBO with a population of 100 and 1500 generations. However, this does not yield a single feasible trajectory in any of the generations or any of the five seeds. This indicates that either no solutions are present within the bounds or that the sensitivity is so high that none are found in the total of 750,000 members. To check this the next section discusses an analysis which splits up the trajectory into its separate legs.

7.2. Separate analyses per leg

In the next step the legs are analyzed separately: Earth-Jupiter, Jupiter-Neptune, Neptune-KBO. This is done with the same departure times for each case and assuming no excess velocity at the start of each leg. Because of this the legs can not be patched together, but this step is performed to rule out that the failure to find trajectories in the previous section comes from an issue in the code. And, as expected, trajectories for the separate legs are found as is shown in Figures 7.1, 7.2, and 7.3. The KBO which is overwhelmingly chosen in the Neptune-KBO leg is 15760, also known as Albion. The point at a time-of-flight of 0 years with a ΔV of 10^6 km/s represents all infeasible trajectories, which are thus still present in each figure.

One issue which is encountered at this stage is the runtime limitation. Running for 1500 generations will, especially for the longer legs towards Neptune and the KBOs, result in runtimes of several days. Therefore the number of generations in this thesis has to be reduced or other smarter methods need to be found. The latter is discussed in subsequent sections, but for now the generation number is limited to 500 for the leg to Jupiter and 100 for the other legs. These limits were chosen based on a trade-off regarding convergence and runtime.

One element which is missing in these successful runs compared to the earlier failed attempts in this chapter is the gravity assist. Tuning in Chapter 6 shows that the gravity-assist calculator works as intended, but it is suspected that the sensitivity of GAs is the main reason for the lack of solutions in the analysis so far. One way to try to solve this is to (partially) fix the trajectory legs. Before this is discussed, two other issues regarding convergence and the root finder function are described.

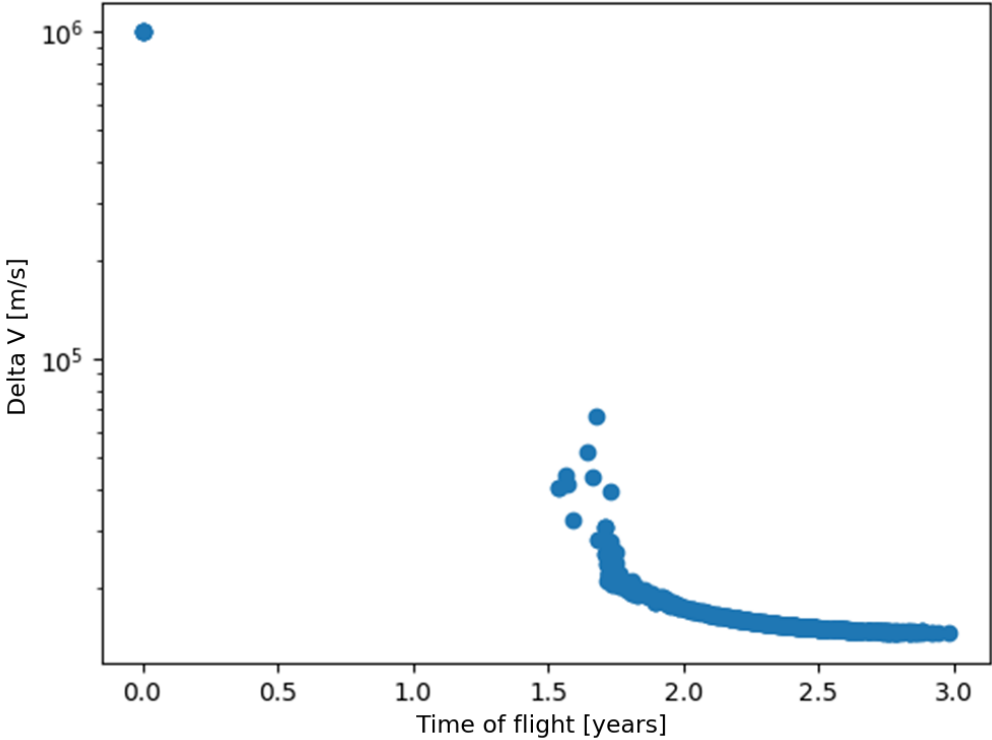


Figure 7.1: The ΔV and TOF of all members in the low-thrust analysis for the separate Earth-Jupiter leg for 500 generations per seed.

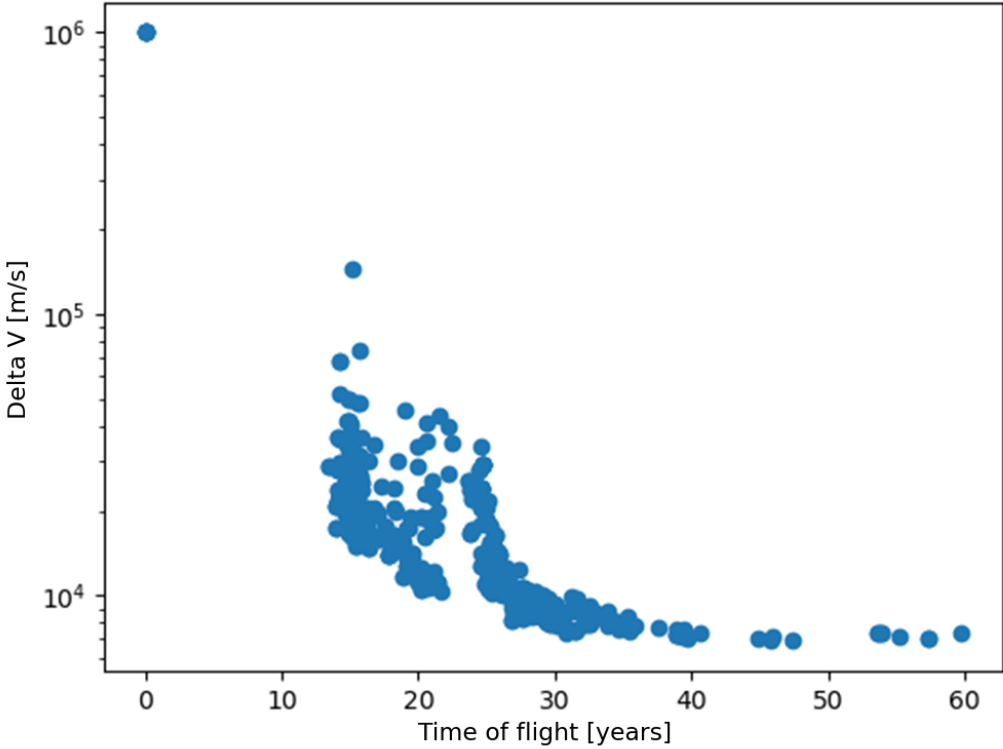


Figure 7.2: The ΔV and TOF of all members in the low-thrust analysis for the separate Jupiter-Neptune leg for 100 generations per seed.

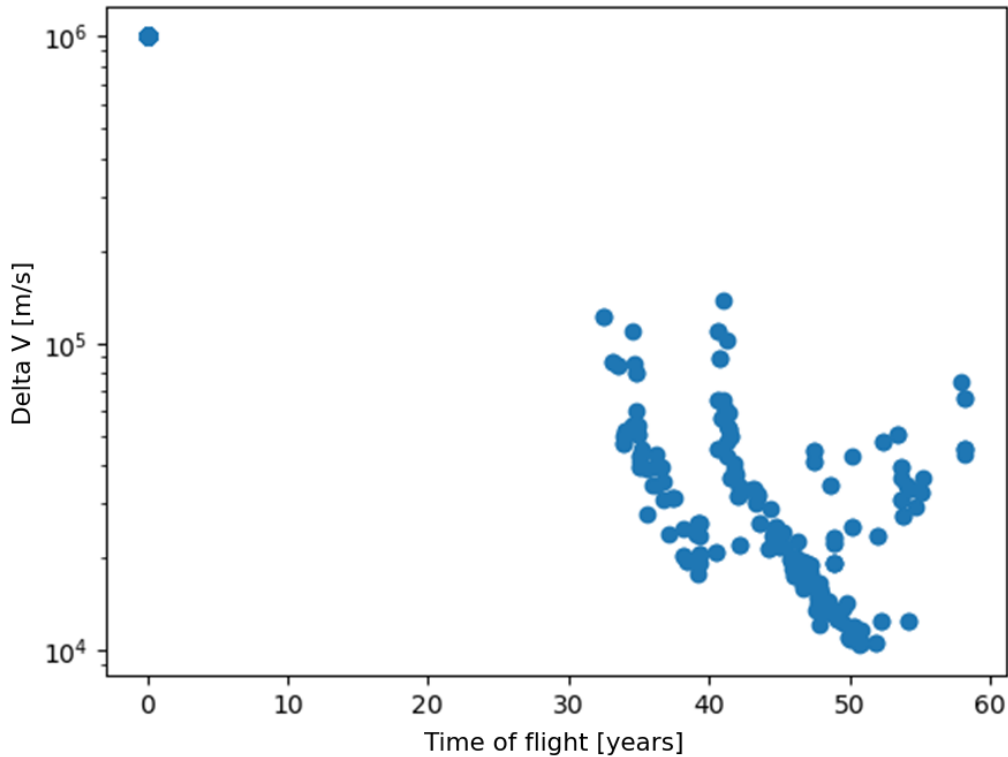


Figure 7.3: The ΔV and TOF of all members in the low-thrust analysis for the separate Neptune-KBO leg for 100 generations per seed.

7.3. Convergence and root finder

One of the main conclusions drawn from the initial analyses is that the number of generations required for convergence varies wildly depending on the type of leg. Furthermore, the 1500 generation number from the tuning phase is also not feasible due to the associated runtime of the low-thrust optimizer. Therefore, a new method for convergence is required.

The solution is to use a variable convergence check which analyzes in real-time when a solution has converged sufficiently for each seed. The convergence check works with four variables. The first one is called the stable length (L_{stable}) and describes the number of generations that a solution should be stable before a population is considered to have converged. The second one is the convergence criterium (C_{crit}) which specifies how much the solution can change before it is no longer considered stable. For this only the ΔV value of the lowest member in the population is considered. The third one is the ΔV limit (ΔV_{lim}) which specifies how low the ΔV of the best member in the population should be at the very least before stability is even considered.

For example take an L_{stable} value of 50, a C_{crit} of 1 m/s and a ΔV_{lim} of 10,000 m/s. This means that a population is considered converged if the best member in that population is below 10,000 m/s for 50 generations in a row and never changes its ΔV value by more than 1 m/s during those generations. Finally, to prevent this method from running endlessly, a maximum number of generations gen_{lim} is also specified after which the optimization stops independent of whether convergence has been reached. Based on trial-and-error with the different methods discussed throughout this chapter the following nominal settings are found: [50, 1, 20400, 2000]. This means that the problem is considered to be converged when the lowest ΔV member in the generation does not change more than 1 m/s in terms of ΔV for 50 generations in a row. This counter towards 50 stable generations only starts when the minimum ΔV value within the population is below 20,400 m/s. This is roughly the maximum available ΔV for this mission based on the propellant fraction limit. If no convergence has been reached after 2000 generations the problem is interrupted. Depending on the complexity of the problem or the ex-

pected ΔV , L_{stable} , ΔV_{lim} and gen_{lim} are varied throughout the analysis process. However C_{crit} is always kept at 1 m/s.

A second remark based on the initial analyses regards the root-finder method for the a_2 variable of the spherical-shaping trajectory. During the analyses of all the trajectory legs in one go many members return an error regarding a wrong curvature of the trajectory which is not curved towards the central body or another error in the bisection method related to the a_2 value. Furthermore, with the separate legs analysis it is found that by varying the range over which the a_2 variable is searched the trajectory could go from infeasible to feasible. This implies that in the first search range no root was found or that multiple roots for a_2 exist, but that not all of them lead to feasible trajectories.

Thus, the root-finder function for the a_2 variable is looked at in more detail and its results are analyzed. An example of plots for the a_2 variable are shown in Figures 7.4 and 7.5. In Figure 7.5 there is only one intersection point whose a_2 value corresponds with a feasible trajectory. However, in Figure 7.4 there are two solutions, but only the negative root with an a_2 value of -0.2 results in a feasible trajectory. These root-finder plots can, in the current structure of Tudat, only be requested once a trajectory is already deemed feasible. Inspecting the a_2 graph of infeasible trajectories to see whether another a_2 root is nearby is thus not possible and would require a rework of some of Tudat's mechanics. The latter is not implemented in this thesis, but is strongly recommended for future research to gain more insight in the behavior of seemingly infeasible trajectories. Related to this, T. Roegiers also mentions a few alternative methods to determine the a_2 value which would be interesting to look at in further research [106]. For now the search range of the a_2 value is placed at -1 to 1 based on ranges in previous studies [121] [106].

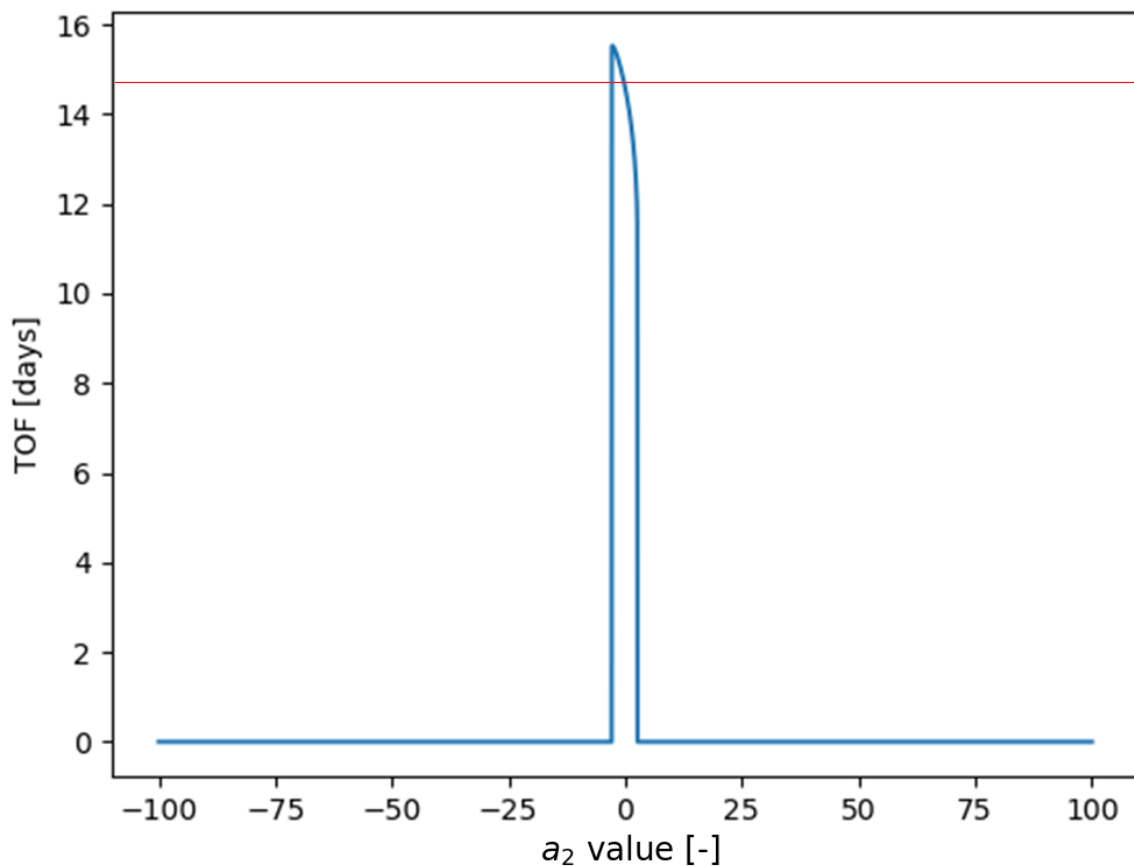


Figure 7.4: The time-of-flight as a function of the a_2 variable for a trajectory from Neptune to Albion. The blue line shows the time-of-flight as a function of a_2 while the red line indicates the true time-of-flight, which is 14.7 years.

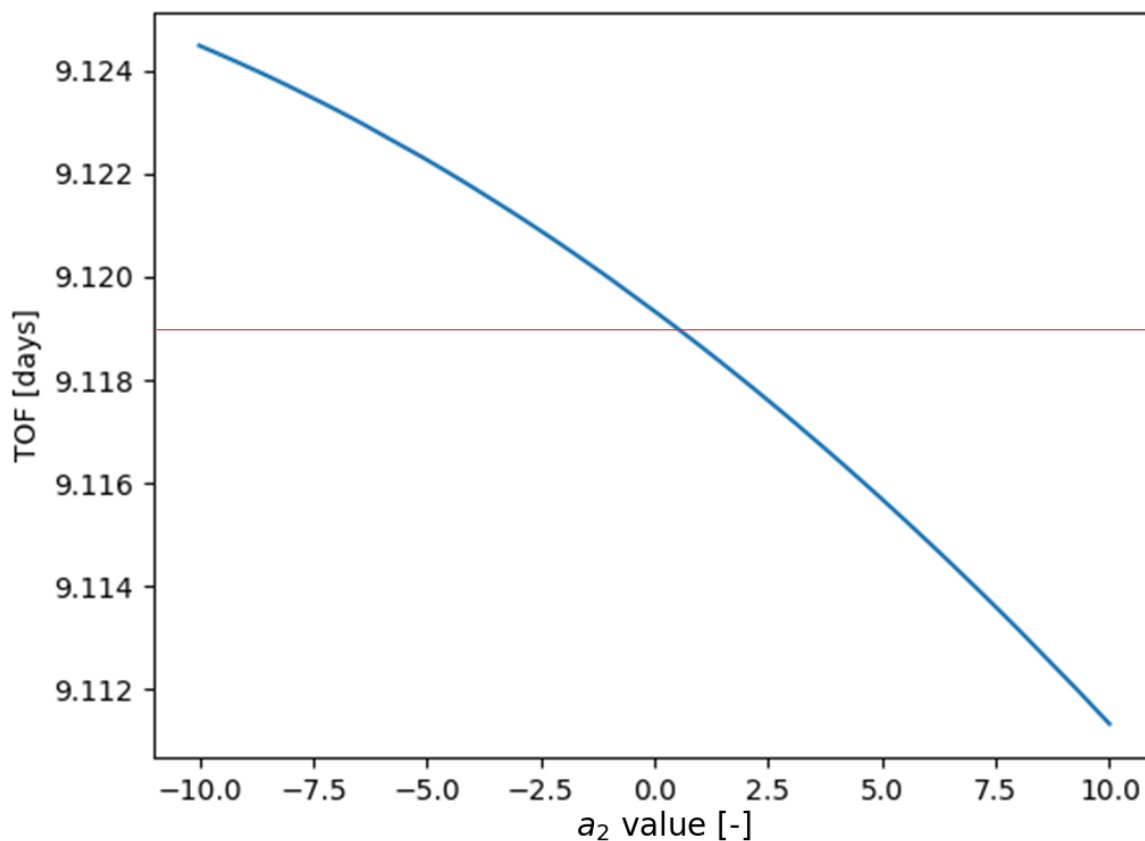


Figure 7.5: The time-of-flight as a function of the a_2 variable for a trajectory from Jupiter to Neptune. The blue line shows the time-of-flight as a function of a_2 while the red line indicates the true time-of-flight, which is 9.119 years.

7.4. Free, locked, and constrained trajectory solutions

After the initial analyses new methods have to be used to find feasible trajectories for a low-thrust KBO mission. Instead of optimizing the trajectory in one go as was done before, three different methods are investigated now: free, locked, and constrained trajectories. This is first done only for the JN trajectory, so without a KBO flyby. Despite not performing an extra flyby with Earth, the separate legs are referred EJ (Earth-Jupiter) and JN (Jupiter-Neptune) in the rest of this report for clarity.

The free trajectory is virtually the same as what was done before where the full range was given for all inputs and the entire trajectory is optimized in one go. The only change now is the use of the convergence check. With the locked trajectory method each leg is optimized separately. So for Earth to Neptune via Jupiter first the EJ leg is optimized. Once an optimum is found the decision variables of this leg are locked, in other words fixed at the values previously found. Afterwards the JN leg is optimized, but settings such as the departure time and the arrival velocity at Jupiter are already set in stone due to the locked first leg of the trajectory. The gravity assist with Jupiter is only optimized in the JN leg. This process continues until the entire trajectory is optimized. Then the different legs can simply be patched together since they have the same position, velocity, and time at each boundary.

Finally, there is the constrained trajectory method. This method largely works the same as the locked method. However, instead of completely locking the trajectory after each leg, the old legs are only partially constrained. Consider the EJ leg again. After an optimum is found for the EJ section, the EJ and JN legs are optimized together. The decision variables in the JN leg are still free. However, unlike the locked trajectory method the decision variables in the EJ part of the trajectory are not fully fixed, but have a freedom margin around the solution for the decision variables of the optimum member of the previous phase. This could for example be a 10% freedom for the variables in the EJ leg. This is a compromise between free and locked, as it shrinks the input space without removing all wiggle room.

All tests are performed with a population of 100 and the nominal convergence settings. Unfortunately, the free trajectory method does not yield any feasible results even upon reaching the maximum number of generations. This method is therefore definitively discarded.

Both the locked and the constrained method do yield results. The results for the five seeds combined can be seen in Figures 7.6 and 7.7 for locked and constrained, respectively. For the constrained method a freedom of $\pm 10\%$ is allowed in the EJ leg while optimizing the JN leg. This percentage is determined by means of trial-and-error. The lowest ΔV found by the locked method is 9,755 m/s, while the constrained method's optimum lies at 10,442 m/s, roughly 7% higher. Both plots use the same convergence checks and one would thus assume both to be roughly equally stable. However, the ΔV variation across different seeds is larger for the constrained method than the locked method indicating convergence to sub-optima.

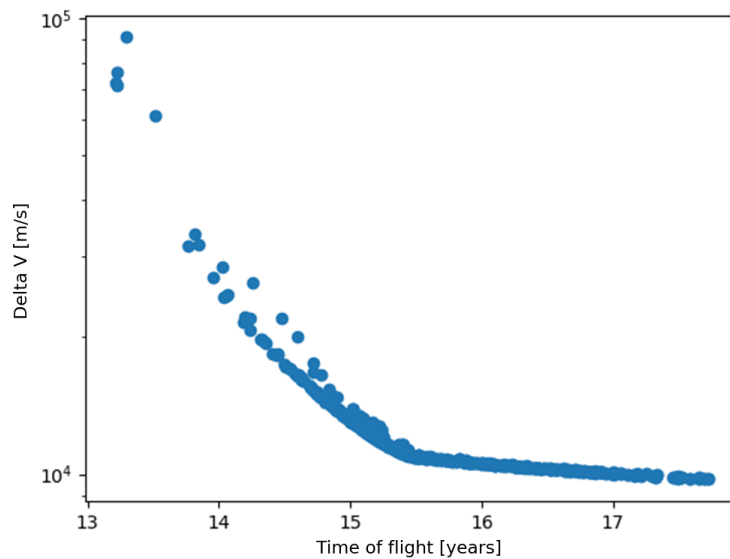


Figure 7.6: The ΔV and TOF of all members in the low-thrust analysis from Earth to Neptune via Jupiter with the locked method.

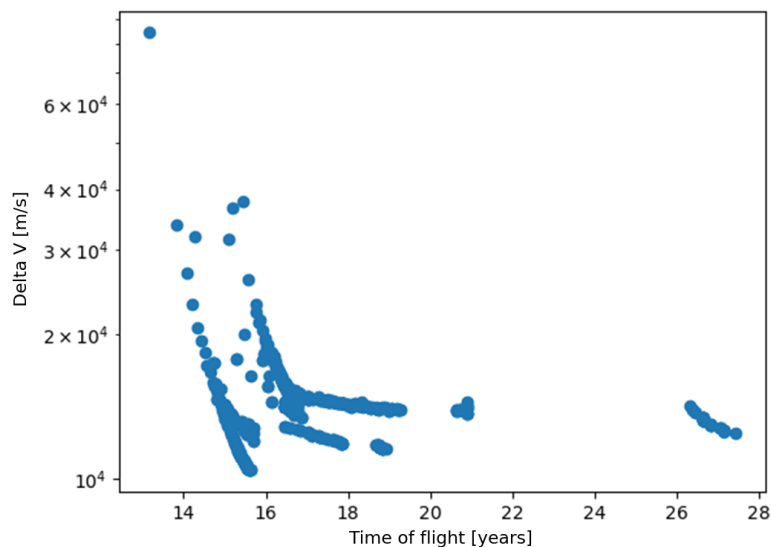


Figure 7.7: The ΔV and TOF of all members in the low-thrust analysis from Earth to Neptune via Jupiter with the constrained method. A freedom margin of $\pm 10\%$ is used after each leg.

Based on this analysis one might conclude to continue with the locked method. However, instead the constrained method is used for further tests. This is because in later stages of this chapter when KBOs are added the tests with the locked method start to perform worse than the constrained method. Due to its certainty to find a solution the locked method is better than the constrained method at first. However, once the number of legs becomes too large the lack of flexibility of the locked method starts to become dominant. Still, the current performance with the constrained method and its lack of robust convergence is not comforting. Another method is thus required to reduce the convergence issues of the constrained method and also to decrease its ΔV in general since the optimal results with the constrained method are still roughly 7% higher than with the locked method. How this is done is explained in the next section.

7.5. High-thrust intermediate step

In the previous section solutions were found for the trajectory to Neptune by using a constrained trajectory design strategy. However, there are still issues with the convergence of this method. This issue becomes even greater when a KBO is added to the trajectory by adding the N_{KBO} variable such that each trajectory gets a randomly assigned KBO from the 22 high-priority KBOs. In this case no feasible trajectories are found. Figure 7.8 shows the position of the KBOs (in orange) with respect to the spacecraft when it reaches Neptune (in blue). This figure contains all KBOs which conform with the uncertainty parameter and the 15 degree inclination limit and thus not only the high-priority cases. As can be seen there should be ample of KBOs close enough for the spacecraft to perform a flyby with. However, even with this expanded set no feasible trajectories are found. If only the closest KBOs with respect to the spacecraft are chosen, the closest being 47171 Lempo, some sporadic results are found. However, these solutions have high ΔV values of 20+ km/s and local refinement around the found decision variables does not reduce the ΔV to realistic values.

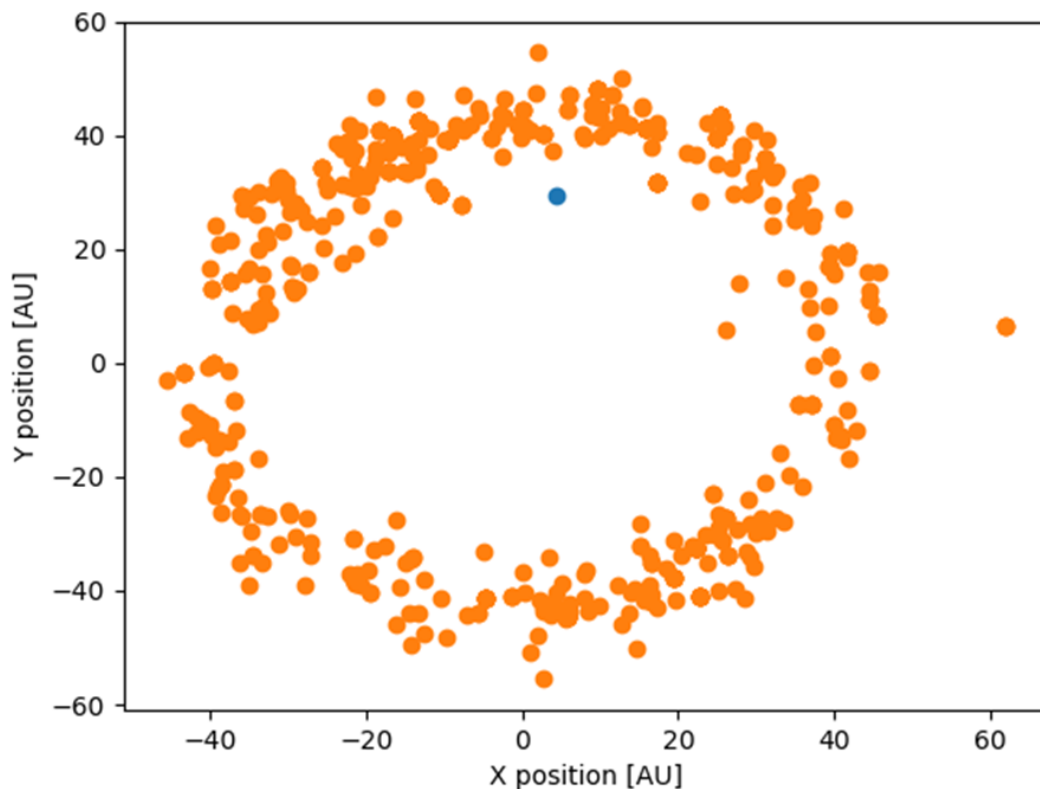


Figure 7.8: The position of all KBOs (orange) complying with the uncertainty parameter and inclination limits, at the same time that the spacecraft (blue) reaches Neptune in the optimal trajectory found so far with the constrained trajectory method.

One method attempted to improve the solution is to use a single-objective DE optimizer instead of MOEA/D and to only optimize for ΔV . However, this results in even more sporadic results with ΔV values above 20 km/s as can be seen in Figure 7.9 for the JN trajectory. Infeasible trajectories are represented here by setting their ΔV value to 10^6 m/s. Only rudimentary tuning of the single-objective DE optimizer is performed since it is not the main optimizer for the thesis. It is possible that a more carefully tuned DE optimizer would give better results, but this is out of scope for this thesis and is instead recommended for future research.

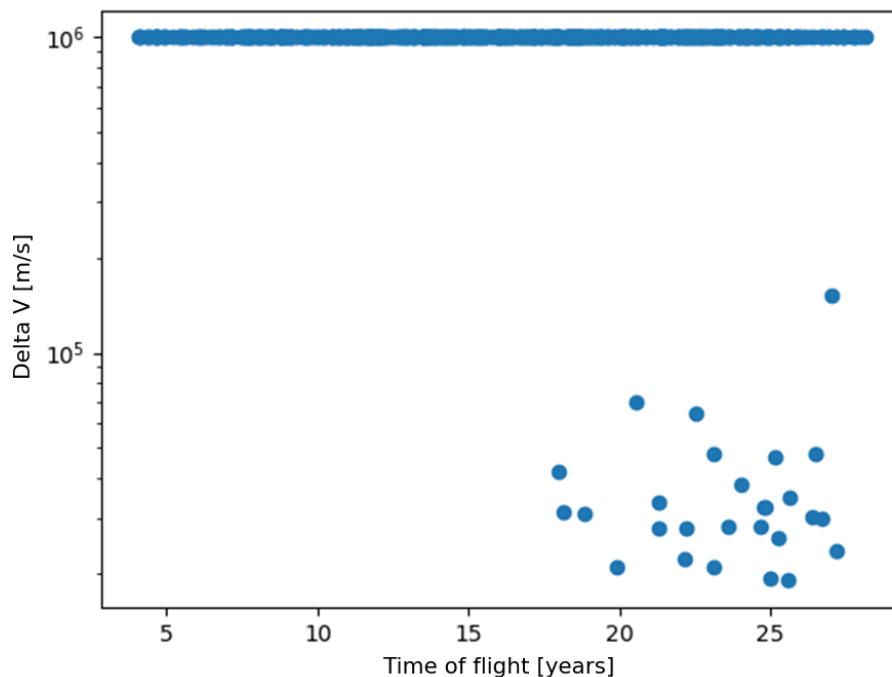


Figure 7.9: The ΔV and TOF of all members in the low-thrust analysis from Earth to Neptune via Jupiter with the constrained method by means of a single-objective optimizer. For the constrained method a freedom of $\pm 10\%$ was used after each leg.

Another concept is to use high-thrust trajectories to explore the design space for the low-thrust trajectories. While high-thrust trajectories with DSMs are not the same as low-thrust trajectories, it stands to reason that their shapes will be fairly similar, especially if the DSM ΔV is small. Thus, high-thrust trajectory optimization can be performed first and the results of these high-thrust cases can be used to steer and constrain the low-thrust optimization process.

There are two main advantages to this method. The first one is that high-thrust trajectory optimization does not have an issue with the a_2 variable or a requirement for specific shaping. While their results might not always be very realistic, almost any input can theoretically result in a high-thrust trajectory which benefits the convergence process and wider search of the input space. Secondly, high-thrust trajectory optimization is orders of magnitude faster than low-thrust trajectory optimization. Single seeds for the EJN-KBO trajectory in a low-thrust scenario already take many hours to run and do not provide very useful results so far. If a high-thrust step can be performed in a fraction of the time which benefits the subsequent low-thrust step, then the total calculation time is significantly reduced.

The JN trajectory is so simple in the high-thrust case that it can be optimized in one go without the step-wise constrained method. Similarly, the trajectories including one KBO can also be optimized in one go. In this case the reduced set of 22 KBOs is used again. The results for the JN and JN-KBO optimization processes with high-thrust are shown in Figures 7.10 and 7.11, respectively. Note that for the high-thrust trajectory optimization the adjusted high-thrust optimizer settings are used. The results show that this method to generate high-thrust JN-KBO trajectories works. Note that in reality these

trajectories are not realistic. They require in the order of 10 km/s of high-thrust ΔV from DSMs, which is far from the heritage values in Chapter 2. In reality if one would want to calculate high-thrust deep-space trajectories one would need very high departure velocities from a LV. However, the goal here is not to create good high-thrust trajectories, but instead to create theoretically possible high-thrust trajectories which are similarly shaped to low-thrust trajectories. The translation from the high-thrust solutions to low-thrust solutions is discussed in the next section.

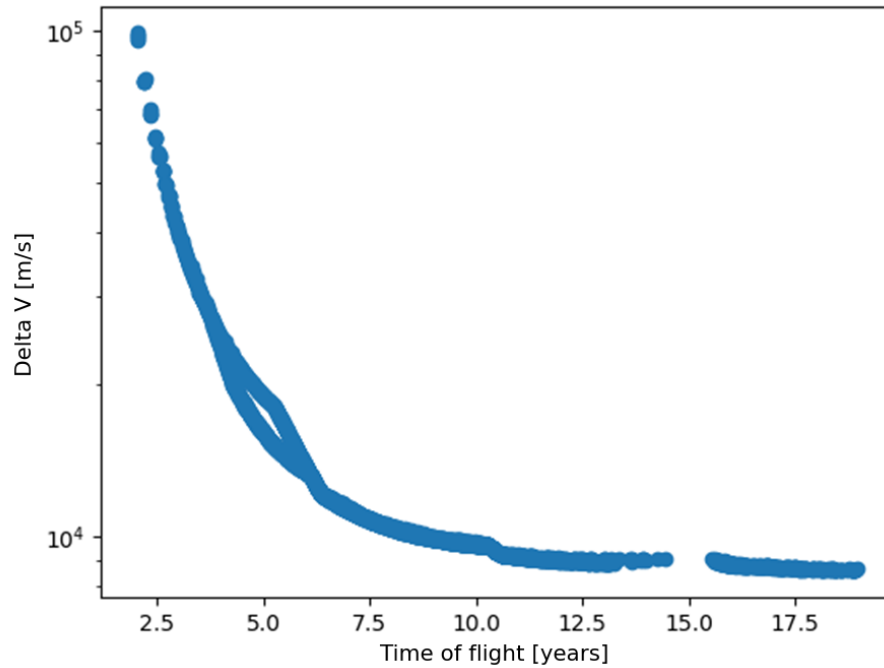


Figure 7.10: The ΔV and TOF of all members of the high-thrust analysis for the JN trajectory (EJ and JN legs).

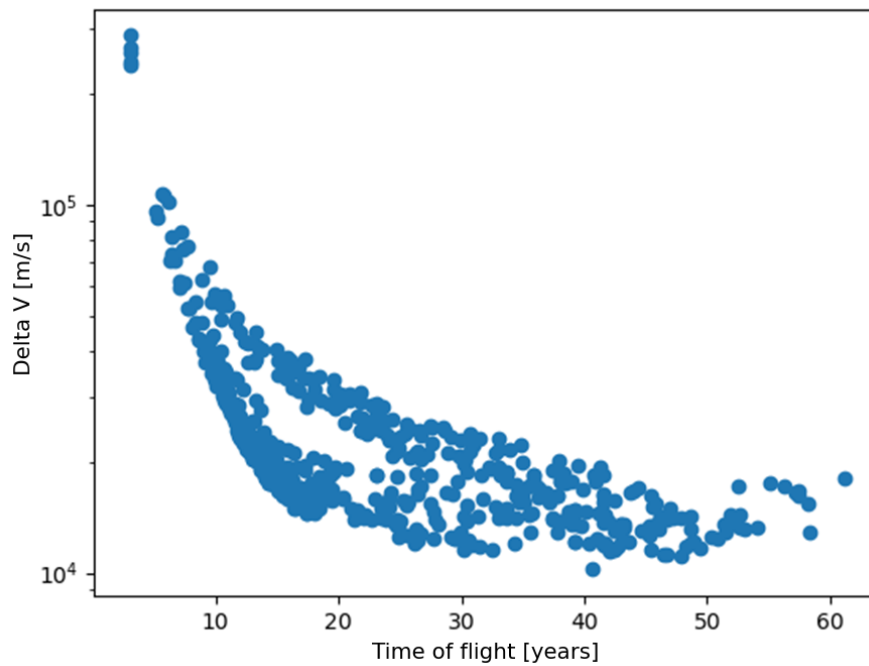


Figure 7.11: The ΔV and TOF of all members of the high-thrust analysis for the JN-KBO trajectory (EJ, JN, and J-KBO legs).

7.6. High-thrust to low-thrust translation

The next step is to translate the high-thrust results to inputs for the low-thrust problem. First the optimal member for the EJ leg of the high-thrust trajectory optimization is chosen and given as input for the low-thrust EJ optimization with a $\pm 20\%$ freedom in the input values around the high-thrust optimum. The 20% value was selected after more trial and error. The results of this are shown in Figure 7.12. The lowest ΔV in this plot is 8,927 m/s, which is the lowest value found so far for the low-thrust EJ leg. Doing the same process for the EJ and JN legs combined from high- to low-thrust results in an optimal low-thrust ΔV of 9,910 m/s. This is better than the constrained performance so far, but still not as good as the fully locked method for EJ and JN combined as was shown in Figure 7.7. Furthermore, multiple sub-optimal fronts have formed since not every seed finds the bottom-left front.

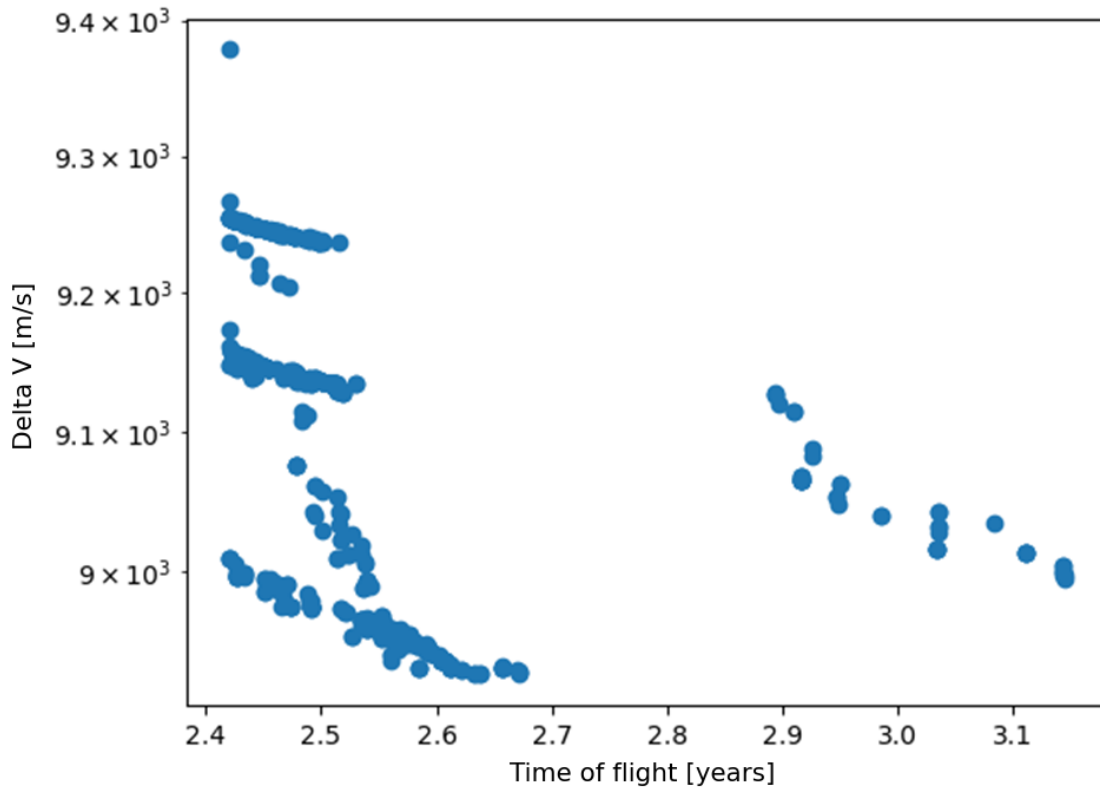


Figure 7.12: The ΔV and TOF of all members in the low-thrust analysis for an EJ trajectory leg. The inputs for the optimization process are taken from the optimal member of a high-thrust EJ trajectory leg with $\pm 20\%$ freedom.

One way to improve the results is to also split up the high- to low-thrust trajectory conversion in multiple steps by taking the legs separately. This does require information about the arrival and departure velocity magnitude and angles in both the high- and low-thrust cases in order to accurately translate the inputs back-and-forth. This is done in several steps. For the arrival velocity the state of both the spacecraft and the planet need to be known just before the flyby. Afterwards, these velocities are rotated to the TNW (thrust, normal, out-of-plane) frame of the respective planet or KBO. Afterwards the difference between the velocity can be taken. The arrival excess velocity magnitude is then the norm of this velocity difference.

For the two angles Equations 7.1 and 7.2 are used. To ensure that θ is in the right quadrant the 2-argument arctangent is required. Due to the definition of the velocity magnitudes within Tudat a minus sign is required for V_y . The addition of π is needed since the used definition of θ runs from 0 to 2π instead of the $-\pi$ to π range of the atan2 function. In a similar manner the departure velocity can also be retrieved. The previous results in this section do not use any information from the departure or arrival velocity to translate the high-thrust to the low-thrust case so this addition should improve the results further.

$$\theta = \text{atan2}(-V_y, V_x) + \pi \quad (7.1)$$

$$\phi = \sin^{-1}\left(\frac{V_z}{V_\infty}\right) \quad (7.2)$$

This method of going back-and-forth between high- and low-thrust solutions results in a procedure which gives satisfactory results. The final procedure is explained step-by-step in the next section.

7.7. Final procedure

This section provides the final procedure used to get a low-thrust trajectory with one KBO flyby. All steps in this procedure are repeated for five seeds and use the nominal convergence criteria.

Step 1: EJ high-thrust (optional)

The first step is to perform the EJ leg in high-thrust such that it can be used as extra input data for the low-thrust EJ leg optimization. Due to the simplicity of the EJ leg this step is not required and is left out in later examples.

Step 2: EJ low-thrust (optional)

The second step is to translate the EJ result from high-thrust to low-thrust. Like step 1, this step is left out in later examples since instead of EJ followed by EJM, the EJM trajectory can be optimized in one go.

Step 3: EJM high-thrust

Usually the calculation thus starts at step 3. Here the EJM trajectory is optimized using a high-thrust trajectory. The optimal trajectory found with this method has a ΔV of 8,580 m/s. Unlike low-thrust, the high-thrust optimizer does allow a small hyperbolic excess velocity as launch. This is the case since no excess velocity provides issues as high-thrust has an impulsive thrust profile instead of a continuous one like low-thrust. This excess velocity is in the order of 2 m/s.

Step 4: EJM low-thrust

Using the input from the high-thrust step the low-thrust EJM trajectory is optimized. The inputs for the decision variables have +/-20% freedom around the optimal values found during step 3. This results in a trajectory with a time-of-flight of 17.9 years and a ΔV of 9,172 m/s.

Step 5: EJM high-thrust correction

The next two steps are corrections to ensure that the high- and low-thrust trajectories are equivalent to each other upon arriving at Neptune. This is required for step 7. In step 5 the high-thrust EJM problem is performed again, but now with exactly the same decision variables as the low-thrust example. Only the time of the DSMs is kept free. This ensures that for example the arrival time at Neptune is the same for both high thrust and low thrust. This step results in a high-thrust trajectory with a time-of-flight of 17.9 years and a ΔV of 8,886 m/s.

Step 6: EJM low-thrust correction

The previous step results in a high-thrust EJM trajectory with a similar but not identical arrival velocity at Neptune as the low-thrust EJM trajectory. Here the EJM low-thrust trajectory is calculated again with as its only update the fact that the arrival velocity at Neptune is now exactly the same as that of the trajectory from step 5. This results in a low-thrust trajectory with a time-of-flight of 17.9 years and a ΔV of 10,132 m/s.

Step 7: EJM-KBO high-thrust

Everything up to arrival at Neptune is now fully locked. The only freedom remaining is the gravity assist around Neptune and then the flight to a KBO. Multiple methods exist to find a KBO. This can be done with a random KBO from the reduced list of 22 high-priority targets. Also, the larger data set of over 500 bodies can be used, or it is possible to pick a single KBO due to its proximity to the spacecraft (see

Figure 7.8). For this specific example Albion is directly chosen as the KBO target as the spacecraft already flies past it very closely without any added ΔV . This step results in a high-thrust trajectory with a time-of-flight of 27.0 years and a ΔV of still 8,886 m/s, rounded.

Step 8: N-KBO low-thrust

Next the leg from Neptune to the KBO, in this case Albion, is optimized for the low-thrust trajectory. The departure velocity from Neptune after the gravity assist is taken from the high-thrust case and used as the start velocity for the N-KBO leg. By only optimizing N-KBO instead of EJN-KBO the low-thrust optimization process runs orders of magnitudes faster. A constrained method is used based on the results from step 7, but the freedom given is much smaller this time: in the order of 0.1% to 1% depending on the variable. This is because, due to its low ΔV beyond Neptune, step 7 already has almost perfect decision variable values for low-thrust as well. The precise freedom margins per variable are determined using a trial-and-error approach.

Step 9: EJN-KBO low-thrust

The EJN and N-KBO sections of the low-thrust trajectory can be patched together since their position, timing, and velocity is the same at the boundary point. Now the whole trajectory can be visualized. This total trajectory has a time-of-flight of 27.0 years and a ΔV of 10,169 m/s, roughly half of the total low-thrust ΔV budget. The time-of-flight is much longer than for example the 9.5 years which it took New Horizons to reach the Kuiper belt [86], but this is caused by setting the launch energy to zero in this thesis. In future research where the launch energy is included it is expected that similar time-of-flight values can be attained as New Horizons.

Step 10: Further optimization cycles

Finally, further optimization cycles can be performed on the full EJN-KBO low-thrust trajectory to see whether a more refined optimum can be found near the solution from step 9. Once again, the freedom margin taken for all the variables is based on trial-and-error and an educated guess from the user. With this method a better trajectory with a time-of-flight of 27.0 years and a ΔV of 9,956 m/s is found. The ΔV is split as follows: 9610 m/s for the EJ leg, 324 m/s for the JN leg, and 22 m/s for the N-KBO leg. This corresponds to a spacecraft wet-to-dry ratio mass of roughly 1.40, which has already been attained by previous low-thrust missions described in Chapter 2. This final trajectory is visualized in Figure 7.13.

7.8. Summary

This chapter describes the different attempted methods to design a single KBO low-thrust flyby mission. The original method is to optimize an entire low-thrust mission in one go, but due to the vast input space this does not yield any feasible trajectories. After issues regarding convergence and the root finder are tackled, a comparison is made between free, locked, and constrained trajectories. It is decided to continue with the constrained trajectory method where each leg is solved subsequently, but only limited freedom is allowed in the input space for legs preceding the current one in the optimization process.

When expanding this constrained method to a KBO flyby it is still insufficient. Therefore, the decision is made to perform back-and-forth optimization between high-thrust and low-thrust trajectories. The high-thrust trajectories are easier and faster to calculate and are thus used as input for the low-thrust optimization process. Using a ten-step procedure where different legs are optimized in high-thrust and low-thrust scenarios, a robust method has been generated to calculate single-flyby low-thrust KBO trajectories.

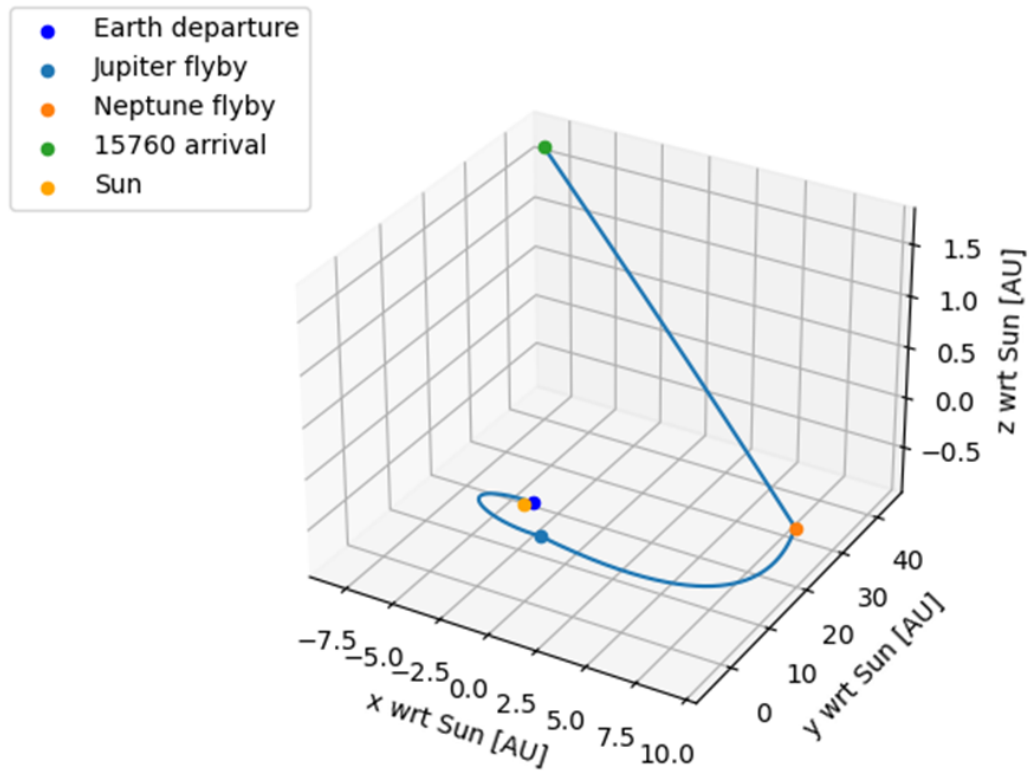
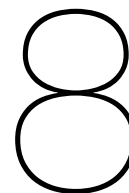


Figure 7.13: A 3D representation of the final found trajectory from Earth to 15760/Albion using low-thrust propulsion. This trajectory has a time-of-flight of 27.0 years and a total low-thrust ΔV of 9,956 m/s.



Multiple KBO flyby analysis

The previous chapter has provided a method to produce a low-thrust trajectory which ends with a flyby at a KBO after performing gravity assists with Jupiter and Neptune. The next step is to test whether it is possible to extend this flyby sequence with more CFBs. First the same methodology is applied as before with alternating high-thrust and low-thrust legs. Afterwards, a list of alternative attempts is discussed. Finally, a new method with so-called close-approach graphs is explained.

8.1. High-thrust to low-thrust leg

After the flyby with Albion in Chapter 7 the next step for a second KBO flyby is to continue with the previous methodology of performing a high-thrust trajectory optimization followed by a low-thrust one. One simplification now is that no gravity-assist calculations are required as all KBOs are assumed to have no gravitational influence on the spacecraft. The departure velocity from Albion is thus exactly the same as the spacecraft's arrival velocity at the KBO.

The high-thrust analysis is performed with two different KBO sets. The first set is the most limiting one: the filtered set of 36 bodies brought down further to 22 bodies due to the 15 degrees inclination constraint. The second set also uses the inclination constraint, but allows all bodies with an uncertainty parameter U of 2 or lower. This set contains 590 bodies.

For the high-thrust analysis the trajectory is locked up until and including Albion. For both data sets results are found. The Pareto front for the data set with 590 bodies is shown in Figure 8.1. Here the Pareto front for the second KBO flyby has converged to three KBO targets as can be seen by the three distinct fronts in the figure. The trailing front with the lowest ΔV corresponds to the transfer from Albion to the KBO (15789) 1993 SC. Note the significant increase in the total ΔV compared to the single-KBO case in Figure 7.11. The extra ΔV fully stems from the DSM during the leg between Albion and the second KBO.

However, when this trajectory case for 15789 is optimized in low-thrust no results are found independent of the freedom margin taken for the decision variables. Consistently the error which is returned is that the trajectory is not curved towards the central body thus indicating the issue with the D-parameter. Further exploration of the a_2 value is performed to try to find an a_2 root for which the D-parameter is non-zero, but this is unsuccessful. The most probable reason for the failure of the optimizer to find a feasible low-thrust trajectory is the high ΔV of more than 5 km/s required after the Albion flyby based on the high-thrust results.

Another issue could be Albion itself, whose flyby might not be well situated for a follow-up leg. Therefore, other high-priority objects from the list of 22 KBOs are attempted to be reached for the first KBO flyby using the same procedure as in Chapter 7. The time-of-flight from Neptune to each of these KBOs as well as the total ΔV of the mission for the high-thrust cases is shown in Figure 8.2. The dot in the bottom-left corner of the figure represents the trajectory to Albion. All the dots at the right-hand side

indicate that for an optimal trajectory they would require a time-of-flight above the 25 years limit. Only three other KBOs with a reasonable time-of-flight are available from this list, but all require at least 2 km/s more ΔV than the trajectory to Albion and are above the desired average time-of-flight between KBOs of 10 years. Clearly other methods are required. The different attempts to try to find better KBO pairs or second KBO visits are discussed in the next section.

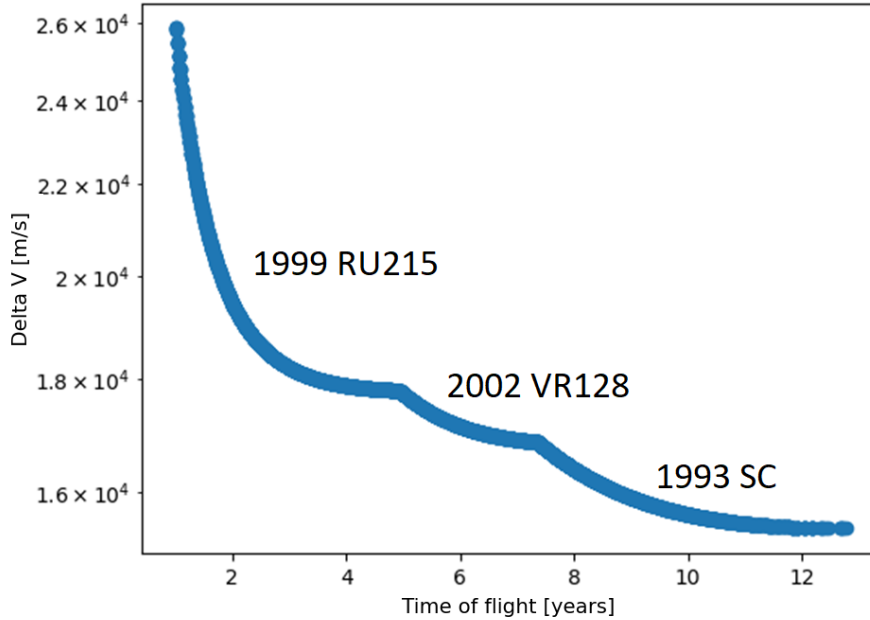


Figure 8.1: The ΔV and TOF of all members in the high-thrust trajectory analysis from Albion to a second KBO by using all known KBOs with an uncertainty parameter of 2 or lower and an inclination of no more than 15 degrees. The time-of-flight represents the time between Albion and the second KBO flyby.

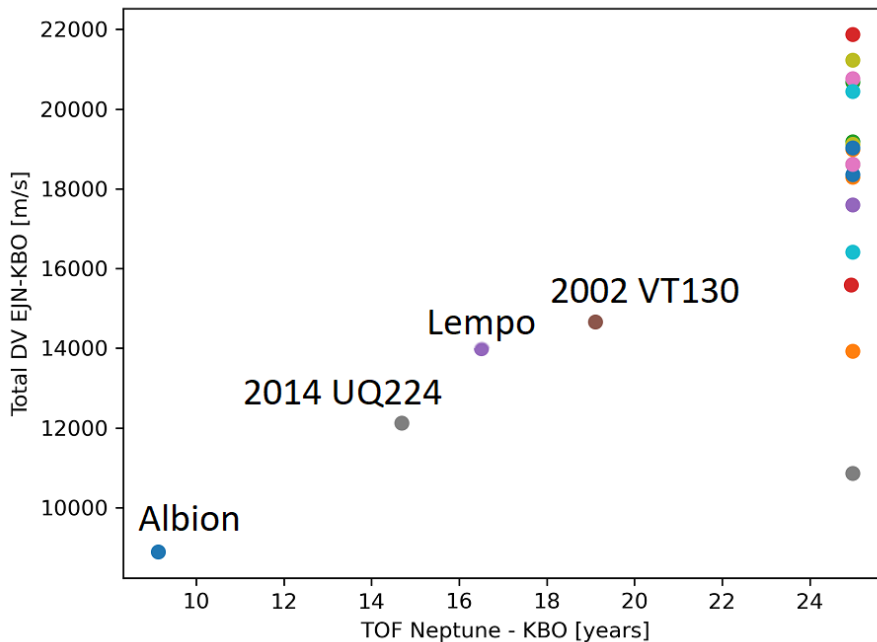


Figure 8.2: The total ΔV and TOF from Neptune to each of the KBOs from the high-priority list for a high-thrust trajectory analysis. Each dot represents the optimal trajectory in terms of ΔV to a specific KBO.

8.2. Alternative attempts

This section discusses the alternative attempts to get at least two KBO flybys with a low-thrust mission. This can either be done by changing the method to find a second KBO flyby after Albion or by disregarding Albion as a flyby target altogether. The first note from the previous section is the high ΔV required for the second KBO flyby after the flyby with Albion (see Figure 8.1). In the high-thrust trajectory this ΔV is often placed at the very start of the leg to the second KBO, at the lower bound of 1% of the total time-of-flight of the leg. Such an early DSM in the leg is not a good representation of a low-thrust trajectory where thrust is roughly equally distributed over the leg. This could be part of the reason why the high-thrust trajectories have difficulty translating to low-thrust ones in this case. Therefore, the first alternative test is to limit the time for the DSM in the leg from Albion to the second KBO to 40 - 60% of the leg in terms of its time-of-flight. However, this also does not lead to a low-thrust solution and even increases the ΔV of the best high-thrust trajectory solution to almost 18 km/s.

The second set of alternative methods focuses around the idea of optimizing multiple KBOs at the same time. So far the trajectory to Albion is locked and then a second KBO flyby is attempted. The issue with this is that no gravity assist with Albion is possible and as such there is very little wiggle room for future flybys since the departure velocity from Albion is already set. This can partially be resolved by optimizing the trajectory to Albion and the second KBO in one go as a high-thrust trajectory problem. This method is able to bring the total ΔV to the second KBO down to slightly more than 13 km/s for the high-thrust case, but still does not result in low-thrust solutions.

The next step is to optimize the flight to two random KBOs at the same time instead of Albion and a second KBO. Albion might simply be ill-positioned at the flyby date with respect to other KBOs. This is done with both the full DSM range as well as the 40 - 60% range. This results in KBO flybys with a total of 11.9 km/s for the full DSM range and 14.4 km/s for the 40 - 60% DSM range. However, still no low-thrust translation is found.

All the previous methods are also tested with an even more expanded data set of 2232 bodies which includes all known KBOs in the MPC independent of inclination or uncertainty values as long as enough information is present to construct a Kepler orbit. However, this also does not result in any feasible low-thrust trajectories. Considering how well the high- to low-thrust method worked in Chapter 7 the lack of results here is surprising. It could be that the ΔV 's found so far are still too high to find reasonable results. The lack of results can also be caused by the high sensitivity of spherical shaping. This works in tandem with the required positive D-function and search for the correct a_2 value. As explained before, the a_2 value can not be accessed unless the trajectory is already deemed feasible. Looking deeper in the inner workings of spherical shaping in Tudat's C++ code could shed more light on the difficulty to find a second CFB. However, this is out of scope for this thesis and is thus recommended for further research.

8.3. Close-approach graphs

Since the standard methodology to automatically go back-and-forth between high-thrust and low-thrust trajectories does not work as intended, the potential flyby options can also be manually inspected. This is done with so-called close-approach graphs. Such a graph propagates an unperturbed Kepler orbit for the spacecraft into the future and looks at the distance between this orbit and other KBOs at corresponding epochs. In this way it can be seen whether the spacecraft passes close to a potential KBO without using thrust. These closest encounters would then be reasonable picks for flyby targets. The close approach graph for the trajectory after Albion is shown in Figure 8.3 with the full set of 2232 KBOs. The blue line in the figure represents Albion. The two other bodies to which the spacecraft come closest to are first 15789 (green) and then q3738 (yellow). Neither of these bodies are capable of being reached with low-thrust spherical shaping trajectories. Also note how quickly the distance to all KBOs increases. Roughly three years after the flyby with Albion the distance to all KBOs within a reasonable window of 10 AU increase. This indicates that this trajectory quickly moves away from regions in space with many KBOs due to its high radial velocity. In future research the proximity of other KBOs to the primary KBO target could also be taken into account when optimizing trajectories.

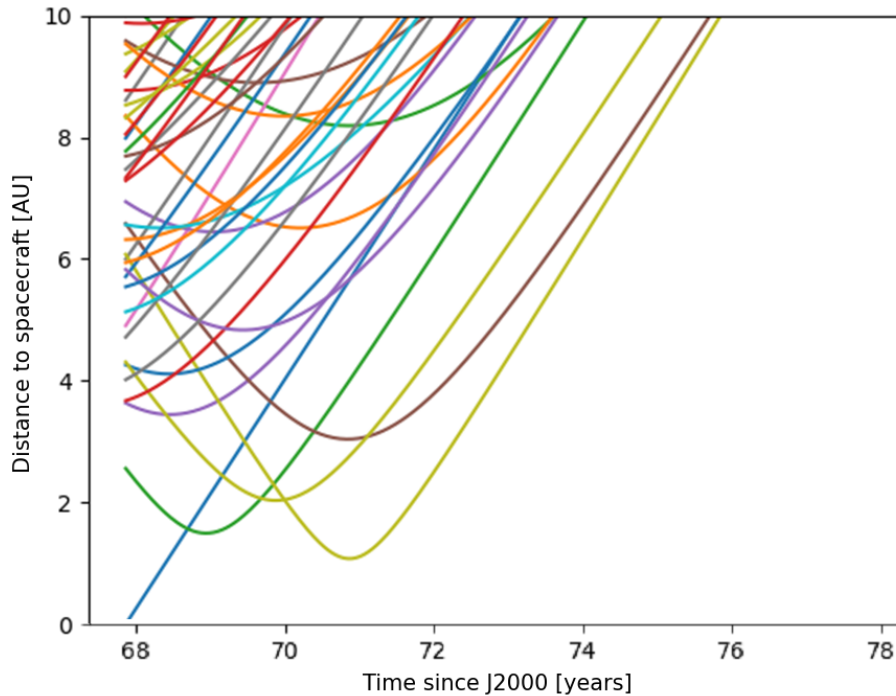


Figure 8.3: The close approach graph for the spacecraft after the nominal flyby with Albion. The figure shows the distance of the spacecraft to 2232 KBOs for 10 years after the Albion flyby. Only KBOs with an approach of 10 AU or less are shown.

Close-approach figures can also be made for alternative first KBO flybys instead of Albion. This means that the variables for the gravity assist at Neptune can also vary again. This results in three KBO candidates for the first flyby which can be reached with low-thrust propulsion using just a few m/s of ΔV . Of these the one with the shortest time-of-flight is D5182, which can be reached from Neptune just five years after the spacecraft enters the Kuiper belt. This body was not shown in Figure 8.2 since it is not present in the set of 590 bodies. Initially no low-thrust transfer towards D5182 could be found. Eventually after varying the search space for the a_2 value a feasible trajectory is found. This once again speaks in favor of the recommendation to look more at this root-finder function in further research and to make an automatic algorithm that performs multiple checks across the input space for the a_2 function to find all possible roots of the function. The close-approach graph for the trajectory after a first flyby with D5182 is shown in Figure 8.4.

This close-approach figure shows a light blue line which has a time-of-flight of six years and only requires 1.5 km/s of high-thrust ΔV . However, no low-thrust version is found for this second transfer. In a last attempt, the close-approach figures are used in combination with the optimization of both the first and second KBO flyby in one go as well. This is done with the full KBO database of 2232 bodies.

This leads to vastly more efficient transfers including a transfer via K13WB4G and K15RS1R with a total ΔV of only 352 m/s after Neptune. 3 m/s is required to go to K13WB4G and the remaining 349 m/s is needed for the leg to K15RS1R. Note that this ΔV value is highly variable depending on the a_2 value found, which is illustrated in more detail in Chapter 9. Replicating the first leg to K13B4G requires a very high value for a_2 above 100. This is due to the large inclination change required as K13WB4G lies more than 1 AU above the XY-plane of the ECLIPJ2000 coordinate system. After the low-thrust flyby of K13WB4G the close-approach graph can be seen in Figure 8.5. The figure shows a flyby of K15RS1R at roughly 10 million km at just over 73 years after J2000. This flyby towards K15RS1R is able to be connected with a low-thrust trajectory. This once again requires trail-and-error exploration of the a_2 range as the function has many roots for this leg, some of which result in infeasible trajectories. With a total ΔV of 352 m/s after Neptune, this trajectory represents a low-thrust flyby mission of two KBOs. The trajectory is discussed in more detail in Chapter 9.

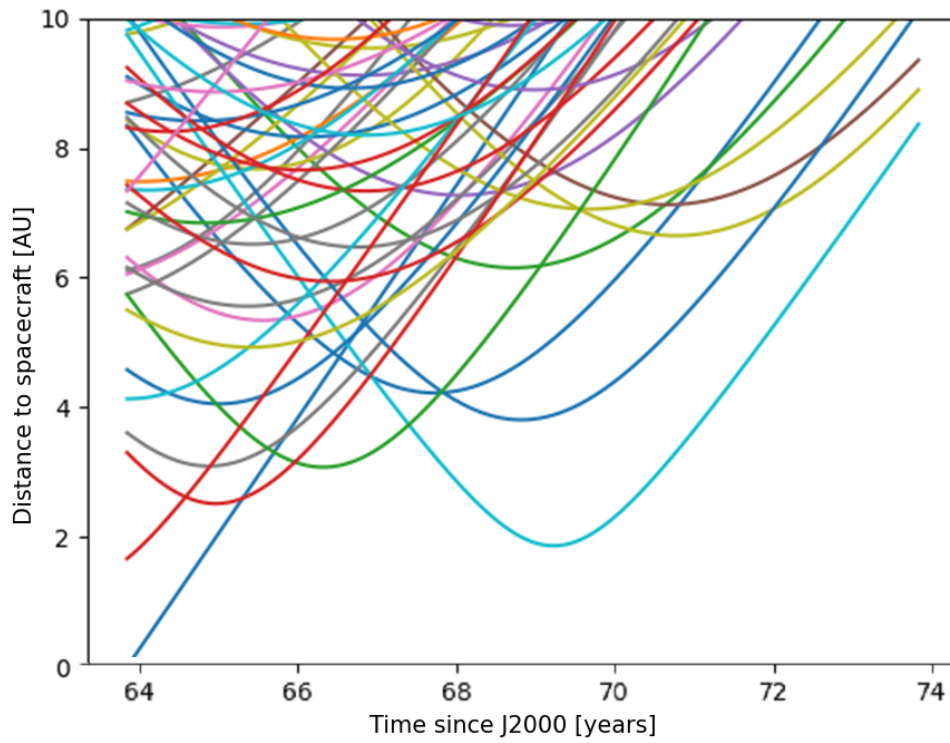


Figure 8.4: The close-approach graph for the spacecraft after the nominal flyby with D5182. The figure shows the distance of the spacecraft to 2232 KBOs for 10 years after the D5182 flyby. Only KBOs with an approach of 10 AU or less are shown.

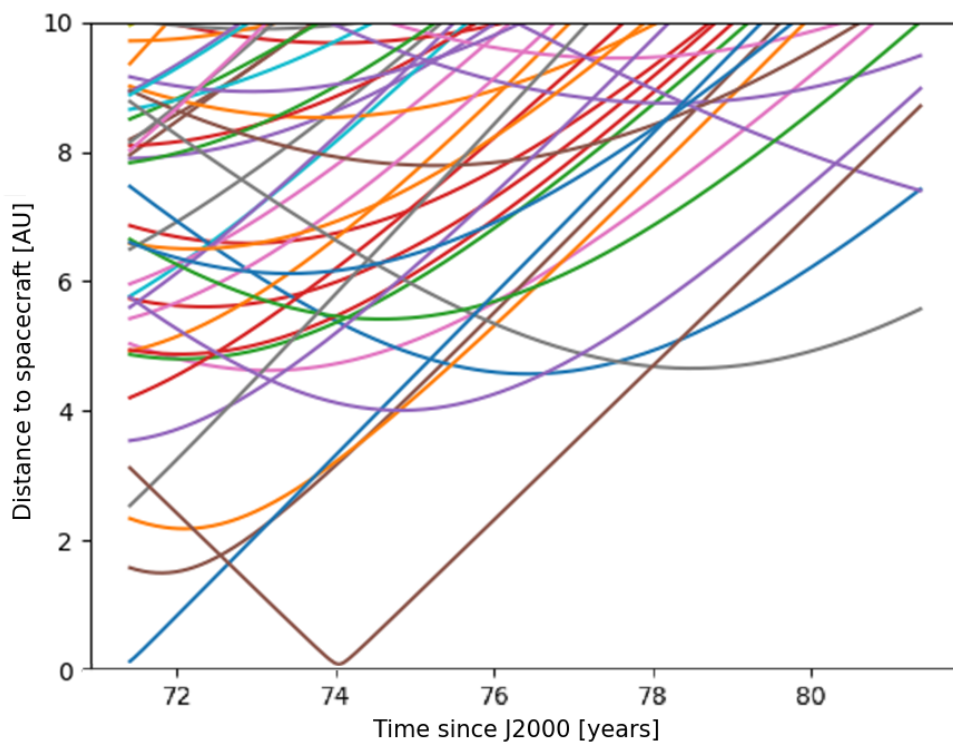


Figure 8.5: The close-approach graph for the spacecraft after the nominal flyby with K13WB4G. The figure shows the distance of the spacecraft to 2232 KBOs for 10 years after the K13WB4G flyby. Only KBOs with an approach of 10 AU or less are shown.

Due to time limitations of the thesis it is decided to focus on only finding a two-KBO flyby mission and to spend the remaining time on other analyses regarding optimization methods. As such, the analyses of three or more KBO visits in one low-thrust mission are left for further research. Despite the very close approach with many second KBOs it still takes many methods to find a single low-thrust trajectory with two KBO flybys compared to the numerous options with high-thrust propulsion. Furthermore, many other trajectories using this last method which eventually found a successful double-flyby KBO mission using high thrust could not be translated to low thrust. Based on their very low ΔV requirement such trajectories should easily be replicable in low thrust.

Based on these results it is concluded that it is most likely possible to perform many more multi-flyby low-thrust KBO missions, but that the description of spherical shaping is limiting the options compared to the real-life possibilities. The main issue here is the requirement for spherical shaping to have a trajectory curving towards the central body. In the current spherical-shaping description the time-of-flight would become a complex value (so with an imaginary component) and would thus not have a real-life interpretation in terms of flight time. An alternative description of spherical shaping could avoid this limitation and possibly lead to feasible multi-flyby trajectories. Such a description would also avoid some of the errors due to the bisection root finder. A more robust exploration of the a_2 range could also help with this to mitigate some of these errors. Finally, in a few rare cases the description of the spherical-shaping method leads to azimuth values which are outside of realistic bounds and can thus not be visualized. The precise cause of this error was not traced back and is thus recommended to be analyzed in further work on the Tudat framework. Furthermore, other (shape-based) parameterization methods such as hodographic shaping can be tested. Hodographic shaping has the option to add more free coefficients for its varying base functions. While the possibility of different base functions and more coefficients increases the complexity of the problem, it could also be key to find feasible KBO trajectories. The analysis of hodographic shaping for low-thrust KBO trajectories is thus recommended for future research.

8.4. Summary

This chapter analyzes the possibility to extend the low-thrust trajectory with more than one KBO flyby. This analysis is done with both the restricted data set of 22 KBOs, an extended set of 590 KBOs based on their inclination and uncertainty parameter, and finally a set of all 2232 KBOs which have sufficient information to generate a Kepler orbit. Extending the method from the previous chapter by switching between high- and low-thrust trajectories for the leg from Albion to a second KBO does not result in feasible low-thrust trajectories.

Many alternative methods are tested such as a limited range for the DSM times in the high-thrust case, using first flybys different from Albion, optimizing both the first and the second KBO at the same time, and using close-approach graphs to manually look at potentially attractive KBO targets. A combination of these methods results in a feasible low-thrust multi-KBO flyby trajectory via K13WB4G and K15RS1R. While a multi-KBO mission is found this took significantly more effort than expected. Furthermore, many more high-thrust versions with just a few tens of m/s beyond Neptune are found, but these could not be replicated in the low-thrust environment. Thus, it is concluded that many multi-flyby KBO missions with low thrust are most likely possible, but that most can not be found with the current method due to the inherent limitations of the shaping of low-thrust trajectories, in part due to the current implementation of the a_2 root-finding process and due to the requirement for the trajectory to be curved towards the central body.

9

Final results

This chapter summarizes the results based on the methodology of the last two chapters. The chapter provides overviews both in terms of the decision variables and the objective values for different trajectories. Note that this chapter only provides a handful of possible trajectories which have optimal objective values or were found first with the methodology of the previous chapters. In reality many more trajectories are possible, but the ones shown here are simply to illustrate the results of the developed methodology. Trajectories to Neptune, a single-KBO flyby, and a second KBO flyby are shown. The most discussed single flyby trajectory to Albion is also accompanied by a sensitivity study. Finally, the thrust magnitude and the real-world implications of the trajectories are discussed.

9.1. Earth to Neptune

The optimal low-thrust trajectory to Neptune in terms of ΔV based on the methodology of Chapter 7 is described by the decision variables in Table 9.1. This results in a trajectory with a ΔV of 9171.8 m/s and a total time-of-flight of roughly 17.9 years. The departure date for this trajectory is December 5, 2040 with an arrival date at Neptune on October 23, 2058. The trajectory is visualized in Figure 9.1. The ΔV of this trajectory is lower than the trajectory eventually used for the KBO flybys, but this is the case because this trajectory does not need to worry about good positioning with respect to subsequent KBO flybys. It is the result at the end of the low-thrust correction in the procedure of Chapter 7.

Table 9.1: An overview of the decision variable values for the optimized Earth-Jupiter-Neptune low-thrust trajectory. The number of revolutions and powered gravity assists are excluded from this table as they equal zero.

Trajectory stage	Variable	Value	Units
Earth departure	t_0	14949.8	MJD ₂₀₀₀
Earth to Jupiter	$t_{f,1}$	1208.7	days
Jupiter to Neptune	$t_{f,2}$	5321.9	days
Departure Earth	$V_{\infty,E}$	2.06	m/s
Departure Earth	θ_E	0.988	rad
Departure Earth	ϕ_E	0.906	rad
Arrival Jupiter	$V_{\infty,J}$	5751.6	m/s
Arrival Jupiter	θ_J	2.85	rad
Arrival Jupiter	ϕ_J	0.00932	rad
GA Jupiter	$r_{p,J}$	151,431	km
GA Jupiter	α_J	-1.36	rad
Arrival Neptune	$V_{\infty,N}$	7852.3	m/s
Arrival Neptune	θ_N	4.42	rad
Arrival Neptune	ϕ_N	0.0141	rad

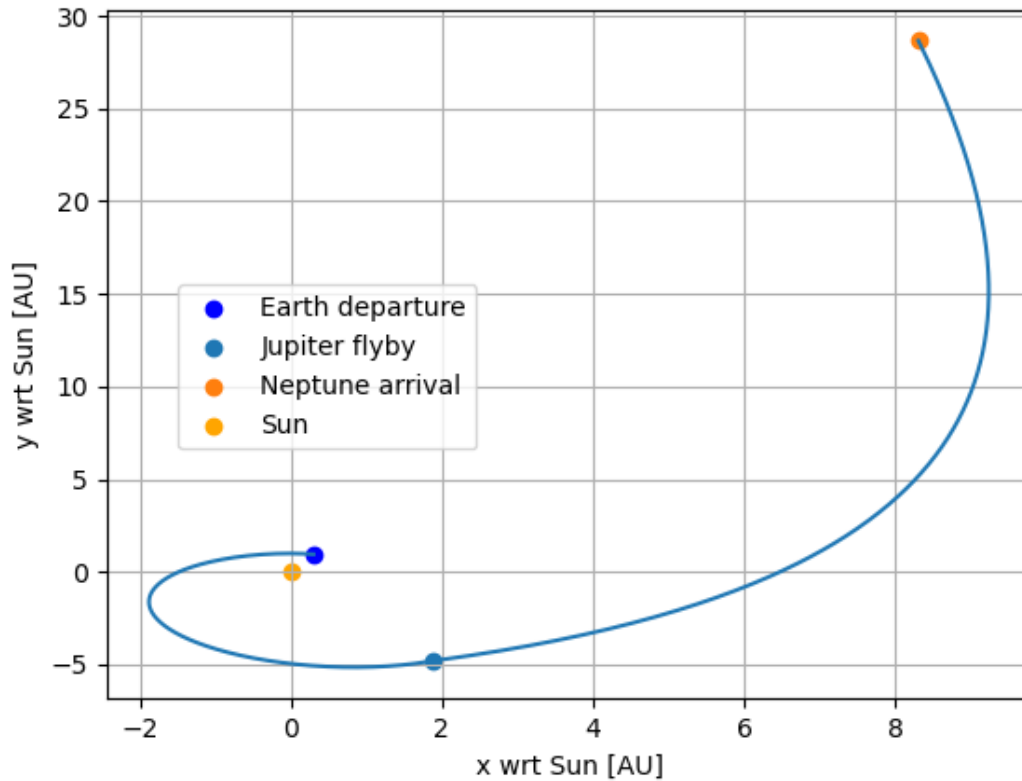


Figure 9.1: A 2D representation of the final optimal trajectory from Earth to Neptune using low-thrust propulsion. This trajectory has a time-of-flight of 17.9 years and a total low-thrust ΔV of 9,172 m/s. Note that the axes in this figure are not equidistant.

9.2. Single flyby results

The main single flyby case which is studied during this thesis is the trajectory to Albion. The decision variables for this trajectory can be found in Table 9.2. The original optimization process results in a ΔV of 9956.2 m/s. However, further refinement cycles where the decision variables can change $\pm 0.01\%$ bring down the ΔV to 9852.9 m/s. This clearly shows how sensitive spherical shaping is as changes in the order of 0.01% in the decision variables lowered the ΔV by roughly 1%. This trajectory has a time-of-flight of roughly 27.0 years. The departure date is December 5, 2040 with an arrival date on November 16, 2067. This ΔV corresponds to a wet-to-dry mass ratio of roughly. In other words, assuming a spacecraft dry mass of 500 kg a total of 200 kg of propellant would be required. A visualization of this trajectory was already given in Figure 7.13.

Besides Albion many other single flyby cases can be designed. A few of these have similarly low ΔV values as the original Albion run and are shown in Table 9.3. The extended local optimization cycles are only performed on Albion so it is expected that the ΔV of these other trajectories can also still be reduced by values in the order of a few percentage points. These trajectories are the same up to Neptune, but differ in their gravity assist with Neptune and their subsequent trajectory. These bodies stem from the full list of more than 2000 KBOs. Since all of these trajectories need only a few m/s or even less of ΔV after Neptune, their total ΔV values are very similar. However, their flight times are vastly lower with one of the trajectories even reaching its KBO target seven years before the trajectory to Albion. As an example the trajectory to D5182 is visualized in Figure 9.2.

Table 9.2: An overview of the decision variable values for the optimized Earth-Jupiter-Neptune-Albion low-thrust trajectory. The number of revolutions and powered gravity assists are excluded from this table as they equal zero.

Trajectory stage	Variable	Value	Units
Earth departure	t_0	14950.0	MJD ₂₀₀₀
Earth to Jupiter	$t_{f,1}$	1208.8	days
Jupiter to Neptune	$t_{f,2}$	5321.2	days
Neptune to Albion	$t_{f,3}$	3311.8	days
Departure Earth	$V_{\infty,E}$	2.06	m/s
Departure Earth	θ_E	0.988	rad
Departure Earth	ϕ_E	0.906	rad
Arrival Jupiter	$V_{\infty,J}$	5907.1	m/s
Arrival Jupiter	θ_J	2.83	rad
Arrival Jupiter	ϕ_J	-0.00215	rad
GA Jupiter	$r_{p,J}$	151,434	km
GA Jupiter	α_J	-1.36	rad
Arrival Neptune	$V_{\infty,N}$	7846.4	m/s
Arrival Neptune	θ_N	4.42	rad
Arrival Neptune	ϕ_N	0.0118	rad
GA Neptune	$r_{p,N}$	115,935	km
GA Neptune	α_N	-1.39	rad
Arrival Albion	$V_{\infty,KBO1}$	8924.2	m/s
Arrival Albion	θ_{KBO1}	5.09	rad
Arrival Albion	ϕ_{KBO1}	0.111	rad

Table 9.3: An overview of the time-of-flight and ΔV of a few optimal low-thrust trajectories to specific KBO targets.

KBO Target	Time-of-flight [days]	ΔV [m/s]
Albion	9842	9853
U9239	9037	9936
q3736	8689	9936
D5182	8586	9935
k9442	8241	9936
K15S20V	7271	9935

9.2.1. Sensitivity study

All the results and intermediate conclusions so far indicate that one of the main issues in finding feasible trajectories is the sensitivity of low-thrust trajectories or at the very least spherical-shaping-based low-thrust trajectories. Therefore, it is also helpful to know how sensitive the trajectory is to unexpected changes. For this the trajectory to Albion is used and the departure time is varied. Variations in the other decision variables are also relevant, but require a detailed literature study to find the relevant uncertainties. This is out of scope for this thesis, but recommended for further research. An uncertainty in the departure date is the most common and most impactful deviation as it often occurs due to for example the weather situation at the launch location.

The launch window for New Horizons was for example 35 days of which only 18 days allowed for the original trajectory with a Pluto flyby in 2015 [38]. For the trajectory to Albion the departure time is varied in intervals of two days over a range of -20 to +20 days with respect to the intended departure date of December 5, 2040. Small variations in the trajectory variables in the order of 0.01% are allowed to improve the ΔV of the cases with a perturbed departure date. Note that a strong increase in the launch energy might also be capable of correcting for the launch date deviation, but this is not analyzed here as launch energy in general is not studied in detail in this thesis project. The results of this sensitivity analysis are visualized in Figure 9.3.

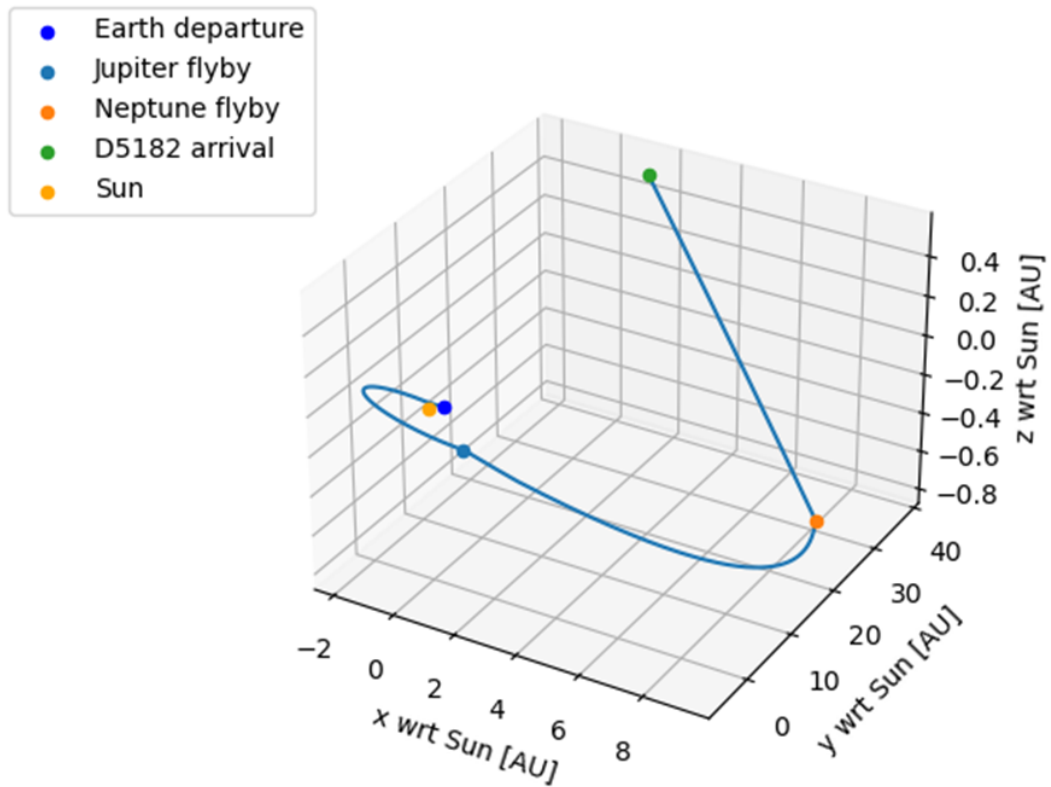


Figure 9.2: A 3D representation of the final optimal trajectory from Earth to D5182 using low-thrust propulsion. This trajectory has a time-of-flight of 23.5 years and a total low-thrust ΔV of 9,935 m/s. Note that the axes in this figure are not equidistant.

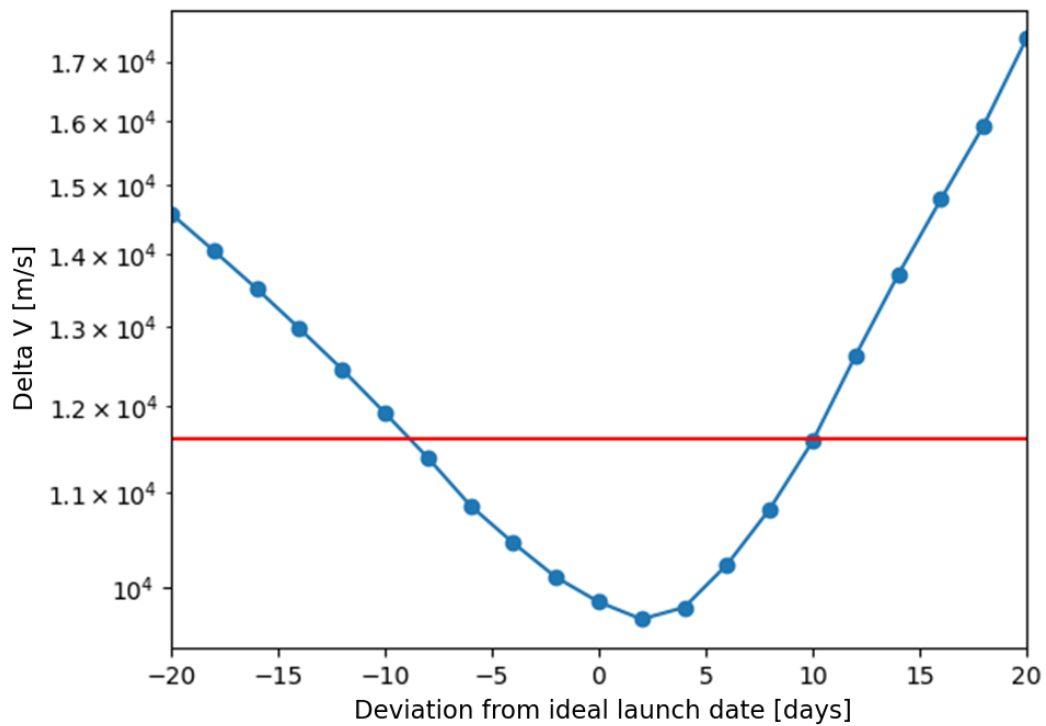


Figure 9.3: The total ΔV required for the low-thrust mission to reach Albion depending on the deviation from the desired departure date of December 5, 2040. The red line represents a 20% value above the lowest found ΔV .

One thing that is immediately visible is that the dip for the lowest ΔV is actually located at a deviation of +2 days instead of at the nominal departure date. At this departure date a ΔV of 9683.3 m/s is found. This shows that, despite the multiple optimization cycles, the trajectory might still only be optimized for a local optimum. This information is important to remember for any analyses on this topic in future study as it underlines the importance of further optimization cycles or perhaps the use of a local optimizer after the global optimization round.

As can be seen in the figure, none of the days in the 40-day window ever have a ΔV which goes above the maximum 20.4 km/s value based on the wet-to-dry mass ratio. However, if one for example wants to stay within 20% of the lowest found ΔV value then a launch window of roughly 18 days is present, which is realistic when compared to other missions such as New Horizons. This 20% window is chosen based on the fact that above roughly 12 km/s other high-priority KBOs would become more attractive than sticking with the Albion flyby (see Figure 8.2). Note that in the case of New Horizons the extra ΔV due to a shifting launch date is corrected by increasing or decreasing the launch energy by roughly 6 km^2/s^2 [38]. This might also be possible for this mission, but the study of the launch energy is out of scope of this analysis. Also note how the ΔV increase is slower for a negative time deviation. This is the case since a negative deviation relates to a longer time-of-flight, while a positive deviation means that the spacecraft would need to speed up to reach the planetary encounter at the right time.

9.3. Multiple flyby results

Chapter 8 looked at possibilities to find multi-flyby KBO trajectories. First some of the unsuccessful attempts at such trajectories are discussed followed by the final trajectory to K13WB4G and K15RS1R.

One of the first tested potential targets found with the close-approach graphs is D5182. This target is found by looking at the close-approach graph for the Albion trajectory in Figure 9.4. But instead of looking at the close approaches after Albion, as was done in Chapter 8, this shows close approaches in the leg from Neptune to Albion. Three targets are found and are indicated with arrows. The earliest relatively close approach, indicated by a red arrow, is D5182.

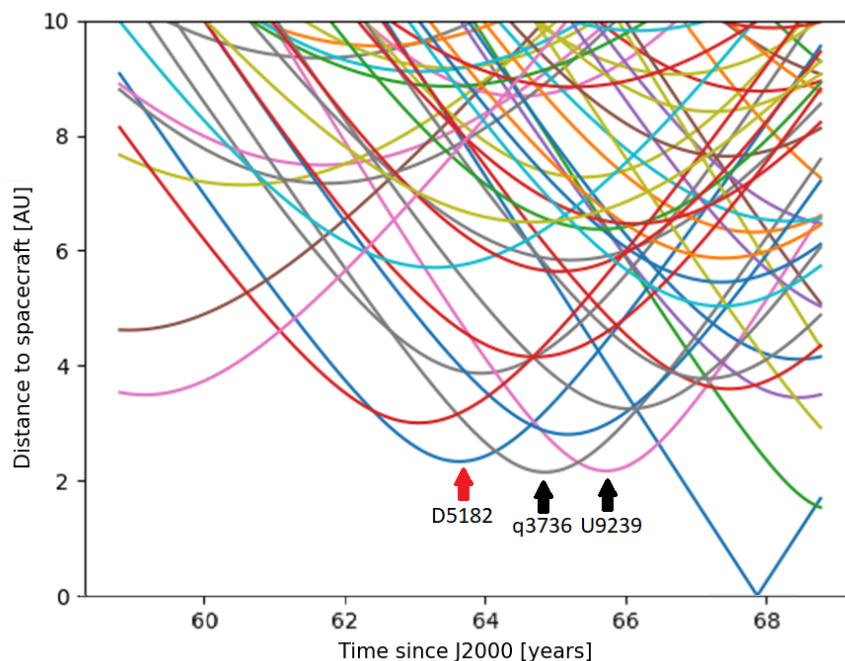


Figure 9.4: The close-approach graph for the spacecraft trajectory to Albion during the phase between Neptune and Albion. The figure shows the relative distance of the spacecraft to KBOs. The blue line which reaches the x-axis near the end of the figure represents Albion itself. Three potential other first KBO flybys are indicated with arrows. The red arrow indicates the approach line for D5182. Only KBOs with an approach of 10 AU or less are shown.

Following the trajectory to this KBO a new search starts for a second KBO flyby, first using high-thrust propulsion. Here the KBO target q5257 is found which can be reached with an additional ΔV of roughly 1.6 km/s. While no low-thrust equivalent for this trajectory is found the time-of-flight of slightly over 2,000 days implies that a continuous ΔV of on average 0.8 m/s per day is required, which is realistic with the low-thrust power requirements. The lack of a suitable trajectory is thus related to the fundamentals of spherical shaping instead of a real-life impossibility. The trajectory to q5257 via D5182 where the last leg assumes the high-thrust maneuver is shown in Figure 9.5.

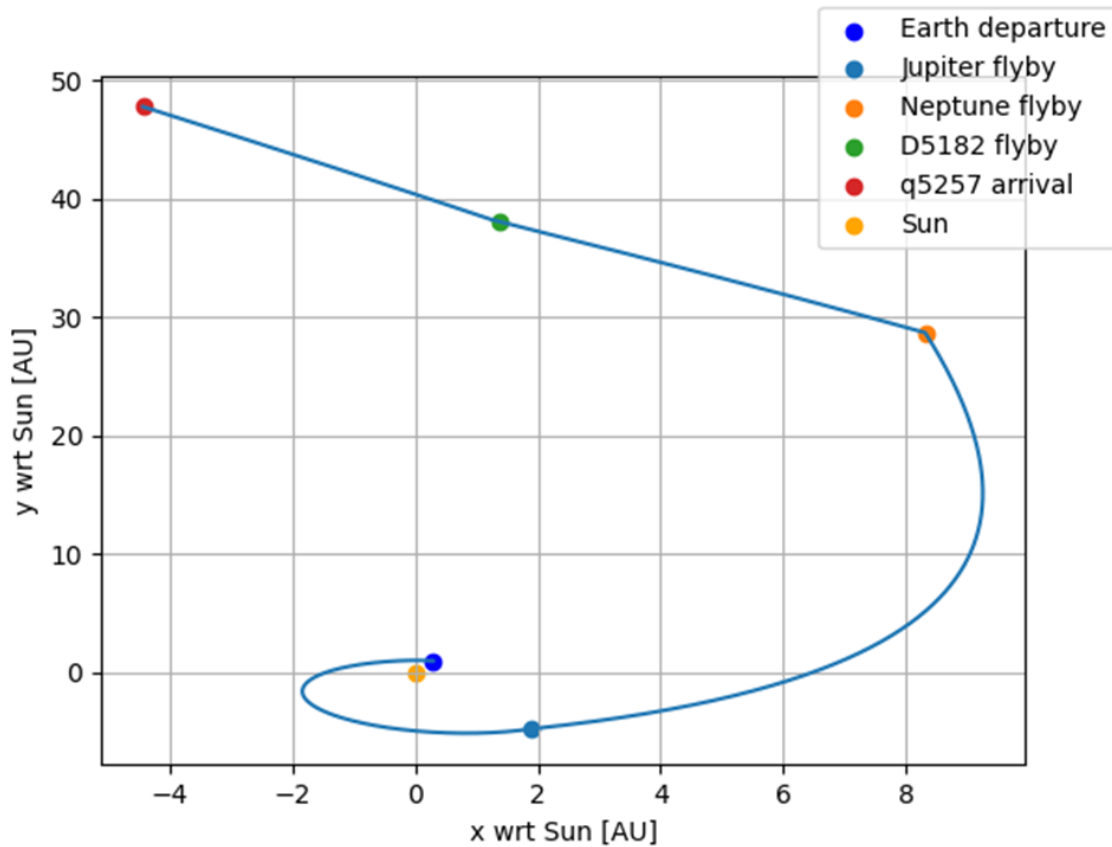


Figure 9.5: A 2D representation of the final optimal trajectory from Earth to D5182 and then to q5257. The last leg uses high-thrust propulsion since no low-thrust spherical-shaping equivalent could be found. Note that the axes in this figure are not equally scaled.

When the full data set of KBOs is used and both the first and second KBOs are optimized together high-thrust trajectories are found which only require a few m/s of ΔV beyond Neptune. Most of these trajectories can be replicated up until and including the first KBO flyby, but fail when including the second KBO due to the same limitations of spherical shaping as discussed before. One example of such a trajectory is shown in Figure 9.6 and concerns flybys of K15RR8F and K10JL0J. This trajectory requires roughly 550 m/s of ΔV after Neptune in the high-thrust case.

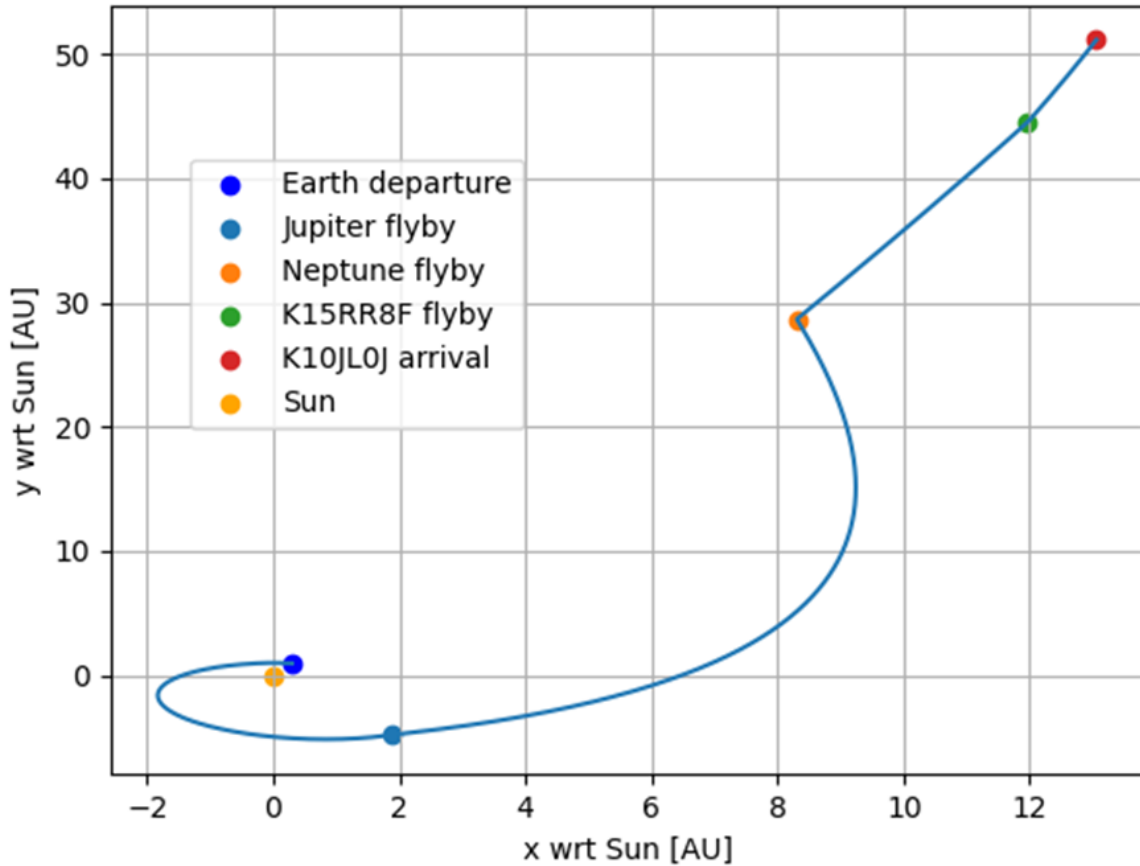


Figure 9.6: A 2D representation of the final optimal trajectory from Earth to K15RR8F and then to K10JL0J. The last leg uses high-thrust propulsion since no low-thrust spherical-shaping equivalent could be found. Note that the axes in this figure are not equally scaled.

Many more cases with two flybys are found using high-thrust trajectories, but most of them could not replicate the second flyby when translated to a low-thrust spherical-shaping trajectory. Most of the time this is caused by the second KBO leg curving away from the central body (= the Sun) during the leg. For future development it is thus recommended to either rework spherical shaping to allow any curvature or to analyze multi KBO low-thrust flybys with a different low-thrust thrust parameterization. To ensure that trajectories with the current parameterization do not optimize trajectories which curve away a simple function has been added to the Python code which checks whether a trajectory curves away from the central body. If so, it is not taken into account during the high-thrust two-KBO exploration run. Even with this method though some high-thrust trajectories with seemingly feasible ΔV values are found which still do not translate to low thrust. This most likely has to do with the multiple roots of the a_2 function, which is why further study of that parameter is the other main recommendation following from the multi-KBO flyby analysis.

The curvature filter method together with the optimization of two KBOs at the same time from the full set of over 2000 KBOs and the use of close-approach graphs eventually results in a two-KBO trajectory which passes by K13WB4G and K15RS1R. It is visualized in Figure 9.7. The full list of decision variables for this trajectory is shown in Table 9.4. Here the GA variables at the KBOs are not included as no gravitational affect is modelled. Note that this method still uses the less optimized JN trajectory which was found in Chapter 7. The multiple local refinement cycles are only used for the trajectory to Albion in this thesis. Running extra optimization rounds for the other trajectories is recommended for future research.

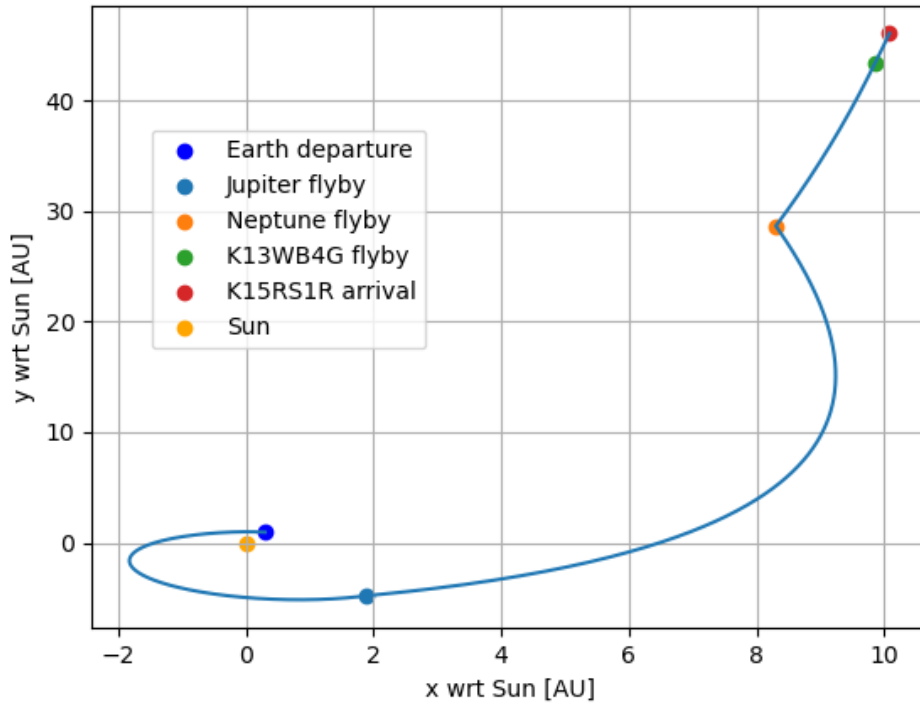


Figure 9.7: A 2D representation of the final optimal trajectory from Earth to K13WB4G and then to K15RS1R. Note that the axes in this figure are not equally scaled.

Table 9.4: An overview of the decision variable values for the optimized Earth-Jupiter-Neptune-K13WB4G-K15RS1R low-thrust trajectory. The number of revolutions, powered gravity assists, and gravity assist variables at KBOs are excluded from this table as they equal zero or are neglected.

Trajectory stage	Variable	Value	Units
Earth departure	t_0	14948.4	MJD ₂₀₀₀
Earth to Jupiter	$t_{f,1}$	1208.7	days
Jupiter to Neptune	$t_{f,2}$	5321.9	days
Neptune to K13WB4G	$t_{f,3}$	4603.1	days
K13WB4G to K15RS1R	$t_{f,4}$	998.3	days
Departure Earth	$V_{\infty,E}$	2.06	m/s
Departure Earth	θ_E	0.988	rad
Departure Earth	ϕ_E	0.906	rad
Arrival Jupiter	$V_{\infty,J}$	5906.2	m/s
Arrival Jupiter	θ_J	2.83	rad
Arrival Jupiter	ϕ_J	-0.00215	rad
GA Jupiter	$r_{p,J}$	151,431	km
GA Jupiter	α_J	-1.36	rad
Arrival Neptune	$V_{\infty,N}$	7846.8	m/s
Arrival Neptune	θ_N	4.42	rad
Arrival Neptune	ϕ_N	0.0118	rad
GA Neptune	$r_{p,N}$	584,504	km
GA Neptune	α_N	1.38	rad
Arrival K13WB4G	$V_{\infty,KBO1}$	5867.9	m/s
Arrival K13WB4G	θ_{KBO1}	4.08	rad
Arrival K13WB4G	ϕ_{KBO1}	0.0674	rad
Arrival K15RS1R	$V_{\infty,KBO2}$	5602.7	m/s
Arrival K15RS1R	θ_{KBO2}	4.07	rad
Arrival K15RS1R	ϕ_{KBO2}	0.0586	rad

This trajectory is found with an older optimized JN trajectory with a total ΔV of 10,169 m/s up to Neptune and with 352 m/s after Neptune for a total of 10,521 m/s. This results in a wet-to-dry mass ratio of 1.43, well below the requirement of 2.0. Assuming a spacecraft dry mass of 500 kg a total of roughly 215 kg of propellant would be required for a total wet mass of 715 kg. The spacecraft spends a total of roughly 19.5 years in the Kuiper belt. Not as long as some of the trajectories found by L. van der Heyden, but much longer than the roughly 7 years that the New Horizons spacecraft spent in the Kuiper belt [86].

The first few legs of this trajectory can be calculated with the standard -1 to 1 range for a_2 . The leg to K13WB4G requires a larger range of a_2 with an upper bound of 150. The leg to K15RS1R is even more laborious to calculate as it has many roots. A visual of the a_2 function for this final KBO leg of the trajectory is provided in Figure 9.8. Even if a step size of 10^{-8} is used for the a_2 value no smooth graph forms. This results in difficulty for the root finder to find a correct a_2 value and also results in wildly different ΔV values depending on the root. Due to the highly fluctuating function the root finder can not find the true intersection point perfectly and this results in slight deviations when it comes to the ephemerides of the spacecraft (more on this in Section 9.4). Therefore, the root is chosen which minimizes this ephemeris deviation. Other roots with a larger deviation do exist and have lower ΔV values after Neptune down to 31 m/s instead of 352 m/s, but are not chosen due to their larger deviation from the true ephemerides of the target KBO. Finally, note that the current implementation in Tudat only allows a single a_2 range per trajectory. Therefore, the legs of the trajectory have to be calculated separately as such no sensitivity study on the trajectory as a whole could be performed.

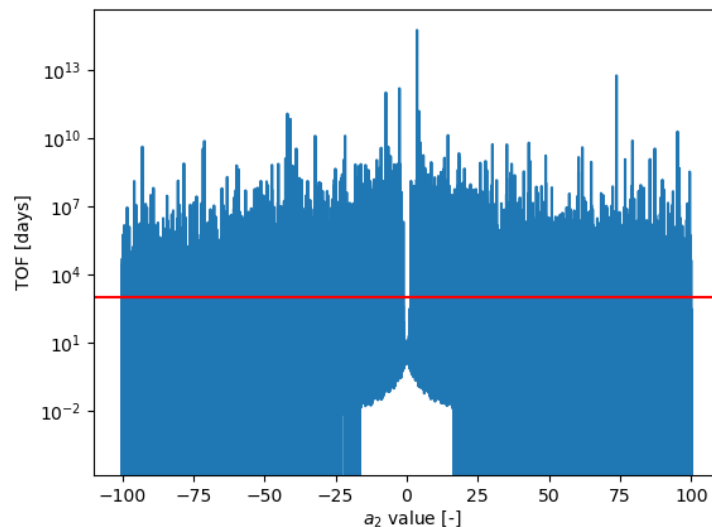


Figure 9.8: The time-of-flight as a function of the a_2 variable for a trajectory leg from K13WB4G to K15RS1R. The blue line shows the time-of-flight as a function of a_2 while the red line indicates the true time-of-flight, which is 2.73 years.

9.4. Distant flyby analysis

The entire trajectory analysis has focused on CFBs. DFBs or VDFBs, which would still allow some scientific study, have not been taken into account during the optimization process. Taking these into account is recommended for future study, but for now they are analyzed in hindsight as by-products of the trajectory. For this the close-approach graphs from Chapter 8 can be used, but now running both forwards and backwards in time such that they capture the entire period the spacecraft is in the Kuiper belt. An overview of all close approaches for the trajectory to Albion while in the Kuiper belt is given by Figure 9.9. Besides the CFB with Albion this trajectory has only one VDFB with q3738 and no DFBs. Similarly, the DFB analysis from Neptune to K13WB4G is shown in Figure 9.10 and gives similar conclusions with two DFBs. An approximation of the close-approach graph for the leg between K13WB4G and K15RS1R was already given by Figure 8.5 and shows no new VDFBs after K13WB4G with the exception of K15RS1R of course. While more research into this topic is recommended, these images suggest that to perform a substantial number of (V)DFBs with known KBOs it should be taken into account in the objective description of the optimization process.

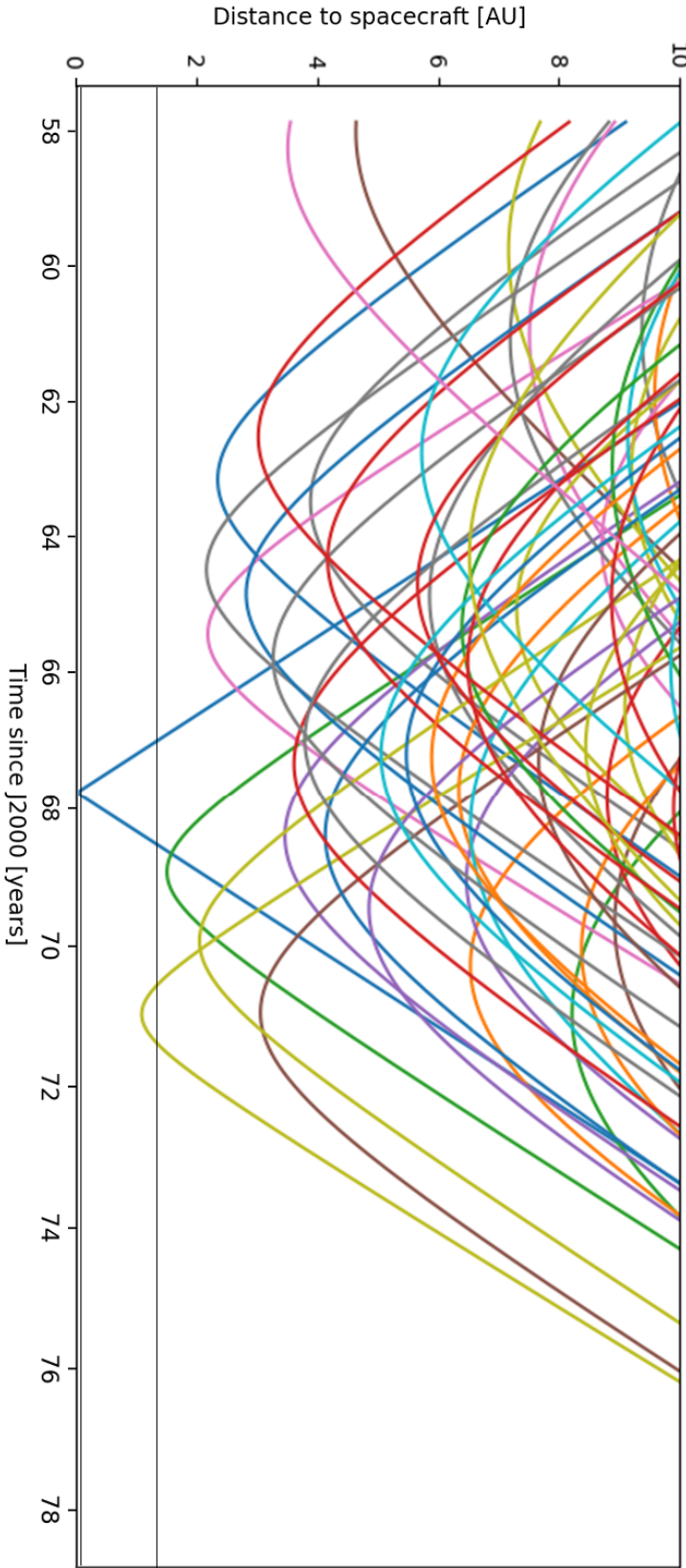


Figure 9.9: An overview of all close approaches for the optimized trajectory from Neptune to Albion. The bottom black horizontal line in the graph is at 0.06 AU which counts as a DFB, while the second horizontal line at 1.34 AU is the most extreme definition of a VDFB.

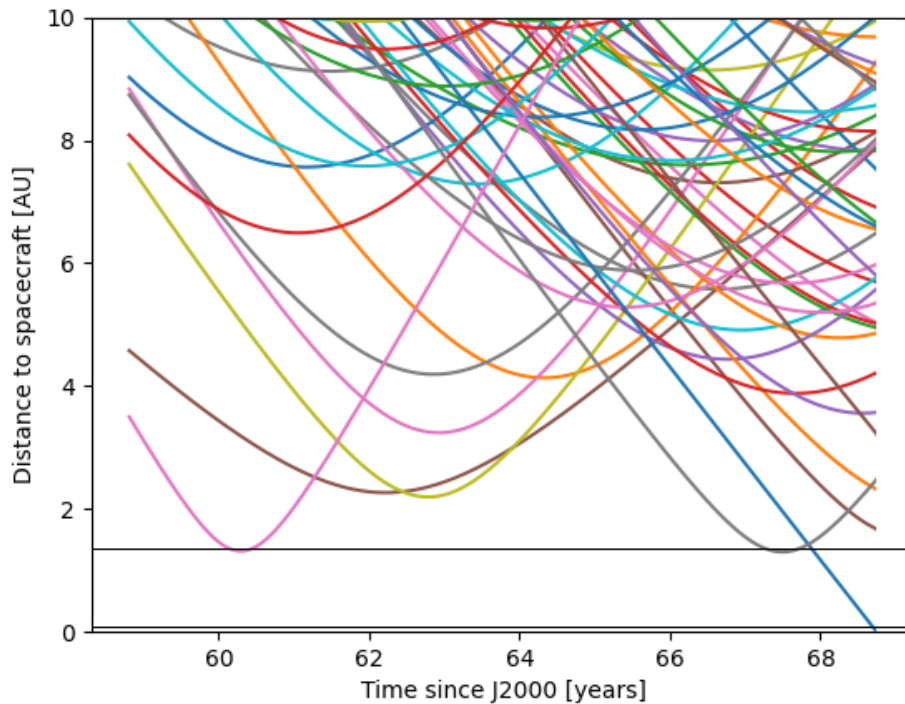


Figure 9.10: An overview of all close approaches for the optimized trajectory from Neptune to K13WB4G. The bottom black horizontal line in the graph is at 0.06 AU which counts as a DFB, while the second horizontal line at 1.34 AU is the most extreme definition of a VDFB.

9.5. Thrust magnitude analysis

Two of the constraints from Chapter 3 have not been discussed yet: the thrust limit and approach distance to the Sun. In none of the optimal trajectories does the distance to the Sun become closer than is described in the constraints list so this is not an issue for the found trajectories. The other constraint regards the thrust profile of the trajectory. Specifically, there is a variable thrust limit depending on the time since launch due to the degradation of the RTG power source. All trajectories have thrust limits with a similar order of magnitude, but as is done so far in this chapter the trajectory to Albion will once again be taken to illustrate the results. The thrust profile of the trajectory to Albion is shown in Figure 9.11. This concerns the improved thrust profile after the sensitivity study. Note that this improvement due to the sensitivity study does not change the thrust profile to a degree which would affect the conclusions of this section.

As can be seen the thrust remains orders of magnitude below the thrust limit during the the majority of the flight. Only near the start of the flight the limit is exceeded. However, in real-life this should not be much of an issue. One of the main reasons why the thrust at the start is so high is because a near-zero excess velocity at departure from Earth is assumed. If later research does include higher launch energy values it is expected that the thrust at the start of the launch will also fall below the thrust limit. Furthermore, since the limit is exceeded at the start of the trajectory it is still possible to temporarily increase the power of the spacecraft at this stage by adding (detachable) solar panels to the spacecraft design.

Later stages of the trajectory do show a sufficient margin with the thrust limit. This becomes even more apparent for the low- ΔV legs towards a KBO such as the thrust profile for the leg from Neptune to K13WB4G in Figure 9.12. This shows that in terms of the power requirement the low-thrust KBO trajectories are realistic with modern technologies. Note that in real-life the thrust profile will probably not look like this. Due to the throttle sensitivity of low-thrust propulsion as well as to prevent wear of the thrust system it is not recommended to have active thrust for the entirety of the decades-long mission. In reality common minimum thrust values for ion engines are in the order of 10^{-3} N [56]. The longest in-flight operational use of a low-thrust propulsion system to date is 16,246 hours or a little under 2

years [127]. A real KBO mission would have short periods of relatively higher thrust levels which would replicate the effect of this continuous thrust profile. The room in the thrust limit budget, beyond the initial phase of the trajectory, indicates that there is plenty of margin for such shorter but stronger thrust sections. The rest of the trajectory would then consist of coasting phases with no thrust. In more detailed design of the mission the study for more realistic thrust profiles with coasting phases is highly recommended.

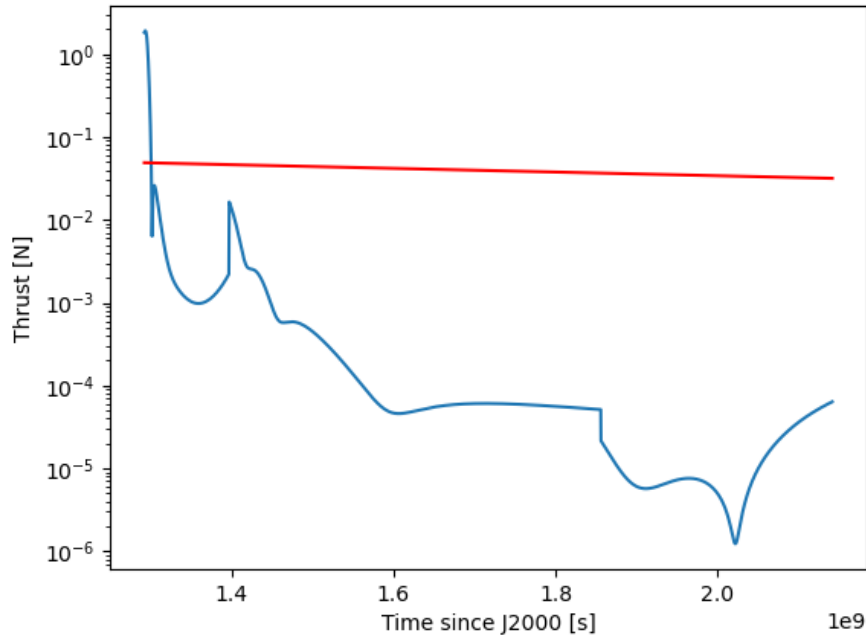


Figure 9.11: The thrust profile for the optimized trajectory from Earth to Albion. The red line indicates the maximum allowable thrust based on the power constraint. Due to the log scale the degradation of the maximum allowable thrust is difficult to see.

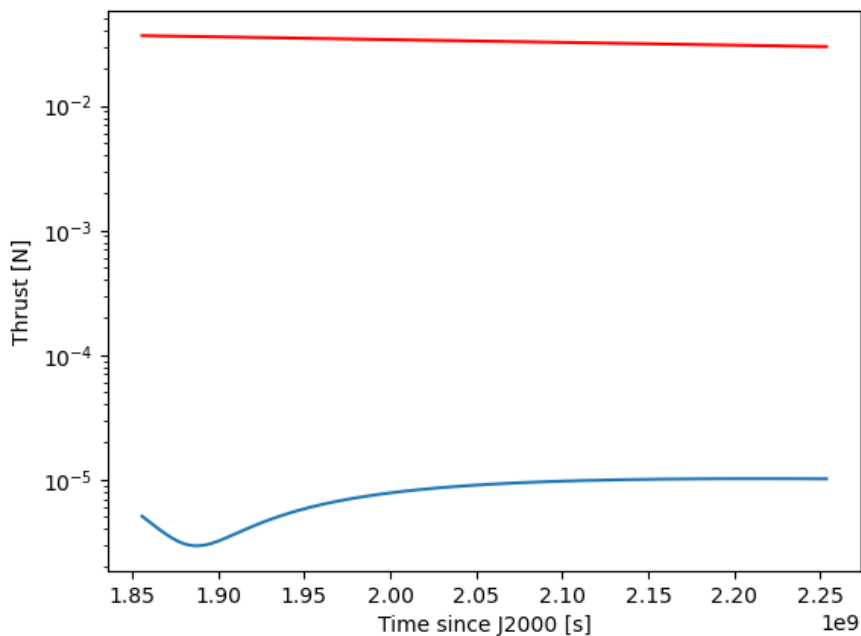


Figure 9.12: The thrust profile for the optimized trajectory from Neptune to K13WB4G. The red line indicates the maximum allowable thrust based on the power constraint. Due to the log scale the degradation of the maximum allowable thrust is difficult to see.

9.6. Requirements recap

In Chapter 3 an overview of mission requirements was given. With the final results of this thesis it is now checked whether these requirements are fulfilled. The list below provides the identifier for each requirement together with a short description. This is followed by a pass/fail and a short explanation if necessary. For a quick overview green text indicates a pass while any (partial) failures of meeting requirements are indicated with red text. All but two of the requirements are passed. Necessary follow-up steps or solutions are presented for the failed requirements.

- KBM-GEN-01 = performing a close flyby with two KBOs. Pass, a trajectory with two KBO CFBs has been found.
- KBM-GEN-02 = the mission ends once the Kuiper belt is left or after 100 years. Pass, the mission objectives of two CFBs are reached before the mission ends.
- KBM-GEN-03 = a wet mass below 1000 kg. Pass, the found ΔV values allow for a spacecraft mass below 1000 kg.
- KBM-GEN-03.1 = a dry mass of at least 500 kg. Pass, the found ΔV values allow for a spacecraft dry-mass of at least 500 kg.
- KBM-INSTR-01 = general usage instrumentation power budget is below 50 W. Pass, the general instrumentation power budget equals 42.2 W.
- KBM-INSTR-01.1 = peak usage instrumentation power budget is below 100 W. Pass, the peak instrumentation power budget equals 82.2 W.
- KBM-PROP-01 = the use of Xenon-ion propulsion. Pass.
- KBM-PROP-01.1 = adherence to the ion power-based thrust limit. Fail, the thrust limit is exceeded for some trajectories during the early stage of the mission (before Jupiter). However, suitable solution strategies are presented such as a higher launch energy.
- KBM-POW-01 = the spacecraft power is delivered with three GPHS-RTGs. Pass.
- KBM-LV-01 = a launch energy below $100 \text{ km}^2/\text{s}^2$. Pass.
- KBM-TIME-01 = a launch date between 2040 and 2050. Pass.
- KBM-TIME-02 = the Kuiper belt is reached within 25 years of launch. Pass, the multi-KBO flyby mission reaches the Kuiper belt in 17.9 years.
- KBM-TIME-03 = the average time between KBO CFBs is lower than 10 years. Pass, the multi-KBO flyby mission has an average flight time between KBOs of 7.7 years.
- KBM-TRAJ-01 = the mission has a Jupiter flyby, a Neptune flyby and KBO CFBs. Pass.
- KBM-TRAJ-01.1 = adherence to the revolution limit around the Sun per leg. Pass.
- KBM-TRAJ-01.2 = adherence to periapsis limits during the gravity assists. Pass.
- KBM-TRAJ-01.3 = adherence to Sun-approach limits during the trajectory. Pass.
- KBM-TRAJ-02 = adherence to the usage of KBOs with an uncertainty factor of 2 or lower for CFBs. Fail, the multi-KBO flyby is performed with a body with an uncertainty factor of 6 and 3, respectively. This results in ephemerides uncertainties of roughly 4 AU and 0.05 AU, respectively, as of launch. Observation of the KBOs during the mission can be used to reduce the uncertainty of the bodies and further research towards the required ΔV buffer is recommended.

9.7. Comparison with high thrust and industry

With the trajectories now fully described a few final remarks can be made regarding the results and the used methodology. Specifically, how the found low-thrust trajectories compare to their high-thrust counterparts and how the found methodology compares to industry low-thrust optimization.

9.7.1. Comparison with high-thrust trajectory performance

Firstly, the comparison with high-thrust trajectories is discussed. In this thesis high-thrust trajectories were used as intermediate steps during the optimization process. However, these trajectories do not function as fair comparison material for the low-thrust trajectories. Due to the lower efficiency of high-thrust propulsion, it is crucial to perform as much of the ΔV with the LV such that the final spacecraft does not become too heavy. Since the trajectories in this thesis neglect the launch energy of the LV

this puts the high-thrust examples at an unfair disadvantage for a direct comparison. Therefore, further research is recommended with the most promising found trajectories where the launch energy limits are increased for both high-thrust and low-thrust cases in order to perform a direct comparison of the payload mass.

Comparisons with heritage and other theses can be done to get some idea of the relative performance of the found low-thrust trajectories. Assuming an I_{sp} of 250 s for high-thrust propulsion the wet-to-dry mass ratio of the spacecraft for the trajectories found in L. van der Heyden's work range from 1.01 to 2.66 depending on the chosen planetary flyby sequence [43]. Research by M. Penas on high-thrust KBO flybys found a two-KBO flyby sequence with a total ΔV of 2.68 km/s from DSMs [98]. This trajectory uses a propellant with an I_{sp} of 228 s, resulting in a wet-to-dry mass ratio of roughly 3.31 [98].

Other papers mentioned in Chapter 2 analyzed high-thrust KBO missions. The trajectory analysis to Haumea found a candidate using a gravity assist with Jupiter with a total of 7.449 km/s of DSM ΔV or a wet-to-dry mass ratio of roughly 12.6 assuming an I_{sp} of 300 s [108] and results with the same order of magnitude were found for trajectories to other well-known KBOs [57]. These trajectories often use high launch energy values in excess of $100 \text{ km}^2/\text{s}^2$. One of the most promising high-thrust results is that of a multi-KBO mission to Huya and Quaoar with a ΔV of 1.30 km/s for a trajectory with a launch energy of roughly $118 \text{ km}^2/\text{s}^2$ and a ΔV of 2.57 km/s for a trajectory with a launch energy of roughly $29 \text{ km}^2/\text{s}^2$ [47]. Using the given specific impulse of 323 s in the paper [47] this results in wet-to-dry mass ratios of 1.51 and 2.25, respectively for the two trajectories.

Comparing these results to the found wet-to-dry mass ratios of 1.39 to 1.43 in this thesis can not result in definitive conclusions, as the experiments in the aforementioned papers are not directly comparable to the ones in this thesis. However, the fact that even with a non-zero launch energy many of the high-thrust KBO missions require a higher wet-to-dry mass ratio for the final stage of the spacecraft than the found low-thrust trajectories indicates the potential of low-thrust KBO missions. Further research is especially recommended to determine whether the addition of a significant non-zero launch energy is capable to reduce the wet-to-dry mass ratio to values comparable as found by L. van der Heyden. Note that with the current C_3 value of roughly $0 \text{ km}^2/\text{s}^2$, the payload mass capabilities of the LV are also much more favorable than the high-thrust counterparts with high launch energy values, as can be seen in Figure 3.1.

9.7.2. Industry optimization methods

Optimizing feasible low-thrust trajectories required much effort during this research project to the point of finding almost no two-KBO low-thrust flyby trajectories. As such, the question arises how other projects such as industry missions by NASA or ESA as well as other papers have calculated and in some cases successfully flown low-thrust missions. There are a few ways in which the methods by these larger institutions differ from the research in this thesis. Firstly, they often have access to more extensive computing systems and supercomputers to increase the number of simulations which can be performed. Secondly, most missions use atypical low-thrust descriptions which are far more complex than the shape-based methods in this thesis. This requires more computational time, but allows far more freedom in the trajectory shape. This is for example illustrated by the frequent use of coasting in Figure 9.13, a more detailed version of the Dawn trajectory (a simplified version was shown in Figure 2.10) [104]. This mission was designed using a tool called Mystic [104].

Thirdly, note that no low-thrust KBO mission has ever flown which means that it is not possible to fully compare it to other mission design projects such as a trajectory to Vesta and Ceres in the case of the Dawn mission. Finally, it is important to note that in hindsight it can be concluded that the current implementation of spherical shaping is one of the major reasons for the difficulty to find KBO flybys. Thus, it is possible that other methods such as Sims-Flanagan or hodographic shaping are more flexible in finding feasible results. Nevertheless, the work in this thesis shows that even with lower computational effort and simplified models it is still possible to design feasible and, compared to other research as described in the previous subsection, competitive low-thrust KBO trajectories.

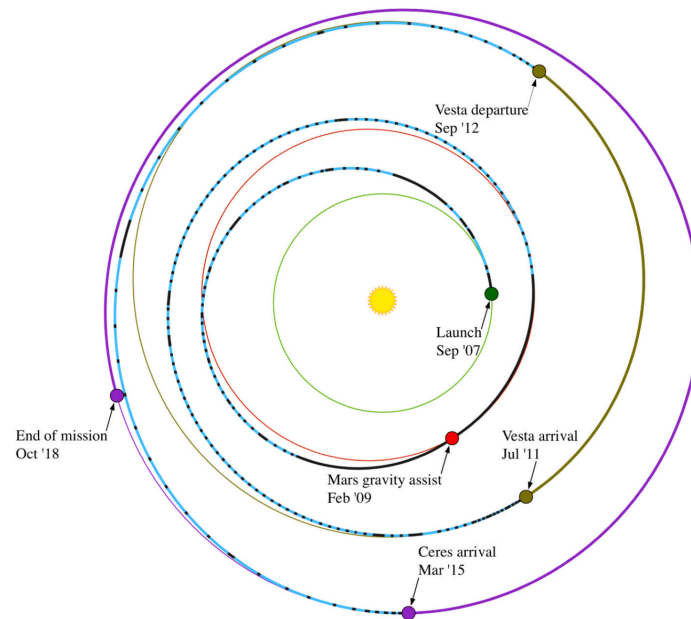


Figure 9.13: An overview of the trajectory of the Dawn mission. The black segments represent coasting phases [104].

9.8. Summary

This chapter provides a comprehensive overview of the resulting final trajectories based on the methodologies described in the previous two chapters. Multiple different trajectories have been described and visualized. First an optimal trajectory to Neptune with a total ΔV of 9,171.8 m/s is shown. Afterwards different single-KBO flyby results are shown including Albion, which is studied in more detail. This latter trajectory has a total ΔV of 9852.9 m/s. A sensitivity study on this Albion trajectory shows that the ΔV can be lowered further to 9683.3 m/s (wet-to-dry mass ratio of 1.39) with a departure date variation of +2 days. Furthermore, this test indicates that by varying some of the decision variables there exists an 18 day launch window if one requires the total ΔV of the mission to be within 20% of the optimal value.

Multiple attempts at multi-KBO flyby missions are also described. While many of these trajectories can be found with high-thrust propulsion, most can not be replicated with low thrust. This is caused by the high sensitivity of low-thrust propulsion and spherical shaping, the requirement for spherical shaping that the trajectory must curve towards the central body, and the varying solutions to the a_2 coefficient solver. For these reasons more study into these aspects is recommended and comparisons with other shape-based low-thrust parameterizations such as hodographic shaping are recommended. One low-thrust mission with two KBO flybys is found. It requires 352 m/s of ΔV after passing Neptune and visits K13WB4G and K15RS1R for a total ΔV of 10,521 m/s (wet-to-dry mass ratio of 1.43).

More analysis of the data is performed including a distant flyby analysis with the trajectory towards Albion. This only shows one VDFB with other known KBOs (besides Albion) and indicates that if one wants many (V)DFBs it would have to be included in the objective description. An analysis of the thrust magnitude for different KBO trajectories shows that the required thrust is orders of magnitude below the maximum available thrust for most of the mission. Only at the start of the mission does the thrust exceed the limitations. It is expected that for a real mission this is not an issue and can be solved with higher values for the launch energy. In later parts of the trajectory the use of coasting arcs is appealing as there is enough space in the thrust magnitude budget. This final check also indicates that the trajectories found in this chapter are realistic with current power-generation technologies.

While no direct comparison is performed with high-thrust comparisons, results from other research indicate that the found low-thrust trajectories are comparable and in some cases more optimal in terms of the wet-to-dry mass fraction than proposed high-thrust KBO missions. Further research with higher launch energy values is recommended in order to perform a direct comparison.

10

Conclusions

This chapter addresses the conclusions of the thesis. The main research question of the project is:

”What methodology is required to optimize realistic low-thrust trajectories with the goal of Kuiper belt object flybys?”

First the subquestions of the thesis are answered one by one and at the end of this chapter these answers are used to provide a general answer to the main research question.

- **How is the science return of a KBO flyby mission defined?**
The science return of a KBO flyby mission in this thesis is defined by the number of close flybys with KBOs in combination with the objectives of a low ΔV and a low time-of-flight. At least two KBO CFBs are required to get the desired science return of the mission. A list of instruments has been provided to perform scientific measurements. This science return is accomplished with a single launch of a low-thrust powered vehicle placed at the edge of Earth’s SOI with (almost) no excess velocity. From here the spacecraft uses low-thrust propulsion to perform planetary gravity assists followed by one or more flybys in the Kuiper belt.
- **Which thrust parameterization and physics description is best used for the low-thrust trajectory design and how does this need to be implemented in Tudat?**
The trajectory design is tackled with a patched-conics approach and semi-analytical low-thrust legs to reduce the runtime and as such increase the number of analyses during the thesis project time span. For the thrust a spherical-shaping approach is used. For the Tudat implementation a three-file object-oriented Python structure is applied with input data for KBOs from MPC.
- **What is the best performing optimizer including tuning for a low-thrust flyby mission?**
Based on heritage research the MOEA/D optimizer is used. To tune this optimizer first a high-thrust tuning problem is tackled to reduce the search space of the optimizer settings. Afterwards, the optimizer is tuned with a low-thrust problem with the following settings as a result: cross-over rate 0.6, scale factor 0.7, distribution index 10, neighborhood size 40, realb 0.6, limit 2. The population number is set at 100 with a generation number based on convergence criteria.
- **What is the optimal planetary gravity-assist sequence for Kuiper belt trajectories?**
Based on previous studies it is chosen to use gravity assists with Jupiter and Neptune to reach the Kuiper belt. With an added convergence method and using constrained trajectories an optimal trajectory case to Neptune is found. This is aided by first using a high-thrust optimization problem to reduce the search space for the low-thrust problem. A low-thrust trajectory to Neptune with a ΔV of 9.17 km/s and a time-of-flight of 17.9 years has been found.
- **What is the required optimization strategy to expand the trajectory to the Kuiper belt with optimal objective values?**
The same process of switching between high-thrust and low-thrust optimization is sufficient to find candidates for the first KBO flyby. Later more local refinement cycles can be used to improve the objective values of these trajectories. A trajectory to the KBO Albion is found with a total ΔV of roughly 9.68 km/s and a total time-of-flight of 27.0 years.

- **What kind of Kuiper belt flyby trajectories are possible with the found optimization strategy?**

Missions with a single KBO flyby are easily found with this optimization strategy. Expanding the trajectory to two KBO flybys is more difficult. By optimizing multiple KBO flybys at the same time, using an expanded set of KBOs, and using close-approach graphs at least one low-thrust KBO mission with two KBO flybys is found with a total ΔV of roughly 10.52 km/s and a time-of-flight of 33.2 years. The difficulty of finding multi-KBO flybys is attributed to the limitations of the current spherical-shaping description, specifically its sensitivity to inputs, its description of the a_2 algorithm, and its requirement to have trajectories curve towards the central body.

- **How many distant flybys can one expect to encounter during a long-term Kuiper belt mission?**

An analysis of the trajectory towards Albion and K13WB4G indicates that, among the known and catalogued KBOs, one should not expect random DFBs during a KBO mission. A few VDFBs might be feasible, but to get a large number of distant flybys this concept should be included in the objective description.

- **What impact does a sensitivity study of the inputs of the trajectory have on the found optimal Kuiper belt trajectories?**

A sensitivity study on the departure date shows that, without changing the launch energy, there is a launch window of roughly 18 days for the Albion KBO mission before the ΔV no longer becomes attractive with respect to alternative trajectories. All ΔV values within the tested 40 day launch window remain below the maximum ΔV budget assigned to the mission.

- **How feasible are the found Kuiper belt flyby trajectories with current power and low-thrust propulsion technologies?**

For the majority of the trajectory the thrust of the found trajectories requires power levels well below the maximum available power. Only at the start of the trajectory the power level is exceeded, but this can be avoided by using a higher launch energy. In reality the thrust would not be continuous, but would have active phases and coasting phases. Trajectories to KBOs are found with a ΔV of roughly 10 km/s. This value is roughly half of the available ΔV budget and the result could be even lowered by increasing the launch energy. Based on this it is concluded that the found KBO flyby trajectories are realistic with the use of current power and low-thrust technologies.

- **How does the the wet-to-dry mass fraction of the designed low-thrust missions compare to potential high-thrust missions?**

The found optimal KBO missions have a wet-to-dry mass ratio in the order of 1.39 to 1.43. No direct fair comparison is performed with high-thrust trajectories in this thesis, which would require an analysis of missions with higher launch energy values. However, based on results from other research it is concluded that at the very least the results found in this thesis are comparable and in some cases even more optimal than the mass fraction found in proposed high-thrust KBO missions.

Based on the conclusions in the itemized list a general conclusion for the thesis can be drawn. In this thesis a methodology based on switching between high-thrust and low-thrust trajectories and separately analyzing trajectory legs is described to constrain the inputs for the low-thrust multi-objective optimization problem. With the use of an evolutionary algorithm this allows for the design of many single flyby KBO missions. By means of combining the optimization steps of multiple KBOs, expanding the KBO database, and the use of close-approach graphs trajectories to more than one KBO in a single mission can also be designed with many high-thrust examples. However, in the end only a single example of such a mission with low thrust has been found. While it is expected that further searches will result in more low-thrust two-KBO trajectories, the difficulty to find these trajectories is mainly caused by the limitations of the used spherical-shaping trajectory method. Nevertheless, this thesis shows that the design and optimization of low-thrust KBO missions is possible and that the resulting trajectories are realistic to perform with current technology in terms of ΔV and thrust levels. The results are even comparable or more optimal compared to high-thrust KBO missions, even though more research is required to definitely quantify this. The thesis thus firmly puts another propulsion possibility on the table when deep-space Kuiper belt missions are considered.

Recommendations

Based on the conclusions of this thesis there are multiple possibilities and recommendations for further research. Furthermore, some topics were not tackled during this thesis to narrow down the research, but are still recommended to do at some point to widen the scope of the research topic. These recommendations are discussed in this chapter. The recommendations are split into four categories: mission design, trajectory design, thrust parameterization, and the optimization process.

Mission design

- The mission design in this thesis only analyzed missions to Kuiper belt objects. However, missions to other TNOs such as SDOs and detached objects can also be included. Due to their far distance from the Sun they can be excellent options for the last flyby of the trajectory after the spacecraft leaves the Kuiper belt.
- The spacecraft for the KBO mission is considered to be a point mass with only a basic description of its components such as the thrust and power system. A more detailed design of the spacecraft of for example the instrumentation subsystem, the telemetry subsystem, and the general spacecraft dimensions and shape would allow more extensive science return descriptions and calculations regarding for example radiation pressure.
- The KBOs in this thesis are modelled using Kepler orbits. In more detailed design stages it is recommended to instead use numerically propagated orbits from the JPL Horizon model to reduce the error of the KBO ephemerides.

Trajectory design

- The inclusion of coasting phases is recommended for future research. The thrust profile in Chapter 9 indicates that the thrust level can be orders of magnitude larger during some sections of the trajectory before reaching the thrust limit. This would reduce the operational time of the thruster and as such increase its lifetime. Furthermore, the use of coasting phases can reduce the total ΔV of a mission as was already studied by A.M. Gonzalez [36].
- The launch is considered to be an instantaneous maneuver in this thesis. A more detailed launch description including launch location and an in-depth analysis of the different launch vehicles is recommended for further research. Specifically, allowing for a larger launch energy can reduce the total ΔV of the mission and reduce the time-of-flight.
- Flybys of the inner Solar System were out of scope for this thesis to reduce the complexity of the problem description. However, with the current results the addition of inner Solar System gravity assists can reduce the total launch energy required and as such the total ΔV . The same goes for other or additional flyby sequences with the outer planets.
- Trajectory design in this thesis is done with semi-analytical thrust arcs. In detailed design it is recommended to switch to a fully propagated trajectory method where perturbations other than the Sun and the thrust system can be taken into account.

- Both powered gravity assists and aerogravity assists have not been included in the trajectory design of this thesis. Research by P. Muelegaas [63] and J. Melman [58] indicates that such maneuvers can further reduce the total ΔV of the mission.
- To improve the implementation of the KBO legs in Tudat it is recommended to add a new type of leg which travels to a node, which represents a KBO, without having to perform a gravity assist or other maneuver at the end of the leg.
- Due to time limitations only missions with a maximum of two KBOs were studied in this thesis. The optimization of missions with more CFBs is recommended.

Thrust parameterization

- This thesis used spherical shaping as its low-thrust parameterization. However, in the conclusions it is mentioned that spherical shaping has severe limitations due to its sensitivity, restrictions regarding trajectory curvature, and current implementation of the a_2 root finder. Therefore, it is recommended to also perform a low-thrust KBO analysis with other low-thrust shape-based methods. Hodographic shaping in particular is recommended due to its large customization by means of base functions and free coefficients. Now that the design space has already been narrowed down the use of Sims-Flanagan also becomes more attractive.
- Related to the previous point, improving the spherical-shaping method in Tudat to remove some of the issues mentioned before is also recommended. This would regard a reformulation of the way the time-of-flight is integrated such that it does allow for trajectories which curve away from the central body as well as a rework of Tudat such that the a_2 function can be accessed more readily and all its different roots can be tested. This also includes the possibility to use different a_2 search ranges for different legs within the same trajectory.
- A direct comparison of this method with high-thrust propulsion would provide an answer on whether low-thrust KBO missions are more attractive than their high-thrust counterpart in terms of the payload mass. Since the research objective of this thesis is different from L. van der Heyden's thesis, these results can not be directly compared at the moment. To allow for a fair comparison an increase in the launch energy would be required in the problem description, which is already discussed in a previous recommendation.
- The calculation of a thrust buffer to account for uncertainties in the position of the planets, KBOs, and errors in the spacecraft instruments is not done in this thesis. Such a buffer could provide a more detailed answer on the realism of performing flybys with KBOs with an uncertainty factor above 2 as was done in later stages of the optimization process.
- The code in this thesis uses the traditional description of spherical shaping. Adjusted descriptions such as the one by A. Vroom [121] can deal better with high inclination trajectories and might thus result in easier trajectory design for some of the more inclined KBO trajectories.

Optimization process

- The optimization process for the KBO flybys does not take any specific information about the KBOs into account. A single mission which performs a flyby of multiple types of KBOs (for example an object from the cold population and one from the hot population of the classical belt) can provide scientific data on the variation of KBOs. The same goes for including information about binary objects and ring systems in the objective description for the optimizer.
- The optimizer method in this thesis used a single island model. Using multiple islands, the so-called archipelago method, allows members of a population to move between different solution clusters and could be especially useful in problems with many local optima as is most likely the case with the problem description from this thesis.
- An expansion of the sensitivity study to other parameters besides the departure date is recommended. This can for example include the sensitivity of the gravity assist variables or, when a fully propagated trajectory is implemented, uncertainties regarding gravity fields and spacecraft characteristics.
- The use of reverse optimization, where the final trajectory leg is optimized first, can improve the chance of finding solutions compared to the current chronological method. This is because due to the low synodic period it is much easier to find solutions for the first few legs of the trajectory

than for the later legs. To do this specific KBO targets have to be selected, which can be taken from the optimal trajectories found during this thesis project.

- The addition of other objectives can increase the scope of the optimization problem. Such new objectives could regard the distant flyby analysis, a penalty system, the launch ΔV , or the duration which the spacecraft spends in the Kuiper belt.
- The multiple steps of the optimization algorithm explained in Chapters 7 and 8 are currently performed manually by running different functions in succession. The construction of an automatic algorithm which runs the necessary functions in sequence would make future analyses of KBO low-thrust missions faster and easier for users unfamiliar with the entire code structure. The advantage of such an algorithm should be weighed against its riskiness since manual intervention was required many times during this thesis to tweak the optimization method.

Bibliography

- [1] K. Alemany and R.D. Braun. "Survey of global optimization methods for low-thrust, multiple asteroid tour missions". In: *Advances in the Astronautical Sciences* 127 PART 2 (2007), pp. 1641–1660.
- [2] S.W. Angrist. *Direct Energy Conversion*. 4th ed. Allyn Bacon, 1982. ISBN: 0205077587.
- [3] ArianeGroup. *Spacecraft Propulsion: With Thrust and Precision into Space*. 2019, p. 6. URL: https://www.ariane.group/wp-content/uploads/2020/06/Orbital_Propulsion_2019_07_PB_EN_Web.pdf.
- [4] Instituto de Astrofísica de Andalucía. *Haumea of the Outer Solar System*. 2017. URL: <https://apod.nasa.gov/apod/ap171017.html> (visited on 03/03/2022).
- [5] E. Baldwin and EJRW-Quartz. "Rosetta: Rendezvous With a Comet". In: *ESA Publications Brochures* (2014), p. 7. ISSN: 0250-1589. URL: https://www.esa.int/About_Us/ESA_Publications/ESA_Publications_Brochures/ESA_BR-318_Rosetta.
- [6] G. Baskaran et al. "A survey of mission opportunities to trans-neptunian objects - Part IV". In: *AIAA/AAS Astrodynamics Specialist Conference 2014* (2014). DOI: 10.2514/6.2014-4353.
- [7] G.L. Bennett et al. "The general-purpose heat source radioisotope thermoelectric generator: A truly general-purpose space RTG". In: *AIP Conference Proceedings* 969 (2008), pp. 663–671. DOI: 10.1063/1.2845028.
- [8] L.B. Beveridge et al. "Optimization of plutonium-238 production in the advanced test reactor for radioisotope thermoelectric generators in deep space exploration applications". In: *Nuclear and Emerging Technologies for Space, NETS 2018* (2016), pp. 364–367.
- [9] F. Biscani and D. Izzo. "A parallel global multiobjective framework for optimization: PaGMO". In: *Journal of Open Source Software* 5 (53 2020), p. 2338. DOI: 10.21105/joss.02338. URL: <https://doi.org/10.21105/joss.02338>.
- [10] F. Biscani and D. Izzo. *PaGMO: C++ API documentation*. 2020. URL: https://esa.github.io/pagmo2/docs/cpp/cpp_docs.html#implemented-algorithms (visited on 12/16/2022).
- [11] F. Biscani and D. Izzo. *PyGMO: Algorithms implemented in Python*. 2021. URL: <https://esa.github.io/pygmo2/algorithms.html> (visited on 12/16/2022).
- [12] F. Biscani and D. Izzo. *PyGMO: List of algorithms*. 2021. URL: <https://esa.github.io/pygmo2/overview.html#list-of-algorithms> (visited on 12/16/2022).
- [13] F. Biscani and D. Izzo. *Using pygmo's moead*. 2021. URL: https://esa.github.io/pygmo2/tutorials/moo_moead.html (visited on 12/16/2022).
- [14] J.R. Brophy et al. "Status of the dawn ion propulsion system". In: *40th AIAA/ASME/SAE/ASEE Joint Propulsion Conference and Exhibit* (2004). DOI: 10.2514/6.2003-4542.
- [15] Minor Planet Center. *Minor Planet Center*. URL: <https://minorplanetcenter.net/> (visited on 04/02/2022).
- [16] J. Chan et al. "Development of advanced Stirling Radioisotope Generator for planetary surface and deep space missions". In: 2008. ISBN: 9781563479441. DOI: 10.2514/6.2008-5768.
- [17] E.Y. Choueiri. "New dawn for electric rockets". In: *Scientific American* 300 (2 2009), pp. 58–65. DOI: 10.1038/scientificamerican0209-58.
- [18] B. Christophe et al. "OSS (Outer Solar System): A fundamental and planetary physics mission to Neptune, Triton and the Kuiper Belt". In: *Experimental Astronomy* 34 (2 2012), pp. 203–242. DOI: 10.1007/s10686-012-9309-y.
- [19] G.E. Costigan et al. "Low-cost opportunity for multiple trans-neptunian object rendezvous and orbital capture". In: *Advances in the Astronautical Sciences* 162 (2018), pp. 1069–1085.

- [20] R. Dawson and R. Murray-Clay. "Neptune's wild days: Constraints from the eccentricity distribution of the classical Kuiper Belt". In: *Astrophysical Journal* 750 (Feb. 2012). DOI: 10.1088/0004-637X/750/1/43.
- [21] TU Delft. *TU Delft Astrodynamics Toolbox*. 2022. URL: <https://docs.tudat.space/en/stable> (visited on 12/15/2022).
- [22] D. Dirx and E. Mooij. *Propagation and Optimisation in Astrodynamics (AE4866) - Global Optimisation*. Unpublished lecture notes. TU Delft, 2021.
- [23] D. Dirx. Private Communication. Zoom (online), June 15, 2021.
- [24] M.K. Dougherty et al. "The Cassini magnetic field investigation". In: *Space Science Reviews* 114 (1-4 2004), pp. 331–383. DOI: 10.1007/s11214-004-1432-2.
- [25] J.L. Elliot et al. "The deep ecliptic survey: A search for kuiper belt objects and centaurs. II. Dynamical classification, the kuiper belt plane, and the core population". In: *Astronomical Journal* 129 (2 2005), pp. 1117–1162. DOI: 10.1086/427395.
- [26] D.H. Ellison. "Robust preliminary design for multiple gravity assist spacecraft trajectories". PhD dissertation. University of Illinois Urbana-Champaign, Feb. 2018.
- [27] D.H. Ellison, J.A. Englander, and B.A. Conway. "Robust global optimization of low-thrust, multiple-flyby trajectories". In: *Advances in the Astronautical Sciences* 150 (2014), pp. 3213–3232.
- [28] ESA. *Global Trajectory Optimisation Problems Database*. 2021. URL: <https://www.esa.int/gsp/ACT/projects/gtop/> (visited on 05/17/2022).
- [29] ESA. *Science Exploration - Rosetta factsheet*. URL: http://www.esa.int/Science_Exploration/Space_Science/Rosetta/Rosetta_factsheet.
- [30] W. Frazier, E. Rice, and K.L. Mitchell. "Architecture of a fault-tolerant and verifiable outer planet flyby". In: *Advances in the Astronautical Sciences* 169 (2019), pp. 173–188. DOI: 2014/51715.
- [31] M.A. Gibson et al. "NASA's Kilowatt reactor development and the path to higher power missions". In: *IEEE Aerospace Conference Proceedings 2017-June* (2017), pp. 1–14. DOI: 10.1109/AERO.2017.7943946.
- [32] E.K.A. Gill and O. Montenbruck. *Satellite orbits: Models, methods and applications*. Springer, 2013. ISBN: 978-3-540-67280-7. DOI: 10.1007/978-3-642-58351-3.
- [33] B. Gladman et al. "The structure of the Kuiper Belt: Size distribution and radial extent". In: *Astronomical Journal* 122 (2 2001), pp. 1051–1066. DOI: 10.1086/322080.
- [34] R. Gomes. "The formation of the cold classical Kuiper Belt by a short range transport mechanism". In: *Icarus* 357 (2021). DOI: 10.1016/j.icarus.2020.114121.
- [35] D. Gondelach. *A Hodographic-Shaping Method for Low-Thrust Trajectory Design*. MSc thesis. Delft University of Technology, Feb. 2012.
- [36] A.M. Gonzalez. *Characterisation of Shape-Based Methods and Combination with Coasting Arcs*. MSc thesis. Delft University of Technology, Feb. 2020.
- [37] E. Gough. *NASA has Figured Out How to Extend the Lives of the Voyagers Even Longer*. 2019. URL: <https://www.universetoday.com/142802/nasa-has-figured-out-how-to-extend-the-lives-of-the-voyagers-even-longer/> (visited on 03/12/2022).
- [38] J. Guo and R.W. Farquhar. "New Horizons Mission Design". In: *Space Sci Reviews* 140 (2008), pp. 49–74. DOI: <https://doi.org/10.1007/s11214-007-9242-y>.
- [39] GVW. *The Minor Planet Ephemeris Service*. 2011. URL: <https://minorplanetcenter.net/iau/info/MPES.pdf> (visited on 04/02/2022).
- [40] M. Hamdan. "The Distribution Index in Polynomial Mutation for Evolutionary Multiobjective Optimisation Algorithms: An Experimental Study". In: *Proceedings of International Conference on Electronics Computer Technology* (2012). URL: https://www.academia.edu/4045692/The_Distribution_Index_in_Polynomial_Mutation_for_Evolutionary_Multiobjective_Optimisation_Algorithms_An_Experimental_Study.

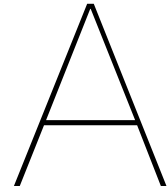
- [41] T.E. Hammel et al. "Multi-Mission Radioisotope Thermoelectric Generator (MMRTG) and performance prediction model". In: *7th International Energy Conversion Engineering Conference* (2009). DOI: 10.2514/6.2009-4576.
- [42] P.K. Henry et al. "Exploring the Kuiper Belt: an extended Pluto mission". In: *Acta Astronautica* 44 (2 1999), pp. 85–90. DOI: 10.1016/S0094-5765(99)00032-6.
- [43] L. van der Heyden. *Exploring the Kuiper Belt*. MSc thesis. Delft University of Technology, Feb. 2020.
- [44] M. Hirabayashi et al. "Hayabusa2 extended mission: New voyage to rendezvous with a small asteroid rotating with a short period". In: *Advances in Space Research* 68 (3 2021), pp. 1533–1555. DOI: 10.1016/j.asr.2021.03.030.
- [45] K. De hulsters. *Trajectory Optimization of a Kuiper Belt Flyby Mission*. MSc thesis literature study. Delft University of Technology, July 2021.
- [46] D. Izzo. "Revisiting Lambert's problem". In: *Celestial Mechanics and Dynamical Astronomy* 121 (1 2015), pp. 1–15. DOI: 10.1007/s10569-014-9587-y.
- [47] D. Johnson et al. "A survey of mission opportunities to trans neptunian objects, part vi: A search for multi-target missions". In: *Advances in the Astronautical Sciences* 171 (2020), pp. 71–82.
- [48] Y. Jul et al. "Complex Network Clustering by a Multi-objective Evolutionary Algorithm Based on Decomposition and Membrane Structure". In: *Scientific Reports* 6 (1 2016). DOI: <https://doi.org/10.1038/srep33870>.
- [49] M.S. Konstantinov and M. Thein. "Method of interplanetary trajectory optimization for the spacecraft with low thrust and swing-bys". In: *Acta Astronautica* 136 (2017), pp. 297–311. DOI: 10.1016/j.actaastro.2017.02.018.
- [50] D. Landau, T. Lam, and N. Strange. "Broad search and optimization of solar electric propulsion trajectories to Uranus and Neptune". In: *Advances in the Astronautical Sciences* 135 (2010), pp. 2093–2112.
- [51] D. Landau, N. Strange, and T. Lam. "Solar electric propulsion with satellite flyby for Jovian capture". In: *Advances in the Astronautical Sciences* 136 (2010), pp. 1043–1056.
- [52] H.F. Levison et al. "Origin of the structure of the Kuiper belt during a dynamical instability in the orbits of Uranus and Neptune". In: *Icarus* 196 (1 2008), pp. 258–273. DOI: 10.1016/j.icarus.2007.11.035.
- [53] H. Li and Q. Zhang. "Multiobjective optimization problems with complicated pareto sets, MOEA/D and NSGA-II". In: *IEEE Transactions on Evolutionary Computation* 13 (2 2009), pp. 284–302. DOI: 10.1109/TEVC.2008.925798.
- [54] J.J. Lissauer and I. de Pater. *Fundamental Planetary Science: Physics, Chemistry and Habitability*. Cambridge University Press, 2019. DOI: 10.1017/9781108304061.
- [55] V. Maiwald. "A new method for optimization of low-thrust gravity-assist sequences". In: *CEAS Space Journal* 9 (3 2017), pp. 243–256. DOI: 10.1007/s12567-017-0147-7.
- [56] S. Mazouffre. "Electric propulsion for satellites and spacecraft: Established technologies and novel approaches". In: *Plasma Sources Science and Technology* 25 (3 2016). DOI: 10.1088/0963-0252/25/3/033002.
- [57] R. Mcgranaghan et al. "A survey of mission opportunities to trans-neptunian objects". In: *JBIS - Journal of the British Interplanetary Society* 64 (9-10 2011), pp. 296–303.
- [58] J. Melman. *Trajectory Optimization for a Mission to Neptune and Triton*. MSc thesis. Delft University of Technology, Feb. 2007.
- [59] K. Michalak. "The effects of asymmetric neighborhood assignment in the MOEA/D algorithm". In: *Applied Soft Computing* 25 (2014), pp. 97–106. DOI: <https://doi.org/10.1016/j.asoc.2014.07.029>.
- [60] K.L. Mitchell et al. "Implementation of Trident: A Discovery-Class Mission to Triton". In: *Lunar and Planetary Science Conference* 50 (2019), p. 3200. URL: <https://www.hou.usra.edu/meetings/lpsc2019/pdf/3200.pdf>.

- [61] D. Morante, M.S. Rivo, and M. Soler. “Multi-objective low-thrust interplanetary trajectory optimization based on generalized logarithmic spirals”. In: *Journal of Guidance, Control, and Dynamics* 42 (3 2019), pp. 476–490. DOI: 10.2514/1.G003702.
- [62] A. Morbidelli, V.V. Emel’yanenko, and H.F. Levison. “Origin and orbital distribution of the trans-Neptunian scattered disc”. In: *Monthly Notices of the Royal Astronomical Society* 355 (3 2004), pp. 935–940. DOI: 10.1111/j.1365-2966.2004.08372.x.
- [63] P. Musegaas. *Optimization of Space Trajectories Including Multiple Gravity Assists and Deep Space Maneuvers*. MSc thesis. Delft University of Technology, Feb. 2013.
- [64] S. Nabiyeu and I. Simonia. “The statistical analysis of the color—orbit parameters and color—inclination distributions of TNOs”. In: *Astrophysics and Space Science* 361 (10 2016). DOI: 10.1007/s10509-016-2913-y.
- [65] NAIF/JPL/NASA. *An Overview of Reference Frames and Coordinate Systems in the SPICE Context*. 2020. URL: https://naif.jpl.nasa.gov/pub/naif/toolkit_docs/Tutorials/pdf/individual_docs/17_frames_and_coordinate_systems.pdf (visited on 12/08/2022).
- [66] NASA. *Advanced Stirling Radioisotope Generator (ASRG)*. 2013. URL: <https://rps.nasa.gov/resources/65/advanced-stirling-radioisotope-generator-asrg/> (visited on 02/25/2022).
- [67] NASA. *Basics of Space Flight*. URL: <https://solarsystem.nasa.gov/basics/chapter4-1/> (visited on 02/24/2022).
- [68] NASA. *In-depth - Kuiper Belt - NASA Solar System Exploration*. URL: <https://solarsystem.nasa.gov/solar-system/kuiper-belt/in-depth/> (visited on 02/22/2022).
- [69] NASA. *In-depth - New Horizons - NASA Solar System Exploration*. URL: <https://solarsystem.nasa.gov/missions/new-horizons/in-depth/> (visited on 02/24/2022).
- [70] NASA. *In-depth - Pioneer 10 - NASA Solar System Exploration*. URL: <https://solarsystem.nasa.gov/missions/pioneer-10/in-depth/> (visited on 02/25/2022).
- [71] NASA. *In-depth - Pioneer 11 - NASA Solar System Exploration*. URL: <https://solarsystem.nasa.gov/missions/pioneer-11/in-depth/> (visited on 02/25/2022).
- [72] NASA. *In-depth - Stardust - NASA Solar System Exploration*. URL: <https://solarsystem.nasa.gov/missions/stardust/in-depth/> (visited on 02/24/2022).
- [73] NASA. *In-depth - Voyager 1 - NASA Solar System Exploration*. URL: <https://solarsystem.nasa.gov/missions/voyager-1/in-depth/> (visited on 02/25/2022).
- [74] NASA. *In-depth - Voyager 2 - NASA Solar System Exploration*. URL: <https://solarsystem.nasa.gov/missions/voyager-2/in-depth/> (visited on 02/25/2022).
- [75] NASA. *NASA’s Launch Services Program - Launch Vehicle Performance Website*. 2021. URL: <https://elvperf.ksc.nasa.gov/Pages/Default.aspx> (visited on 03/10/2022).
- [76] NASA. *NASA’s New Horizons Spacecraft Takes the Inside Course to Ultima Thule*. 2018. URL: <https://solarsystem.nasa.gov/news/795/nasas-new-horizons-spacecraft-takes-the-inside-course-to-ultima-thule/> (visited on 02/24/2022).
- [77] NASA. *New Horizons 2: A Journey to New Frontiers*. 2005. URL: https://www.lpi.usra.edu/opag/meetings/feb2005/presentations/nh2_community_info.pdf (visited on 03/01/2022).
- [78] NASA. *Overview - Dawn - NASA Solar System Exploration*. URL: <https://solarsystem.nasa.gov/missions/dawn/overview/> (visited on 03/01/2022).
- [79] NASA. “Stardust Launch: Press Kit”. In: *JPL Press Kits 1-29-99* (1999). URL: https://www.jpl.nasa.gov/news/press_kits/stardust.pdf.
- [80] NASA. *Voyager Backgrounder*. Vol. 80-160. ID = 19810001583. United States of America, 1980, p. 32. URL: <https://ntrs.nasa.gov/citations/19810001583>.
- [81] (J. Schalkwyk) NASA. *NASA Celebrates Four Decades of Plucky Pioneer 11*. 2013. URL: <https://www.nasa.gov/centers/ames/news/2013/pioneer11-40-years.html> (visited on 02/24/2022).

- [82] NASA/GSFC. *NSSDCA Master Catalog Search - Hayabusa2 (2014-076A)*. URL: <https://nssdc.gsfc.nasa.gov/nmc/spacecraft/display.action?id=2014-076A> (visited on 03/02/2022).
- [83] NASA/GSFC. *NSSDCA Master Catalog Search - New Horizons Pluto Kuiper Belt Flyby (2006-001A)*. URL: <https://nssdc.gsfc.nasa.gov/nmc/spacecraft/display.action?id=2006-001A> (visited on 03/02/2022).
- [84] NASA/JHUAPL/SwRI. *In Depth: Charon - NASA Solar System Exploration*. 2015. URL: <https://solarsystem.nasa.gov/moons/pluto-moons/charon/in-depth/> (visited on 12/18/2022).
- [85] NASA/JPL. *Generic Frame Definition Kernel File for ESA Planetary Missions*. 2021. URL: <https://naif.jpl.nasa.gov/pub/naif/VEX/kernels/fk/RSSD0002.TF> (visited on 12/06/2022).
- [86] NASA/JPL. *HORIZONS Web-Interface*. 2021. URL: <https://ssd.jpl.nasa.gov/horizons.cgi> (visited on 12/08/2022).
- [87] NASA/JPL/USGS. *PIA00317: Global Color Mosaic of Triton*. 1998. URL: <https://photojournal.jpl.nasa.gov/catalog/PIA00317> (visited on 03/03/2022).
- [88] NASA/SRI/APL. *New Horizons Press Launch Kit*. 2012. URL: https://www.nasa.gov/pdf/139889main_PressKit12_05.pdf (visited on 12/08/2022).
- [89] D. Nelson et al. "Navigation and Orbit Estimation for New Horizons' Arrokoth Flyby: Overview, Results and Lessons Learned". In: *Space Science Reviews* 218 (3 Mar. 2022), pp. 331–383. DOI: 10.1007/s11214-022-00877-4.
- [90] Nuclear Newswire. *DOE steps up plutonium production for future space exploration*. 2021. URL: <https://www-ans-org.tudelft.idm.oclc.org/news/article-2658/doe-steps-up-plutonium-production-for-future-space-exploration/> (visited on 04/06/2022).
- [91] D.M. Novak. *Methods and Tools for Preliminary Low Thrust Mission Analyses*. PhD thesis. University of Glasgow, 2012.
- [92] D.M. Novak and M. Vasile. "Improved shaping approach to the preliminary design of low-thrust trajectories". In: *Journal of Guidance, Control, and Dynamics* 34 (1 2011), pp. 128–147. DOI: 10.2514/1.50434.
- [93] NASA Science Mission Directorate/New Horizons II Review Panel. "Final Report on the New Horizons II Review Panel". In: *FY 2005 Omnibus Appropriations Conference Report (2005)*, pp. 1–3.
- [94] R.S. Park et al. "The JPL planetary and lunar ephemerides DE440 and DE441". In: *Astronomical Journal* 161 (3 2021). DOI: 10.3847/1538-3881/abd414.
- [95] NASA/Johns Hopkins University Applied Physics Laboratory/Southwest Research Institute/Alex Parker. *The True Colors of Pluto*. 2018. URL: http://pluto.jhuapl.edu/Galleries/Featured-Images/image.php?page=1&gallery_id=2&image_id=543 (visited on 03/03/2022).
- [96] M.N. De Parolis and W. Pinter-Krainer. *Current and Future Techniques for Spacecraft Thermal Control 1. Design drivers and current technologies*. 1996. URL: <http://www.esa.int/esapub/bulletin/bullet87/paroli87.htm> (visited on 03/16/2022).
- [97] S.P. Parvathi and R.V. Ramanan. "Direct transfer trajectory design options for interplanetary orbiter missions using an iterative patched conic method". In: *Advances in Space Research* 59.7 (2017), pp. 1763–1774. DOI: 10.1016/j.asr.2017.01.023.
- [98] M.B. Penas. *A Rapid Grid-Search Technique for KBO Exploration Trajectories*. MSc thesis. Delft University of Technology, Feb. 2020.
- [99] A.E. Petropoulos and J.M. Longuski. "Shape-based algorithm for automated design of low-thrust, gravity-assist trajectories". In: *Journal of Spacecraft and Rockets* 41 (5 2004), pp. 787–796. DOI: 10.2514/1.13095.
- [100] R.W. Pogge. *Astronomy 161: An Introduction to Solar System Astronomy - Lecture 19: Orbits*. Lecture notes. Ohio State University, 2010.
- [101] L.M. Prockter et al. "Exploring Triton with Trident: A Discovery Class Mission". In: *Lunar and Planetary Science Conference* 50 (2019), p. 3188. URL: <https://www.hou.usra.edu/meetings/lpsc2019/pdf/3188.pdf>.

- [102] Team Hayabusa2 Project. *Hayabusa2 Information Fact Sheet Ver. 2. 3*. 2018. URL: https://global.jaxa.jp/projects/sat/hayabusa2/pdf/sat33_fs_23_en.pdf (visited on 03/02/2022).
- [103] NASA/JPL (M. Rayman). *Dear Dawnniversaries*. 2017. URL: <https://www.jpl.nasa.gov/blog/2017/9/dear-dawnniversaries> (visited on 03/01/2022).
- [104] M.D. Rayman et al. "Lessons from the Dawn mission to Ceres and Vesta". In: *Acta Astronautica* 176 (2020), pp. 233–237. ISSN: 0094-5765. DOI: 10.1016/j.actaastro.2020.06.023.
- [105] D.C. Reuter et al. "Ralph: A visible/infrared imager for the New Horizons Pluto/Kuiper Belt Mission". In: *Space Science Reviews* 140 (1-4 2008), pp. 129–154. DOI: 10.1007/s11214-008-9375-7.
- [106] T.G.R. Roegiers. *Application of the Spherical Shaping Method to a Low-Thrust Multiple Asteroid Rendezvous Mission: Implementation, limitations and solutions*. MSc thesis. Delft University of Technology, Feb. 2014.
- [107] D.M. Sanchez, A.A. Sukhanov, and A.F.B.A. Prado. "Optimal trajectories to kuiper belt objects". In: *Revista Mexicana de Astronomia y Astrofisica* 55 (1 2019), pp. 39–54. DOI: 10.22201/ia.01851101p.2019.55.01.06.
- [108] D.M. Sanchez et al. "Optimal transfer trajectories to the haumea system". In: *13th International Conference on Space Operations, SpaceOps 2014* (2014). DOI: 10.2514/6.2014-1639.
- [109] E Saturnino. *A Piecewise Shaping Method for Preliminary Low-Thrust Trajectory Design*. MSc thesis. Delft University of Technology, Feb. 2017.
- [110] A. Sengupta et al. "An overview of the results from the 30,000 Hr life test of deep space 1 flight spare ion engine". In: *40th AIAA/ASME/SAE/ASEE Joint Propulsion Conference and Exhibit* (2004). DOI: 10.2514/6.2004-3608.
- [111] Y. Shin et al. "Radiation effect for a CubeSat in slow transition from the Earth to the Moon". In: *Advances in Space Research* 31 (Jan. 2015). DOI: 10.1016/j.asr.2015.01.018.
- [112] J.A. Sims and S.N. Flanagan. "Preliminary design of low-thrust interplanetary missions". In: *Advances in the Astronautical Sciences* 103 (PART 1 2000), pp. 583–592.
- [113] A. Stern et al. "New Horizons 2". In: *Outer Planets Assessment Group Archive* (2005), pp. 1–3. URL: https://www.lpi.usra.edu/opag/archive_documents/new_horizons2.pdf.
- [114] S.A. Stern et al. "The New Horizons Kuiper Belt Extended Mission". In: *Space Science Reviews* 214 (4 2018). DOI: 10.1007/s11214-018-0507-4.
- [115] J.F. Stone. "On Julian day notation for meteorological conditions". In: *Agricultural Meteorology* 29 (2 1983), pp. 137–140. DOI: 10.1016/0002-1571(83)90046-8.
- [116] R. Storn and K. Price. "Differential Evolution – A Simple and Efficient Heuristic for global Optimization over Continuous Spaces". In: *Journal of Global Optimization* 11 (4 1997). DOI: 10.1023/A:1008202821328.
- [117] NASA/Johns Hopkins University Applied Physics Laboratory/Southwest Research Institute/Roman Tkachenko. *Enhanced-Color Composite Image of Kuiper Belt Object Arrokoth (2014 MU69)*. 2019. URL: https://solarsystem.nasa.gov/resources/2449/enhanced-color-composite-image-of-kuiper-belt-object-arrokoth-2014-mu69/?category=solar-system/kuiper-belt_arrokoth-2014-mu69 (visited on 03/03/2022).
- [118] C.A. Trujillo, D.C. Jewitt, and J.X. Luu. "Population of the scattered Kuiper Belt". In: *Astrophysical Journal* 529 (2 PART 2 2000). DOI: 10.1086/312467.
- [119] R. Unal and E.B. Dean. "Taguchi Approach To Design Optimization For Quality And Cost: An Overview". In: *Annual Conference of the International Society of Parametric Analysts* (1990).
- [120] M. Vasile and S. Campagnola. "Design of low-thrust multi-gravity assist trajectories to Europa". In: *JBIS - Journal of the British Interplanetary Society* 62 (1 2009), pp. 15–31.
- [121] A. Vroom. *Development of an Improved Spherical Shaping Method for High-Inclination Trajectories*. MSc thesis. Delft University of Technology, Feb. 2017.

- [122] K.F. Wakker. *Fundamentals of Astrodynamics*. Institutional Repository Library, Delft University of Technology, 2015. ISBN: 9789461864192.
- [123] B.J. Wall. "Shape-based approximation method for low-thrust trajectory optimization". In: *AIAA/AAS Astrodynamics Specialist Conference and Exhibit (2008)*. DOI: 10.2514/6.2008-6616.
- [124] H. Weaver and S. Stern. "New Horizons: NASA's Pluto-Kuiper Belt Mission". In: *The Solar System Beyond Neptune* (Feb. 2008), p. 8. URL: http://web.gps.caltech.edu/~mbrown/out/kbbook/Chapters/Weaver_NewHorizons.pdf.
- [125] R.P. Welle. "Availability considerations in the selection of inert propellants for ion engines". In: *AIAA/DGLR/JSASS 21st International Electric Propulsion Conference, 1990* (1990). DOI: 10.2514/6.1990-2589.
- [126] B. Williams et al. "Navigation strategy and results for new Horizons-approach and flyby of the Pluto system". In: *Advances in the Astronautical Sciences*. Vol. 156. 2016, pp. 3271–3290.
- [127] A. Hemant Kumar Yadav et al. "A Study and Brief Research On Electric propulsion Of Spacecraft and Rockets". In: *International Journal of Application or Innovation in Engineering Management (IJAEM)* 218 (12 Dec. 2014). ISSN: 2319-4847.
- [128] D.G. Yarnoz, R. Jehn, and P. De Pascale. "Trajectory design for the bepi-colombo mission to Mercury". In: *JBIS - Journal of the British Interplanetary Society* 60 (6 2007), pp. 202–208.
- [129] A M Zangari et al. "Return to the Kuiper Belt: Launch opportunities from 2025 to 2040". In: *Journal of Spacecraft and Rockets* 56 (3 2019), pp. 919–930. ISSN: 00224650. DOI: 10.2514/1.A34329.
- [130] Q. Zhang and H. Li. "MOEA/D: A multiobjective evolutionary algorithm based on decomposition". In: *IEEE Transactions on Evolutionary Computation* 11 (6 2007), pp. 712–731. DOI: 10.1109/TEVC.2007.892759.
- [131] Q Zong and J He. "Interstellar Heliosphere Probes (IHPs)". In: *42nd COSPAR Scientific Assembly* 42 (2018), PIR.1-2-18. URL: <https://ui.adsabs.harvard.edu/abs/2018cosp...42E3882Z>.
- [132] V.A. Zubko et al. "Analysis of mission opportunities to Sedna in 2029–2034". In: *Advances in Space Research* 68 (7 2021), pp. 2752–2775. DOI: 10.1016/j.asr.2021.05.035.



Overview of unit tests

Tables A.1 and A.2 provide an overview of the unit tests performed on the written code for this thesis. All the unit tests were passed. The numbers in Table A.1 can be used to identify the name of the unit test in Table A.2. The Earth-Mars-Earth example trajectory refers to the trajectory shown in Figure 6.8.

Table A.1: An overview of all the unit tests performed in the code together with their inputs listed.

Number	Unit test	Input
1	Mass fraction maneuver	Value for ΔV (1359.5 m/s) and I_{sp} (200 s)
2	Set up bodies	An array with all planets
3	Set up bodies with KBOs	An array with all planets and KBOs
4	Get trajectory parameters	Earth-Mars-Earth example trajectory
5	Get trajectory object	Earth-Mars-Earth example trajectory
6	Single objective optimization	Cassini-2 GTOPT optimization problem
7	Multi objective optimization	Cassini-2 GTOPT optimization problem
8	Problem object creation	MGATrajectory inputs for Earth-Mars-Earth trajectory
9	Get decision variables	Earth-Mars-Earth example trajectory
10	Get state history	Earth-Mars-Earth example trajectory
11	Get thrust history	Earth-Mars-Earth example trajectory
12	Set optimization type	Optimizer indicator (1) for Earth-Mars-Earth trajectory
13	Get final mass	Earth-Mars-Earth example trajectory
14	Get bounds	Earth-Mars-Earth example trajectory
15	Get nobj	Earth-Mars-Earth example trajectory
16	Position error	Uncertainty parameter (2) and time period (3 years)
17	Mean to eccentric anomaly	Kepler orbit example (M = 30 deg, e = 0.00001)
18	Mean to true anomaly	Kepler orbit example (M = 30 deg, e = 0.1)
19	Epoch to J2000	Letter + number code for an epoch (J981173)
20	Test root finder	Earth-Mars-Earth example trajectory

Table A.2: An overview of all the unit tests performed in the code together with their expected outputs and an indicator whether the unit test was passed.

Number	Expected output	Passed
1	Mass fraction (0.5) based on rocket equation	Yes
2	All planets present	Yes
3	All planets and KBOs present	Yes
4	All inputted values present	Yes
5	Object with correct input values	Yes
6	Correct length and properties of output lists	Yes
7	Correct length and properties of output lists	Yes
8	Correct initialization values of the object	Yes
9	Correct decision variables returned	Yes
10	Correct dimensions and realistic values of the state	Yes
11	Correct dimensions and realistic values of the thrust	Yes
12	Results in a single-objective optimization	Yes
13	Expected final mass based on the trajectory	Yes
14	Same bounds as given in the decision variable range	Yes
15	Expected number of objectives ($1 = \Delta V$)	Yes
16	Expected error (0.17 million km) based on uncertainty parameter	Yes
17	Correct eccentric anomaly (0.524 rad)	Yes
18	Correct true anomaly (0.634 rad)	Yes
19	Correct conversion to J2000 day number (2450832.23)	Yes
20	a_2 value reaches the TOF value at its expected point	Yes